NIST GCR 10-917-8

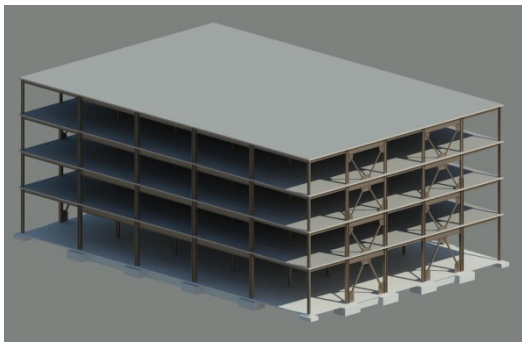

Evaluation of the FEMA P-695 Methodology for Quantification of Building Seismic Performance Factors

NEHRP Consultants Joint Venture
A partnership of the Applied Technology Council and the Consortium of Universities for Research in Earthquake Engineering

nehrp

NIST
National Institute of Standards and Technology
U.S. Department of Commerce

Disclaimers

This report was prepared for the Engineering Laboratory of the National Institute of Standards and Technology (NIST) under the National Earthquake Hazards Reduction Program (NEHRP) Earthquake Structural and Engineering Research Contract SB134107CQ0019, Task Orders 67344 and 68002. The statements and conclusions contained herein are those of the authors and do not necessarily reflect the views and policies of NIST or the U.S. Government.

This report was produced by the NEHRP Consultants Joint Venture, a partnership of the Applied Technology Council (ATC) and the Consortium of Universities for Research in Earthquake Engineering (CUREE). While endeavoring to provide practical and accurate information, the NEHRP Consultants Joint Venture, the authors, and the reviewers assume no liability for, nor express or imply any warranty with regard to, the information contained herein. Users of information contained in this report assume all liability arising from such use.

The policy of NIST is to use the International System of Units (metric units) in all of its publications. However, in North America in the construction and building materials industry, certain non-SI units are so widely used instead of SI units that it is more practical and less confusing to include measurement values for customary units only.

Cover photo – Illustration of steel concentrically braced frame archetype for performance evaluation.

NIST GCR 10-917-8

Evaluation of the FEMA P-695 Methodology for Quantification of Building Seismic Performance Factors

Prepared for
U.S. Department of Commerce
Engineering Laboratory
National Institute of Standards and Technology
Gaithersburg, MD 20899-8600

By
NEHRP Consultants Joint Venture
A partnership of the Applied Technology Council and the Consortium of Universities for Research in Earthquake Engineering

November 2010

U.S. Department of Commerce
Gary Locke, Secretary

National Institute of Standards and Technology
Patrick D. Gallagher, Director

Participants

National Institute of Standards and Technology

John (Jack) R. Hayes, Director, National Earthquake Hazards Reduction Program
John (Jay) L. Harris, Project Manager

NEHRP Consultants Joint Venture

Applied Technology Council
201 Redwood Shores Parkway, Suite 240
Redwood City, California 94065
www.ATCouncil.org

Consortium of Universities for
Research in Earthquake Engineering
1301 S. 46th Street, Building 420
Richmond, California 94804
www.CUREE.org

Joint Venture Management Committee

James R. Harris
Robert Reitherman
Christopher Rojahn
Andrew Whittaker

Joint Venture Program Committee

Jon A. Heintz (Program Manager)
Michael Constantinou
C.B. Crouse
James R. Harris
William T. Holmes
Jack Moehle
Andrew Whittaker

Project Technical Committee

Charles Kircher (Project Director)
Gregory Deierlein
John Hooper
Helmut Krawinkler
Steve Mahin
Benson Shing
John Wallace

Project Review Panel

Ronald O. Hamburger
James R. Harris
William T. Holmes
Richard E. Klingner
Philip Line
Nicolas Luco
Bonnie E. Manley
Laurence Novak
Rafael Sabelli
Kurt Stochlia

Working Group Members

Chui-Hsin Chen
Brian Dean
Aysegul Gogus
Ioannis Koutromanos
Dimitrios Lignos
Farzin Zareian

FEMA Representatives

Michael Mahoney
Robert D. Hanson

Preface

The NEHRP Consultants Joint Venture is a partnership between the Applied Technology Council (ATC) and the Consortium of Universities for Research in Earthquake Engineering (CUREE). In 2007, the National Institute of Standards and Technology (NIST) awarded a National Earthquake Hazards Reduction Program (NEHRP) "Earthquake Structural and Engineering Research" contract (SB1341-07-CQ-0019) to the NEHRP Consultants Joint Venture to conduct a variety of tasks, including Task Orders 67344 and 68002 entitled "Quantification of Building System Performance and Response Parameters."

This work was an extension of work conducted under the ATC-63 Project, funded by the Federal Emergency Management Agency (FEMA), which resulted in the publication of the FEMA P-695 report, *Quantification of Building Seismic Performance Factors* (FEMA 2009). The FEMA P-695 report outlines a procedural methodology for reliably quantifying seismic performance factors, including the response modification coefficient (R factor), the system overstrength factor (Ω_0), and the deflection amplification factor (C_d). While the ATC-63 Project included testing of the Methodology on selected systems (e.g., special and ordinary reinforced concrete moment frames and wood light-frame structural panel shear walls), the purpose of this NIST project was to expand the testing of the Methodology to additional seismic force-resisting systems.

Beta testing was overseen by members of the original ATC-63 Project Team, but was conducted by working groups consisting of individuals who were not directly involved in the development of the Methodology. The following systems were tested as part of this work: (1) special and ordinary reinforced masonry shear walls; (2) special and ordinary reinforced concrete shear walls; (3) special steel concentrically braced frames and buckling-restrained braced frames; and (4) special steel moment frames. With certain exceptions, results confirmed the applicability of the Methodology for quantifying seismic performance factors and verified that currently approved seismic force-resisting systems generally meet the inherent safety against collapse intended by current seismic codes and standards.

The NEHRP Consultants Joint Venture is indebted to the leadership of Charlie Kircher, Project Director, and to the members of the project team for their efforts in testing the Methodology and developing this report. The Project Technical Committee, consisting of Greg Deierlein, John Hooper, Helmut Krawinkler, Steve

Mahin, Benson Shing, and John Wallace monitored and guided the beta testing work. The Working Groups, including Chui-Hsin Chen, Brian Dean, Aysegul Gogus, Ioannis Koutromanos, Dimitrios Lignos, and Farzin Zareian prepared archetype designs and conducted nonlinear response history analyses. The Project Review Panel, consisting of Ron Hamburger, Jim Harris, Bill Holmes, Rich Klingner, Phil Line, Nico Luco, Bonnie Manley, Laurence Novak, Rafael Sabelli, and Kurt Stochlia provided technical review, advice, and consultation at key stages of the work. The names and affiliations of all who contributed to this report are provided in the list of Project Participants.

The NEHRP Consultants Joint Venture also gratefully acknowledges Jack Hayes (NEHRP Director), Jay Harris (NIST Project Manager), Michael Mahoney (FEMA Project Officer), and Robert Hanson (FEMA Technical Monitor) for their input and guidance in the preparation of this report, and Ayse Hortacsu and Peter N. Mork for ATC report production services.

Jon A. Heintz
Program Manager

Table of Contents

List of Figures

List of Tables

Chapter 1
Introduction

The Federal Emergency Management Agency (FEMA) report, FEMA P-695 *Quantification of Building Seismic Performance Factors* (FEMA 2009), outlines a procedural methodology for establishing global seismic performance factors (SPFs), including the response modification coefficient (*R* factor), the system overstrength factor (Ω_0), and deflection amplification factor (C_d). These factors are fundamentally critical in the specification of seismic design loading. The ability to accurately and reliably quantify these factors is important for new seismic force-resisting systems being proposed for adoption, as well as for established systems currently allowed in national model building codes and standards.

In 2007, the National Institute of Standards and Technology (NIST) initiated a project to investigate the FEMA P-695 Methodology in its final stages of development. Performed by the NEHRP Consultants Joint Venture, a partnership of the Applied Technology Council (ATC) and the Consortium of Universities for Research in Earthquake Engineering (CUREE), this work was an extension of work conducted under the FEMA-funded ATC-63 Project. Although the ATC-63 Project included testing of the Methodology on selected systems, the purpose of this NIST project was to expand the testing of the Methodology to additional seismic force-resisting systems.

This report presents the results of expanded testing of the FEMA P-695 Methodology, summarizes findings and conclusions for the systems studied, and provides recommendations for possible improvement of the Methodology and further study related to the specification and use of seismic performance factors in seismic design codes and standards.

1.1 Background and Purpose

Seismic performance factors were initially introduced in the ATC-3-06 report, *Tentative Provisions for the Development of Seismic Regulations for Buildings* (ATC, 1978). They are now used in current seismic codes and standards to estimate strength and deformation demands for seismic force-resisting systems that are designed using linear methods of analysis, but are responding in the nonlinear range. Until recently, derivations of these parameters have been based largely on engineering judgment or qualitative comparisons with systems of known response capabilities.

Advances in performance-based seismic design tools and technologies have resulted in the ability to use nonlinear collapse simulation techniques to link seismic

performance factors and system performance on a probabilistic basis. The FEMA P-695 Methodology uses these techniques in a probabilistic procedure that directly accounts for potential variations in structural configuration, ground motion, and available experimental data on the behavioral characteristics of structural components and systems.

Currently there are more than 75 individual systems contained in the 2003 Edition of the *National Earthquake Hazards Reduction Program (NEHRP) Recommended Provisions for Seismic Regulations for New Buildings and Other Structures, Part 1: Provisions* (FEMA, 2004a). Development of the FEMA P-695 Methodology included testing on selected seismic force-resisting systems. To date, this has included investigation of special reinforced concrete moment frames, ordinary reinforced concrete moment frames, and light-framed walls with wood structural panel sheathing.

Although these investigations served to test, refine, and illustrate the application of the Methodology, additional testing was necessary to further verify the accuracy and reliability of the procedures. The primary objective of this work was to test the FEMA P-695 Methodology on additional seismic force-resisting systems, evaluate the results for the system of interest, and develop recommendations for improving the Methodology, if needed. A secondary objective was to identify possible improvements to the specification and use of seismic performance factors in model codes and standards, and to recommend areas for further study. It is anticipated that, once validated, the FEMA P-695 Methodology will be used by model codes and standards organizations to set minimum acceptable design criteria for code-approved systems, and to provide guidance in the selection of appropriate design criteria for alternative systems when linear design methods are applied.

1.2 Scope of the Beta Testing Effort

The beta testing effort was structured to cover a broad range of building types, response characteristics, and seismic detailing requirements. The availability of reliable test data on component and system performance, as well as the ability to simulate significant failure modes and component degrading behavior in analytical models, were also considered in system selection. The following seismic force-resisting systems were investigated:

- Special reinforced masonry shear wall (special RMSW) systems
- Ordinary reinforced masonry shear wall (ordinary RMSW) systems
- Special reinforced concrete shear wall (special RCSW) systems
- Ordinary reinforced concrete shear wall (ordinary RCSW) systems
- Special steel concentrically braced frame (special SCBF) systems

- Buckling-restrained braced frame (BRBF) systems
- Special steel moment frame (special SMF) systems

Beta testing was overseen by members of the original ATC-63 Project Team, but was conducted by working groups consisting of individuals who were not directly involved in the development of the Methodology. Systems were divided across four teams as follows: (1) reinforced masonry shear walls; (2) reinforced concrete shear walls; (3) steel concentrically braced frames and buckling-restrained braced frames; and (4) steel moment frames. Each team was headed by a researcher with active research on the material and system of interest, and was advised by a practicing structural engineer with design expertise on the material and system of interest.

Teams were given the autonomy to develop system archetypes, prepare trial designs, and conduct nonlinear analyses using software of their choosing. Although teams performed their work independently, they did not operate in isolation. At key developmental stages, work was coordinated with regard to the scope of the archetype design space, analytical assumptions, design decisions, criteria for non-simulated collapse modes, and overall compliance with the requirements of the Methodology. Tables 1-1 through 1-4 summarize key information for each of the systems selected for beta testing.

Table 1-1 Summary of Design Coefficients and Factors from Table 12.2-1 of ASCE/SEI 7-05 for Each System

Seismic Force-Resisting System			Primary Analysis Procedure	ASCE/SEI 7-05, Table 12.2-1					
No.	Type	Detailing		No.	R	Ω_0	C_d	SDC	Limit (ft)
1	RMSW	Special	ELF	A.7	5	2.5	5	D	160
2	RMSW	Ordinary	ELF	A.9	2	2.5	1.75	C	160
3	RCSW	Special	ELF	B.5	6	2.5	5	D	240
4	RCSW	Ordinary	ELF	B.6	5	2.5	4.5	C	NL
5	SCBF	Special	ELF	B.3	6	2	5	D	240
6	BRBF	n/a	ELF	B.26	8	2.5	5	D	240
7a	SMF	Special	ELF	C.1	8	3	5.5	D	NL
7b	SMF	Special	RSA	C.1	8	3	5.5	D	NL

Table 1-1 provides a summary of the coefficients and factors taken from Table 12.2-1 of ASCE/SEI 7-05, *Minimum Design Loads for Buildings and Other Structures* (ASCE 2006a). Archetype designs for each system were developed using the R factors shown in this table. In a departure from current seismic design practice, the FEMA P-695 Methodology specifies the use of $C_d = R$. To test the effects of this requirement, archetype designs were developed using code-specified drift limits and

values of $C_d = R$. The C_d values from ASCE/SEI 7-05 are provided for reference but were not used.

Table 1-2 summarizes design criteria used to prepare index archetype configurations for each system, including analysis procedures, seismic design levels, and gravity load levels. In most cases, the Equivalent Lateral Force (ELF) procedure of Section 12.8 of ASCE/SEI 7-05 was used as the basis for design. In certain cases the Response Spectrum Analysis (RSA) procedure of Section 12.9 of ASCE/SEI 7-05 was used, particularly when RSA methods are commonly used in design practice. Special SMF archetypes were purposely designed using both the ELF and RSA procedures to investigate differences in performance due to the choice of analytical method. Selected taller archetypes for other systems were also designed using the RSA procedure.

Table 1-2 Summary of Design Criteria Used to Prepare Index Archetype Configurations for Each System

Seismic Force-Resisting System			Primary Analysis Procedure	Seismic Design		Gravity Design	
No.	Type	Detailing		Max.	Min.	High	Low
1	RMSW	Special	ELF	D_{max}	D_{min}	✓	✓
2	RMSW	Ordinary	ELF	C_{max}	C_{min}	✓	✓
3	RCSW	Special	ELF	D_{max}	D_{min}	✓	✓
4	RCSW	Ordinary	ELF	C_{max}	C_{min}	✓	✓
5	SCBF	Special	ELF	D_{max}	D_{min}	Typical	
6	BRBF	n/a	ELF/RSA	D_{max}	D_{min}	Typical	
7a	SMF	Special	ELF	D_{max}	D_{min}	Typical	
7b	SMF	Special	RSA	D_{max}	D_{min}	Typical	

Archetypes were designed for maximum and minimum spectral acceleration intensities (e.g., D_{max}, D_{min}, C_{max}, and C_{min}) associated with the governing Seismic Design Category (SDC). Although FEMA P-695 requires checking of other SDCs to fully evaluate system performance, studies have shown that the SDC with the highest permitted level of seismicity governs the evaluation of the *R* factor, and beta testing was limited to archetypes within the governing SDC.

To evaluate the influence of gravity load on performance, archetypes for masonry and concrete wall systems were designed for both high and low levels of gravity load intensity. For steel braced frame and steel moment frame systems, in which the effects of gravity loads were judged to be insignificant, a single (typical) level of gravity load was used to design system archetypes.

Table 1-3 lists the index archetype heights (in number of stories) that were evaluated for each system. Heights were selected to represent both short-period ($T < T_s$) and

long-period ($T > T_s$) systems, as defined in FEMA P-695. In certain cases, the number of stories was considered above (or below) the practical limit for the system of interest. For example, shear wall configurations greater than 12 stories and braced frame configurations less than 2 stories were not designed.

Table 1-3 Summary of Index Archetype Heights (Number of Stories) for Each System

Seismic Force-Resisting System			Primary Analysis Procedure	Index Archetype Heights (Number of Stories)					
No.	Type	Detailing							
1	RMSW	Special	ELF	1	2	4	8	12	n/a
2	RMSW	Ordinary	ELF	1	2	4	8	12	n/a
3	RCSW	Special	ELF	1	2	4	8	12	n/a
4	RCSW	Ordinary	ELF	1	2	4	8	12	n/a
5	SCBF	Special	ELF	n/a	2	3	6	12	16
6	BRBF	n/a	ELF/RSA	n/a	2	3	6	12	16
7a	SMF	Special	ELF	1	2	4	n/a	n/a	20
7b	SMF	Special	RSA	1	2	4	8	12	20

Performance groups are used to evaluate the average performance of archetypes with common design features and behavioral characteristics. Key features that were considered include building height (e.g., short-period or long-period systems), level of gravity loading (e.g., high, low, or typical gravity loads), and level of seismic loading (e.g., maximum or minimum spectral acceleration intensities for the governing SDC). To fully evaluate a system of interest, a sufficient number of performance groups must be populated with a sufficient number of archetypes to encompass the permissible design space over the range of applicability of the system.

A total of 120 archetypes were developed for the seven systems selected for beta testing. Table 1-4 summarizes the performance groups and number of archetypes used to evaluate each system. Each cell in the table corresponds to one performance group, and the number shown in the cell is the number of archetypes in that performance group.

Because of practical limitations in available resources, the scope of the beta testing effort was necessarily limited. The primary objective of this work was to test the FEMA P-695 Methodology on as many seismic force-resisting systems as possible, so it was considered more beneficial to evaluate a larger number of systems with a carefully selected, but limited, number of archetypes per system, rather than to evaluate fewer systems with a larger number of archetypes per system.

Table 1-4 Summary of Performance Groups and Total Number of Archetypes Used to Evaluate Each System

Seismic Force-Resisting System			No. of Archetypes by Performance Group					Total
			Gravity Loads	Short-Period		Long-Period		
No.	Type	Detailing		Seismic Loads (Maximum or Minimum of SDC)				
				Max.	Min.	Max.	Min.	
1	RMSW	Special	High	3	2	2	3	20
			Low	3	2	2	3	
2	RMSW	Ordinary	High	2	3	2	3	20
			Low	2	3	2	3	
3	RCSW	Special	High	3	2	2	3	20
			Low	3	2	2	3	
4	RCSW	Ordinary	High	2	3	2	3	20
			Low	2	3	2	3	
5	SCBF	Special	Typical	2	3	2	3	10
6	BRBF	n/a	Typical	2	3	2	3	10
7a	SMF	Special	Typical	2	1	2	3	8
7b	SMF	Special	Typical	2	1	4	5	12

Full implementation of the FEMA P-695 Methodology, however, would require at least three archetypes to evaluate the statistics within each performance group. Also, additional performance groups for each system would likely be required to fully evaluate the design space permitted by current code requirements. For example, shear walls could be constructed with varying thicknesses in pierced, flanged, or T-shaped configurations, and steel braced frames could be constructed with tube, wide-flange, or double channel braces arranged in single-diagonal, "X," or multistory configurations.

To test the feasibility of full implementation of the Methodology, the buckling-restrained braced frame (BRBF) system was selected for further study. In this study, the process for developing a full set of archetypes for evaluation of the complete design space was tested. Although nonlinear analyses and performance evaluations were not performed as part of this work, this expanded trial application demonstrated how systematic identification of controlling characteristics can be used to limit the number of archetypes needed for full implementation of the Methodology.

1.3 Report Organization and Content

This report summarizes modeling methods, assumptions, and results for the beta testing effort. It is organized to present findings and conclusions for each individual system of interest and to allow comparison of results across different systems.

Chapter 1 provides background information and describes the scope of the beta testing effort.

Chapter 2 provides a brief overview of the FEMA P-695 Methodology for context, introducing the basic theory and concepts as they relate to the beta testing effort.

Chapters 3 through 6 describe the application of the FEMA P-695 Methodology to reinforced masonry shear wall systems, reinforced concrete shear wall systems, steel braced frame systems, and steel moment frame systems, respectively. Each chapter follows a common organizational format that includes identification of structural system information, development of index archetype configurations, conduct of nonlinear analyses, and system performance evaluation. Results for each system are summarized in tables in a consistent manner. Each chapter concludes with a summary of observations on the FEMA P-695 Methodology, observations on system performance, and recommendations for possible future experimental and analytical research.

Chapter 7 illustrates the development of a complete set of archetypes that would be necessary to cover the code-permitted design space for performance evaluation of buckling-restrained braced frame systems.

Chapter 8 summarizes general findings and conclusions across all systems, recommendations for possible improvement or refinement of the FEMA P-695 Methodology, and recommendations for further study on the specification and use of seismic performance factors in model codes and standards.

Appendices A through E provide additional information on the development of index archetype configurations, the resulting archetype designs, and analytical model development for each system of interest.

Chapter 2

Overview of the FEMA P-695 Methodology

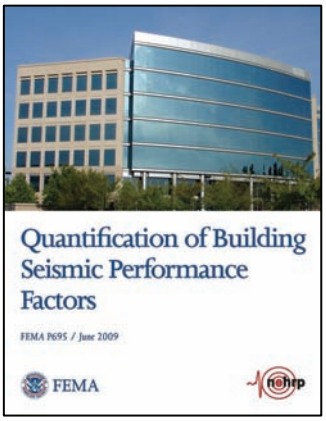

This chapter provides a brief summary of the scope and basis of the methodology contained in FEMA P-695 *Quantification of Building Seismic Performance Factors* (FEMA 2009). It defines terminology and key concepts used in the trial applications described herein. Readers are referred to the FEMA P-695 report for complete information on the specific requirements of the Methodology, and guidance on its implementation and use.

The purpose of the FEMA P-695 Methodology is to provide a rational basis for determining global seismic performance factors, including the response modification coefficient (R factor), the system overstrength factor (Ω_0), and deflection amplification factor (C_d) that, when properly implemented in the seismic design process, will result in "equivalent safety against collapse in an earthquake, comparable to the inherent safety against collapse intended by current seismic codes, for buildings with different seismic-force-resisting systems," (FEMA 2009).

The Methodology is intended for use with model building codes and standards to set minimum acceptable design criteria for code-approved seismic-force-resisting systems when linear design methods are applied. It also provides a basis for evaluation of current code-approved systems and their ability to meet the seismic performance intent of the code.

2.1 Selected Terminology

The following selected terminology is key to the FEMA P-695 Methodology and is used in descriptions of the beta testing effort:

- **Archetype:** A prototypical representation of a seismic-force-resisting system.
- **Archetype Design Space:** The overall range of permissible configurations, structural design parameters, and other features that define the application limits for a seismic-force-resisting system.
- **Collapse Level Earthquake Ground Motions:** The level of earthquake ground motions that cause collapse of the seismic force-resisting system of interest.
- **Collapse Margin Ratio:** The primary parameter used to characterize the collapse safety of a system, taken as the ratio between the median collapse intensity and the Maximum Considered Earthquake (MCE) ground motion intensity.

- **Design Requirements-Related Uncertainty:** Collapse uncertainty associated with the quality of the design requirements of the system of interest.
- **Index Archetype Configuration:** A prototypical representation of a seismic-force-resisting system configuration that embodies key features and behaviors related to collapse performance when subjected to earthquake ground motions.
- **Index Archetype Design:** An index archetype configuration that has been proportioned and detailed using the design requirements of the system of interest.
- **Index Archetype Model:** An idealized mathematical representation of an index archetype design used to simulate collapse using nonlinear static and dynamic analyses.
- **Maximum Considered Earthquake (MCE) Ground Motions:** The most severe earthquake effects considered, as defined by Section 11.4 of ASCE/SEI 7-05.
- **Modeling Uncertainty:** Collapse uncertainty associated with the quality of the index archetype models.
- **Non-Simulated Collapse:** Structural collapse caused by collapse modes that are not represented in the analytical model. Non-simulated collapse occurs when a component limit state is exceeded, as defined by component fragility functions.
- **Performance Group:** A subset of the archetype design space containing a group of index archetype configurations that share a set of common features or behavioral characteristics, binned for statistical evaluation of collapse performance.
- **Record-to-Record Uncertainty:** Collapse uncertainty due to variability in response to different ground motions.
- **Simulated Collapse:** Structural collapse caused by collapse modes that are directly represented in the analytical model.
- **Test Data-Related Uncertainty:** Collapse uncertainty associated with the quality of the test data for the system of interest.

2.2 Elements of the Methodology

Key elements of the FEMA P-695 Methodology are illustrated in Figure 2-1. The Methodology involves the development of detailed design information and test data for the system of interest. It utilizes nonlinear analysis techniques and explicitly considers uncertainties in ground motion, modeling, design, and test data in the probabilistic assessment of collapse risk.

Implementation of the Methodology involves uncertainty, judgment, and potential for variation. In its envisioned application, decisions regarding an appropriate level of detail for adequately characterizing the performance of a proposed system are made in collaboration with an independent peer review panel.

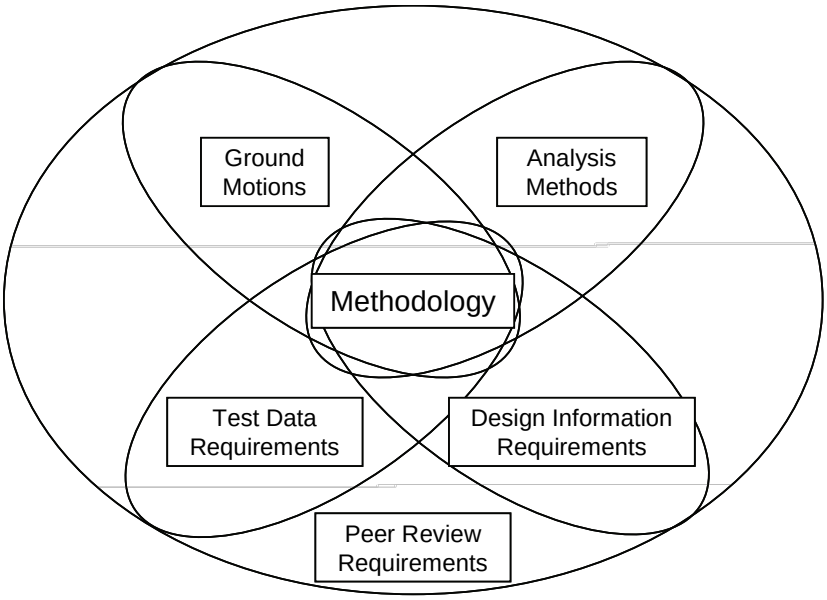

Figure 2-1 Key elements of the FEMA P-695 Methodology (FEMA 2009).

2.3 Scope and Basis of the Methodology

The following principles outline the scope and basis of the FEMA P-695 Methodology:

- **Applicable to New Building Structural Systems.** The Methodology applies to the determination of seismic performance factors appropriate for the design of seismic-force-resisting systems in new building structures. Nonstructural systems, non-building structures, and retrofit of existing seismic-force-resisting systems are not explicitly considered.
- **Compatible with the NEHRP Recommended Provisions and ASCE/SEI 7-05.** The Methodology is intended for use with applicable design criteria and requirements of the *NEHRP Recommended Provisions for Seismic Regulations for New Buildings and Other Structures, Part 1: Provisions* (FEMA, 2004a), and the seismic provisions of ASCE/SEI 7-05, *Minimum Design Loads for Buildings and Other Structures* (ASCE 2006).
- **Consistent with the Life Safety Performance Objective.** The Methodology is consistent with the primary "life safety" performance objective of seismic regulations in model building codes, identified as "minimum criteria considered prudent for protection of life safety in structures subject to earthquakes" (FEMA 2004b).
- **Based on Acceptably Low Probability of Structural Collapse.** The Methodology achieves the primary life safety performance objective by requiring an acceptably low probability of collapse of the seismic-force-resisting system when subjected to MCE ground motions.

- **Earthquake Hazard based on MCE Ground Motions.** The Methodology evaluates collapse under MCE ground motions for various geographic regions of seismicity, as defined by the coefficients and mapped acceleration parameters of the general procedure of ASCE/SEI 7-05, based on the maps and procedures contained in the *NEHRP Recommended Provisions.*
- **Concepts Consistent with Current Seismic Performance Factor Definitions.** The Methodology is consistent with the definitions of seismic performance factors given in ASCE/SEI 7-05, and the underlying nonlinear static analysis (pushover) concepts described in the Commentary to the *NEHRP Recommended Provisions*. The *R* factor is keyed to the ratio between the MCE ground motion intensity and the design strength of a system, but there are differences related to the system overstrength factor (Ω_0), and deflection amplification factor (C_d), which is taken as equal to the *R* factor.

2.4 Outline of the Process

The steps comprising the FEMA P-695 Methodology are shown in Figure 2-2. They outline a process for developing system design information with enough detail and specificity to identify the permissible range of application for the proposed system, adequately simulate nonlinear response, and reliably assess the collapse risk over the proposed range of applications. The process includes the following steps:

- **Obtain Required Information.** Obtain required system information in the form of detailed design requirements and system and component test data.
- **Characterize Behavior.** Characterize system behavior through consideration of configuration issues and behavioral effects, development of index archetype configurations, definition of an archetype design space, and identification of performance groups.
- **Develop Models.** Develop nonlinear models by applying design requirements and using test data to prepare index archetype designs, develop mathematical models for explicit simulation of collapse modes, calibrate models, and establish criteria for non-simulated collapse modes.
- **Analyze Models.** Perform nonlinear static (pushover) and nonlinear dynamic (response history) analyses using a set of predefined (Far-Field) ground motion records.
- **Evaluate Performance.** Evaluate system collapse performance by assessing total uncertainty (based on the quality of test data, design requirements, and analytical models), determining the collapse margin ratio, and comparing an adjusted collapse margin ratio to acceptable values based on an acceptably low probability of collapse.
- **Document Results.** Identify sources of required system information, and document information on system behavior, development of index archetype

designs, nonlinear model development, analytical results, quality ratings, and system performance evaluation criteria.

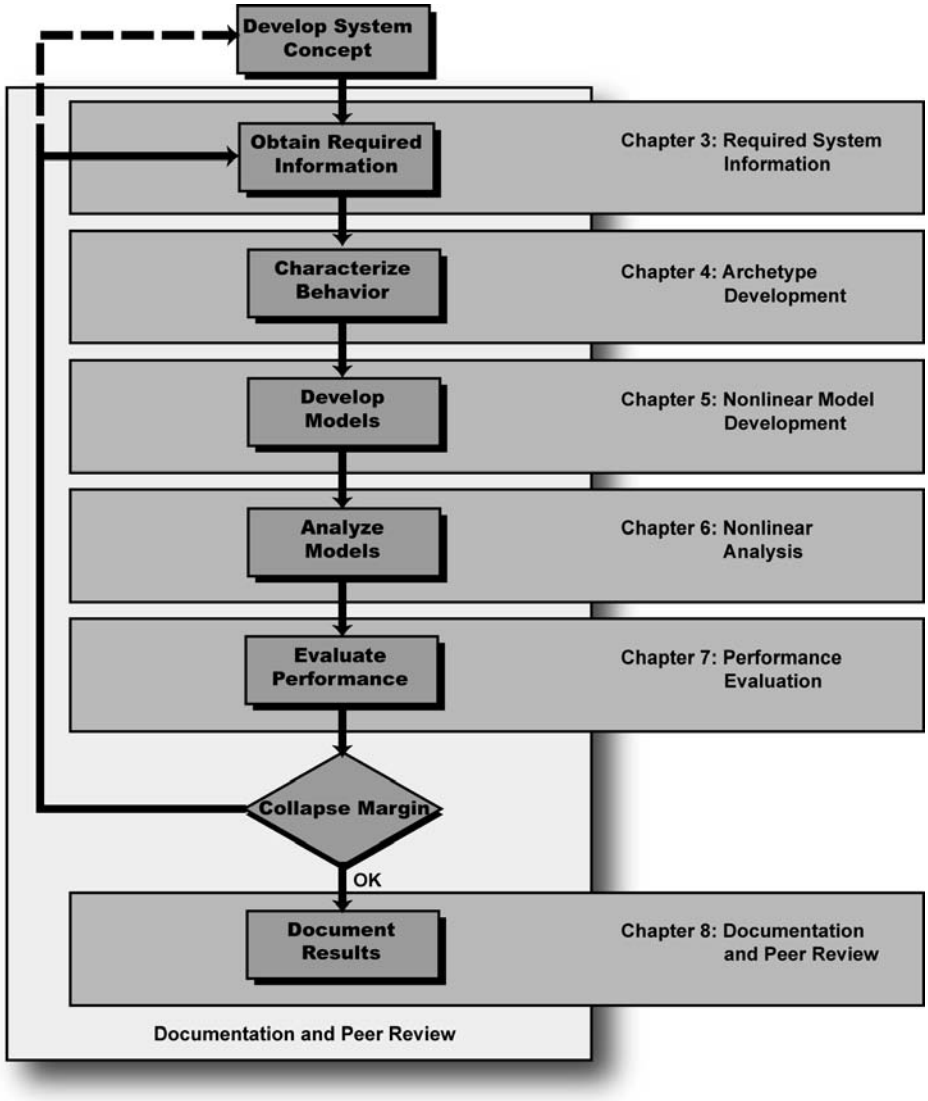

Figure 2-2 Outline of process for quantitatively establishing and documenting seismic performance factors (FEMA 2009).

2.5 Implementation of the Performance Evaluation

The performance of a structural system is deemed acceptable if the probability of collapse due to MCE ground motions is limited to an acceptably low value. Within each performance group, systems are required to meet a 10% collapse probability limit, on average, across all archetypes in the performance group. Recognizing that some individual archetypes could have collapse probabilities that exceed this value, a limit of twice that value, or 20%, is used as the criterion for evaluating the acceptability of potential "outliers" within a performance group. In the trial applications that follow, collapse performance evaluation is performed for each system as follows:

Probability of collapse is measured through the use of collapse margin ratios. A collapse margin ratio (*CMR*) is the ratio of the median collapse intensity, $\hat{S}_{CT}$, obtained from nonlinear dynamic analysis to the MCE ground motion spectral demand, S_{MT}.

$$CMR = \frac{\hat{S}_{CT}}{S_{MT}} \tag{2-1}$$

Adjusted collapse margin ratios (*ACMR*s) are obtained by multiplying the *CMR*s, computed from nonlinear dynamic analysis results, by a spectral shape factor, *SSF*.

$$ACMR_i = SSF_i \times CMR_i \tag{2-2}$$

The *SSF* for each archetype is determined using Table 7-1 of FEMA P-695, based on the code-based fundamental period, *T*, and period-based ductility, μ_T. Period-based ductility is obtained by dividing the ultimate roof drift by the effective yield drift obtained from static pushover analysis:

$$\mu_T = \frac{\delta_u}{\delta_{y,eff}} \tag{2-3}$$

The acceptable average value of *ACMR* for each performance group is denoted by $ACMR_{10\%}$. The acceptable value of *ACMR* for individual archetypes within a performance group is denoted by $ACMR_{20\%}$. Values of $ACMR_{10\%}$ and $ACMR_{20\%}$ are specified in Table 7-3 of FEMA P-695, based on total system collapse uncertainty, β_{TOT}. Collapse uncertainty is a function of the quality ratings associated with the design requirements, test data, and nonlinear models, as well as record-to-record uncertainty. Values of β_{TOT} are determined from Table 7-2 of FEMA P-695 or from the following equation:

$$\beta_{TOT} = \sqrt{\beta_{RTR}^2 + \beta_{DR}^2 + \beta_{TD}^2 + \beta_{MDL}^2} \tag{2-4}$$

Calculated values of *ACMR* are compared on average across a performance group and individually for each archetype:

$$\overline{ACMR_i} \geq ACMR10\% \tag{2-5}$$

$$ACMR_i \geq ACMR20\% \tag{2-6}$$

The overstrength factor, Ω, for each archetype is calculated as the ratio between the maximum shear force obtained from pushover analysis, V_{max}, and the design shear force, *V*:

$$\Omega = \frac{V_{\max}}{V} \tag{2-7}$$

Chapter 3
Trial Application: Reinforced Masonry Shear Wall Structures

3.1 Introduction

This chapter presents a trial application of the FEMA P-695 Methodology on special reinforced masonry shear wall (special RMSW) and ordinary reinforced masonry shear wall (ordinary RMSW) structures. It summarizes design requirements and available test data for reinforced masonry shear walls, explains the development of masonry shear wall archetype configurations, documents the nonlinear modeling approach, presents the results of a performance evaluation, and summarizes observations on the Methodology specific to reinforced masonry shear wall systems.

3.2 Overview and Approach

In this trial application, special and ordinary reinforced masonry shear wall systems, as defined in ACI 530-08/ASCE 5-08/TMS 402-08, Masonry Standards Joint Committee (MSJC), *Building Code Requirements for Masonry Structures* (ACI, 2008b), were considered as if they were new systems proposed for inclusion in ASCE/SEI 7-05, *Minimum Design Loads for Buildings and Other Structures* (ASCE, 2006). Although the intent was to treat special and ordinary masonry shear wall systems as if they were new systems, the purpose was not to re-derive or validate seismic performance factors (R, Ω_0, and C_d) for these systems. Rather, it was to examine whether masonry shear wall systems would satisfy the acceptance criteria of the FEMA P-695 Methodology, test the application of the Methodology with respect to these systems, and identify possible improvements to the Methodology or current masonry shear wall design provisions.

The system design requirements of ASCE/SEI 7-05, including minimum base shear and story drift limits, were used as the basis for design, with the exception that C_d was taken equal to R, as specified in the FEMA P-695 Methodology. Values of R for load-bearing special RMSW and ordinary RMSW systems are 5 and 2, respectively.

Reinforced masonry shear wall systems can have many different configurations, including perforated walls with regular or irregularly shaped openings, cantilever walls with strong or weak coupling beams, and walls with rectangular or flanged cross sections. For practical reasons, the scope of the beta testing effort on reinforced masonry shear walls was necessarily limited. A single wall configuration, cantilever with rectangular cross section, was used to investigate results for a range of building

heights and design parameters. The selection of this configuration, and the development of corresponding index archetype designs for masonry shear wall buildings, is described below.

Cantilever walls with weak coupling and rectangular cross sections can be found in both low-rise and midrise masonry shear wall buildings. Compared to other wall types, they are easier to design and detail to achieve a desired seismic performance. Furthermore, rectangular cantilever wall systems can be analyzed with a higher level of confidence than other configurations using currently available nonlinear modeling capabilities.

Focus on a single wall configuration allows a broad range of design variables to be examined with a reasonable number of building archetypes. Design variables that were considered include the number of stories, wall aspect ratio, level of gravity load, Seismic Design Category (SDC), and full or partial grouting.

In this study, special RMSWs are fully grouted, while ordinary RMSWs are partially grouted (grouted only in cells containing longitudinal reinforcement). This is not a code requirement, but reflects current design practice for special and ordinary walls. Strictly speaking, partially grouted special walls and fully grouted ordinary walls should also be considered in the design space, as they are permitted by the code.

Special RMSWs are most prevalent in the western United States, where these walls are normally fully grouted. Partially grouted ordinary RMSWs are used in other regions of the country where the seismic risk is perceived to be less severe. Since partially grouted walls are not expected to perform as well as fully grouted walls, consideration of partially grouted special walls would bias the results for special RMSWs in a way that is contrary to common design practice. Results of this study should be interpreted with this condition in mind.

In the design of taller (e.g., 12-story) special RMSW configurations, use of the Equivalent Lateral Force (ELF) procedure was found to result in a design that was governed by story drift. In this case, use of $C_d = R$ resulted in a more conservative design than would have been obtained using the value of C_d given in ASCE/SEI 7-05. If the Response Spectrum Analysis (RSA) procedure was used, calculated story drifts were smaller, and did not govern the design. For shorter wall configurations and ordinary RMSWs, drift did not control, regardless of the analysis procedure used. To avoid biasing the results with drift-controlled (conservative) designs, 12-story special RMSW archetypes were designed using the RSA procedure. Other archetypes were designed using the ELF procedure.

3.3 Structural System Information

3.3.1 Design Requirements

Reinforced masonry shear walls were designed and detailed in accordance with the strength design requirements of the ACI 530-08/ASCE 5-08/TMS 402-08, MSJC code. According to the MSJC code, special RMSWs are required for SDC D, while ordinary RMSWs can be used for SDC C. Special RMSWs are very often fully grouted, while ordinary RMSWs are partially grouted. In this study, fully grouted special RMSWs were used for SDC D archetypes, and partially grouted ordinary RMSWs were used for SDC C archetypes.

With the strength design provisions of the MSJC code, it is possible that a wall could develop very high compressive strains and exhibit severe toe-crushing behavior when subjected to combined vertical and lateral loads, even when special boundary elements are not required. On the other hand, alternative conditions specified to assure adequate flexural ductility can be too stringent, leading to uneconomical design solutions. Consistent with typical engineering practice, wall designs satisfying strength design requirements were checked against the allowable stress design requirements and modified, if necessary, so that the maximum compressive stress limit of $f'_m / 3$ was not violated (where f'_m is the specified masonry compressive strength). This allowable stress requirement was found to govern the design of some of the taller, partially grouted archetypes.

3.3.2 Quality Rating of Design Requirements

The design requirements for special RMSWs are considered well developed and reasonably substantiated by experimental data. They are based on a capacity design approach and have reasonable safeguards against unanticipated failure modes. A quality rating of (B) Good was assigned to the design requirements for special RMSWs.

The design requirements for ordinary RMSWs are not well substantiated by experimental data. Ordinary walls are partially grouted, and as a result, their behavior is not as consistent as that of special RMSWs. A quality rating of (C) Fair was assigned to the design requirements for ordinary RMSWs.

3.3.3 Test Data

To develop and calibrate analytical models for the evaluation of the seismic performance of the archetype wall systems, past experimental studies were reviewed, and suitable data were selected for model validation. Tests on fully grouted walls have been conducted by Shing et al. (1991), Voon and Ingham (2006), Shedid et al. (2008), Merryman et al. (1990), and Kingsley et al. (1994).

Shing et al. (1991) tested 24 one-story walls with a height-to-length ratio of one and axial compressive load ratios, $P / (f'_m A_n)$, not greater than 0.10, where A_n is the net

cross-sectional area. Seven of the walls had flexure-dominated behavior, most of which satisfied the requirements for special walls, while the rest had flexure-shear or shear-dominated behavior. Voon and Ingham (2006) tested eight fully grouted and two partially grouted reinforced concrete masonry cantilever shear walls under cyclic loading. Different height-to-length ratios (0.6, 1.0, and 2.0), reinforcement ratios, and axial loads were considered. Most specimens exhibited shear-dominated behavior. Shedid et al. (2008) tested six small-scale walls with a height-to-length ratio of 2.0. Merryman et al. (1990) tested two 2-story coupled wall systems with the coupling forces introduced by floor and roof slabs. Kingsley et al. (1994) tested a 5-story masonry wall system with coupled flanged walls.

3.3.4 Quality Rating of Test Data

There is a reasonable amount of data from tests on fully grouted walls that are well documented and considered to be reliable. However, they do not cover the broad range of reinforcement ratios, wall aspect ratios, and axial load levels that are encountered in the archetype design space. Furthermore, there are not enough data to determine the statistical variability of the test results. Data on multistory wall systems are scarce, and there are only limited data available to determine the influence of the wall aspect ratio and loading condition on the effective plastic-hinge length of a flexure-dominated wall. Given the reasonable availability of data along with the limitations noted above, test data for special RMSWs were assigned a quality rating of (B) Good.

Test data on partially grouted walls are extremely limited, especially with respect to flexure-dominated behavior. Most of the walls tested by Ingham et al. (2001) had shear-dominated behavior. Ghanem et al. (1992) tested three small-scale partially grouted walls, which exhibited shear, flexure-shear, and flexure-dominated behaviors as the distribution of the vertical and horizontal reinforcement was varied. In general, the observed behavior of partially grouted walls in available test data is not as consistent as that of fully grouted walls. Given these limitations, test data for ordinary RMSWs were assigned a quality rating of (C) Fair.

3.4 Archetype Configurations

The design space for reinforced masonry shear wall systems includes many different configurations. They can be perforated wall systems, with regular or irregular openings, which are common in low-rise buildings. In midrise and taller buildings, cantilever wall systems are often used. Cantilever walls can be strongly or weakly coupled and can include flanged or rectangular cross sections.

The design of perforated wall systems is not addressed well in current code provisions. These walls may not possess the desired ductility even if they are detailed in accordance with the requirements for special RMSWs. In contrast, cantilever wall systems are easier to design and detail to attain a desired seismic

performance. They can also be analyzed with a higher level of confidence using currently available nonlinear modeling capabilities. For these reasons, archetypes considered in this trial application were limited to cantilever wall systems with rectangular cross sections.

Focus on rectangular shear wall configurations allowed consideration of the following additional design variables: special versus ordinary detailing, fully grouted versus partially grouted construction, level of seismic design loading (SDC), level of gravity load, number of stories, period, and wall aspect ratio. Two plan configurations were selected as representative of realistic reinforced masonry shear wall arrangements in buildings encompassing these design variables. To produce lower-bound designs without excessive overstrength, the number of walls and plan dimensions of these typical configurations were varied in each archetype to optimize strength relative to the level of seismic design loading.

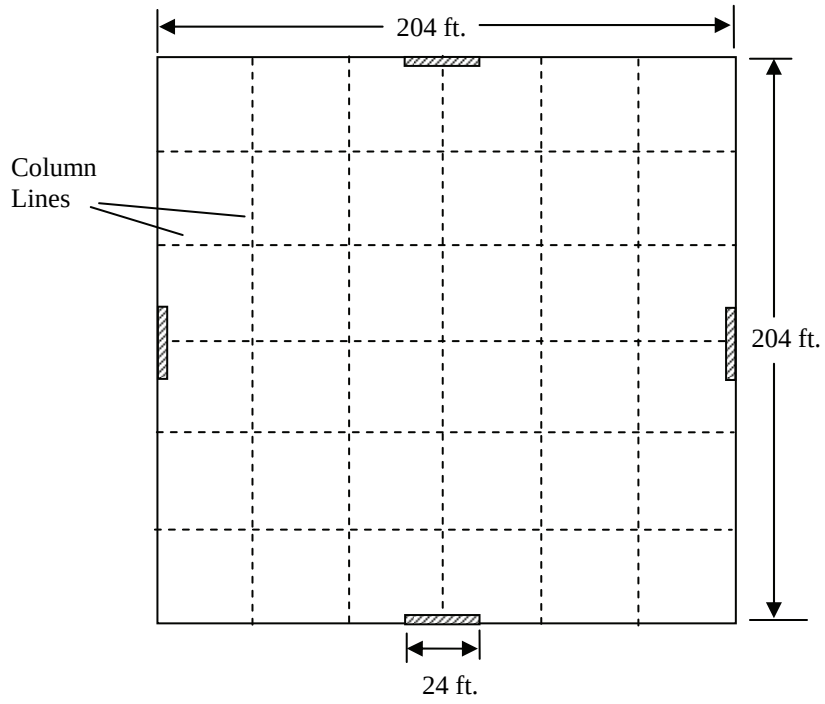

Figure 3-1 Plan view of typical single-story reinforced masonry shear wall building configuration (design for SDC D_{max} shown).

Single-story archetype configurations (Figure 3-1) were selected to be representative of masonry buildings used in retail-type occupancies. They are one-story structures with a roof height of 12 feet and shear walls located on the building perimeter. As idealized in this study, the archetypes included large storefront windows and minimal (24 feet long) reinforced masonry walls as the exterior enclosure. All walls had a fixed aspect ratio of 0.5 to 1. The number of walls and the total length of shear wall in each archetype were kept to the minimum required for strength, based on the plan dimensions and Seismic Design Category. Gravity loads were distributed to interior columns and exterior wall lines based on tributary roof area. Since all walls carry the

same level of gravity load, the same one-story wall archetype design is used for both the low and high gravity load conditions for each Seismic Design Category.

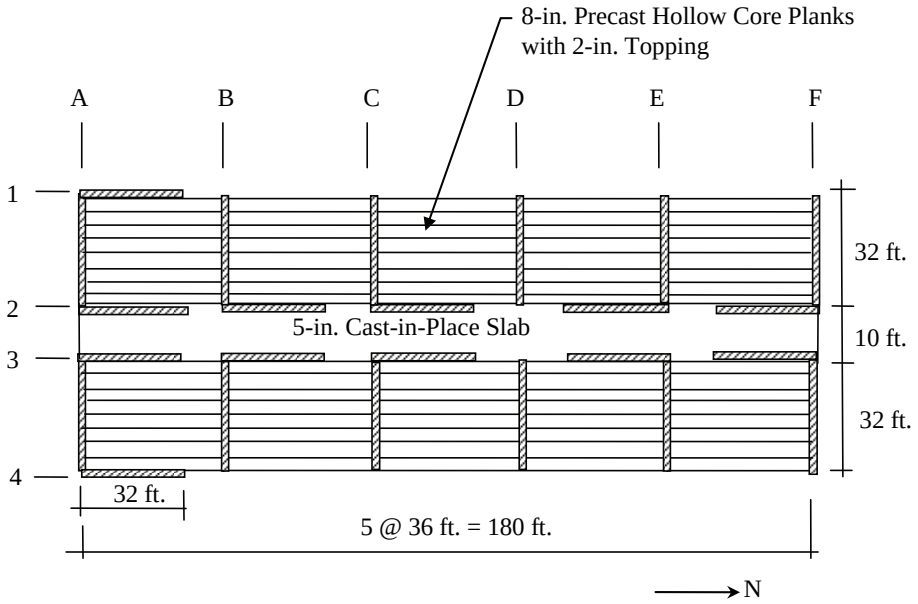

Figure 3-2 Plan view of typical multistory reinforced masonry shear wall building configuration (design for 12-story SDC D_{max} shown).

Multistory archetype configurations (Figure 3-2) were selected to be representative of masonry buildings used in hotels, condominiums, and college dormitory residential-type occupancies. Story heights are 10 feet in all cases, and building heights of 2, 4, 8, and 12 stories were considered. All shear walls are 32 feet long, so wall aspect ratios varied with the number of stories (Figure 3-3). Shear walls in the transverse and longitudinal directions are not structurally connected, so walls were assumed to act as independent rectangular sections in each direction. The number of walls provided in each direction for each archetype was reduced to the minimum required for strength, based on Seismic Design Category and number of stories.

For the purpose of estimating design gravity loads, the floor and roof systems were assumed to consist of cast-in-place concrete slabs in the corridors and precast hollow core planks with a cast-in-place concrete topping slab elsewhere. Although the absolute magnitude of axial load on a wall depends on the height of the building, relatively higher gravity load conditions occurred on transverse walls and relatively lower gravity load conditions occurred on longitudinal walls as a result of the orientation of the floor framing. Although Merryman et al. (1990) and Kingsley et al. (1994) have shown that axial compression loads introduced into a wall by the coupling action of the slabs can significantly increase lateral resistance, coupling moments and forces induced by the floor and roof slabs were neglected in the design and analysis of the archetypes.

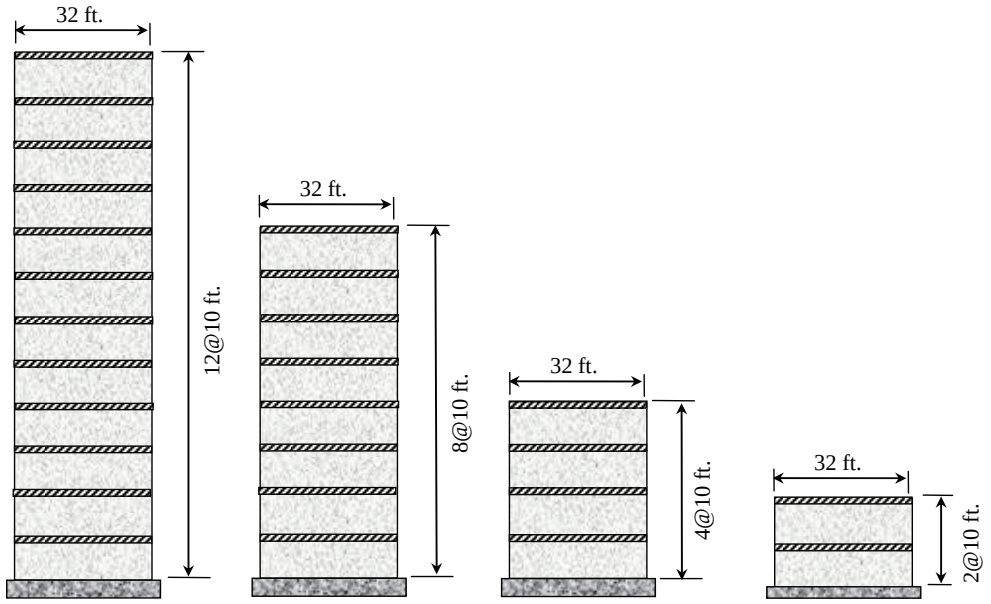

Figure 3-3 Dimensions of multistory reinforced masonry shear walls.

Walls were assumed to be constructed of hollow concrete masonry units with nominal widths ranging from 8 inches to 16 inches. In multistory walls, reinforcement quantities and nominal masonry design strength, f'_m, were changed every other story, as needed, for economies in design. Wall thicknesses, however, remained constant over the height of a building.

Both special and ordinary RMSW archetypes were considered. Fully grouted special RMSW archetypes were designed for the maximum and minimum seismic criteria associated with SDC D (i.e., D_{max} and D_{min}). Partially grouted ordinary RMSW archetypes were designed for the maximum and minimum seismic criteria associated with SDC C (i.e., C_{max} and C_{min}).

Archetypes were grouped into performance groups containing a set of common features or behavioral characteristics, including Seismic Design Category, gravity load level, and code-based period of the structure. Considering the design variables listed above, a total of 40 archetypes were developed. These were divided into 16 performance groups, eight attributed to special RMSWs and eight attributed to ordinary RMSWs, as shown in Tables 3-1 and 3-2. Performance groups with less than three archetypes did not meet the minimum number of archetypes per performance group required in a full application of the Methodology.

Tables 3-3 and 3-4 summarize the design variables for the 40 archetypes considered in this trial application, including the number of stories, the wall geometry, the number of walls in each direction, and the seismic weight per floor shared by each wall.

Table 3-1 Summary of Performance Groups and Total Number of Archetypes Used to Evaluate Each System

Performance Group Summary					
Group No.	Grouping Criteria				Number of Archetypes
	Basic Config.	Design Load Level		Period Domain	
		Gravity	Seismic		
PG-1S	Cantilever	High	SDC D_{max}	Short	3^1
PG-2S				Long	2^2
PG-3S			SDC D_{min}	Short	2^3
PG-4S				Long	3^4
PG-5S		Low	SDC D_{max}	Short	3^1
PG-6S				Long	2^2
PG-7S			SDC D_{min}	Short	2^3
PG-8S				Long	3^4

[1] Short-period, SDC D_{max}, performance groups, PG-1 and PG-5, include 1-story, 2-story and 4-story archetypes.

[2] Long-period, SDC D_{max}, performance groups, PG-2 and PG-6, include 8-story and 12-story archetypes.

[3] Short-period, SDC D_{min}, performance groups, PG-3 and PG-7, include 1-story and 2-story archetypes.

[4] Long-period, SDC D_{min}, performance groups, PG-4 and PG-8, include 4-story, 8-story and 12-story archetypes.

Table 3-2 Performance Groups for Evaluation of Ordinary Reinforced Masonry Shear Wall Archetypes

Performance Group Summary					
Group No.	Grouping Criteria				Number of Archetypes
	Basic Config.	Design Load Level		Period Domain	
		Gravity	Seismic		
PG-1O	Cantilever	High	SDC C_{max}	Short	2^1
PG-2O				Long	3^2
PG-3O			SDC C_{min}	Short	2^1
PG-4O				Long	3^2
PG-5O		Low	SDC C_{max}	Short	2^1
PG-6O				Long	3^2
PG-7O			SDC C_{min}	Short	2^1
PG-8O				Long	3^2

[1] Short-period performance groups, PG-1, PG-3, PG-5 and PG-7, include 1-story and 2-story archetypes.

[2] Long-period performance groups, PG-2, PG-4, PG-6 and PG-8, include 4-story, 8-story and 12-story archetypes.

Table 3-3 Special Reinforced Masonry Shear Wall Archetype Design Variables

Arch. Design ID No.	Design Parameters						
	No. of Stories	Wall Height/ Length (ft.)	Gravity Loads	SDC	No. of Walls in Each Direct.	Seismic Weight Per Wall at Roof (kips)	Seismic Weight Per Wall at Floor (kips)
Performance Group No. PG-1S and PG-5S							
S1/S11	1	12/24	High/Low	D_{max}	2	1,292	NA
S2/S12	2	20/32	High/Low	D_{max}	4	516	617
S3/S13	4	40/32	High/Low	D_{max}	8	231	286
Performance Group No. PG-2S and PG-6S							
S4/S14	8	80/32	High/Low	D_{max}	12	115	151
S5/S15	12	120/32	High/Low	D_{max}	12	126	174
Performance Group No. PG-3S and PG-7S							
S6/S16	1	12/24	High/Low	D_{min}	2	1,756	NA
S7/S17	2	20/32	High/Low	D_{min}	4	893	1,053
Performance Group No. PG-4S and PG-8S							
S8/S18	4	40/32	High/Low	D_{min}	4	642	762
S9/S19	8	80/32	High/Low	D_{min}	4	390	464
S10/S20	12	120/32	High/Low	D_{min}	4	402	493

Table 3-4 Ordinary Reinforced Masonry Shear Wall Archetype Design Variables

Arch. Design ID No.	Design Parameters						
	No. of Stories	Wall Height/ Length (ft.)	Gravity Loads	SDC	No. of Walls in Each Direct.	Seismic Weight Per Wall at Roof (kips)	Seismic Weight Per Wall at Floor (kips)
Performance Group No. PG-1O and PG-5O							
O1/O11	1	12/24	High/Low	C_{max}	4	318	NA
O2/O12	2	20/32	High/Low	C_{max}	4	381	450
Performance Group No. PG-2O and PG-6O							
O3/O13	4	40/32	High/Low	C_{max}	8	158	193
O4/O14	8	80/32	High/Low	C_{max}	12	107	135
O5/O15	12	120/32	High/Low	C_{max}	12	111	144
Performance Group No. PG-3O and PG-7O							
O6/O16	1	12/24	High/Low	C_{min}	4	873	NA
O7/O17	2	20/32	High/Low	C_{min}	4	631	740
Performance Group No. PG-4O and PG-8O							
O8/O18	4	40/32	High/Low	C_{min}	4	319	374
O9/O19	8	80/32	High/Low	C_{min}	8	192	232
O10/O20	12	120/32	High/Low	C_{min}	8	163	200

Key seismic design parameters for the special RMSW and ordinary RMSW archetypes are summarized in Tables 3-5 and 3-6. Values of the seismic base shear coefficient, V/W, and the Maximum Considered Earthquake (MCE) spectral acceleration, S_{MT}, for SDC D_{max}, D_{min}, C_{max}, and C_{min} were determined using the code-based structural period, T, and the spectral values given in Table 5-1 of FEMA P-695. The code-based period is the upper-limit approximate fundamental period calculated using the equation, $T=C_uT_a$, provided in ASCE/SEI 7-05, assuming a lower bound value of 0.25 seconds in accordance with the Methodology.

Table 3-5 Special Reinforced Masonry Shear Wall Archetype Design Properties

Archetype Design ID Number	No. of Stories	Key Archetype Design Parameters						
		Gravity Loads	Seismic Design Criteria					$S_{MT}(T)$ (g)
			SDC	R	T (sec)	T_1 (sec)	V/W (g)	
Performance Group No. PG-1S								
S1	1	High	D_{max}	5	0.25	0.10	0.200	1.50
S2	2	High	D_{max}	5	0.26	0.13	0.200	1.50
S3	4	High	D_{max}	5	0.45	0.21	0.200	1.50
Performance Group No. PG-2S								
S4	8	High	D_{max}	5	0.75	0.55	0.160	1.20
S5	12	High	D_{max}	5	1.02	0.93	0.118	0.89
Performance Group No. PG-3S								
S6	1	High	D_{min}	5	0.25	0.14	0.100	0.75
S7	2	High	D_{min}	5	0.28	0.19	0.100	0.75
Performance Group No. PG-4S								
S8	4	High	D_{min}	5	0.48	0.35	0.084	0.63
S9	8	High	D_{min}	5	0.80	1.12	0.050	0.37
S10	12	High	D_{min}	5	1.09	1.74	0.037	0.28
Performance Group No. PG-5S								
S11	1	Low	D_{max}	5	0.25	0.10	0.200	1.50
S12	2	Low	D_{max}	5	0.26	0.13	0.200	1.50
S13	4	Low	D_{max}	5	0.45	0.26	0.200	1.50
Performance Group No. PG-6S								
S14	8	Low	D_{max}	5	0.75	0.61	0.160	1.20
S15	12	Low	D_{max}	5	1.02	0.93	0.118	0.89
Performance Group No. PG-7S								
S16	1	Low	D_{min}	5	0.25	0.14	0.100	0.75
S17	2	Low	D_{min}	5	0.28	0.21	0.100	0.75
S18	4	Low	D_{min}	5	0.48	0.43	0.084	0.63
S19	8	Low	D_{min}	5	0.80	1.16	0.05	0.37
S20	12	Low	D_{min}	5	1.09	1.94	0.037	0.28

Table 3-6 Ordinary Reinforced Masonry Shear Wall Archetype Design Properties

Archetype Design ID Number	No. of Stories	Key Archetype Design Parameters						
		Gravity Loads	Seismic Design Criteria					$S_{MT}(T)$ (g)
			SDC	R	T (sec)	T_1 (sec)	V/W (g)	
Performance Group No. PG-1O								
O1	1	High	C_{max}	2	0.25	0.10	0.250	0.75
O2	2	High	C_{max}	2	0.28	0.19	0.250	0.75
Performance Group No. PG-2O								
O3	4	High	C_{max}	2	0.48	0.28	0.210	0.63
O4	8	High	C_{max}	2	0.80	0.59	0.125	0.37
O5	12	High	C_{max}	2	1.09	1.0	0.092	0.28
Performance Group No. PG-3O								
O6	1	High	C_{min}	2	0.25	0.16	0.150	0.45
O7	2	High	C_{min}	2	0.31	0.20	0.150	0.45
Performance Group No. PG-4O								
O8	4	High	C_{min}	2	0.52	0.43	0.128	0.38
O9	8	High	C_{min}	2	0.87	0.72	0.076	0.23
O10	12	High	C_{min}	2	1.18	1.19	0.056	0.17
Performance Group No. PG-5O								
O11	1	Low	C_{max}	2	0.25	0.10	0.250	0.75
O12	2	Low	C_{max}	2	0.28	0.17	0.250	0.75
Performance Group No. PG-6O								
O13	4	Low	C_{max}	2	0.48	0.28	0.210	0.63
O14	8	Low	C_{max}	2	0.80	0.59	0.125	0.37
O15	12	Low	C_{max}	2	1.09	1.04	0.092	0.28
Performance Group No. PG-7O								
O16	1	Low	C_{min}	2	0.25	0.16	0.150	0.45
O17	2	Low	C_{min}	2	0.31	0.20	0.150	0.45
Performance Group No. PG-8O								
O18	4	Low	C_{min}	2	0.52	0.42	0.128	0.38
O19	8	Low	C_{min}	2	0.87	0.82	0.076	0.23
O20	12	Low	C_{min}	2	1.18	1.24	0.056	0.17

Values of code-based period, T, and fundamental period, T_1 (calculated from eigenvalue analysis), are shown for comparison in Table 3-5 and Table 3-6. Eigenvalue periods, T_1, were calculated using linear elastic models, which considered the flexural and shear flexibility of the walls. The effective moment of inertia, I_e, was taken as 50% of the uncracked net masonry wall section, and the modulus of elasticity was estimated using the formula given in the MSJC code, based on the expected masonry compressive strength.

For the low-rise (1- and 2-story) archetypes, T_1 tends to be much smaller than T. Low values of T_1 can be attributed to the low aspect ratios of the low-rise walls. On the other hand, values of T_1 for the 12-story special walls designed for SDC D_{min} are much higher than T. This can be attributed to the large seismic mass carried by each wall in these archetypes. Variations in structural properties such as these are not accounted for in the code-based period formulation.

Because design wind load varies with geographic location, wind load was ignored in the designs so that archetypes in lower Seismic Design Categories (where wind might control) were not effectively over-designed for seismic load. Out-of-plane seismic forces were not critical in the design of the walls, given the unsupported story heights considered in this application.

Detailed information used in design, along with additional details for the resulting reinforced masonry shear wall archetypical designs, including plan configurations and wall reinforcing patterns, are provided in Appendix A.

3.5 Nonlinear Model Development

3.5.1 Modeling Approach

For nonlinear analysis, each archetype was idealized as an uncoupled cantilever wall with appropriate gravity load and seismic mass determined based on tributary area. Because walls in the two orthogonal directions are not structurally connected, each wall was considered as a rectangular section. The base of each wall was assumed to be perfectly fixed, without consideration of soil-structure interaction effects.

The analyses were conducted using OpenSees, *Open System for Earthquake Engineering Simulation* (OpenSees, 2007), with displacement-based fiber-section beam-column elements to model the flexural behavior of the walls. For calculating story drift, an effective moment of inertia, I_e, equal to 50% of the uncracked net masonry section was used. Shear deformation was modeled with zero-length elastic springs. Inelastic shear behavior was not accounted for, and shear failure was treated as a non-simulated collapse mode.

Figure 3-4 shows a representative element assembly used in a typical archetype model. One shear spring was used for each story, with stiffness equal to the elastic shear stiffness of the story below. Vertical degrees of freedom for the two nodes connected with a horizontal shear spring are constrained to be equal. The discretization scheme adopted for each archetype model, i.e., the number and size of beam-column elements used, was determined by the effective plastic-hinge length at the base of the wall and the height of the first story. If the plastic-hinge length was on the order of (or larger than) the story height, the bottom story was represented by one beam-column element. Otherwise, the bottom story was modeled with two beam-column elements, and the length of the element at the base was set equal to the

effective plastic-hinge length. In either case, the upper stories were represented by one beam-column element.

The same modeling approach was used for fully grouted and partially grouted walls. Ungrouted sections of partially grouted walls were represented by a reduced section thickness corresponding to the total thickness of the face shells of a masonry unit. Grouted and ungrouted sections were assumed to have the same compressive strength, taken as the expected strength of masonry. Test data for concrete masonry have indicated that the compressive strengths of grouted and ungrouted masonry prisms are only slightly lower than that of masonry units.

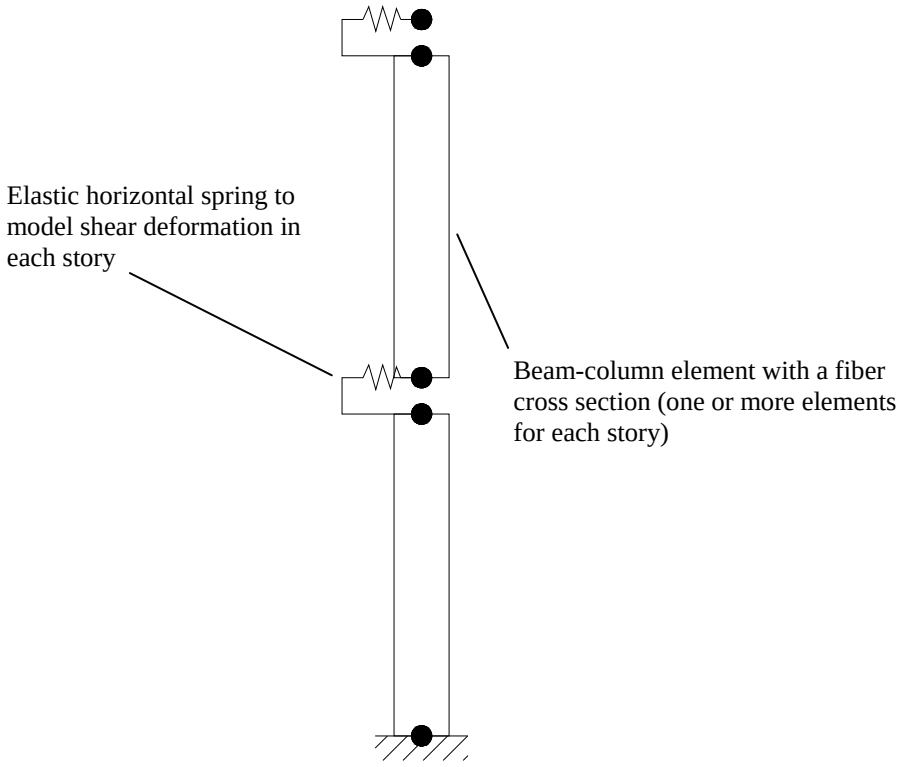

Figure 3-4 Representative element assembly in a typical archetype model.

In some archetype configurations, the seismic mass for the horizontal degree of freedom at each floor can be much larger than the gravity mass directly supported by the wall because a large portion of the gravity load might be carried by other adjacent elements (e.g., gravity frames or walls oriented in the perpendicular direction). Although the gravity load is applied as a static load at the nodal point at each floor level, mass is still needed for the vertical degrees of freedom to account for inertia effects introduced by a rocking wall. In the dynamic analyses, this resulted in unrealistically large vertical accelerations introduced by the rocking of a cracked wall, resulting in a large oscillatory axial inertial force when the actual mass was specified for vertical translational degrees of freedom. This large vertical acceleration was believed to be an artifact of the fiber-section beam-column model

due to shifting of the neutral axis for bending after cracking occurs. As a result, the mass for each vertical degree of freedom was set to a negligibly small value. P-Delta effects were accounted for using the co-rotational transformation in the beam-column elements, but this influence was found to be insignificant for the in-plane response of the walls.

3.5.2 Nonlinear Material Models for Reinforced Masonry

With appropriate material models selected for the fibers, a fiber-section element can simulate the axial load-moment interaction phenomenon and the nonlinear moment-curvature relation of a wall section. In all archetype models, the cross section of a wall element was divided into 400 fiber layers, and a uniaxial stress-strain material relation was adopted to describe the behavior of each fiber. Given the axial deformation and curvature at an element section, the strain in each fiber was calculated based on the assumption that plane sections remain plane, and the stresses were determined from the assigned stress-strain relation. Based on the cross-sectional area of each fiber and its position in the element cross section, the resultant internal forces (axial force and bending moment) at the section were calculated by numerical integration. Finally, the element nodal axial forces and moments were determined by Gauss integration using two Gauss points for each element. The nodal shear forces were determined from the nodal moments using the equilibrium condition. Shear failure was assumed to occur when the shear force in a wall element reached the shear strength calculated using the formula in the MSJC code without the resistance factor, ϕ.

Two uniaxial stress-strain relations were needed to model the flexural behavior of the reinforced masonry walls: one for the masonry and another for the reinforcing steel. A reference stress-strain relation, considered as the true material property, is determined for each material, based on the expected strengths of the materials.

Even though the analytical models developed for reinforced masonry and concrete shear walls are similar, there are major differences in modeling assumptions and material model calibration, mainly due to the differences in design details for the two types of wall systems. For example, reinforced masonry walls normally do not have special boundary elements, and, therefore, the flexural reinforcement near the extreme compression fibers in these walls is more vulnerable to buckling than in reinforced concrete walls. Furthermore, masonry walls tend to have larger spacing between shear reinforcement, so post-peak shear behavior can be more brittle.

The Kent-Park model for concrete (Kent and Park, 1971), available in OpenSees, was adopted to model the compression behavior of masonry. The model assumes zero tensile strength and exhibits stiffness degradation in compressive unloading and reloading. The expected masonry compressive strength, f'_m, was assumed to be 1.25 times the nominal strength chosen for design. This was deduced from prism test data provided in the Commentary of the MSJC code. Figure 3-5 shows the reference

stress-strain curve selected for masonry with the stress value normalized by the expected compressive strength.

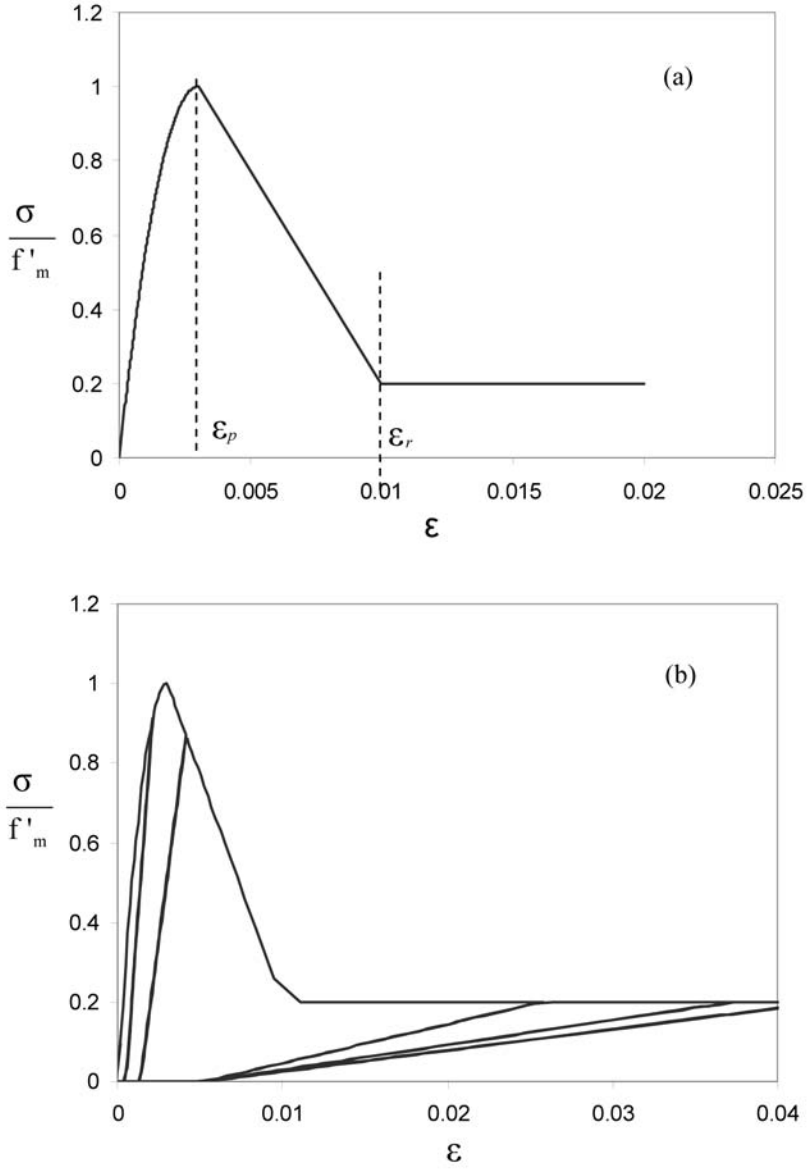

Figure 3-5 Normalized reference stress-strain curves used for compressive behavior of masonry: backbone curve (top) and cyclic loading and unloading curves (bottom).

In Figure 3-5, the strain ε_p, corresponding to the peak stress, was taken as 0.003. This is based on the prism test data of Atkinson and Kingsley (1985). The strain ε_r, marking the end of the descending branch, was taken as 0.01, which is about two times the strain level shown by most prism test data. This value was chosen because it provides a good match between numerical results and wall test data. It can be expected that the post-peak compression behavior of a masonry prism may not be the same as that in a wall because of differences in geometry (such as aspect ratio) and boundary conditions. According to the Kent-Park model, the initial modulus of

elasticity of masonry is equal to $2 f'_m / \varepsilon_p$. Hence, with ε_p equal to 0.003, the initial modulus of elasticity is assumed to be 667 f'_m, which is less than the elastic modulus of 900 f'_m calculated according to the MSJC code. However, the shear modulus of masonry used to determine the stiffness of the shear spring was based on the MSJC specification, i.e., $G = 0.4 \times 900 \times f'_m$.

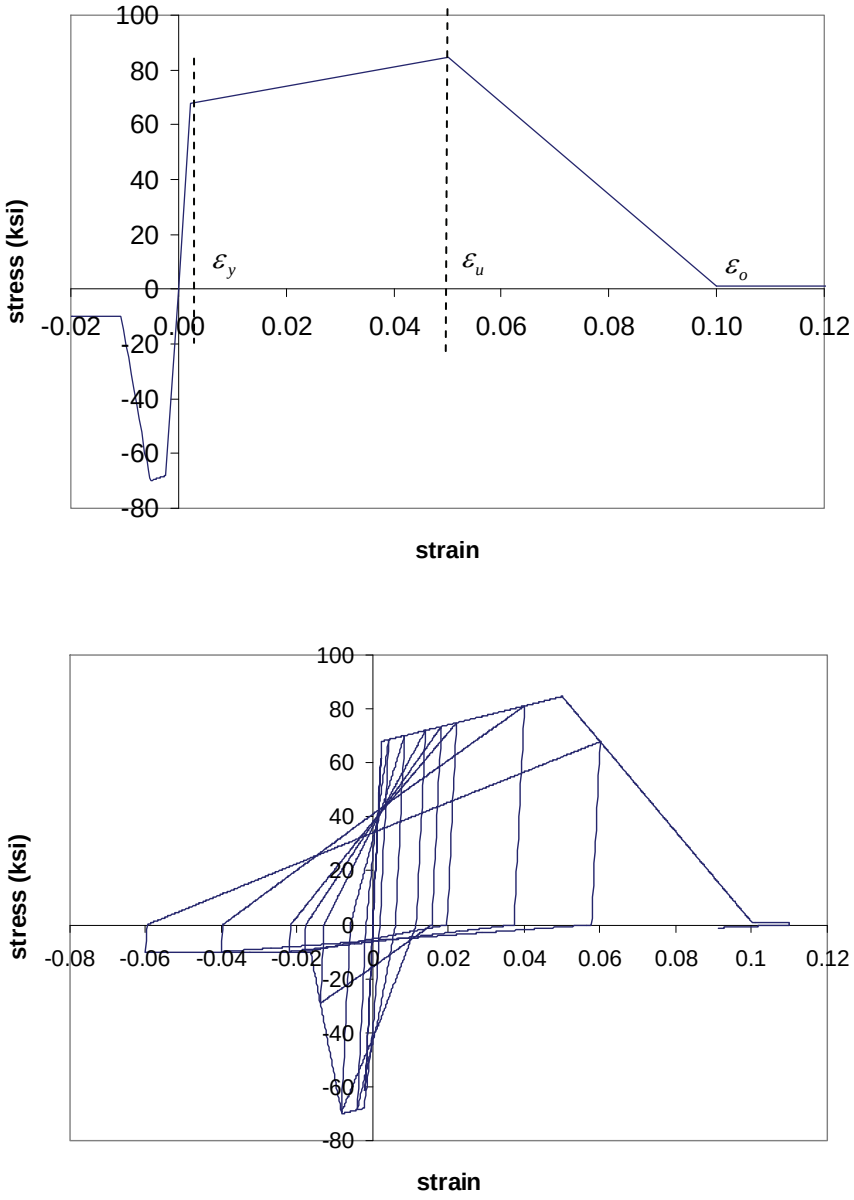

Figure 3-6 Reference stress-strain relations used for reinforcing steel: backbone curve (top) and cyclic loading and unloading curves (bottom).

The reference stress-strain relations selected for reinforcing steel are shown in Figure 3-6. Grade 60 reinforcing steel was chosen for design of the archetypes. Expected yield and tensile strengths were taken as 1.13 times the nominal strengths, based on data provided by Nowak et al. (2008), resulting in an expected yield strength of 68 ksi and an expected tensile strength of 102 ksi for the reinforcing steel.

The steel model in OpenSees cannot simulate buckling or rupture, which is important for assessing the collapse capacity of a reinforced masonry shear wall archetype. Hence, the stress-strain relation used in this study was modified based on user-defined material limit states. It was assumed that tensile rupture of a steel reinforcing bar would occur at a strain of 0.05, which is about half of the strain at which a bar reaches its tensile strength. This accounts for low-cycle fatigue phenomena, which could happen under cyclic load reversals. After this limit was reached, the tensile strength of the bar was assumed to decrease linearly, reaching zero at a tensile strain of 0.10.

A bar will buckle when the masonry around the bar spalls significantly. This was simulated in the user-defined model by introducing compressive strain softening, which started at a compressive strain of 0.0083 in the reference material model. At this strain level the masonry compressive strength drops to 40 percent of the peak value, intended to signify the occurrence of severe spalling. After buckling, it was assumed that the compressive strength of a bar drops to 10 percent of the yield strength at a strain of 0.016, after which the residual strength was assumed to remain constant.

3.5.3 Non-Simulated Collapse Criteria

Although the flexure-dominated yielding mechanisms of reinforced masonry shear walls were calibrated with test data and explicitly simulated in the analytical models, additional criteria were needed to establish the collapse of flexure-critical walls. Based on results observed in pushover analyses, collapse of a flexure-critical wall was assumed to occur when either of the following conditions was met:

- Excessive crushing in the wall cross section, defined as the condition when 30% of the cross section has reached the end of the softening branch of the masonry stress-strain relation.
- Rupture or buckling of a large portion of the flexural reinforcement, defined as the condition when 30% or more of the bars in a wall cross section have lost their tensile resistance due to rupture or reached their residual compressive resistance due to buckling.

These criteria were consistently observed in conjunction with a sudden and significant drop in lateral strength of the system. Even though extensive bar rupture was observed to cause a significant drop in lateral strength, this condition alone may not induce collapse of low-rise shear wall archetypes. In contrast with high-rise walls, low-rise walls have a greater potential to rock or slide along the base without collapse. Though potentially overconservative in the case of 1- and 2-story shear walls, the bar rupture criterion was used in evaluating these archetypes because of a lack of experimental evidence to the contrary.

The curvature at which either of these conditions was first reached was established for each archetype using static pushover analysis. In the nonlinear dynamic analyses, flexural collapse was considered to occur when the maximum wall curvature exceeded the established curvature limits. The use of these criteria in lieu of a full incremental dynamic analysis (IDA), in which collapse is often signified by excessive story drift or lateral dynamic instability, had several advantages. First, the reliability of a nonlinear model in capturing the post-peak response of a structure at large drift levels is often questionable, and use of non-simulated criteria avoids this. Second, these criteria can be applied in an objective manner without relying on a visual estimation of instability. Third, the use of these criteria can significantly reduce the number of incremental dynamic analyses needed to identify the collapse capacity of an archetype, and is easily implementable with the simplified IDA procedure suggested as part of the Methodology.

Similarly, because nonlinear shear behavior was not explicitly simulated in the analytical models, additional criteria were needed to establish the collapse of shear-critical walls. Collapse due to shear-controlled behavior was considered to occur when the shear force in a wall exceeded the nominal shear strength calculated based on MSJC code formulas. This assumption is appropriate considering that shear behavior is often brittle in reinforced masonry shear walls and post-peak shear resistance is not reliable, as indicated by test data from Shing et al. (1991).

3.5.4 Model Calibration and Validation

When using displacement-based beam-column elements with distributed plasticity and strain-softening material laws to model a shear wall, plastic deformation tends to concentrate in a single element closest to the base of the wall while the rest of the model remains elastic. This phenomenon, termed strain localization, leads to numerical results that are sensitive to the length of the element in which the plastic strain is localized. To circumvent this problem, the reference material stress-strain relations should be modified, based on element size, to obtain realistic total fracture-energy dissipation. This modification is called regularization, which ensures that the numerical solution will be objective and not sensitive to element size.

The regularization method adopted in this study is described in Appendix A. It is based on the premise that the reference stress-strain relations shown in Figure 3-5 and Figure 3-6 will result in a numerical solution that represents the true behavior of a wall, provided that the length of the beam-column element where plastic strain will be localized is equal to the effective plastic-hinge length, L_p, of the wall. As the length, L_e, of the element is varied, the plastic strain will be localized over the new length, and the value of ε_r in the masonry material model must be varied to obtain the same total compressive fracture energy, G_m^f, that would have been dissipated in a unit area of a fiber over the effective plastic-hinge length.

A good estimation of the effective plastic-hinge length is crucial to the accuracy of such an analysis. Paulay and Priestley (1993) have suggested a formula to estimate the effective plastic-hinge length in reinforced concrete walls. However, this formula has not provided good results for some of the masonry wall tests considered here. Experimental data from Shing et al. (1991) have shown a large scatter of plastic-hinge lengths among the single-story specimens, all of which had an aspect ratio of one. However, the average effective plastic-hinge length identified for masonry wall specimens is about 20% of the wall height. This ratio has been found to be a good estimate of the effective plastic-hinge length of the more slender walls tested by Merryman et al. (1990), and Shedid et al. (2008). Hence, this ratio has been used in the development of archetype models.

A set of model validation studies was conducted using Specimens 1 and 12 tested by Shing et al. (1991). These walls are fully grouted, single-story walls with the design and loading scheme shown in Figure 3-7. The two specimens had the same reinforcing, but Specimen 1 had an axial load ratio ($P / A_n f'_m$) of 0.08, while Specimen 12 had an axial load ratio of 0.04.

In the models, each wall was represented by two elements. The bottom element was sized to match the plastic hinge length (equal to 20% of the wall height) so that the reference stress-strain relations shown in Figure 3-5 and Figure 3-6 are used without modification. Analytical results were compared to the experimental results for the two specimens in Figures 3-8 and 3-9. It can be seen that the strength, ductility, and hysteretic behavior of the walls are captured well by the analytical models. Results from additional model validation studies are provided in Appendix A.

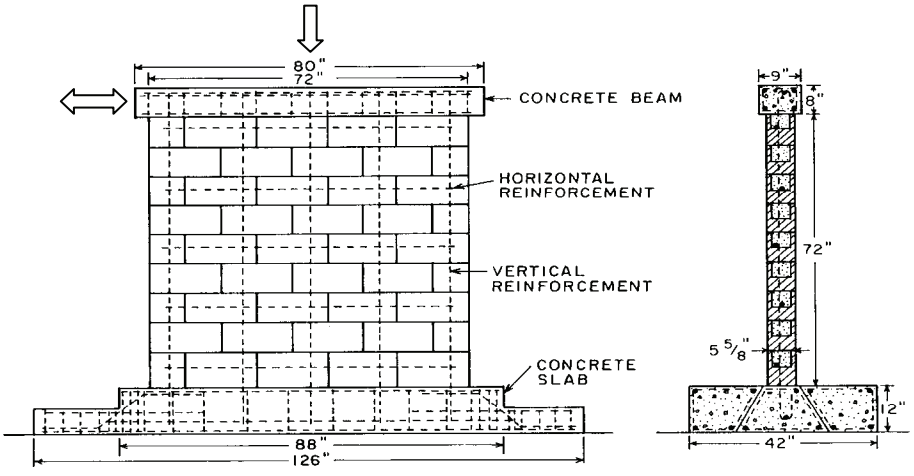

Figure 3-7 Single-story walls tested by Shing et al. (1991).

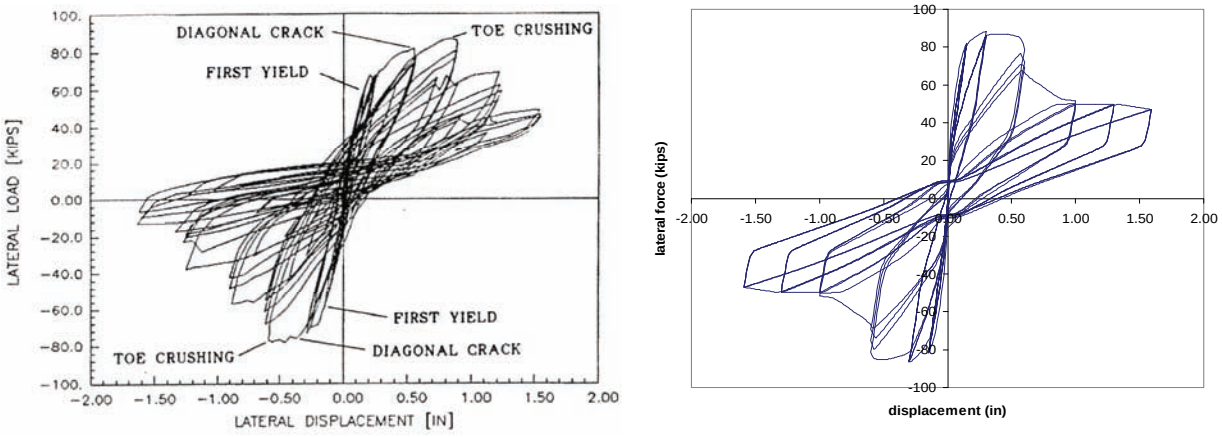

(a) (b)

Figure 3-8 Lateral load versus displacement curves for Specimen 1 tested by Shing et al. (1991): (a) experimental results; (b) analytical model.

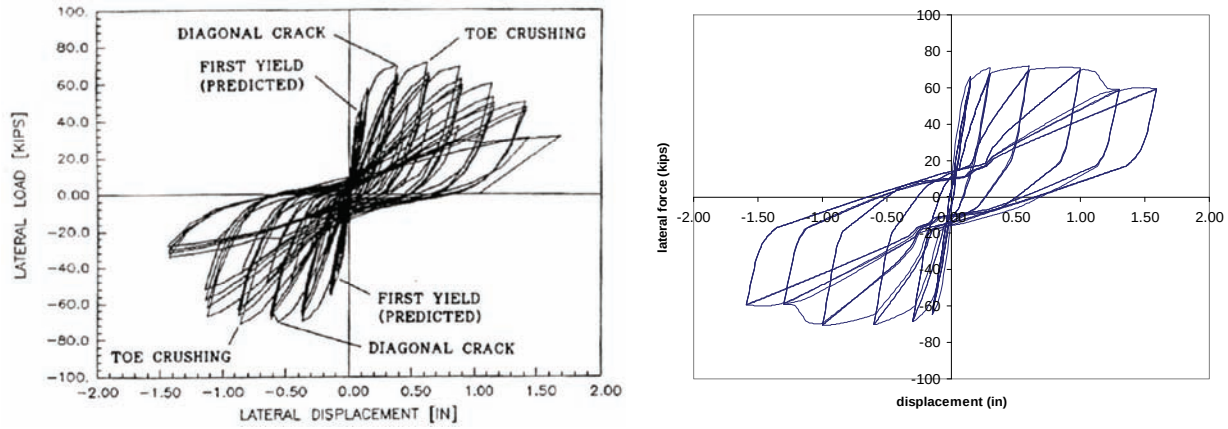

(a) (b)

Figure 3-9 Lateral load versus displacement curves for Specimen 12 tested by Shing et al. (1991): (a) experimental results; (b) analytical model.

3.5.5 Quality Rating of Analytical Models

Model calibration and validation studies demonstrated that the flexural behavior of fully grouted and partially grouted walls can be reasonably simulated with the adopted modeling approach. Shear failure, however, must be treated as a non-simulated collapse mode, which has been assumed to occur when the maximum shear force in a wall reaches the shear strength calculated based on MSJC code formulas. In addition, the influence of flexural deformation on shear resistance is not considered.

The effective plastic-hinge length was assumed to be 20% of the total wall height, which had a major influence on the ductility of a wall. Although reasonable, this value was based on limited experimental data. While models were able to simulate flexural behavior reasonably well, in consideration of the limitations noted above,

analytical models for reinforced masonry shear wall archetypes were assigned a quality rating of B (Good).

3.6 Nonlinear Analyses

Nonlinear static pushover analyses and simplified incremental dynamic analyses (IDAs) were used to evaluate system overstrength, period-based ductility, and the collapse capacity of reinforced masonry shear wall archetypes.

3.6.1 Static Pushover Analyses

For each archetype, a pushover analysis was conducted with a lateral load distribution corresponding to the fundamental mode shape and mass distribution of the structure. An eigenvalue analysis was performed for each archetype to determine the fundamental period, T_1, and modal shape. The base shear obtained from the pushover analysis was then plotted against the roof drift ratio. From this plot, the maximum base shear V_{max} was identified, and the overstrength factor was calculated as $\Omega = V_{max}/V$, where V is the design base shear. The fundamental period, T_1, obtained from the eigenvalue analysis was compared to the code-based period, T, and the larger of the two used to compute the effective yield drift $\delta_{y,eff}$ at the roof. The roof drift, δ_u, corresponding to a 20% drop in base shear was identified, and the period-based ductility was calculated as $\mu_T = \delta_u / \delta_{y,eff}$. A plot of base shear versus roof drift (pushover curve) for the 2-story, high axial load, SDC D_{max} archetype is shown in Figure 3-10. The effective yield drift, $\delta_{y,eff}$, calculated for this archetype was $0.00155h_r$, and the drift δ_u identified from the plot was $0.0125h_r$, where h_r is the roof height. The resulting period-based ductility, μ_T, was 8.1.

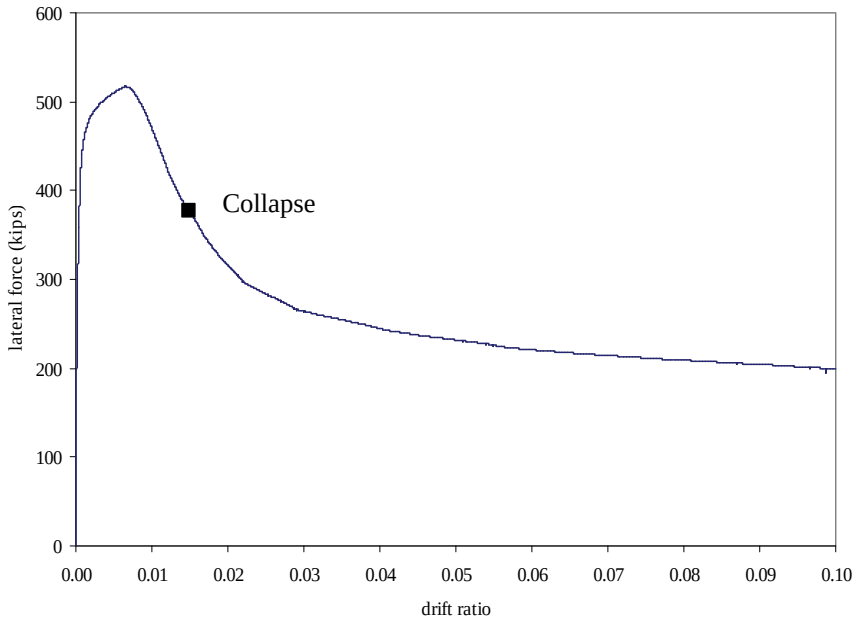

Figure 3-10 Pushover curve for the 2-story, high axial load, SDC D_{max} archetype.

The pushover curve for the 12-story, high axial load, SDC D_{max} archetype is shown in Figure 3-11. The effective yield drift $\delta_{y,eff}$ calculated for this archetype was $0.00205h_r$, and the drift δ_u identified from the plot was $0.0299h_r$. This resulted in a period-based ductility, μ_T, of 14.6.

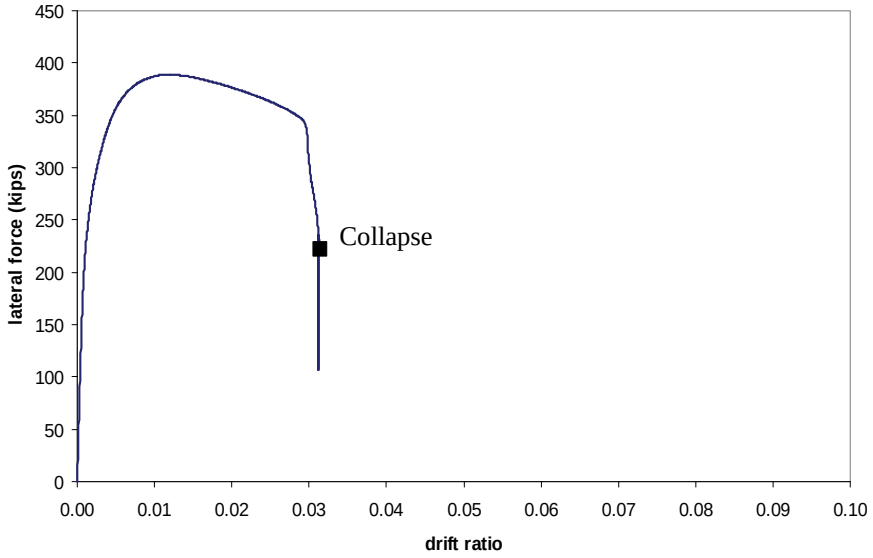

Figure 3-11 Pushover curve for the 12-story, high axial load, SDC D_{max} archetype.

Figure 3-12 shows the result for the 12-story, low axial load, SDC D_{max} archetype. This wall exhibited very ductile behavior. For this case, $\delta_{y,eff} = 0.00187h_r$.

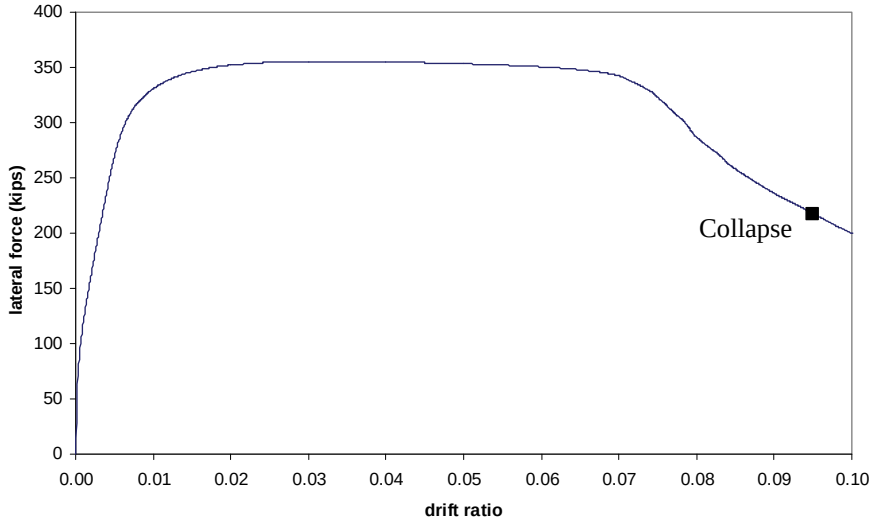

Figure 3-12 Pushover curve for the 12-story, low axial load, SDC D_{max} archetype.

Figure 3-13 shows the pushover curve for the 12-story, high axial load, SDC C_{max} archetype. The behavior exhibited by this partially grouted wall was relatively ductile in comparison with the response of most partially grouted walls subjected to high axial load. This was attributed to the larger number (in a relative sense) of

grouted cells in the wall. The pushover curve for the 4-story, high axial load, SDC C_{max} archetype is shown in Figure 3-14. This behavior was more representative of the expected behavior of partially grouted walls subjected to high axial load.

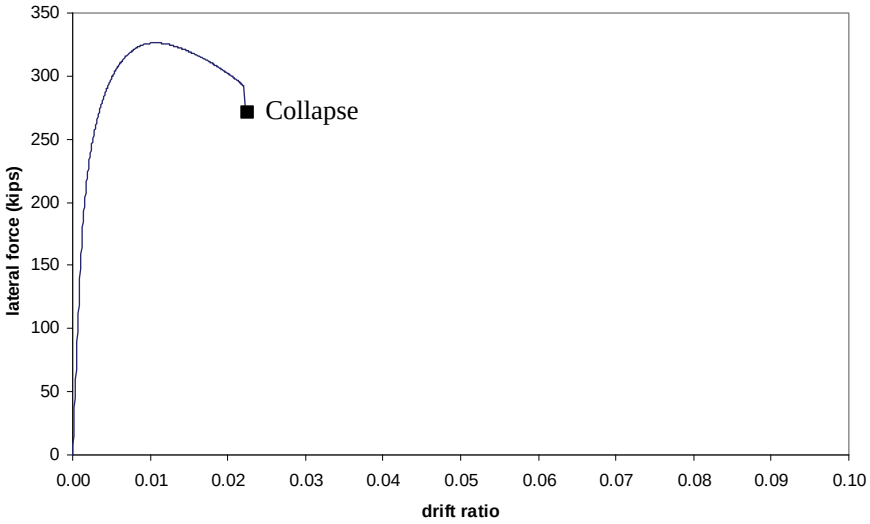

Figure 3-13 Pushover curve for the 12-story, high axial load, SDC C_{max} archetype.

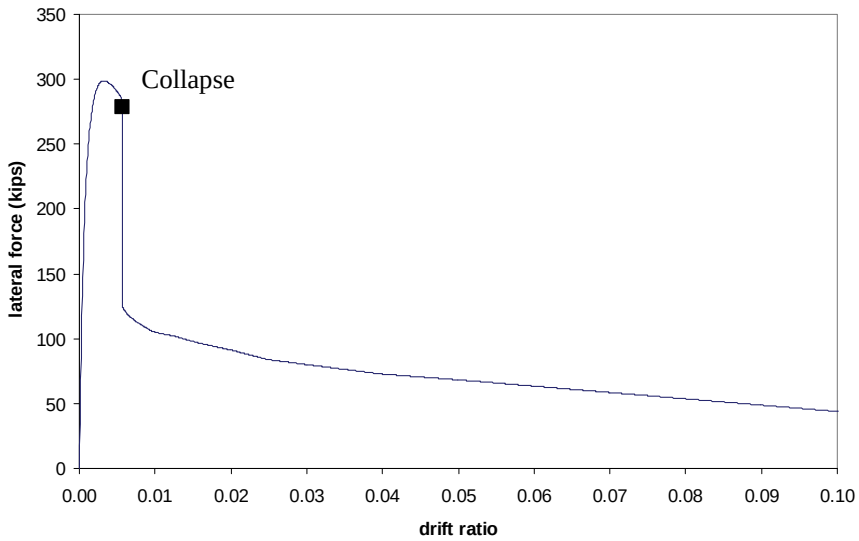

Figure 3-14 Pushover curve for the 4-story, high axial load, SDC D_{max} archetype.

The sudden drop in lateral resistance for the 2-story, high axial load, SDC D_{max} archetype shown in Figure 3-13 was caused by the rupture of a large portion of flexural reinforcement. This condition controlled for all 1- and 2-story fully grouted archetypes, as well as the 4-story fully grouted archetypes with low axial loads. For all other archetypes, including the taller 8- and 12-story configurations with partially grouted walls, the drop in lateral strength was caused by excessive masonry crushing.

In general, it was observed that walls subjected to higher axial loads were less ductile (based on severe toe crushing) and that low-rise walls were less ductile than high-rise walls. The latter was partially attributed to the fact that for low-rise walls, the code-based periods were much longer than the fundamental periods calculated by eigenvalue analysis, leading to effective yield drifts that were higher than would have been calculated based on the physical properties of the system. Furthermore, the low-rise walls designed for SDC D_{min} appeared to be more ductile than those for SDC D_{max}.

A number of low-rise partially grouted walls had shear strengths that were lower than the flexural strengths exhibited in the pushover curves. Because shear failure was a non-simulated mode, the ductility of these walls was assumed to be 1.5 based on experimental observations (e.g., Shing et al., 1991). In general, partially grouted walls were observed to be less ductile, as expected.

3.6.2 Nonlinear Dynamic Analyses

Each archetype was subjected to nonlinear dynamic (response history) analysis with the set of 44 far-field ground motion records provided as part of the Methodology. In accordance with the simplified IDA procedure suggested in the Methodology, all the records in the set were scaled up gradually by the same factor in each increment until collapse was obtained for 50% of the record set. The median collapse spectral intensity, S_{CT}, was taken as the median spectral acceleration at the code-based structural period, T.

Care was taken to ensure that the damping model used in the analyses did not introduce too much damping into the system when the structural elements became nonlinear. When Rayleigh damping is used, the damping matrix can be constructed using the initial stiffness or the tangent stiffness of the structure. In either case, if the damping properties are determined based on the fundamental frequency and a higher-mode frequency, the damping effect can increase when the structure softens, and the fundamental frequency decreases. On the other hand, the effect of Rayleigh damping, in general, is much less significant than that of hysteretic damping in an inelastic system.

Most of the archetype models exhibited severe strain softening with negative stiffness, as exemplified in the moment-curvature relation. In these cases, use of tangent stiffness-proportional Rayleigh damping can lead to numerical problems. For this reason, initial stiffness-proportional Rayleigh damping, with 5% damping in the first and third modes, was used for 4-story and taller archetypes. Initial stiffness for this purpose was based on uncracked section properties.

For the 1-story and 2-story archetypes, which can develop significant rocking under severe seismic loads, the Rayleigh damping model was observed to introduce unrealistically large oscillatory axial damping forces. Hence, for these cases, the

Rayleigh damping matrix was determined so that very small damping was introduced into the higher modes, which are not important for the response of low-rise archetypes. This was achieved by using a very small coefficient for the stiffness-proportional term.

Values of overstrength, Ω, from the pushover analyses, and collapse margin ratio, *CMR*, calculated as S_{CT}/S_{MT} from the simplified incremental dynamic analyses, are summarized in Table 3-7 for special RMSWs and Table 3-8 for ordinary RMSWs.

Table 3-7 Summary of Collapse Results for Special Reinforced Masonry Shear Wall Archetype Designs

Archetype Design ID Number	Design Configuration			Pushover and IDA Results			
	No. of Stories	Gravity Loads	SDC	Static Ω	S_{MT} [*T*] (g)	S_{CT} [*T*] (g)	*CMR*
Performance Group No. PG-1S							
S1	1	High	D_{max}	1.84	1.50	0.78	0.52
S2	2	High	D_{max}	2.28	1.50	1.71	1.14
S3	4	High	D_{max}	1.87	1.50	2.33	1.55
Performance Group No. PG-2S							
S4	8	High	D_{max}	1.89	1.20	1.57	1.31
S5	12	High	D_{max}	1.61	0.89	1.72	1.94
Performance Group No. PG-3S							
S6	1	High	D_{min}	1.62	0.75	0.78	1.04
S7	2	High	D_{min}	2.61	0.75	1.44	1.92
Performance Group No. PG-4S							
S8	4	High	D_{min}	1.65	0.63	1.04	1.65
S9	8	High	D_{min}	1.93	0.37	0.60	1.63
S10	12	High	D_{min}	1.68	0.28	0.58	2.07
Performance Group No. PG-5S							
S11	1	Low	D_{max}	1.84	1.50	0.78	0.52
S12	2	Low	D_{max}	1.82	1.50	2.57	1.71
S13	4	Low	D_{max}	1.73	1.50	2.48	1.65
Performance Group No. PG-6S							
S14	8	Low	D_{max}	1.59	1.20	1.57	1.31
S15	12	Low	D_{max}	1.47	0.89	1.72	1.94
Performance Group No. PG-7S							
S16	1	Low	D_{min}	1.62	0.75	0.78	1.04
S17	2	Low	D_{min}	1.80	0.75	1.79	2.38
Performance Group No. PG-8S							
S18	4	Low	D_{min}	1.41	0.63	1.04	1.65
S19	8	Low	D_{min}	1.64	0.37	0.61	1.63
S20	12	Low	D_{min}	1.46	0.28	0.59	2.13

In some cases, incremental dynamic analyses were stopped before the median collapse condition was attained because the performance group was observed to pass the performance evaluation criteria. In the 8-story and 12-story special RMSW archetypes with low axial loads, shear collapse was observed to occur in a number of cases due to higher-mode effects. Shear collapse was also observed in the low-rise ordinary RMSWs and attributed to the absence of capacity design requirements for these walls.

Table 3-8 Summary of Collapse Results for Ordinary Reinforced Masonry Shear Wall Archetype Designs

Archetype Design ID Number	Design Configuration			Pushover and IDA Results			
	No. of Stories	Gravity Loads	SDC	Static Ω	S_{MT} [T] (g)	S_{CT} [T] (g)	*CMR*
Performance Group No. PG-1O							
O1	1	High	C_{max}	2.33	0.75	1.33	1.77
O2	2	High	C_{max}	1.44	0.75	0.80	1.06
Performance Group No. PG-2O							
O3	4	High	C_{max}	1.94	0.63	0.74	1.18
O4	8	High	C_{max}	2.21	0.37	0.54	1.45
O5	12	High	C_{max}	2.09	0.28	0.39	1.42
Performance Group No. PG-3O							
O6	1	High	C_{min}	1.36	0.45	0.70	1.56
O7	2	High	C_{min}	1.46	0.45	0.55	1.23
Performance Group No. PG-4O							
O8	4	High	C_{min}	1.63	0.38	0.56	1.48
O9	8	High	C_{min}	2.07	0.23	0.41	1.79
O10	12	High	C_{min}	2.26	0.17	0.30	1.81
Performance Group No. PG-5O							
O11	1	Low	C_{max}	2.33	0.75	1.33	1.77
O12	2	Low	C_{max}	1.49	0.75	1.48	1.97
Performance Group No. PG-6O							
O13	4	Low	C_{max}	1.68	0.63	1.04	1.65
O14	8	Low	C_{max}	1.70	0.37	0.81	2.17
O15	12	Low	C_{max}	1.63	0.28	0.81	2.95
Performance Group No. PG-7O							
O16	1	Low	C_{min}	1.36	0.45	0.70	1.56
O17	2	Low	C_{min}	1.37	0.45	0.97	2.15
Performance Group No. PG-8O							
O18	4	Low	C_{min}	1.45	0.38	0.71	1.85
O19	8	Low	C_{min}	1.65	0.23	0.73	3.21
O20	12	Low	C_{min}	1.82	0.17	0.49	2.89

3.7 Performance Evaluation

In the Methodology, adjusted collapse margin ratios (*ACMR*s) are obtained by multiplying the *CMR*s obtained from nonlinear dynamic analysis results by the spectral shape factor (*SSF*). The acceptable average value of *ACMR* for each performance group is denoted by $ACMR_{10\%}$. The acceptable value of *ACMR* for individual archetypes within a performance group is denoted by $ACMR_{20\%}$.

Values of $ACMR_{10\%}$ and $ACMR_{20\%}$ are determined based on total system collapse uncertainty, β_{TOT}. Collapse uncertainty is a function of the quality ratings associated with the design requirements, test data, and nonlinear models, as well as record-to-record uncertainty. Quality ratings assigned to design requirements, test data, and nonlinear models for reinforced masonry shear walls are summarized in Table 3-9.

Table 3-9 Summary of Quality Ratings for Reinforced Masonry Shear Wall Systems

System	Design Requirements	Test Data	Nonlinear Modeling
Special RMSWs	B	B	B
Ordinary RMSWs	C	C	B

3.7.1 Summary of Performance Evaluation Results

To pass the performance evaluation criteria, individual archetypes must have adjusted collapse margin ratios exceeding $ACMR_{20\%}$. Performance evaluation results for individual special RMSW archetypes are summarized in Table 3-10, and results for individual ordinary RMSW archetypes are summarized in Table 3-11. For special RMSWs, all 2-, 4-, 8-, and 12-story archetypes passed this criterion, with only one exception (2-story archetype ID S2). All 1-story special RMSW archetypes, however, failed this criterion.

In the case of ordinary RMSWs, results were mixed. While all 8- and 12-story ordinary RMSW archetypes passed this criterion, many of the shorter period archetypes did not. In general, 1-, 2-, and 4-story ordinary RMSW archetypes subjected to low axial load passed the criterion, while archetypes of the same height subjected to high axial load did not.

The relatively poor performance of low-rise special RMSW archetypes can be attributed to two factors. One is the high ductility demand that earthquake ground motions placed on short-period archetypes, which is a well-documented and expected result in the case of short-period structures. The other is the lower ductility capacity of shorter walls, as observed in the pushover curves of Figures 3-13 through 3-17. This had the combined effect of producing a lower collapse margin ratio as a starting point, a lower spectral shape factor, and ultimately a lower adjusted collapse margin ratio for comparison.

Table 3-10 Summary of Collapse Performance Evaluations of Special Reinforced Masonry Shear Wall Archetypes

Arch. Design ID No.	Design Configuration			Computed Overstrength and Collapse Margin Parameters					Acceptance Check	
	No. of Stories	Gravity Loads	SDC	Static Ω	*CMR*	μ_T	*SSF*	*ACMR*	Accept. *ACMR*	Pass/ Fail
Performance Group No. PG-1S										
S1	1	High	D_{max}	1.84	0.52	5.2	1.26	0.66	1.56	Fail
S2	2	High	D_{max}	2.28	1.14	8.1	1.33	1.52	1.56	Fail
S3	4	High	D_{max}	1.87	1.55	11.8	1.33	2.06	1.56	Pass
Mean of Performance Group:				**2.00**				**1.41**	**1.96**	**Fail**
Performance Group No. PG-2S										
S4	8	High	D_{max}	1.89	1.31	6.4	1.35	1.76	1.56	Pass
S5	12	High	D_{max}	1.61	1.94	14.6	1.47	2.84	1.56	Pass
Mean of Performance Group:				**1.75**				**2.30**	**1.96**	**Pass**
Performance Group No. PG-3S										
S6	1	High	D_{min}	1.62	1.04	13.3	1.14	1.19	1.56	Fail
S7	2	High	D_{min}	2.61	1.92	14.4	1.14	2.18	1.56	Pass
Mean of Performance Group:				**2.12**				**1.69**	**1.96**	**Fail**
Performance Group No. PG-4S										
S8	4	High	D_{min}	1.65	1.65	28.4	1.14	1.88	1.56	Pass
S9	8	High	D_{min}	1.93	1.63	7.1	1.25	2.03	1.56	Pass
S10	12	High	D_{min}	1.68	2.07	16.0	1.37	2.84	1.56	Pass
Mean of Performance Group:				**1.75**				**2.25**	**1.96**	**Pass**
Performance Group No. PG-5S										
S11	1	Low	D_{max}	1.84	0.52	5.2	1.26	0.66	1.56	Fail
S12	2	Low	D_{max}	1.82	1.71	8.3	1.33	2.27	1.56	Pass
S13	4	Low	D_{max}	1.73	1.65	11.3	1.33	2.19	1.56	Pass
Mean of Performance Group:				**1.80**				**1.71**	**1.96**	**Fail**
Performance Group No. PG-6S										
S14	8	Low	D_{max}	1.59	1.31	13.6	1.40	1.82	1.56	Pass
S15	12	Low	D_{max}	1.47	1.94	42.8	1.47	2.84	1.56	Pass
Mean of Performance Group:				**1.53**				**2.33**	**1.96**	**Pass**
Performance Group No. PG-7S										
S16	1	Low	D_{min}	1.62	1.04	13.3	1.14	1.19	1.56	Fail
S17	2	Low	D_{min}	1.80	2.38	14.4	1.14	2.71	1.56	Pass
Mean of Performance Group:				**1.71**				**1.95**	**1.96**	**Fail**
Performance Group No. PG-8S										
S18	4	Low	D_{min}	1.41	1.65	29.0	1.14	1.88	1.56	Pass
S19	8	Low	D_{min}	1.64	1.63	17.7	1.26	2.05	1.56	Pass
S20	12	Low	D_{min}	1.46	2.13	20.7	1.37	2.92	1.56	Pass
Mean of Performance Group:				**1.50**				**2.28**	**1.96**	**Pass**

Table 3-11 Summary of Collapse Performance Evaluations of Ordinary Reinforced Masonry Shear Wall Archetypes

Arch. Design ID No.	Design Configuration			Computed Overstrength and Collapse Margin Parameters					Acceptance Check	
	No. of Stories	Gravity Loads	SDC	Static Ω	*CMR*	μ_T	*SSF*	*ACMR*	Accept. *ACMR*	Pass/ Fail
Performance Group No. PG-1O										
O1	1	High	C_{max}	2.33	1.77	2.7	1.08	1.91	1.69	Pass
O2	2	High	C_{max}	1.44	1.06	1.5	1.04	1.10	1.66	Fail
Mean of Performance Group:				**1.89**				**1.51**	**2.23**	**Fail**
Performance Group No. PG-2O										
O3	4	High	C_{max}	1.94	1.18	2.4	1.07	1.26	1.69	Fail
O4	8	High	C_{max}	2.21	1.45	3.8	1.09	1.57	1.76	Fail
O5	12	High	C_{max}	2.09	1.42	9.4	1.27	1.80	1.76	Pass
Mean of Performance Group:				**2.08**				**1.54**	**2.38**	**Fail**
Performance Group No. PG-3O										
O6	1	High	C_{min}	1.36	1.56	1.5	1.04	1.63	1.66	Fail
O7	2	High	C_{min}	1.46	1.23	1.5	1.04	1.28	1.66	Fail
Mean of Performance Group:				**1.41**				**1.46**	**2.16**	**Fail**
Performance Group No. PG-4O										
O8	4	High	C_{min}	1.63	1.48	1.5	1.04	1.54	1.66	Fail
O9	8	High	C_{min}	2.07	1.79	5.3	1.17	2.09	1.76	Pass
O10	12	High	C_{min}	2.26	1.81	5.6	1.24	2.24	1.76	Pass
Mean of Performance Group:				**1.99**				**1.96**	**2.38**	**Fail**
Performance Group No. PG-5O										
O11	1	Low	C_{max}	2.33	1.77	2.7	1.08	1.91	1.69	Pass
O12	2	Low	C_{max}	1.49	1.97	1.5	1.04	2.05	1.66	Pass
Mean of Performance Group:				**1.91**				**1.98**	**2.23**	**Fail**
Performance Group No. PG-6O										
O13	4	Low	C_{max}	1.68	1.65	1.5	1.04	1.72	1.66	Pass
O14	8	Low	C_{max}	1.70	2.17	10.2	1.20	2.60	1.76	Pass
O15	12	Low	C_{max}	1.63	2.95	10.6	1.27	3.74	1.76	Pass
Mean of Performance Group:				**1.67**				**2.69**	**2.38**	**Pass**
Performance Group No. PG-7O										
O16	1	Low	C_{min}	1.36	1.56	1.5	1.04	1.63	1.66	Fail
O17	2	Low	C_{min}	1.37	2.15	1.5	1.04	2.24	1.66	Pass
Mean of Performance Group:				**1.37**				**1.94**	**2.16**	**Fail**
Performance Group No. PG-8O										
O18	4	Low	C_{min}	1.45	1.85	9.8	1.04	1.92	1.76	Pass
O19	8	Low	C_{min}	1.65	3.21	17.4	1.21	3.90	1.76	Pass
O20	12	Low	C_{min}	1.82	2.89	24.6	1.29	3.74	1.76	Pass
Mean of Performance Group:				**1.64**				**3.19**	**2.38**	**Pass**

The mixed performance of ordinary RMSW archetypes can also be attributed to two factors. One is lower quality ratings, as compared to special RMSW archetypes, caused by additional uncertainty in design requirements and test data for ordinary walls. The other is lower ductility capacity of ordinary walls, which was the controlling factor affecting the values of *ACMR* for ordinary RMSW archetypes. For the 1- and 2-story archetypes, collapse was signaled by diagonal shear failure. In the 4-, 8-, and 12-story archetypes, collapse was signaled by excessive crushing of the masonry.

Table 3-12 Summary of Results by Performance Group for Special Reinforced Masonry Shear Walls

Performance Group Summary					
Group No.	Grouping Criteria				Performance Result
	Basic Config.	Design Load Level		Period Domain	
		Gravity	Seismic		
PG-1S	Cantilever	High	SDC D_{max}	Short	Fail
PG-2S				Long	Pass
PG-3S			SDC D_{min}	Short	Fail
PG-4S				Long	Pass
PG-5S		Low	SDC D_{max}	Short	Fail
PG-6S				Long	Pass
PG-7S			SDC D_{min}	Short	Fail
PG-8S				Long	Pass

Table 3-13 Summary of Results by Performance Group for Ordinary Reinforced Masonry Shear Walls

Performance Group Summary					
Group No.	Grouping Criteria				Performance Result
	Basic Config.	Design Load Level		Period Domain	
		Gravity	Seismic		
PG-1O	Cantilever	High	SDC C_{max}	Short	Fail
PG-2O				Long	Fail
PG-3O			SDC C_{min}	Short	Fail
PG-4O				Long	Fail
PG-5O		Low	SDC C_{max}	Short	Fail
PG-6O				Long	Pass
PG-7O			SDC C_{min}	Short	Fail
PG-8O				Long	Pass

Performance evaluation results by performance group are summarized in Table 3-12 for special RMSW archetypes and Table 3-13 for ordinary RMSW archetypes. To pass the performance evaluation criteria, the adjusted collapse margin ratio (*ACMR*) averaged across all archetypes in a performance group must exceed $ACMR_{10\%}$.

For special RMSWs, long-period performance groups passed this criterion while short-period performance groups did not. In the case of ordinary RMSWs, long-period, low axial load performance groups passed this criterion while the long-period, high axial load performance groups did not. Additionally all short-period ordinary RMSW performance groups failed the criterion.

3.8 Evaluation of System Overstrength

In the Methodology, the system overstrength factor, Ω_0, is taken as the largest average value of the overstrength factor, Ω, computed for each performance group. Values of overstrength for individual archetypes and average values for each performance group are shown in Table 3-10 and Table 3-11. Calculated values of Ω_0 were 2.12 for special RMSWs and 2.08 for ordinary RMSWs. These values are smaller, but on the same order of magnitude as the value of 2.5 provided for both systems in ASCE/SEI 7-05.

Reinforced masonry shear wall archetypes were deliberately configured to minimize the potential for overstrength. The close agreement between calculated and code-specified values of Ω_0 is likely related to this design objective.

3.9 Observations and Recommendations

3.9.1 Observations on System Performance

Neither the special RMSW archetypes nor the ordinary RMSW archetypes evaluated in this trial application fully met the acceptance criteria of the Methodology. System overstrength factors obtained in this study, however, are comparable to values provided for both systems in ASCE/SEI 7-05. Differences in observed performance for the two systems can be largely attributed to full versus partial grouting of the masonry cells. If special RMSW archetypes were partially grouted, which is permitted by the code but uncommon in practice, their assessed performance would have been less favorable.

Although the individual pass/fail statistics were different between the special and ordinary systems, taller archetypes, in general, were observed to pass the acceptance criteria while shorter archetypes, in general, were observed to fail the criteria. This result was not entirely unexpected, as differences in seismic response characteristics between short-period and long-period systems are not specific to reinforced masonry shear wall systems and have been well documented in the literature. This raises a question as to whether or not low-rise RMSW buildings should have the same seismic performance factors (e.g., *R* factor) as high-rise RMSW buildings.

Additionally, these differences in performance also raise questions as to whether or not the same collapse criteria are appropriate.

Observed results were sensitive to assumptions made about the collapse behavior of reinforced masonry shear walls and decisions made in nonlinear modeling. Because of difficulties in quantifying collapse for low-rise walls, it was decided that collapse would be defined as excessive crushing of the masonry cross section or rupture of a significant percentage of the vertical reinforcement. Neither of these conditions would necessarily lead to collapse in a low-rise shear wall system. Rather, collapse would more likely be expected to occur when drifts are so large that other gravity-load carrying elements lose their ability to carry vertical loads.

Additionally, the fixed-base modeling assumption likely increased ductility demands on low-rise walls. Because of the stiffness of low-rise shear wall systems, demands on these structures can be more significantly influenced (i.e., lowered) through consideration of soil-structure interaction effects, which were not accounted for in the analyses. If the non-simulated collapse criteria were less conservative, and if soil-structure interaction was considered in assessing the ductility demands on low-rise walls, the performance of special RMSW archetypes would have likely been significantly improved.

In the design of some archetypes, it was found that the special boundary element requirements in the strength design provisions of the MSJC code do not adequately control the maximum compressive strain induced by combined flexure and axial load. The ductility of some high-rise ordinary RMSW archetypes would have been further reduced if the maximum stress limit specified in the allowable stress design provisions of the code were not imposed. To improve the performance of ordinary shear wall systems, partial grouting should be avoided unless more experimental data are obtained to demonstrate that partially grouted walls have sufficient ductility capacity to perform satisfactorily.

Although some archetype designs were initially controlled by drift, the story drift limit in ASCE/SEI 7-05 did not seem to be closely related to the performance of a cantilever wall system. In such systems, a large portion of the drift in an upper story could be caused by rigid-body rotation of the wall about a plastic hinge formed at the base.

3.9.2 Observations on the Methodology

The Methodology provides a systematic and rational procedure to determine the seismic performance factors for structural systems. However, it relies on the ability of an analytical model to simulate the collapse state of a structural system with reasonable accuracy. In the case of low-rise shear wall systems, total collapse is rare and difficult to define. A sudden drop in strength caused by rupture of flexural reinforcement might not necessarily lead to collapse in such systems. Additionally,

the reliability of an analytical model in simulating the response of a low-rise shear wall system close to collapse requires special attention because of numerical issues related to softening of a very stiff structural system and the importance of modeling assumptions.

Values of the period-based ductility, μ_T , calculated for some of the special RMSWs are very large. In many cases, this is due to the very small effective yield drifts, $\delta_{y,eff}$, calculated using the equation provided in the Methodology. This equation utilizes the structural period (taken as the larger of the code-based period and the fundamental period determined by eigenvalue analysis) divided by the total weight. When the code-based period controls the effective period, the calculated value of period-based ductility is insensitive to the weight of the archetype, and structures with different weights have the same calculated effective yield point and values of period-based ductility. The code based-period was found to control for most of archetypes. This results in a situation where a structure with a larger weight tends to have a lower $\delta_{y,eff}$, implying a higher equivalent stiffness, which is counter-intuitive. Very large values of μ_T , however, do not have a major impact on the spectral shape factor, *SSF*, because there is a low saturation point in the relation between μ_T and *SSF*.

The Methodology requires consideration of the performance of structures subjected to earthquake ground motions exceeding the Maximum Considered Earthquake (MCE). While stringent criteria can be justified for assuring a uniform risk of collapse, this is especially demanding on less ductile systems that are not appropriately detailed for severe seismic loading. This might be a contributing factor as to why the ordinary RMSW archetypes generally failed the performance evaluation criteria.

3.9.3 Recommendations for Further Investigation

This study focused on rectangular cantilever wall systems, but masonry buildings can have many different wall configurations, including flanged walls and coupled walls. Many masonry buildings are low-rise box systems with perforated shear walls of many different and irregular opening sizes and arrangements. All these system variations would need to be studied to fully characterize the seismic performance of reinforced masonry structures and identify appropriate seismic performance factors.

Additional experimental data are needed to calibrate analytical models for different wall systems. The modeling of perforated wall systems presents a major challenge, and experimental data for wall components in such systems are extremely limited. This study has indicated that even for cantilever walls, the current analytical modeling capabilities with beam-column elements leave much room for improvement. The reliability of an analytical model depends on a good estimate of the effective plastic-hinge length in a flexure-dominated wall. Furthermore, reliable analytical models are needed to simulate the shear failure of a wall system.

Experimental data on this are limited, especially for walls with height to length ratios greater than one.

Current code provisions do not adequately distinguish between the wide range of performance characteristics of different masonry wall systems for which the use of the same *R* factor might not be appropriate. In particular, current codes do not account for the fact that the ductility demands induced by an earthquake ground motion on low-rise walls and high-rise walls can be very different. Their ductility capacities can be very different as well, so that different *R* factors may be needed for low-rise and high-rise walls. Furthermore, the assessment of the ductility demands and the collapse condition for low-rise walls requires additional information. Further research is needed to clarify these issues and to provide general and consistent guidelines for modeling of reinforced masonry shear walls.

Chapter 4
Trial Application: Reinforced Concrete Shear Wall Structures

4.1 Introduction

This chapter presents a trial application of the FEMA P-695 Methodology on special reinforced concrete shear wall (special RCSW) and ordinary reinforced concrete shear wall (ordinary RCSW) structures. It summarizes design requirements and available test data for reinforced concrete shear walls, explains the development of concrete shear wall archetype configurations, documents the nonlinear modeling approach, presents the results of a performance evaluation, and summarizes observations on the Methodology specific to reinforced concrete shear wall systems.

4.2 Overview and Approach

In this trial application, special and ordinary reinforced concrete shear wall systems, as defined in ACI 318-08, *Building Code Requirements for Structural Concrete* (ACI, 2008a), were considered as if they were new systems proposed for inclusion in ASCE/SEI 7-05, *Minimum Design Loads for Buildings and Other Structures* (ASCE, 2006). Although the intent was to treat special and ordinary concrete shear wall systems as if they were new systems, the purpose was not to re-derive or validate seismic performance factors (R, Ω_0, and C_d) for these systems. Rather it was to examine whether concrete shear wall systems would satisfy the acceptance criteria of the FEMA P-695 Methodology, test the application of the Methodology with respect to these systems, and identify possible improvements to the Methodology or current concrete shear wall design provisions.

The system design requirements of ASCE/SEI 7-05, including minimum base shear and story drift limits, were used as the basis for design, with the exception that C_d was taken equal to R, as specified in the FEMA P-695 Methodology. Values of R for non-load-bearing special RCSW and ordinary RCSW systems are 6 and 5, respectively.

Reinforced concrete shear wall systems can have many different configurations, including pier-spandrel systems with regular or irregularly shaped openings, cantilever or coupled wall systems, and walls with rectangular or flanged cross sections. For practical reasons, the scope of the beta testing effort on reinforced concrete shear walls was necessarily limited. A single wall configuration, cantilever with rectangular cross section, was used to investigate results for a range of building

heights and design parameters. The selection of this configuration, and the development of corresponding index archetype designs for concrete shear wall buildings, is described below.

4.3 Structural System Information

4.3.1 Design Requirements

Proportioning and detailing of reinforced concrete walls was based on ACI 318-08 requirements, subject to ASCE/SEI 7-05 Chapter 14 amendments. In the case of special RCSWs, the requirements of ACI 318-08 Chapter 21 were applied. For ordinary RCSWs, the requirements of Chapter 14 were applied.

Shear and anchorage requirements for web reinforcement were based on ACI 318-08 Chapter 21 for special RCSWs, and Chapter 14 (including Chapter 11 for shear design) for ordinary RCSWs.

4.3.2 Quality Rating of Design Requirements

The quality of design requirements for special and ordinary walls varies significantly depending on the design action. Determination of wall yield and nominal moment strengths in the presence of relatively low levels of axial load (i.e., $P < 0.15 A_g f_c'$) are generally within 10% of values determined from experimental tests on walls governed by flexure. Test results for higher levels of axial load are not available.

Code provisions for shear strength are generally quite conservative and can significantly underestimate actual shear strength. ACI 318-08 provisions for shear strength of special RCSWs have been shown to provide essentially a lower-bound estimate of shear strength (Wood, 1990; Orakcal et al., 2009), with mean shear strength on the order of 1.5 times the code nominal strength. The ACI 318-08 equation for shear strength of special RCSWs does not account for the effects of axial compression or well-confined boundary zones on shear strength. Test results (Wallace, 1996; Orakcal et al., 2009) have shown that both of these factors can measurably increase shear strength.

Recommendations for effective bending, shear, and axial stiffness generally specify a single value to reflect the cracked stiffness of a wall section (e.g., $E_c I_{eff} = 0.5 E_c I_g$). It has been well documented in the literature (e.g., Wallace, 2007) that bending stiffness varies with moment yield strength and axial load, and that a single value is not appropriate in all cases. In consideration of the above limitations, a quality rating of (B) Good was assigned to the design requirements for special and ordinary RCSWs.

4.3.3 Test Data

Comparisons between test data and model results were used to help determine appropriate modeling parameters for material relations and failure modes (e.g.,

crushing, buckling). Modeling parameters associated with axial-bending behavior were based primarily on test data reported by, or summarized in, Orakcal et al. (2004), Orakcal and Wallace (2006), and Wallace (2007). Additional information for relatively slender walls was taken from Corley et al. (1981), Oesterle et al. (1976, 1979), Shiu et al. (1981), Aktan et al. (1985), Goodsir (1985), Wallace (1996), Thomsen and Wallace (1995, 2004), and Waugh et al. (2008). Test data for low-rise walls were taken from Wood (1990), Massone et al. (2006), Massone (2006), Wallace (2007), Orakcal et al. (2009), and Massone et al. (2009).

The tests conducted by Corley et al. (1981), Oesterle et al. (1976, 1979), and Shiu et al. (1981), address the influence of shear on the behavior of relatively slender walls (most with aspect ratio of 2.4), including the impact of shear stress level on wall deformation capacity and web crushing failures. The upper-bound ACI 318-08 wall design shear stress limit of $10\sqrt{f_c'}$ is based on these tests.

The results reported by Thomsen and Wallace (2004), Orakcal and Wallace (2006), Wallace (2007), and Waugh et al. (2008) were used to define modeling and material parameters for axial-bending behavior, such as uniaxial material stress-strain relations for concrete and reinforcement. Where uniaxial material relations are used, the bending stiffness and yield moment vary with axial load per the defined material relations. Modeling of confined concrete behavior, tension-stiffening, and the impact of surrounding concrete on the yield strength of longitudinal reinforcement are based on well-established research results. Comparisons between experimental and analytical results based on these material parameters indicate that overall load versus deformation response of walls dominated by nonlinear flexural responses is well captured (Orakcal and Wallace 2006); however, additional comparisons were performed to assess how best to define modeling parameters within the OpenSees, *Open System for Earthquake Engineering Simulation* (OpenSees, 2007) analysis platform used in this study.

4.3.4 Quality Rating of Test Data

Although available test results provide useful data to help define modeling and material parameters for axial-bending behavior and shear strength, the number of tests that have been conducted is generally insufficient to assess uncertainty and the range of variability in design limits. They do not enable determination of lateral strength degradation or collapse as influenced by, for example, concrete crushing, rebar buckling, and rebar fracture. Nor are they sufficient for characterizing behavior of walls loaded with significant axial stress. In general, tests were stopped after only modest to moderate levels of lateral strength degradation was observed, so they do not provide data for determining residual strength or collapse (e.g., loss of axial load capacity). In consideration of the above limitations, a quality rating of (B) Good was assigned to the test data for special and ordinary RCSWs.

4.4 Archetype Configurations

The design space for reinforced concrete shear wall systems includes many different configurations. Possible configurations include cantilever walls, coupled walls, core walls, and perimeter walls. For each of these configurations, various wall cross sections are possible, including rectangular, T-shaped, C-shaped, and barbell. Each of these can be perforated wall systems, with regular or irregular openings, and can be strongly or weakly coupled with adjacent walls in the system.

In coupled wall systems, the degree of coupling can vary substantially. For example, slabs typically provide only minor coupling. Coupling beams with aspect ratios between 2.0 and 4.0 provide substantial coupling, whereas horizontal wall segments with aspect ratios less than 1.0 provide strong or full coupling. Overall system behavior is also impacted by foundation behavior. Large overturning forces at the foundation can produce significant rigid body rotations in the system if the soil-structure interface is flexible or can increase plastic deformation demands in the walls if the foundation is stiff.

Given the large design space for reinforced concrete shear wall systems, the scope of the investigation was necessarily limited. Many subsets were considered, including cantilever walls with non-rectangular cross sections and coupled walls with rectangular or non-rectangular cross sections. Because of the range of possible design variables for non-rectangular, coupled wall sections, including flange length, longitudinal reinforcement ratio, and coupling beam aspect ratio, more potential archetypes existed than could be meaningfully considered within this limited study.

A single wall configuration, cantilever with rectangular cross section, was selected to investigate results for a range of building heights and design parameters. This subset was selected because the vast majority of test data and comparisons between experimental and analytical results reported in the literature are focused on this subset, and because the design space could be limited to a sufficient number of cases within each sub-group to enable meaningful determination of performance group data.

Within ASCE/SEI 7-05, reinforced concrete shear walls are permitted in both bearing wall systems and building frame systems. To further limit the design space, archetypes were configured as shear walls within a building frame system because it was difficult to vary key design parameters and maintain archetype configurations that remotely resembled a bearing wall system. Other key design variables that were considered included special versus ordinary detailing, building height, wall aspect ratio (height/length), axial load level, shear stress level, and the amount of transverse reinforcement provided at the wall boundary.

The plan configuration selected for reinforced concrete shear wall archetypes is shown in Figure 4-1. Both special RCSW and ordinary RCSW archetypes were

considered. Special RCSWs were designed for Seismic Design Category (SDC) D_{max} and SDC D_{min}, while ordinary RCSWs were designed for SDC C_{max} and SDC C_{min}. To produce lower-bound designs without excessive overstrength, the plan dimensions and length of walls in each direction were varied in each archetype to optimize strength relative to the level of seismic design loading. Archetypes were configured to maximize the shear stress and adjust the axial load levels to control other important behaviors.

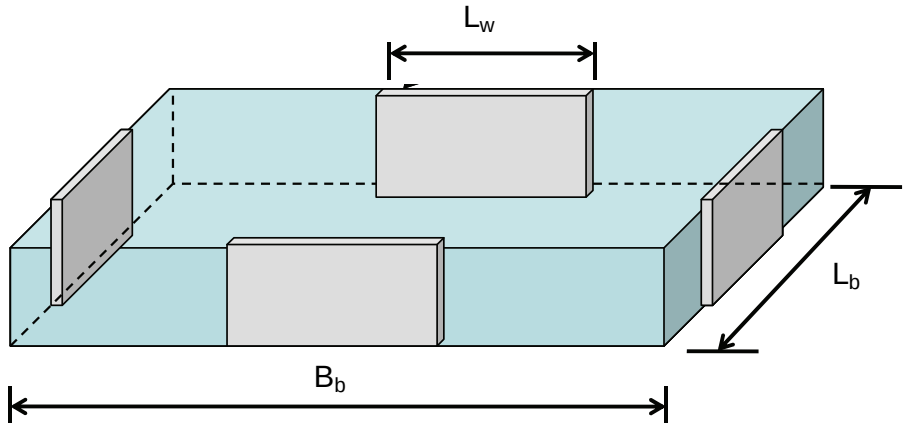

Figure 4-1 Plan configuration for reinforced concrete shear wall archetypes.

For the purpose of estimating design gravity loads, the floor and roof systems were assumed to consist of cast-in-place concrete slabs. While the absolute magnitude of axial load on a wall will depend on the height of the building, two levels of axial load were included to address the potential impact of axial load on collapse behavior.

Building heights of 1, 2, 4, 8, and 12 stories were considered. Above 12 stories, use of cantilever walls is not economical (i.e., in practical applications, a coupled wall would be used), so taller archetypes were not considered. Story heights were selected to be 13 feet in the first story and 12 feet in the remaining stories, although story height was not a critical design parameter. Wall aspect ratios were selected for a given story height to produce wall behaviors ranging from shear-controlled to flexure-shear or flexural-controlled. Variation in axial stress was considered for each aspect ratio.

Archetypes were grouped into performance groups containing a set of common features or behavioral characteristics, including Seismic Design Category, gravity load level, and code-based period of the structure. Considering the design variables listed above, a total of 40 archetypes were developed. These were divided into 16 performance groups, eight attributed to special RCSWs and eight attributed to ordinary RCSWs, as shown in Table 4-1 and Table 4-2. Performance groups with less than three archetypes did not meet the minimum number of archetypes per performance group required in a full application of the Methodology.

Table 4-1 Performance Groups for Evaluation of Special Reinforced Concrete Shear Wall Archetypes

Performance Group Summary					
Group No.	Grouping Criteria				Number of Archetypes
	Basic Config.	Design Load Level		Period Domain	
		Gravity	Seismic		
PG-1S	A	High	SDC D_{max}	Short	3[1]
PG-2S				Long	2[2]
PG-3S			SDC D_{min}	Short	2[3]
PG-4S				Long	3[4]
PG-5S		Low	SDC D_{max}	Short	3[1]
PG-6S				Long	2[2]
PG-7S			SDC D_{min}	Short	2[3]
PG-8S				Long	3[4]

[1] Short-period, SDC D_{max}, performance groups, PG-1 and PG-5, include 1-story, 2-story and 4-story archetypes.

[2] Long-period, SDC D_{max}, performance groups, PG-2 and PG-6, include 8-story and 12-story archetypes.

[3] Short-period, SDC D_{min}, performance groups, PG-3 and PG-7, include 1-story and 2-story archetypes.

[4] Long-period, SDC D_{min}, performance groups, PG-4 and PG-8, include 4-story, 8-story, and 12-story archetypes.

Table 4-2 Performance Groups for Evaluation of Ordinary Reinforced Concrete Shear Wall Archetypes

Performance Group Summary					
Group No.	Grouping Criteria				Number of Archetypes
	Basic Config.	Design Load Level		Period Domain	
		Gravity	Seismic		
PG-1O	A	High	SDC C_{max}	Short	2[1]
PG-2O				Long	3[2]
PG-3O			SDC C_{min}	Short	2[1]
PG-4O				Long	3[2]
PG-5O		Low	SDC C_{max}	Short	2[1]
PG-6O				Long	3[2]
PG-7O			SDC C_{min}	Short	2[1]
PG-8O				Long	3[2]

[1] Short-period performance groups, PG-1, PG-3, PG-5 and PG-7, include 1-story and 2-story archetypes.

[2] Long-period performance groups, PG-2, PG-4, PG-6 and PG-8, include 4-story, 8-story, and 12-story archetypes.

Key seismic design parameters for the special RCSW and ordinary RCSW archetypes are summarized in Table 4-3 and Table 4-4. These include the code-based period, T (calculated using the equation, $T=C_uT_a$, provided in ASCE/SEI 7-05), fundamental period, T_1 (calculated from eigenvalue analysis), the seismic base shear coefficient, V/W, and the MCE-level spectral acceleration, S_{MT}.

Table 4-3 Special Reinforced Concrete Shear Wall Archetype Design Properties

Archetype Design ID Number	No. of Stories	Key Archetype Design Parameters						
		Gravity Loads	Seismic Design Criteria					$S_{MT}(T)$ (g)
			SDC	R	T (sec)	T_1 (sec)	V/W (g)	
Performance Group No. PG-1S								
1	1	High	D_{max}	6	0.25	0.26	0.17	1.50
2	2	High	D_{max}	6	0.31	0.50	0.17	1.50
3	4	High	D_{max}	6	0.52	0.55	0.17	1.50
Performance Group No. PG-2S								
4	8	High	D_{max}	6	0.87	0.76	0.12	1.03
5	12	High	D_{max}	6	1.17	0.99	0.09	0.77
Performance Group No. PG-3S								
6	1	High	D_{min}	6	0.25	0.25	0.08	0.75
7	2	High	D_{min}	6	0.31	0.38	0.08	0.75
Performance Group No. PG-4S								
8	4	High	D_{min}	6	0.52	0.53	0.06	0.58
9	8	High	D_{min}	6	0.87	0.71	0.04	0.34
10	12	High	D_{min}	6	1.17	0.94	0.03	0.26
Performance Group No. PG-5S								
11	1	Low	D_{max}	6	0.25	0.26	0.17	1.50
12	2	Low	D_{max}	6	0.31	0.50	0.17	1.50
13	4	Low	D_{max}	6	0.52	0.66	0.17	1.50
Performance Group No. PG-6S								
14	8	Low	D_{max}	6	0.87	0.73	0.12	1.03
15	12	Low	D_{max}	6	1.17	1.23	0.09	0.77
Performance Group No. PG-7S								
16	1	Low	D_{min}	6	0.25	0.25	0.08	0.75
17	2	Low	D_{min}	6	0.31	0.38	0.08	0.75
Performance Group No. PG-8S								
18	4	Low	D_{min}	6	0.52	0.53	0.06	0.58
19	8	Low	D_{min}	6	0.87	0.74	0.04	0.34
20	12	Low	D_{min}	6	1.17	0.92	0.03	0.26

Values of the seismic base shear coefficient, *V*/*W*, and the MCE-level spectral acceleration, S_{MT}, for SDC D_{max}, D_{min}, C_{max}, and C_{min} were determined using the code-based structural period, *T*, assuming a lower-bound value of 0.25 seconds in accordance with the Methodology.

Table 4-4 Ordinary Reinforced Concrete Shear Wall Archetype Design Properties

Archetype Design ID Number	No. of Stories	Key Archetype Design Parameters						
		Gravity Loads	Seismic Design Criteria					$S_{MT}(T)$ (g)
			SDC	*R*	*T* (sec)	T_1 (sec)	*V*/*W* (g)	
Performance Group No. PG-1O								
21	1	High	C_{max}	5	0.25	0.25	0.10	0.75
22	2	High	C_{max}	5	0.31	0.37	0.10	0.75
Performance Group No. PG-2O								
23	4	High	C_{max}	5	0.52	0.54	0.08	0.58
24	8	High	C_{max}	5	0.87	0.62	0.05	0.34
25	12	High	C_{max}	5	1.17	0.82	0.03	0.26
Performance Group No. PG-3O								
26	1	High	C_{min}	5	0.25	0.25	0.07	0.5
27	2	High	C_{min}	5	0.31	0.37	0.07	0.5
Performance Group No. PG-4O								
28	4	High	C_{min}	5	0.52	0.54	0.05	0.38
29	8	High	C_{min}	5	0.87	0.62	0.03	0.23
30	12	High	C_{min}	5	1.17	0.82	0.02	0.17
Performance Group No. PG-5O								
31	1	Low	C_{max}	5	0.25	0.25	0.10	0.75
32	2	Low	C_{max}	5	0.31	0.37	0.10	0.75
Performance Group No. PG-6O								
33	4	Low	C_{max}	5	0.52	0.54	0.08	0.58
34	8	Low	C_{max}	5	0.87	0.66	0.05	0.34
35	12	Low	C_{max}	5	1.17	0.87	0.03	0.26
Performance Group No. PG-7O								
36	1	Low	C_{min}	5	0.25	0.25	0.07	0.5
37	2	Low	C_{min}	5	0.31	0.37	0.07	0.5
Performance Group No. PG-8O								
38	4	Low	C_{min}	5	0.52	0.54	0.05	0.38
39	8	Low	C_{min}	5	0.87	0.66	0.03	0.23
40	12	Low	C_{min}	5	1.17	0.87	0.02	0.17

Design forces were determined using the Equivalent Lateral Force (ELF) procedure defined in ASCE/SEI 7-05 and the code-based period. Vertical story forces were determined using the computed period T_1 (calculated from eigenvalue analysis). Archetypes were assumed to be fixed at the base, so the potential effects of soil-structure interaction were not considered. Torsional response was also not considered.

For the 1- and 2-story archetypes, wall aspect ratios were set at 0.5 and 1.0, respectively, to produce walls that were likely governed by shear behavior. In the taller archetypes (4-, 8-, and 12-stories), aspect ratios were set at approximately 2.0, 3.0, and 3.5, respectively. In the 4- and 8-story archetypes, nonlinear responses tended to be dominated by flexural deformations, although failure could be defined by shear (e.g., web crushing). In the 12-story archetypes, the relatively high-aspect ratio walls were more likely to be governed by flexural failure modes, such as rebar buckling or fracture at wall boundaries.

Both low ($0.075A_g f_c'$) and high ($0.2A_g f_c'$) axial stress levels were considered, except in the case of 1- and 2-story buildings, in which only the $0.075A_g f_c'$ axial load level was used. In the 1- and 2-story archetypes, wall thicknesses were selected to limit the shear stress to $8\sqrt{f_c'}$, allowed on average for all walls in ACI 318-08, because flexural yielding was not expected to occur prior to shear failure.

In the taller (4-, 8-, and 12-story) archetypes, it was not possible to design walls near a shear stress level of $8\sqrt{f_c'}$ without using unrealistically large quantities of boundary reinforcement or unrealistically narrow web thicknesses. In these cases, walls were designed to produce as high a shear stress as possible while still resulting in a wall section that was deemed to be reasonably constructible. Over the height of multistory archetypes, quantities of reinforcing steel were varied at every two floor levels to account for changes in design forces.

The need for boundary elements was checked using both the displacement-based and stress-based approaches contained in ACI 318-08. Transverse reinforcement at the wall boundaries was based on the minimum required using the two approaches to ensure that the design satisfied minimum requirements. In all cases, the displacement-based approach produced less overall required transverse reinforcement, which is common in the case of planar, cantilever walls.

In general, strength requirements governed proportioning of the wall cross sections; however, in some cases (e.g., 8- and 12-story archetypes), drift limits governed. Detailed information used in design, along with additional details for the resulting reinforced concrete shear wall designs, including plan configurations and wall reinforcing patterns for each archetype, are provided in Appendix B.

4.5 Nonlinear Model Development

4.5.1 Modeling Approach

For nonlinear analysis, each archetype was idealized as an uncoupled cantilever wall with appropriate gravity load and seismic mass determined based on respective tributary areas. The base of each wall was assumed to be perfectly fixed, without consideration of soil-structure interaction effects.

Displacement-based beam-column elements were used to model the inelastic flexural behavior of the walls, and zero-length translational shear springs were used to model shear deformation. All models included a leaning column with no lateral stiffness to account for P-Delta effects from the gravity load in the system that was not directly tributary to the wall elements. The number of elements and number of integration points used in the models were optimized based on the results of sensitivity studies reported in Appendix B.

4.5.2 Nonlinear Material Model for Concrete

Various concrete material models are available in OpenSees, including a simplified version of the Chang and Mander (1994) model, designated C07; and a cyclic version of the modified Kent-Park model (Scott et al., 1982) developed by Yassin (1994), designated C02. Sensitivity studies presented by Orakcal et al. (2006) indicate that analytical results produced using the C07 model match experimental results modestly better than the C02 model; however, numerous convergence problems were encountered with the C07 model.

As a result, the OpenSees C02 model shown in Figure 4-2 was used for both confined and unconfined concrete. For unconfined concrete, the peak strength parameter, f_{pc}, was selected as 6.1 ksi, and the strain at peak strength, e_{psc0}, was selected to be 0.0027, which yields an initial modulus ($E_0 = 2f_{pc}/e_{psc0}$) of around 4500 ksi. Stress and strain values used to define the post-peak descending branch of the unconfined stress-strain relation (f_{pcU} and e_{psU}) were selected to be 1.4 ksi and 0.01, respectively.

For confined concrete, the parameters (f_{pc}, e_{psc0}, e_{psU}, f_{pcU}) were determined based on the Razvi and Saatcioglu (1999) model, which uses the unconfined concrete parameters (f_{pc} and e_{psc0}) and the boundary reinforcement details to determine the confined concrete peak stress and strain (f_{pc} and e_{psc}) and to define the post-peak behavior parameters (e_{psU} and f_{pcU}).

In this study, concrete crushing was taken as the point where the post-peak linear descending branch reaches the residual concrete stress (defined as 20% of the peak confined concrete stress). Confined concrete model parameters were varied over the wall height at locations where transverse reinforcement changed.

Concrete tensile strength, f_t, concrete tensile modulus, E_t, and unloading parameter, λ, which defines the unloading slope in terms of the initial concrete modulus (i.e.,

unloading slope = λE_0), were selected to be 0.586 ksi, 410 ksi, and 0.1, respectively, based on the information provided by Orakcal and Wallace (2006).

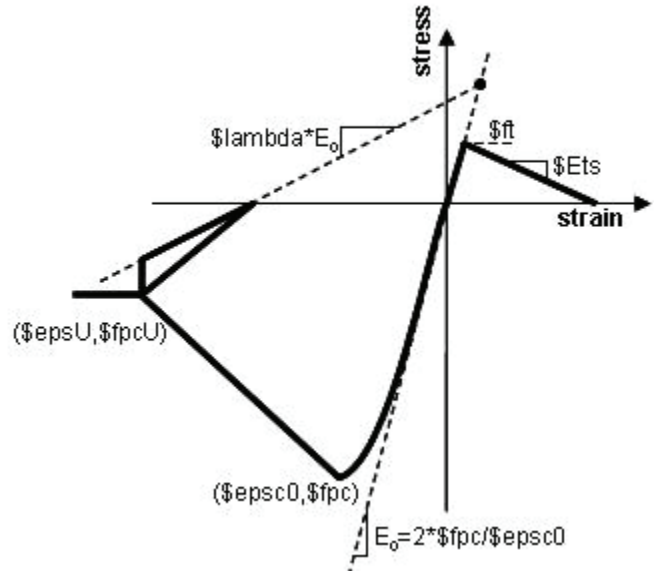

Figure 4-2 Concrete stress-strain behavior model (C02) contained in OpenSees.

4.5.3 Nonlinear Material Model for Reinforcing Steel

Reinforcing steel was modeled as a hysteretic material in OpenSees, as shown in Figure 4-3. Expected values of yield and ultimate strength were taken as 68 ksi and 100 ksi, respectively, based on results reported by Mirza et al. (1979) and Bournonville et al. (2004). Studies of walls with rectangular cross sections, tested by Thomsen and Wallace (1995, 2004), indicate that strength loss at a strain of 0.03 to 0.035 produced good comparisons between modeled and tested results.

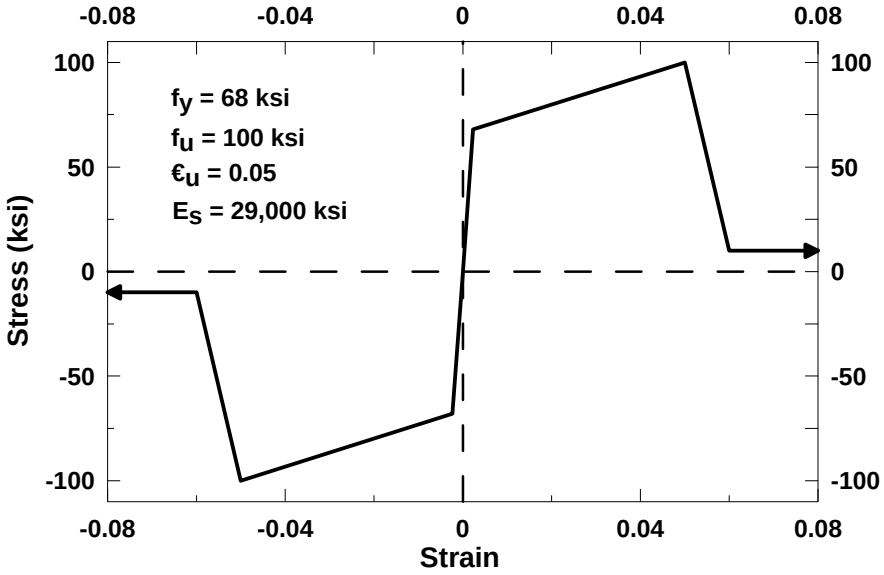

Figure 4-3 Hysteretic material model for reinforcing steel.

Pantazopoulou (1998) investigated the relationship among transverse reinforcement (quantity, spacing), longitudinal bar diameter, and concrete compressive strain on rebar buckling. Findings showed that the concrete compressive strain at buckling increases with an increase in the effective confinement (quantity and effectiveness of the transverse reinforcement) and with a decrease in the ratio of hoop/tie spacing to longitudinal bar diameter (s/d_b). Rodriguez et al. (1999) reported reverse cyclic test results of rebar (in air) and relate rebar bucking to the magnitude of the strain reversal.

Based on these results, a tensile strain value of 0.05 was selected to correspond to failure associated with rebar buckling and subsequent rebar fracture. In the model, the stress capacity of the reinforcing steel was assumed to be near zero once a strain of 0.05 is reached. Use of a more complex model was not justified given the uncertainty associated with existing test results and models.

4.5.4 Extension and Slip of Reinforcing Steel

The potential impact of reinforcing steel extension and slip was included in the models through the addition of rotational springs at the base of the walls to account for softening of the load-versus-deformation response (Figure 4-4). The model assumes that a crack forms along the entire length of the base of the wall and reduces the flexural rigidity of the wall, leading to a softer moment-rotation response.

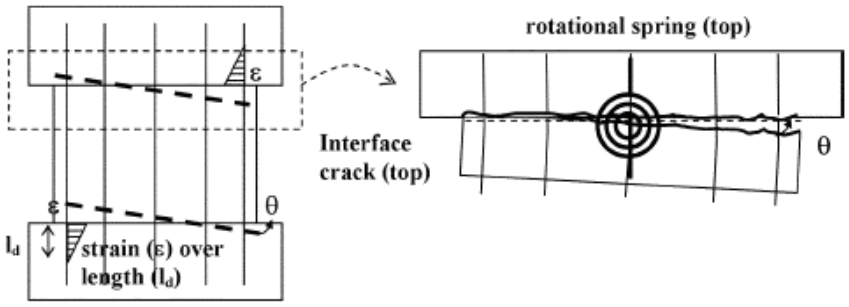

Figure 4-4 Rotational spring model for reinforcing steel extension and slip (Massone et al., 2009).

Moment-curvature relations were computed at the base of all walls for all archetypes to determine the yield moment, M_y, considering actual material properties, confinement effects, and steel hardening together with the applied axial load. As illustrated in the figure, a linear strain distribution was assumed along the development length, l_d, of the longitudinal bars with maximum strains developing at the wall-foundation interface. Cumulative displacements (bar extensions) were then obtained by integrating the strains along l_d, and were divided by the neutral axis depth to achieve the wall base rotation (θ_y). Rotational springs that were implemented in OpenSees consisted of elastic materials having moment-rotation stiffness values of M_y/θ_y.

4.5.5 Shear Model

In most structural analysis programs, limited options exist to model nonlinear shear behavior. These include multilinear segments used to define key points associated at cracking, yielding, and degradation of strength. In some cases, additional points are included to model residual strength and loss of vertical-load-carrying capacity. One such generalized model for shear backbone behavior is provided in ASCE/SEI 41-06, *Seismic Rehabilitation of Existing Buildings* (ASCE, 2007).

Test results indicate that nonlinear shear deformations occur due to coupling between axial-bending and shear behavior (Massone and Wallace, 2004), and available cyclic material models in OpenSees do not include this coupled behavior. A sensitivity study was conducted where the cracking force (stress) level and the post-cracking slope were varied. This study is presented in Appendix B, and results showed that the shear modulus should be reduced to account for nonlinear shear deformations.

The model used in this study for slender walls, where flexural yielding limits the wall shear demands, is shown in Figure 4-5. This relation is similar to that given in ASCE/SEI 41-06, except the cracking level is taken as 0.5 times the shear force required to reach the yield moment at the wall base, where $V=M_{pr}/h_{eff}$, $M_{pr}=1.25M_n$, h_{eff} is the effective height of the resultant lateral force for the code prescribed distribution of lateral forces, and the shear strain at yield is taken as 0.0015. This relationship was used for the 4-, 8-, and 12-story walls with aspect ratios of 2.0, 3.0, and 3.5, respectively.

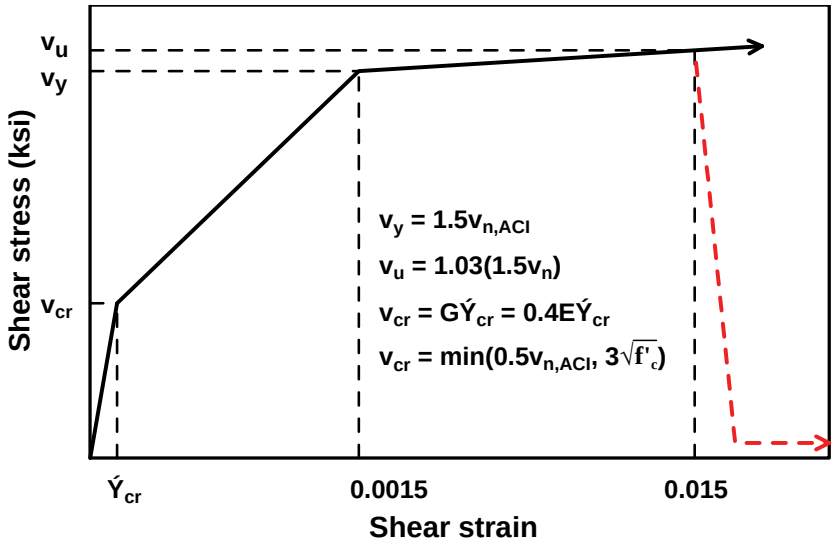

Figure 4-5 Generalized shear model adapted from ASCE/SEI 41-06.

For walls that were expected to be controlled by shear (i.e., 1- and 2-story walls with aspect ratios of 0.5 and 1.0, respectively), the relation used in ASCE/SEI 41-06 was modified slightly to consider the level of axial stress used in this study ($0.075A_g f_c'$). Test results reported by Massone (2006) indicate that a shear strain of approximately

0.0015 at shear yield for axial load levels of between $0.05A_g f_c'$ and $0.10A_g f_c'$. Cracking was assumed to occur at $3\sqrt{f_c'}$, but not greater than $0.5V_n$ (which is slightly less than the value of $0.6V_n$ used in ASCE/SEI 41-06, to be consistent with the relation developed for walls controlled by flexure). Strength degradation was assumed to occur at a strain of 0.015, which is 50% more than allowed in ASCE/SEI 41-06, because the values in ASCE/SEI 41-06 are based on lightly-reinforced and poorly detailed walls, and new walls with code-conforming details were assumed to be capable of achieving more rotation at strength degradation (Hidalgo et al., 2002; Salonikios, 2001; Salonikios et al., 1999; Wood, 1991).

4.5.6 Damping

ASCE/SEI 7-05 specifies that periods of $0.2T_1$ and $1.5T_1$ be used to determine Rayleigh damping coefficients for nonlinear analysis. Consistent with recommendations contained in the PEER/ATC 72-1 report (PEER/ATC, 2010), a damping ratio of 2.5% was used. It is noted that $0.2T_1$ is approximately equal to the third mode period of a frame building (i.e., $T_3 = T_1/5$) but in shear wall buildings, the third mode period is closer to $T_1/7$, or approximately $0.15T_1$. The difference between $0.2T_1$ and $0.15T_1$ was not considered significant, and a value of $0.2T_1$ was used for consistency with common practice. The Rayleigh damping model is plotted in Figure 4-6.

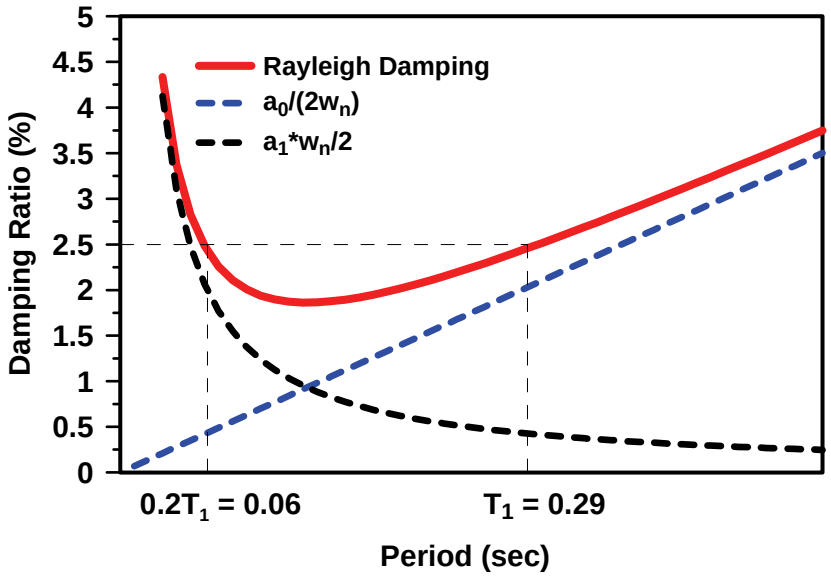

Figure 4-6 Plot of Rayleigh damping model, ζ = 2.5%, at T_1 and $0.2T_1$, for archetype ID 8.

4.5.7 Model Validation

The modeling approach described herein has been validated with experimental data in the literature. Parameters for uniaxial material models for concrete and reinforcement were developed based on the results reported by Orakcal and Wallace (2006) and Orakcal et al. (2006), which also included test and model

comparisons indicating that similar material models could reproduce the measured force versus flexural deformation behavior well.

Comparisons between test and model results have also been performed to assess how well models capture measured load versus top displacement behavior. Wall specimen RW2, a relatively slender (h_w/l_w = 3) cantilever wall with rectangular cross section tested by Thomsen and Wallace (1995, 2004) was used for this purpose. Comparisons showing good agreement between test results and model predictions are presented in Orakcal and Wallace (2006) and Waugh et al. (2008).

4.5.8 Non-Simulated Failure Criteria

Because of analytical limitations, several failure modes important to shear wall behavior were not explicitly simulated. Criteria for non-simulated failure modes are summarized in the sections that follow.

4.5.8.1 Reinforcing Steel Buckling and Fracture

A strain of 0.05 was used to define buckling (and fracture) of a single reinforcing bar. Failure of a single bar, however, was not considered sufficient to cause collapse of a shear wall archetype. This conclusion is supported by tests in the literature (e.g. Thomsen and Wallace, 1995). Failure indicative of collapse was assumed to occur when the reinforcing steel within one-quarter of the wall length fractures or buckles (Figure 4-7). This condition would be expected to produce a substantial drop in lateral strength and stiffness, and a substantial increase in the potential for both side-sway collapse due to P-Delta effects, and loss of axial-load-carrying capacity.

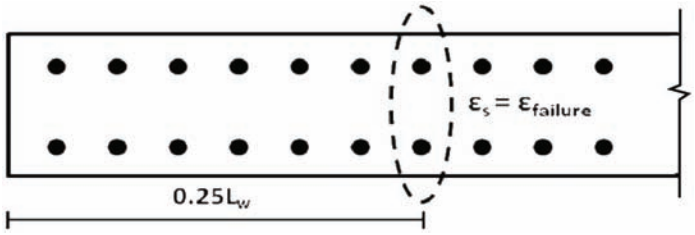

Figure 4-7 Non-simulated criteria for buckling and fracture of reinforcing steel.

Failure strains, $\varepsilon_{failure}$, were taken as 0.05 for all special RCSW archetypes, 0.05 for ordinary RCSW archetypes under low axial loading, and 0.02 for ordinary RCSW archetypes under high axial loading. Results of pushover analyses were used to assess whether or not these values were reasonable. Results for the 4-story, low axial load, SDC C_{max} archetype (ID 33) are shown in Figure 4-8, and results for the 4-story, high axial load, SDC C_{max} archetype (ID 23) are shown in Figure 4-9.

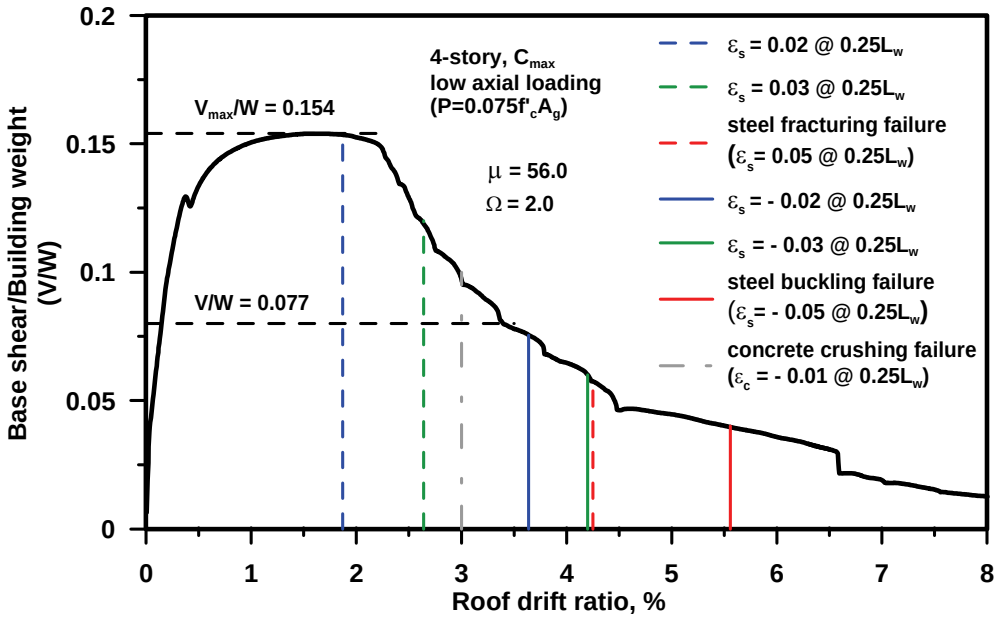

Figure 4-8 Pushover analysis results for the 4-story, low axial load, SDC C_{max} archetype (ID 33).

In the case of walls subjected to low axial load levels (Figure 4-8), when reinforcing steel located at $0.25L_w$ reached strain values of 0.02, 0.03, and 0.05, the wall section was observed to lose 2%, 20%, and 60% of its lateral strength, respectively. Because losses of 2% and 20% would not be expected to cause failure, a steel strain of 0.05 at fracture was considered reasonable. In the case of walls subjected to high axial load levels (Figure 4-9), steel strains of 0.02 and 0.05 at $0.25L_w$ produced reductions of 70% and 93% in peak lateral strength, so a lower criterion for steel strain at fracture was justified.

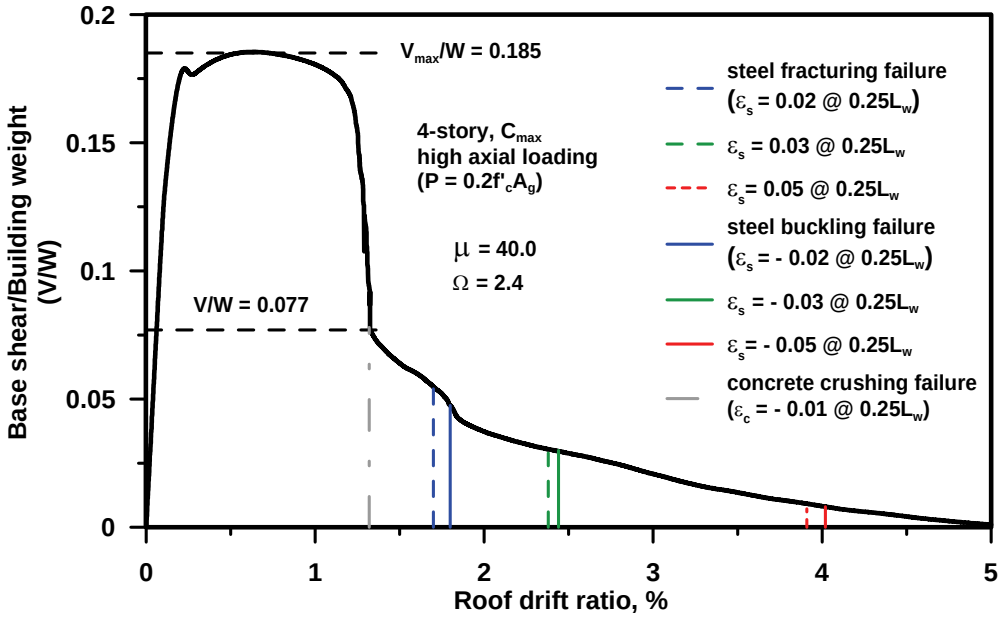

Figure 4-9 Pushover analysis results for the 4-story, high axial load, SDC C_{max} archetype (ID 23).

4.5.8.2 Concrete Crushing

The criteria established for concrete crushing were based on a specified wall length reaching a critical compressive strain, as illustrated in Figure 4-10.

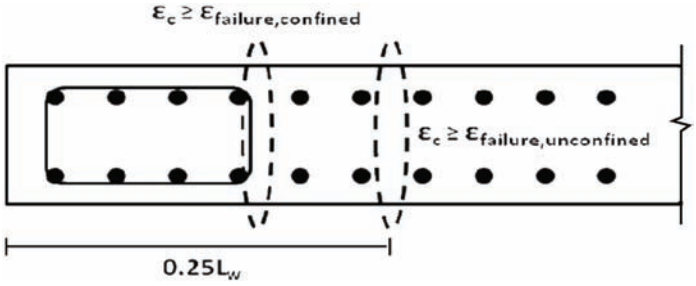

(a) Special RCSW archetypes

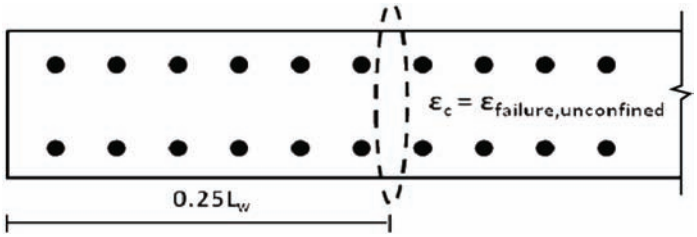

(b) Ordinary RCSW archetypes

Figure 4-10 Non-simulated criteria for crushing and spalling of concrete in: (a) special RCSW archetypes; and (b) ordinary RCSW archetypes.

Different criteria were established for special RCSWs and for ordinary RCSWs. Concrete crushing for well-confined walls (special RCSWs) was taken as the point where the post-peak linear descending branch in concrete stress-strain relation reached the residual concrete stress (defined as 20% of the peak confined concrete stress). For unconfined walls (ordinary RCSWs), the crushing strain was taken as the strain value when the stress in the post-peak, linear descending branch reached zero.

4.5.8.3 Shear Failure

For walls controlled by shear, the shear force versus deformation relation shown in Figure 4-5 was used. Within OpenSees, however, only three points are available to define shear behavior. Given the need to model uncracked and cracked stiffness, the strength-degrading portion of the relation could not be modeled, so non-simulated criteria were needed to assess this failure mode.

For walls controlled by flexure, the potential for shear failure also exists, similar to columns. However, unlike columns, specific recommendations do not exist for relatively slender walls, which are likely to yield in flexure, but will still be subjected to modest shear stress levels. Test data for low-rise and relatively slender walls with aspect ratios between 1.5 and 2.4 were reviewed to develop a relation that could be used for this study.

A review of test data indicates that a good estimate of the median shear strength is 1.5 times the nominal shear strength predicted using the equations in ACI 318-08 (Orakcal et al., 2009; Wood, 1990; Wallace, 1996). However, for walls that yield in flexure, the expected shear strength at failure is reduced from this value, depending on the level of flexural deformation. Data available to assess this relationship are plotted in Figure 4-11, for both low-rise and moderately slender walls.

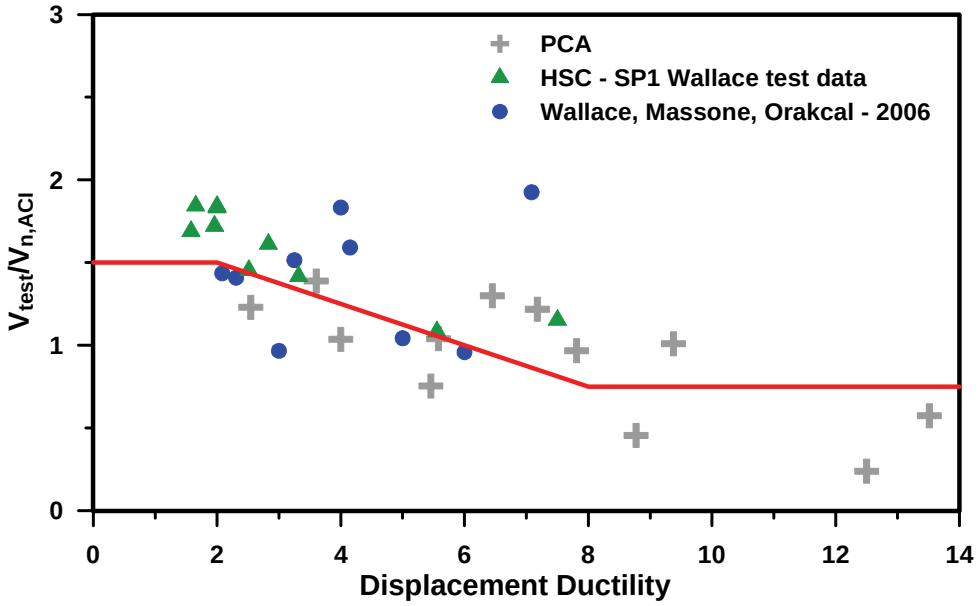

Figure 4-11 Approximate shear failure criterion used to account for the effects of flexural demand on shear behavior.

Insufficient data exist to do a detailed statistical assessment, but a simple trend was fitted to the data, as indicated in the figure. This trend is anchored at a shear strength of $1.5V_n$ for displacement ductility values less than 2.0, degrades linearly to a strength of $0.7V_n$ at a displacement ductility of 8.0, and then remains constant at $0.7V_n$ for larger ductility values. This relationship can be modified to relate shear strength to either curvature or strain ductility using various assumptions (Paulay, 1986).

4.5.8.4 Axial Failure

A model developed to predict axial load failure for lightly reinforced wall piers (Wallace et al., 2008) was used to establish a basis to assess axial failure of the archetypes. Based on results presented in Appendix B, very high drift values could be obtained from the axial failure model, especially for the 1- and 2-story archetypes. Because no test data were available to justify the use of large predicted values, lower values were selected based on judgment. Axial failure was assumed to occur if the drift ratio reached 3% in the 1- and 2-story archetypes, and 5% in the 4-, 8-, and 12-story archetypes.

4.5.9 Quality Rating of Analytical Models

Overall, the modeling approach in this study is detailed and comprehensive. Comparisons between models and test results for relatively slender cantilever walls indicate that overall load-displacement relations in flexure can be captured quite well. However, the models are known to be less accurate in predicting local strains, and several of the failure modes considered are based on local strain estimates. Also, the criteria used to assess some failure modes (e.g., rebar buckling and concrete crushing) are somewhat subjective because to a lack of data to develop more comprehensive models.

Extension and slip of reinforcing steel was not directly modeled, and the interaction between flexure and shear was accounted for in an approximate way. In consideration of the above limitations, a quality rating of B (Good) was assigned to the analytical models used in this study.

4.6 Nonlinear Analyses

Nonlinear static pushover analyses and simplified incremental dynamic analyses (IDAs) were used to evaluate system overstrength, period-based ductility, and the collapse capacity of reinforced concrete shear wall archetypes. Selected pushover results are shown in Figures 4-12 through 4-16.

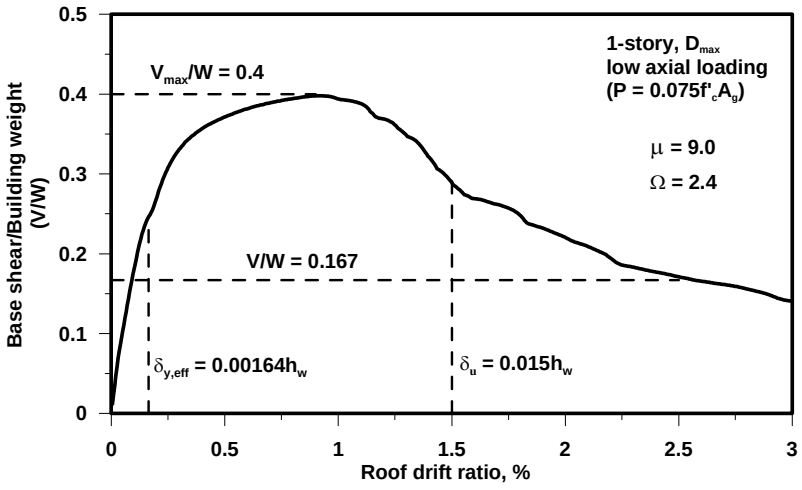

Figure 4-12 Pushover results for the 1-story, low axial load, SDC D_{max} archetype (ID 11).

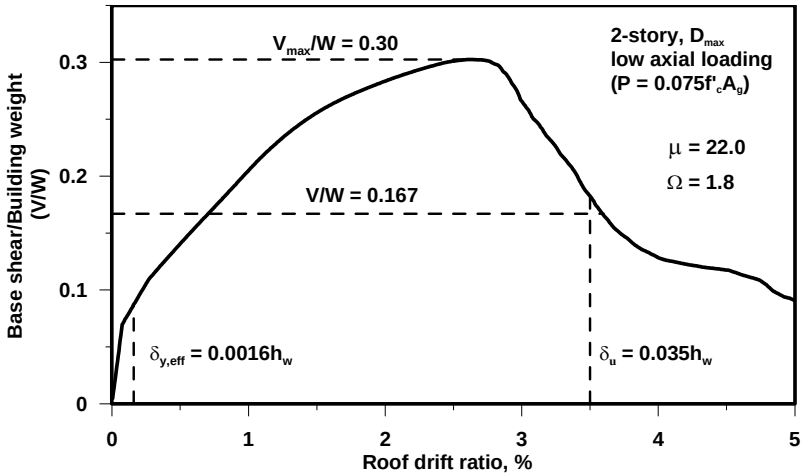

Figure 4-13 Pushover results for the 2-story, low axial load, SDC D_{max} archetype (ID 12).

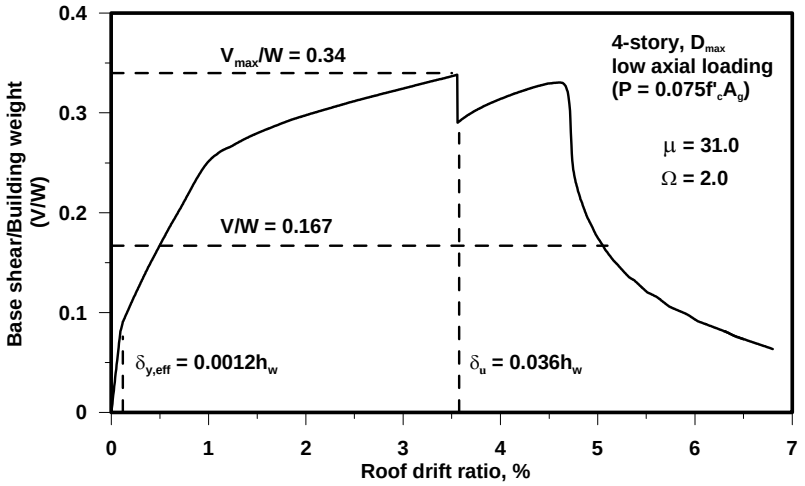

Figure 4-14 Pushover results for the 4-story, low axial load, SDC D_{max} archetype (ID 13).

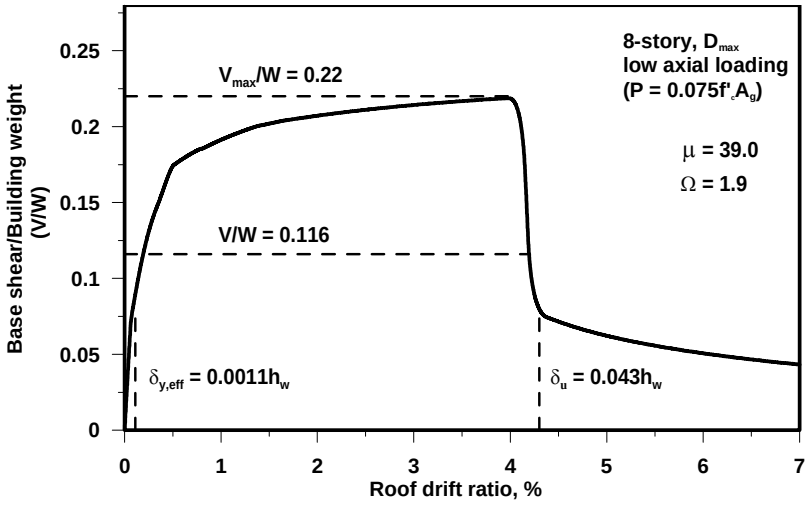

Figure 4-15 Pushover results for the 8-story, low axial load, SDC D_{max} archetype (ID 14).

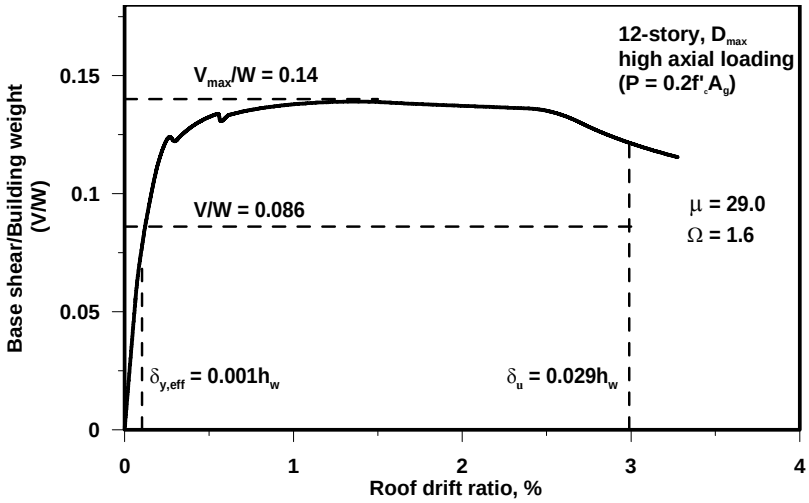

Figure 4-16 Pushover results for the 12-story, high axial load, SDC D_{max} archetype (ID 5).

For each archetype, pushover analyses were used to compute the system overstrength factor, Ω_0, and period-based ductility, μ_T, and to assess the validity or consistency of the results. The ultimate roof drift in the above figures was governed by shear failure in the 1-story, low axial load SDC D_{max} archetype (Figure 4-12), and by fracture of the reinforcing steel in the other archetypes.

Each archetype was analyzed using the simplified incremental dynamic analysis (IDA) procedure suggested by the Methodology in conjunction with the set of 44 far-field ground motion records provided as part of the Methodology. The median collapse spectral intensity, S_{CT}, was taken as the median spectral acceleration at the code-based structural period, T, and the analyses were discontinued as soon as half of the records were observed to result in collapse.

Values of overstrength, Ω, from the pushover analyses, and collapse margin ratio, *CMR*, from the simplified incremental dynamic analyses, are summarized in Table 4-5 for special RCSWs and Table 4-6 for ordinary RCSWs.

Table 4-5 Summary of Collapse Results for Special Reinforced Concrete Shear Wall Archetype Designs

Archetype Design ID Number	Design Configuration			Pushover and IDA Results			
	No. of Stories	Gravity Loads	SDC	Static Ω	S_{MT} [T] (g)	S_{CT} [T] (g)	*CMR*
Performance Group No. PG-1S							
1	1	High	D_{max}	2.39	1.5	1.18	0.79
2	2	High	D_{max}	1.82	1.5	1.69	1.13
3	4	High	D_{max}	1.72	1.5	2.20	1.47
Performance Group No. PG-2S							
4	8	High	D_{max}	1.45	1.03	1.93	1.87
5	12	High	D_{max}	1.63	0.77	1.88	2.44
Performance Group No. PG-3S							
6	1	High	D_{min}	2.98	0.75	1.05	1.40
7	2	High	D_{min}	1.83	0.75	0.92	1.23
Performance Group No. PG-4S							
8	4	High	D_{min}	2.91	0.58	1.74	3
9	8	High	D_{min}	4.44	0.34	1.59	4.68
10	12	High	D_{min}	4.93	0.26	1.61	6.19
Performance Group No. PG-5S							
11	1	Low	D_{max}	2.39	1.5	1.18	0.79
12	2	Low	D_{max}	1.82	1.5	1.69	1.13
13	4	Low	D_{max}	2.03	1.5	3.05	2.03
Performance Group No. PG-6S							
14	8	Low	D_{max}	1.89	1.03	2.32	2.25
15	12	Low	D_{max}	1.50	0.77	1.62	2.10
Performance Group No. PG-7S							
16	1	Low	D_{min}	2.98	0.75	1.05	1.40
17	2	Low	D_{min}	1.83	0.75	0.92	1.23
Performance Group No. PG-8S							
18	4	Low	D_{min}	1.85	0.58	1.74	3.00
19	8	Low	D_{min}	5.64	0.34	1.81	5.32
20	12	Low	D_{min}	3.08	0.26	1.68	6.46

Table 4-6 Summary of Collapse Results for Ordinary Reinforced Concrete Shear Wall Archetype Designs

Archetype Design ID Number	Design Configuration			Pushover and IDA Results			
	No. of Stories	Gravity Loads	SDC	Static Ω	S_{MT} [T] (g)	S_{CT} [T] (g)	*CMR*
Performance Group No. PG-1O							
21	1	High	C_{max}	3.71	0.75	1.25	1.67
22	2	High	C_{max}	1.98	0.75	1.07	1.43
Performance Group No. PG-2O							
23	4	High	C_{max}	2.40	0.58	1.57	2.71
24	8	High	C_{max}	3.64	0.34	1.74	5.12
25	12	High	C_{max}	4.26	0.26	1.68	6.46
Performance Group No. PG-3O							
26	1	High	C_{min}	4.26	0.5	1.1	2.2
27	2	High	C_{min}	2.15	0.5	0.90	1.8
Performance Group No. PG-4O							
28	4	High	C_{min}	3.7	0.38	1.57	2.71
29	8	High	C_{min}	3.64	0.23	1.74	7.57
30	12	High	C_{min}	6.44	0.17	1.68	9.88
Performance Group No. PG-5O							
31	1	Low	C_{max}	3.71	0.75	1.25	1.25
32	2	Low	C_{max}	1.98	0.75	1.07	1.07
Performance Group No. PG-6O							
33	4	Low	C_{max}	1.99	0.58	1.90	3.28
34	8	Low	C_{max}	2.37	0.34	2.05	6.03
35	12	Low	C_{max}	2.71	0.26	1.66	6.38
Performance Group No. PG-7O							
36	1	Low	C_{min}	4.26	0.5	1.10	2.2
37	2	Low	C_{min}	2.15	0.5	0.90	1.8
Performance Group No. PG-8O							
38	4	Low	C_{min}	2.35	0.38	1.59	4.18
39	8	Low	C_{min}	2.37	0.23	2.05	8.91
40	12	Low	C_{min}	4.10	0.17	1.66	9.76

4.7 Performance Evaluation

In the Methodology, adjusted collapse margin ratios (*ACMR*s) are obtained by multiplying the *CMR*s, computed from nonlinear dynamic analysis results by the spectral shape factor (*SSF*). The acceptable average value of *ACMR* for each performance group is denoted by $ACMR_{10\%}$. The acceptable value of *ACMR* for individual archetypes within a performance group is denoted by $ACMR_{20\%}$.

Values of $ACMR_{10\%}$ and $ACMR_{20\%}$ are determined based on total system collapse uncertainty, β_{TOT}. Collapse uncertainty is a function of the quality ratings associated with the design requirements, test data, and nonlinear models, as well as record-to-record uncertainty. Quality ratings assigned to design requirements, test data, and nonlinear models for reinforced concrete shear wall systems are summarized in Table 4-7.

Table 4-7 Summary of Quality Ratings for Reinforced Concrete Shear Wall Systems

System	Design Requirements	Test Data	Nonlinear Modeling
Special RCSWs	B	B	B
Ordinary RCSWs	B	B	B

4.7.1 Summary of Performance Evaluation Results

To pass the performance evaluation criteria, individual archetypes must have adjusted collapse margin ratios exceeding $ACMR_{20\%}$. Performance evaluation results for individual special RCSW archetypes are summarized in Table 4-8, and results for individual ordinary RCSW archetypes are summarized in Table 4-9. For special RCSWs, all 4-, 8-, and 12-story archetypes passed this criterion, while 1- and 2-story, short-period archetypes failed the criterion. In the case of ordinary RCSWs, all short-period and long-period archetypes passed this criterion.

Performance evaluation results by performance group are summarized in Table 4-10 for special RCSW archetypes and Table 4-11 for ordinary RCSW archetypes. To pass the performance evaluation criteria, the adjusted collapse margin ratio averaged across all archetypes in a performance group must exceed $ACMR_{10\%}$. For special RCSWs, all long-period performance groups passed this criterion. In the case of ordinary RCSWs, short-period, SDC C_{min} performance groups and all long-period performance groups passed this criterion.

4.8 Evaluation of System Overstrength

In the Methodology, the system overstrength factor, Ω_0, is taken as the largest average value of the overstrength, Ω, computed for each performance group. Values of overstrength for individual archetypes and average values for each performance group are shown in Table 4-10 and Table 4-11. For special RCSWs, average values varied between 1.54 and 3.88. The resulting value of Ω_0 equal to 3.88 is larger than the value of 2.5 provided for special RCSW systems in ASCE/SEI 7-05.

For ordinary RCSWs, average values of overstrength varied between 2.37 and 5.2. The resulting value of Ω_0 equal to 5.2 is significantly larger than the value of 2.5 provided for special RCSW systems in ASCE/SEI 7-05. Per the Methodology, however, values of Ω_0 need not be taken larger than 3.0, as a practical limit.

Table 4-8 Summary of Collapse Performance Evaluations of Special Reinforced Concrete Shear Wall Archetypes

Arch. Design ID No.	Design Configuration			Computed Overstrength and Collapse Margin Parameters					Acceptance Check	
	No. of Stories	Gravity Loads	SDC	Static Ω	*CMR*	μ_T	*SSF*	*ACMR*	Accept. *ACMR*	Pass/ Fail
Performance Group No. PG-1S										
1	1	High	D_{max}	2.39	0.79	9	1.33	1.05	1.56	Fail
2	2	High	D_{max}	1.82	1.13	12	1.33	1.50	1.56	Fail
3	4	High	D_{max}	1.72	1.47	23	1.34	1.96	1.56	Pass
Mean of Performance Group:				**1.98**				**1.5**	**1.96**	**Fail**
Performance Group No. PG-2S										
4	8	High	D_{max}	1.45	1.87	22	1.43	2.68	1.56	Pass
5	12	High	D_{max}	1.63	2.44	19	1.51	3.68	1.56	Pass
Mean of Performance Group:				**1.54**				**3.18**	**1.96**	**Pass**
Performance Group No. PG-3S										
6	1	High	D_{min}	2.98	1.40	25	1.14	1.60	1.56	Pass
7	2	High	D_{min}	1.83	1.23	17	1.14	1.40	1.56	Fail
Mean of Performance Group:				**2.41**				**1.50**	**1.96**	**Fail**
Performance Group No. PG-4S										
8	4	High	D_{min}	2.91	3.0	35	1.14	3.42	1.56	Pass
9	8	High	D_{min}	4.44	4.68	21	1.22	5.71	1.56	Pass
10	12	High	D_{min}	4.30	6.29	18	1.29	7.99	1.56	Pass
Mean of Performance Group:				**3.88**				**5.71**	**1.96**	**Pass**
Performance Group No. PG-5S										
11	1	Low	D_{max}	2.39	0.79	9	1.33	1.05	1.56	Fail
12	2	Low	D_{max}	1.82	1.13	12	1.33	1.50	1.56	Fail
13	4	Low	D_{max}	2.03	2.03	13	1.33	2.70	1.56	Pass
Mean of Performance Group:				**2.08**				**1.75**	**1.96**	**Fail**
Performance Group No. PG-6S										
14	8	Low	D_{max}	1.89	2.25	21	1.43	3.22	1.56	Pass
15	12	Low	D_{max}	1.50	2.10	38	1.51	3.17	1.56	Pass
Mean of Performance Group:				**1.70**				**3.20**	**1.96**	**Pass**
Performance Group No. PG-7S										
16	1	Low	D_{min}	2.98	1.40	25	1.14	1.60	1.56	Pass
17	2	Low	D_{min}	1.83	1.23	17	1.14	1.40	1.56	Fail
Mean of Performance Group:				**2.41**				**1.50**	**1.96**	**Fail**
Performance Group No. PG-8S										
18	4	Low	D_{min}	1.85	3.0	50	1.14	3.42	1.56	Pass
19	8	Low	D_{min}	5.64	1.81	30	1.22	2.21	1.56	Pass
20	12	Low	D_{min}	3.08	6.46	24	1.29	8.33	1.56	Pass
Mean of Performance Group:				**3.52**				**4.65**	**1.96**	**Pass**

Table 4-9 Summary of Collapse Performance Evaluations of Ordinary Reinforced Concrete Shear Wall Archetypes

Arch. Design ID No.	Design Configuration			Computed Overstrength and Collapse Margin Parameters					Acceptance Check	
	No. of Stories	Gravity Loads	SDC	Static Ω	*CMR*	μ_T	*SSF*	*ACMR*	Accept. *ACMR*	Pass/ Fail
Performance Group No. PG-1O										
21	1	High	C_{max}	3.7	1.67	10	1.14	1.90	1.56	Pass
22	2	High	C_{max}	2.0	1.43	14	1.14	1.63	1.56	Pass
Mean of Performance Group:				**2.85**				**1.77**	**1.96**	**Fail**
Performance Group No. PG-2O										
23	4	High	C_{max}	2.4	2.71	11	1.14	3.09	1.56	Pass
24	8	High	C_{max}	3.6	5.12	8	1.21	6.22	1.56	Pass
25	12	High	C_{max}	4.3	6.46	6.3	1.25	8.08	1.56	Pass
Mean of Performance Group:				**3.43**				**5.80**	**1.96**	**Pass**
Performance Group No. PG-3O										
26	1	High	C_{min}	4.3	2.2	13	1.14	2.51	1.56	Pass
27	2	High	C_{min}	2.2	1.8	19	1.14	2.05	1.56	Pass
Mean of Performance Group:				**3.25**				**2.28**	**1.96**	**Pass**
Performance Group No. PG-4O										
28	4	High	C_{min}	3.7	2.71	13	1.14	3.09	1.56	Pass
29	8	High	C_{min}	5.5	7.57	8	1.21	9.19	1.56	Pass
30	12	High	C_{min}	6.4	9.88	6.3	1.25	12.4	1.56	Pass
Mean of Performance Group:				**5.2**				**8.23**	**1.96**	**Pass**
Performance Group No. PG-5O										
31	1	Low	C_{max}	3.7	1.67	10	1.14	1.90	1.56	Pass
32	2	Low	C_{max}	2.0	1.43	14	1.14	1.63	1.56	Pass
Mean of Performance Group:				**2.85**				**1.77**	**1.96**	**Fail**
Performance Group No. PG-6O										
33	4	Low	C_{max}	2.0	3.28	30	1.14	3.74	1.56	Pass
34	8	Low	C_{max}	2.4	6.03	30	1.21	7.30	1.56	Pass
35	12	Low	C_{max}	2.7	6.38	23	1.29	8.23	1.56	Pass
Mean of Performance Group:				**2.37**				**6.42**	**1.96**	**Pass**
Performance Group No. PG-7O										
36	1	Low	C_{min}	4.3	2.2	13	1.14	2.51	1.56	Pass
37	2	Low	C_{min}	2.2	1.8	19	1.14	2.05	1.56	Pass
Mean of Performance Group:				**3.25**				**2.28**	**1.96**	**Pass**
Performance Group No. PG-8O										
38	4	Low	C_{min}	2.4	4.18	47	1.14	4.77	1.56	Pass
39	8	Low	C_{min}	3.6	8.91	35	1.21	10.78	1.56	Pass
40	12	Low	C_{min}	4.1	9.76	23	1.29	12.59	1.56	Pass
Mean of Performance Group:				**3.37**				**9.38**	**1.96**	**Pass**

Table 4-10 Summary of Results by Performance Group for Special Reinforced Concrete Shear Walls

Performance Group Summary					
Group No.	Grouping Criteria				Performance Result
	Basic Config.	Design Load Level		Period Domain	
		Gravity	Seismic		
PG-1S	A	High	SDC D_{max}	Short	Fail
PG-2S				Long	Pass
PG-3S			SDC D_{min}	Short	Fail
PG-4S				Long	Pass
PG-5S		Low	SDC D_{max}	Short	Fail
PG-6S				Long	Pass
PG-7S			SDC D_{min}	Short	Fail
PG-8S				Long	Pass

Table 4-11 Summary of Results by Performance Group for Ordinary Reinforced Concrete Shear Walls

Performance Group Summary					
Group No.	Grouping Criteria				Performance Result
	Basic Config.	Design Load Level		Period Domain	
		Gravity	Seismic		
PG-1O	A	High	SDC C_{max}	Short	Fail
PG-2O				Long	Pass
PG-3O			SDC C_{min}	Short	Pass
PG-4O				Long	Pass
PG-5O		Low	SDC C_{max}	Short	Fail
PG-6O				Long	Pass
PG-7O			SDC C_{min}	Short	Pass
PG-8O				Long	Pass

4.9 Observations and Recommendations

4.9.1 Observations on System Performance

With the exception of short-period performance groups, special RCSW and ordinary RCSW archetypes met the acceptance criteria of the Methodology. In addition, ordinary RCSW, short-period, SDC C_{min} archetypes also met the acceptance criteria. Calculated values of system overstrength factor, Ω_0, for both special and ordinary RCSW archetypes exceeded values provided for these systems in ASCE/SEI 7-05.

In general, results indicated that archetypes with high seismic demands (SDC D_{max} and SDC C_{max}) had lower collapse margin ratios than archetypes with low seismic demands (SDC D_{min} and SDC C_{min}). Similarly, archetypes subjected to high axial loads had lower collapse margin ratios than archetypes subjected to low axial loads. These trends were apparent in both special and ordinary shear wall systems.

For the 1- and 2-story archetypes, flexural yielding followed by shear failure was the most common collapse mode, followed by buckling and fracture of longitudinal reinforcing steel. In taller (4-, 8-, and 12-story) archetypes, buckling and fracture of longitudinal reinforcing steel was the most common collapse mode, followed by shear failure (after flexural yielding).

One- and 2-story archetypes failed to achieve acceptable collapse margin ratios primarily because shear failures used as a proxy for collapse occurred at relatively low drift levels (e.g., 1.5%). In general, collapse of low-rise shear wall buildings has not been observed in earthquakes (Wallace et al., 2008), except in cases where the floor system failed (e.g., precast parking structures). This suggests that findings related to low-rise walls were biased by the modeling assumptions and potentially conservative criteria used to assess collapse. At this time, however, insufficient information exists to establish more liberal failure criteria.

Archetypes with low seismic demands (SDC D_{min} and SDC C_{min}) had higher calculated overstrength than archetypes with high seismic demands (SDC D_{max} and SDC C_{max}). Furthermore, calculated overstrength for ordinary RCSWs was, in general, larger than for special RCSWs. This result was likely due to bias caused by conservatism in the archetype designs. In general, it was more difficult to design ordinary RCSW archetypes to just meet the limits of code-permitted flexure, shear, and axial strengths, than it was for special RCSW archetypes. As a result, ordinary RCSW archetypes had more inherent conservatism built into their designs.

4.9.2 Observations on the Methodology

Nonlinear response history analyses to collapse are inherently difficult for a non-redundant system, such as a cantilever shear wall, because yielding at a single location (e.g., base of a wall element) can produce instabilities that make modeling convergence difficult. Specific recommendations related to modeling various failure modes that could lead to collapse generally do not exist. Assumptions regarding non-simulated collapse behaviors on the part of the analyst can substantially impact the performance evaluation results.

The potential impact of soil-structure interaction is not considered in the process. In the case of stiff systems, such as shear wall buildings, the added flexibility associated with foundation rotation could significantly alter the response, likely enabling many short-period archetypes to achieve acceptable collapse margin ratios. However, it is noted that by neglecting such effects, minimum design requirements were evaluated.

4.9.3 Recommendations for Further Investigation

This study focused on rectangular cantilever wall systems, but reinforced concrete shear wall buildings can have many different wall configurations, including flanged walls, core walls, coupled walls, and non-rectangular wall systems. All these variations would need to be studied in order to fully characterize the seismic performance of reinforced concrete shear wall structures and identify appropriate seismic performance factors.

Results appear to be generally consistent with expectations. Relatively slender cantilever walls with rectangular cross sections and low shear stresses are expected to perform well. Recently, ACI Committee 318-H has been balloting material to define a shear wall governed by flexure. Results related to taller shear wall archetypes would appear to support this effort. However, this study would need to be extended to the full range of possible wall configurations used in practice (coupled walls, core walls, walls with non-rectangular cross sections) in order to comprehensively contribute to the ACI Committee 318-H effort.

Results for 1- and 2-story archetypes were sensitive to the axial failure criteria used to measure loss of vertical load-carrying capacity. Investigation of an axial failure model was presented in Appendix B. These studies highlight the need for more research and improved criteria to define loss of vertical-load-carrying capacity and collapse of shear wall components.

The Equivalent Lateral Force (ELF) procedure was used in the design of special and ordinary RCSW archetypes. Results for other systems have shown that use of the Response Spectrum Analysis (RSA) procedure produces designs that perform differently. Depending on how minimum code requirements impact the design (e.g., minimum reinforcement requirements, drift limits), use of the RSA procedure may or may not be significant in the case of reinforced concrete shear wall systems. The potential impact of using the RSA procedure on reinforced concrete shear wall systems should be investigated.

In this study, a fairly significant body of research was synthesized to assess and support the modeling assumptions. Despite this effort, the ability to model the influence of certain failure modes on collapse is limited due to lack of information, lack of large-scale test data, and lack of data from actual buildings subjected to strong ground shaking. Sensitivity of the results to variations in modeling assumptions and identification of which assumptions have the greatest impact on the performance evaluation should be investigated.

Chapter 5
Trial Application: Steel Braced Frame Structures

5.1 Introduction

This chapter presents a trial application of the FEMA P-695 Methodology on steel braced frame structures consisting of special steel concentrically braced frames (SCBFs) or buckling-restrained braced frames (BRBFs). It summarizes design requirements and available test data for steel braced frames, explains the development of braced frame archetype configurations, documents the nonlinear modeling approach, presents the results of a performance evaluation, and summarizes observations on the Methodology specific to steel braced frame systems. Results are investigated for a range of building heights and design parameters.

5.2 Overview and Approach

In this trial application, special steel concentrically braced frame and buckling-restrained braced frame systems, as defined in ANSI/AISC 341-05, *Seismic Provisions for Structural Steel Buildings* (AISC, 2005a), were considered as if they were new systems proposed for inclusion in ASCE/SEI 7-05 *Minimum Design Loads for Buildings and Other Structures* (ASCE, 2006). Although the intent was to treat SCBF and BRBF systems as if they were new systems, the purpose was not to re-derive or validate seismic performance factors (R, Ω_0, and C_d) for these systems. Rather, it was to examine whether SCBF and BRBF systems would satisfy the acceptance criteria of the FEMA P-695 Methodology, test the application of the Methodology with respect to these systems, and identify possible improvements to the Methodology or current SCBF and BRBF design provisions.

The system design requirements of ASCE/SEI 7-05, including minimum base shear and story drift limits, were used as the basis for design, with the exception that C_d was taken equal to R, as specified in the FEMA P-695 Methodology. Values of R for special SCBF and BRBF systems are 6 and 8, respectively.

Special SCBFs have been widely used for many types of steel buildings because of their efficiency in resisting lateral forces. Under severe lateral loading, the braces will buckle, first laterally and then locally, eventually leading to deterioration of the strength and stiffness of the system. Under repeated cycles of inelastic deformation, braces can fracture, transferring the burden of lateral force-resistance to the remaining braces and the beam-column framing system.

During the past decade, BRBFs have been increasingly used. The braces in these systems provide more ductile behavior, exhibit fuller hysteretic loops, and generally exhibit considerably more energy dissipation capacity before rupture. In recognition of this improved ductility, BRBFs have higher *R* factors, and are designed for lower lateral forces, than SCBFs.

Braced frame systems can have many different configurations, including single-diagonal, X-braced, chevron, and other arrangements, and these configurations can occur over one or more stories. Also, braces can also be constructed with different types of cross sections, including singly-symmetric, doubly-symmetric, closed, or open sections. For practical reasons, the scope of the beta testing effort on braced frames was necessarily limited.

The evaluations presented herein do not constitute a complete study of the full range of braced frame behaviors, as only a subset of structural configurations, proportions, and detailing options could be considered. Recent research and design practice has favored the use of two-story X-brace configurations. Two-story X-bracing helps to avoid large unbalanced beam loads that can occur when braces in chevron (or inverted chevron) configurations buckle. Current code requirements result in very large beam sizes to resist this unbalanced loading, even when buckling-restrained braces are used. For these reasons, the two-story X-brace configuration was selected for investigation of special SCBF and BRBF systems over a range of building heights and design parameters.

Many aspects of component, connection, and system behavior of both SCBF and BRBF systems are still uncertain, and numerous studies are underway to improve understanding of their inelastic response. Although the hysteretic properties and failure modes associated with the braces dominate the behavior of concentrically braced frame systems, previous analytical studies have shown that the moment frame behavior of beams and columns in a braced frame play an important role in determining the ultimate behavior of the system after the braces buckle or fail.

Global buckling of braces, possible rupture of braces, and beam-column framing action were explicitly considered in the computational models. The beam-column connections and brace-to-framing connections were assumed to have adequate stiffness, strength, and detailing to avoid failure before brace rupture. As such, they were not designed or analyzed in detail. Critical failure modes for beams, columns, and other components that were not explicitly included in the analytical models were indirectly accounted for using non-simulated failure criteria based on available test data.

5.3 Structural System Information

5.3.1 Design Requirements

Braced frame systems were designed and detailed in accordance with the strength design requirements in ANSI/AISC 341-05 and the seismic design requirements in ASCE/SEI 7-05. These requirements focus mainly on the proportioning of braces, beams, and columns. Although the provisions control certain aspects of connection design, there is considerable flexibility in how beam-column connections, gusset-to-framing connections, and brace-to-gusset connections are made.

5.3.2 Quality Rating of Design Requirements

Flexibility in design assumptions and acceptable connection configurations can lead to designs that can have significantly different overall system behavior and variability in system performance. As a consequence, a quality rating of (B) Good was assigned to the design requirements for special SCBF and BRBF systems.

5.3.3 Test Data

There are many studies in the literature that have included testing of braces, braced frame components, and braced frame assemblies (e.g., Black et al., 1980 and 2004; Zayas et al., 1980; Tremblay, 2002 and 2008; Powell et al., 2008; and Yoo et al., 2008). Material properties have been known to vary by the date and location of the test, and many of these tests were conducted some time ago.

Data from recent tests (Yang and Mahin, 2005; Uriz, 2005) were used to calibrate the analytical models used in this trial application. These data include the cyclic responses of tube braces, pipe braces, buckling-restrained braces, chevron frames with conventional braces, and chevron frames with buckling-restrained braces. Considerable data are available, but the following important limitations should be considered:

- **Variations in Member Sizes.** Test specimens used in the calibration all had similar beam, column, and brace member sizes. Conventional braces in the test specimens measured about six inches across the section. The archetypical designs, however, resulted in considerably heavier, or in some cases lighter, sections. Sections of a different size could have different local and global low-cycle fatigue response characteristics.
- **Variations in Loading Conditions.** Because of limitations in laboratory test setups, cyclic loading was applied only at the roof level, and test specimens were not subjected to gravity loading during the tests. The idealized load pattern reduces the complexity for examining component response during the tests but may or may not be representative of seismic loading.

- **Variations in Slab Details.** Concrete slabs were not included in the test specimens. As such, changes in stiffness and strength because of composite behavior were not reflected in the frame tests.
- **Variations in Drift Range.** Test specimens were subjected to cyclic loading with increasing amplitudes of story drift until significant damage occurred in the critical elements. For the safety and protection of experimental facilities, however, tests were stopped before the specimens collapsed. Information on how the specimens behaved between the stages of significant damage and total collapse is, therefore, not available.

5.3.4 Quality Rating of Test Data

Although considerable test data are available on concentrically braced frame systems, these data have limitations that reduce confidence in certain modeling parameters and failure criteria. As a consequence, a quality rating of (B) Good was assigned to the test data for special SCBF and BRBF systems.

5.4 Archetype Configurations

A two-story X-brace configuration was selected for investigation of special SCBF and BRBF systems over a range of building heights and design parameters. Recent research and design practice has favored the use of this type of bracing configuration. It also has additional advantages, including: (1) a more straightforward load path for transfer of seismic forces throughout the system; (2) avoidance of large unbalanced beam forces when braces buckle; and (3) avoidance of possible failure modes at intersecting brace connections located at mid-story.

Focus on a single brace configuration allowed consideration of the following additional design variables: conventional versus buckling-restrained brace types, level of seismic design loading, level of gravity load, number of stories, and period. A rectangular plan configuration (Figure 5-1) was selected as representative of realistic braced frame structures encompassing these design variables. Building heights of 2, 3, 6, 12, and 16 stories were considered (Figure 5-2). To produce lower-bound designs without excessive overstrength, the plan dimensions and number of braced bays were varied to optimize strength relative to the level of seismic design loading.

The height limit for steel braced frame archetypes was taken as 240 feet, which is extended from the basic limit of 160 feet prescribed in ASCE/SEI 7-05, assuming that there are no extreme torsional irregularities and that braced frames in any one plane take less than 60% of the total seismic force in each direction (neglecting torsional effects). Archetypes were assumed to have no horizontal irregularities, so they could be idealized as rigid in-plane. They were also assumed to be regular in plan, with braced frames located at the building perimeter. The redundancy factor (ρ) was determined to be equal to 1.0.

For the purpose of estimating design gravity loads, floor and roof systems were assumed to consist of metal deck with concrete fill. The potential for variation in design gravity loads was considered irrelevant to the design of brace elements, and insignificant in comparison with column axial forces due to brace component forces and overturning effects, so a typical level of gravity load was assumed in the design of all archetypes.

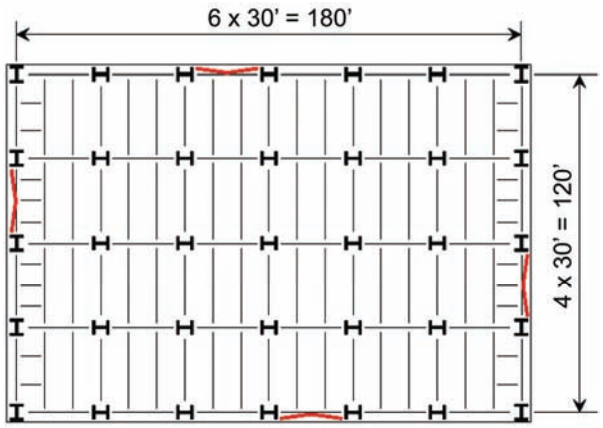

Figure 5-1 Typical plan configuration of special SCBF and BRBF archetypes (design for 3-story and 6-story configurations shown).

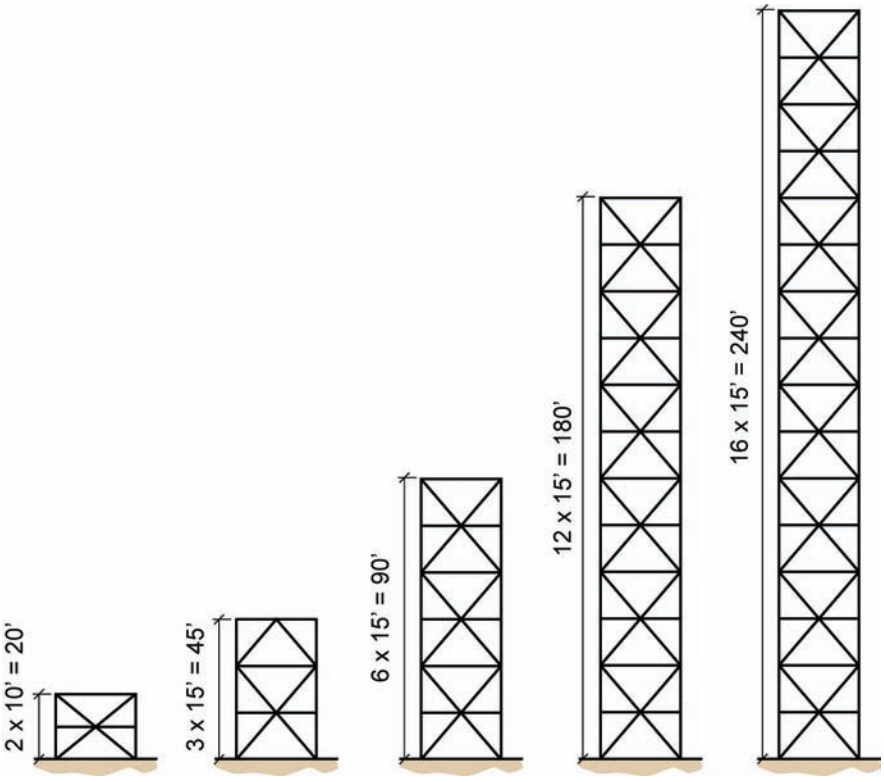

Figure 5-2 Elevation of 2-, 3-, 6-, 12-, and 16-story braced frame archetypes

Archetypes were grouped into performance groups containing a set of common features or behavioral characteristics, including Seismic Design Category (SDC),

gravity load level, and code-based period of the structure. Considering the design variables listed above, a total of 20 archetypes were developed. These were divided into eight performance groups, four attributed to special SCBFs and four attributed to BRBFs, as shown in Table 5-1 and Table 5-2. Performance groups with less than three archetypes did not meet the minimum number of archetypes per performance group required in a full application of the Methodology.

Table 5-1 Performance Groups for Evaluation of Special Steel Concentrically Braced Frame Archetypes

Performance Group Summary					
Group No.	Grouping Criteria				Number of Archetypes
	Basic Config.	Design Load Level		Period Domain	
		Gravity	Seismic		
PG-1SCB	Double Story X-Braces	Typical	SDC D_{max}	Short	2[1]
PG-2SCB				Long	3[2]
PG-3SCB			SDC D_{min}	Short	2[1]
PG-4SCB				Long	3[2]

[1] Short-period performance groups, PG-1 and PG-3, include 2-story and 3-story archetypes.

[2] Long-period performance groups, PG-2 and PG-4, include 6-story, 12-story and 16-story archetypes.

Table 5-2 Performance Groups for Evaluation of Buckling-Restrained Brace Frame Archetypes

Performance Group Summary					
Group No.	Grouping Criteria				Number of Archetypes
	Basic Config.	Design Load Level		Period Domain	
		Gravity	Seismic		
PG-1BRB	Double Story X-Braces	Typical	SDC D_{max}	Short	2[1]
PG-2BRB				Long	3[2]
PG-3BRB			SDC D_{min}	Short	2[1]
PG-4BRB				Long	3[2]

[1] Short-period performance groups, PG-1 and PG-2, include 2-story and 3-story archetypes.

[2] Long-period performance groups, PG-2 and PG-4 include 6-story, 12-story and 16-story archetypes.

Conventional brace cross sections consisted of hollow structural sections (HSS) and wide-flange sections, while beam and column framing consisted of wide-flange sections. Buckling-restrained brace sections were sized based on the area of the yielding core. Overstrength factors in ASCE/SEI 7-05 were used to determine design axial forces on the columns.

Key seismic design parameters for the special SCBF and BRBF archetypes are summarized in Table 5-3 and Table 5-4. These include the code-based period, T (calculated using the equation, $T=C_uT_a$, provided in ASCE/SEI 7-05), fundamental period, T_1 (calculated from eigenvalue analysis), the seismic base shear coefficient, V/W, and the MCE-level spectral acceleration, S_{MT}.

Table 5-3 Special Steel Concentrically Braced Frame Archetype Design Properties

Archetype Design ID Number	No. of Stories	Key Archetype Design Parameters						
		Analysis Procedure	Seismic Design Criteria					$S_{MT}(T)$ (g)
			SDC	R	T (sec)	T_1 (sec)	V/W (g)	
Performance Group No. PG-1SCB								
2SCBFDmax	2	ELF	D_{max}	6	0.26	0.40	0.167	1.50
3SCBFDmax	3	ELF	D_{max}	6	0.49	0.58	0.167	1.50
Performance Group No. PG-2SCB								
6SCBFDmax	6	ELF	D_{max}	6	0.82	1.05	0.122	1.10
12SCBFDmax	12	ELF	D_{max}	6	1.38	1.91	0.073	0.65
16SCBFDmax	16	RSA	D_{max}	6	1.71	3.16	0.059	0.53
Performance Group No. PG-3SCB								
2SCBFDmin	2	ELF	D_{min}	6	0.28	0.55	0.083	0.75
3SCBFDmin	3	ELF	D_{min}	6	0.52	0.80	0.064	0.58
Performance Group No. PG-4SCB								
6SCBFDmin	6	ELF	D_{min}	6	0.88	1.51	0.038	0.34
12SCBFDmin	12	ELF	D_{min}	6	1.47	3.04	0.023	0.20
16SCBFDmin	16	RSA	D_{min}	6	1.83	4.67	0.022	0.16

Table 5-4 Buckling-Restrained Brace Frame Archetype Design Properties

Archetype Design ID Number	No. of Stories	Key Archetype Design Parameters						
		Analysis Procedure	Seismic Design Criteria					$S_{MT}(T)$ (g)
			SDC	R	T (sec)	T_1 (sec)	V/W (g)	
Performance Group No. PG-1BRB								
2BRBFDmax	2	ELF	D_{max}	8	0.40	0.50	0.125	1.50
3BRBFDmax	3	ELF	D_{max}	8	0.73	0.80	0.103	1.23
Performance Group No. PG-2BRB								
6BRBFDmax	6	ELF	D_{max}	8	1.23	1.35	0.061	0.73
12BRBFDmax	12	RSA	D_{max}	8	2.06	2.82	0.044	0.44
16BRBFDmax	16	RSA	D_{max}	8	2.56	3.73	0.044	0.35
Performance Group No. PG-3BRB								
2BRBFDmin	2	ELF	D_{min}	8	0.43	0.68	0.059	0.70
3BRBFDmin	3	ELF	D_{min}	8	0.78	1.25	0.032	0.38
Performance Group No. PG-4BRB								
6BRBFDmin	6	ELF	D_{min}	8	1.31	2.34	0.022	0.23
12BRBFDmin	12	RSA	D_{min}	8	2.21	3.49	0.022	0.14
16BRBFDmin	16	RSA	D_{min}	8	2.74	4.83	0.022	0.11

In certain taller (e.g., 12-, and 16-story) configurations, use of the Equivalent Lateral Force (ELF) procedure was found to result in a design that was overly conservative. In these cases, the Response Spectrum Analysis (RSA) procedure was used to avoid a conservative bias in the results. P-Delta effects were not observed to govern any of the archetype designs. More detailed information on the design of all special SCBF and BRBF archetypes is provided in Appendix C.

5.5 Nonlinear Model Development

5.5.1 Modeling Approach

For nonlinear analysis, each archetype was idealized using two-dimensional plane frame models, as shown in Figure 5-3. Models were implemented in OpenSees, *Open System for Earthquake Engineering Simulation* (OpenSees, 2007). To model inelastic behavior, nonlinear beam-columns elements were used. Critical locations where yielding might occur were modeled using fiber elements.

Braces were assumed to have pinned end connections to the framing. Beam-column connections at the braces were assumed to be fully-restrained because gusset plate connections provide considerable fixity. To simplify design and analysis, all other beam-column connections were also assumed to be fully-restrained. Beams were assumed to be laterally supported at quarter points along the span, and columns were assumed to be fixed at the base, orientated to resist lateral forces through strong-axis bending.

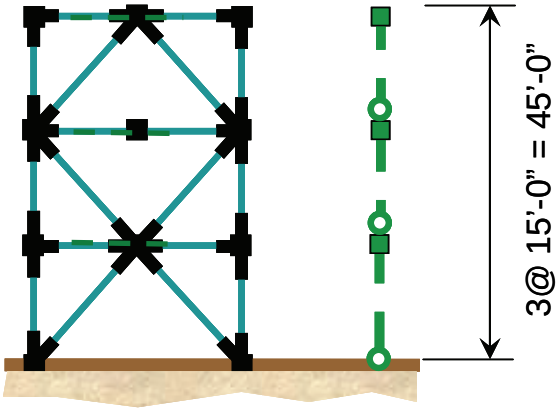

Figure 5-3 Two-dimensional plane frame model with a leaning column (3-story archetype shown).

Rigid offsets were assumed at the beam-column connections and brace-to-framing connections to represent the physical size and stiffening effect of the gusset plates. The assumed effective length of the braces was 70% of the work-point-to-work-point length. The effective stiffness of the buckling-restrained braces was modified to 1.4 times the stiffness of the steel core to account for added stiffness contributions from tapered end zones and typical connection configurations. Analytical models of

BRBF archetypes were essentially the same as SCBF archetypes, except for the modeling of buckling-restrained braces, which were assumed not to buckle.

A co-rotational formulation was used to simulate large deformations and P-Delta effects. The gravity framing system was idealized as a leaning column, which was assumed to be axially rigid, but without any lateral strength so that the lateral stiffness and strength of the gravity framing system was not considered. The axial load on a leaning column was taken as the portion of the total system gravity load that could be attributed to a braced bay, but not directly tributary to the column elements.

The vertical floor mass tributary to the beam in the braced frame was modeled as recommended by Khatib et al. (1988). Any rotation of the floor diaphragms about a vertical axis was ignored. As such, torsional effects due to mass and stiffness eccentricities or premature deterioration of bracing on one side of the building were not accounted for in the analyses.

5.5.2 Nonlinear Models of Braces

The hysteretic characteristics of conventional braces were modeled using an approach developed by Uriz (2005). In this approach, each brace is subdivided into 10 nonlinear beam-column elements, with fibers used to model the shape and hysteretic characteristics of the brace at three integration points along each element. A Menegotto-Pinto material model with isotropic strain hardening is used to simulate the mechanical properties of the steel material, and a co-rotational formulation is used to model the braces so the effects of buckling and large deformation could be taken into account.

To model buckling and low-cycle fatigue rupture of braces, the strain history in each fiber was tracked, and a rainflow counting algorithm was used to determine the amplitude of each inelastic cycle. A Manson-Coffin relation calibrated to multiple brace tests was used to characterize low-cycle fatigue damage to each fiber during each cycle, and Miner's rule was then used to determine whether the fatigue life had been exceeded. For simplicity in two-dimensional modeling, brace buckling was modeled to occur in-plane rather than out-of-plane.

The analytical model shown in Figure 5-4 illustrates the geometric parameters of the buckling brace elements. A small initial camber was imposed in the middle of the brace to induce the buckling phenomenon. To better capture the behavior, more elements are used in the middle of the brace where inelastic behavior often concentrates.

Parameters such as initial camber, number of nonlinear sub-elements, number of integration points, and number of fibers affect the global and local response of a brace under cyclic loading. Results from Uriz (2005) suggest an initial camber between 0.05% and 0.1% of the brace length, a minimum of three integration points

in each element, and 10 to 15 fibers across the depth of the cross section are sufficient to accurately estimate the inelastic strains at critical sections of the braces.

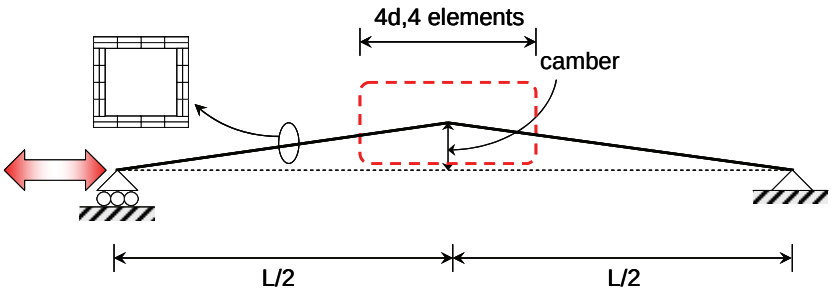

Figure 5-4 Initial camber used to model buckling behavior of brace elements.

The modeling of buckling-restrained braces was more straightforward because buckling behavior was not considered for these elements. Buckling-restrained braces were assumed to conform to the code-required ductility capacity for testing of these braces and were considered to have the ability to achieve a cumulative inelastic axial deformation of 200 times the yield deformation before fracture.

5.5.3 Non-Simulated Failure Modes

Failure modes due to damage in the braces have been calibrated with test data and explicitly simulated in the analytical models. Although brace failure is a critical response parameter related to potential collapse, there are other important deterioration modes that should be accounted for in the performance evaluation of steel braced frame systems. Not all of these modes were included in the models. Table 5-5 lists critical deterioration modes for steel braced frame structures and identifies their modeling status.

Most of the failure modes that have been neglected in the analyses were assumed to be prevented through adequate design, detailing, or quality control during construction. One such example is connection failure. Beam-column connections and brace-to-framing connections were assumed to have adequate stiffness, strength, and detailing to avoid failure before brace rupture. Similarly, possible net-section failures at the brace-to-gusset-plate connections were assumed to be adequately reinforced per ANSI/AISC 341-05, and members were assumed to be adequately braced to prevent out-of-plane buckling and lateral torsional buckling.

Non-simulated deterioration modes were incorporated in the performance evaluation process through post-processing of results and comparison of force or deformation response quantities to predetermined criteria outside of the analysis. Based on available test data, a drift-related failure criterion was used as a measure for column fracture. This was necessary because of the absence of calibrated low-cycle fatigue criteria for the columns used in the archetype designs.

Table 5-5 Modeling Status of Critical Deterioration Modes in Steel Braced Frame Structures

Critical Deterioration Mode	Modeling Status		
	Explicitly Modeled	Non-Simulated Criteria	Neglected
Braces			
Global buckling	✓		
Low-cycle fatigue	✓		
Local buckling		✓	
Net-section failure			✓
Beams			
Global beam buckling		✓	
Lateral torsional buckling			✓
Columns			
Fracture		✓	
Splice/ base plate failure (tension)		✓	
Global column buckling		✓	
Torsion			✓
Connections			
Failure			✓

Earlier tests on wide flange columns by Newell and Uang (2006) showed that columns begin to lose capacity after 7% to 9% story drift under cyclic axial and lateral load interactions. Accounting for differences between the boundary conditions in the test specimens and those of the archetypes, a story drift capacity of 10% was selected for the non-simulated failure criteria of the columns. Additionally, since global buckling of columns was not explicitly modeled, force and deformation demands in columns were tracked to see if column geometric instability was initiated.

5.5.4 Model Validation

The ability to simulate brace fracture is especially important in braced frame analyses because this behavior is expected to dominate frame response near collapse. The design of the 2-story, special SCBF, SDC D_{max} archetype coincides with the specimen tested by Uriz (2005). A comparison of experimental data and nonlinear simulation is shown in Figure 5-5. The model satisfactorily captures the strength of the specimen and the time when the brace fractures. The analytical parameters were well-calibrated for this specimen so high confidence was placed in the ability of the computational model to capture the cyclic response of the 2-story archetypes.

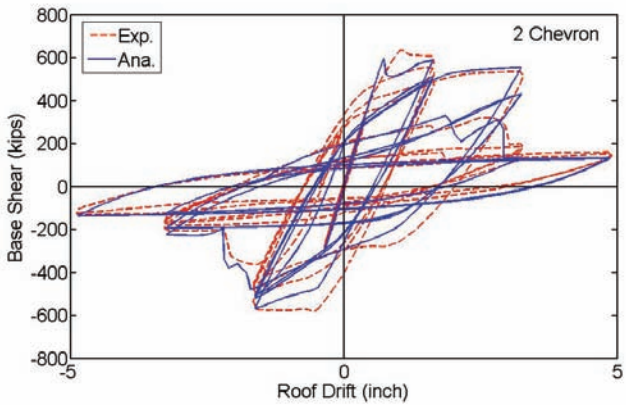

Figure 5-5 Comparison of experimental data and nonlinear simulation for the 2-story special SCBF archetype.

5.5.5 Quality Rating of Analytical Models

Brace elements were calibrated with test data, and braced frame archetype models have been shown to coincide with data from braced frame subassembly tests. There are, however, non-simulated failure modes that were not explicitly included in the analytical models. Also, fiber-based elements have limited ability to simulate local buckling behavior, and many three-dimensional response characteristics have not been explicitly modeled. Recognizing that the modeling approach is able to directly simulate structural response up to collapse, but that some limitations still exist, a quality rating of (B) Good was assigned to the analytical models for special SCBF and BRBF systems.

5.6 Nonlinear Analyses

Nonlinear static pushover analyses and incremental dynamic analyses (IDAs) were used to evaluate system overstrength, period-based ductility, and the collapse capacity of steel braced frame archetypes.

For each archetype, a pushover analysis was conducted with a lateral load distribution corresponding to the fundamental mode shape and mass distribution of the structure. Figure 5-6 shows examples of pushover curves for the set of 3-story special SCBF and BRBF archetypes.

For the 3-story, special SCBF, SDC D_{max} archetype (3SCBFD$_{max}$), brace buckling occurred at a roof drift ratio of about 0.002 radians, which corresponds to the drift ratio at maximum strength. The strength then degraded rapidly as the braces lost compression capacity with increasing lateral displacement. P-Delta effects added to the negative tangent stiffness until complete collapse occurred. The overstrength factor for this archetype was computed as Ω = 730k/519k = 1.41, and the period-based ductility capacity was computed as μ_T = 0.012/0.002 = 6.01.

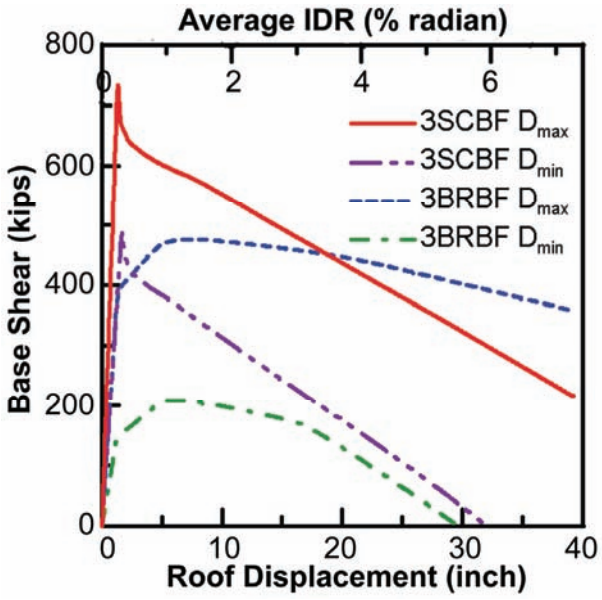

Figure 5-6 Pushover curves for the set of 3-story special SCBF and BRBF archetypes.

For the 3-story, BRBF, SDC D_{min} archetype (3BRBFD$_{min}$), the system yielded at a roof drift ratio of about 0.003 radians. The maximum strength of 210 kips occurred at a roof drift ratio of about 0.01 radians. The negative tangent stiffness was primarily caused by P-Delta effects.

Each archetype was analyzed using an incremental dynamic analysis (IDA) approach and the set of 44 far-field ground motion records provided as part of the Methodology. Figure 5-7 shows IDA results for the 3-story, special SCBF, SDC D_{max} archetype (3SCBFD$_{max}$). The spectral acceleration at collapse, S_{CT}, was computed for each of the 44 ground motion records, and the median collapse level, $\hat{S}_{CT}$, was determined to be 2.4 g. The collapse margin ratio was calculated as the ratio of $\hat{S}_{CT}$ to the Maximum Considered Earthquake (MCE) ground motion spectral demand, S_{MT}, equal to 1.60 for this archetype.

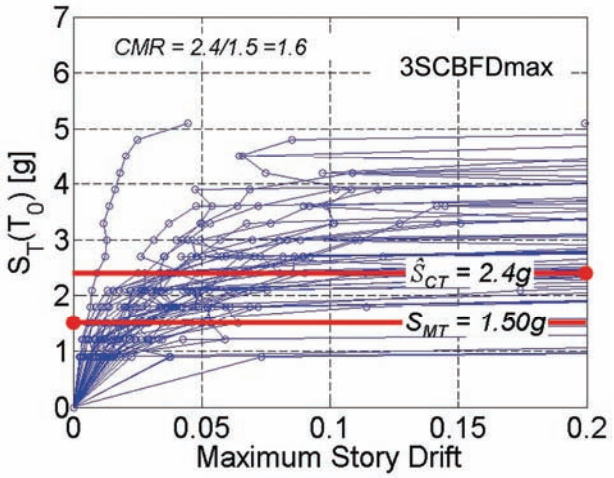

Figure 5-7 IDA results for 3-story special SCBF D_{max} archetypes

Values of overstrength, Ω, from the pushover analyses, and collapse margin ratio, *CMR*, from the incremental dynamic analyses are summarized in Table 5-6 for special SCBFs and Table 5-7 for BRBFs.

Table 5-6 Summary of Collapse Results for Special Steel Concentrically Braced Frame Archetype Designs

Archetype Design ID Number	Design Configuration			Pushover and IDA Results			
	No. of Stories	Gravity Loads	SDC	Static Ω	S_{MT} [T] (g)	S_{CT} [T] (g)	*CMR*
Performance Group No. PG-1SCB							
2SCBFDmax	2	Typical	D_{max}	1.44	1.50	1.5	1.00
3SCBFDmax	3	Typical	D_{max}	1.41	1.50	2.4	1.60
Performance Group No. PG-2SCB							
6SCBFDmax	6	Typical	D_{max}	1.28	1.10	2.4	2.18
12SCBFDmax	12	Typical	D_{max}	1.60	0.65	2.1	3.23
16SCBFDmax	16	Typical	D_{max}	2.11	0.53	1.4	2.64
Performance Group No. PG-3SCB							
2SCBFDmin	2	Typical	D_{min}	1.38	0.75	1.3	1.73
3SCBFDmin	3	Typical	D_{min}	2.41	0.58	2.1	3.62
Performance Group No. PG-4SCB							
6SCBFDmin	6	Typical	D_{min}	1.86	0.34	1.2	3.53
12SCBFDmin	12	Typical	D_{min}	2.18	0.20	1.0	5.00
16SCBFDmin	16	Typical	D_{min}	1.56	0.16	0.7	4.38

Table 5-7 Summary of Collapse Results for Buckling-Restrained Braced Frame Archetype Designs

Archetype Design ID Number	Design Configuration			Pushover and IDA Results			
	No. of Stories	Gravity Loads	SDC	Static Ω	S_{MT} [T] (g)	S_{CT} [T] (g)	*CMR*
Performance Group No. PG-1BRB							
2BRBFDmax	2	Typical	D_{max}	1.31	1.50	2.6	1.73
3BRBFDmax	3	Typical	D_{max}	1.48	1.23	3.5	2.85
Performance Group No. PG-2BRB							
6BRBFDmax	6	Typical	D_{max}	1.47	0.73	2.4	3.29
12BRBFDmax	12	Typical	D_{max}	1.17	0.44	1.0	2.27
16BRBFDmax	16	Typical	D_{max}	1.00	0.35	1.1	3.14
Performance Group No. PG-3BRB							
2BRBFDmin	2	Typical	D_{min}	1.44	0.70	1.2	1.71
3BRBFDmin	3	Typical	D_{min}	2.11	0.38	1.2	3.16
Performance Group No. PG-4BRB							
6BRBFDmin	6	Typical	D_{min}	1.28	0.23	0.7	3.04
12BRBFDmin	12	Typical	D_{min}	1.44	0.14	0.4	2.86
16BRBFDmin	16	Typical	D_{min}	1.15	0.11	0.5	4.55

Results indicate that short-period archetypes (i.e., 2- and 3-story archetypes) have lower collapse margin ratios than longer-period archetypes. Results also indicate that special SCBF archetypes designed for lower seismic demands have higher collapse margin ratios. These trends are not as apparent in the results for BRBF archetypes.

5.7 Performance Evaluation

In the Methodology, adjusted collapse margin ratios (*ACMR*s) are obtained by multiplying the *CMR*s computed from nonlinear dynamic analysis results by the spectral shape factor (*SSF*). The acceptable average value of *ACMR* for each performance group is denoted by $ACMR_{10\%}$. The acceptable value of *ACMR* for individual archetypes within a performance group is denoted by $ACMR_{20\%}$.

Values of $ACMR_{10\%}$ and $ACMR_{20\%}$ are determined based on total system collapse uncertainty, β_{TOT}. Collapse uncertainty is a function of the quality ratings associated with the design requirements, test data, and nonlinear models, as well as record-to-record uncertainty. Quality ratings assigned to design requirements, test data, and nonlinear models for steel concentrically braced frame systems are summarized in Table 5-8.

Table 5-8 Summary of Quality Ratings for Steel Braced Frame Systems

System	Design Requirements	Test Data	Nonlinear Modeling
Special SCBFs	B	B	B
BRBFs	B	B	B

5.7.1 Summary of Performance Evaluation Results

To pass the performance evaluation criteria, individual archetypes must have adjusted collapse margin ratios exceeding $ACMR_{20\%}$. Performance evaluation results for individual special SCBF archetypes are summarized in Table 5-9, and results for individual BRBF archetypes are summarized in Table 5-10.

For special SCBFs, all long-period (i.e., 6-, 12-, and 16-story) archetypes passed this criterion regardless of seismic design level, and short-period (i.e., 2- and 3-story) archetypes designed for SDC D_{min} also passed. Short-period special SCBF archetypes designed for SDC D_{max} failed this criterion. In the case of BRBFs, all archetypes passed this criterion.

Trends in the *ACMR* values mirrored trends observed in the incremental dynamic analyses and the resulting *CMR* values. Special SCBF archetypes with shorter periods generally had lower *ACMR* values than archetypes with longer periods. Similarly, archetypes designed for high seismic demands (SDC D_{max}) tended to have lower *ACMR* values than those designed for low seismic demands (SDC D_{min}).

Table 5-9 Summary of Collapse Performance Evaluations of Special Steel Concentrically Braced Frame Archetypes

Arch. Design ID No.	Design Configuration		Computed Overstrength and Collapse Margin Parameters					Acceptance Check	
	No. of Stories	SDC	Static Ω	*CMR*	μ_T	*SSF*	*ACMR*	Accept. *ACMR*	Pass/ Fail
Performance Group No. PG-1SCB									
2SCBFDmax	2	D_{max}	1.44	1.00	4.3	1.22	1.22	1.56	Fail
3SCBFDmax	3	D_{max}	1.41	1.60	6.1	1.28	2.05	1.56	Pass
Mean of Performance Group:			**1.42**				**1.63**	**1.96**	**Fail**
Performance Group No. PG-2SCB									
6SCBFDmax	6	D_{max}	1.28	2.18	2.4	1.21	2.64	1.56	Pass
12SCBFDmax	12	D_{max}	1.60	3.23	3.2	1.32	4.26	1.56	Pass
16SCBFDmax	16	D_{max}	2.11	2.64	1.8	1.21	3.20	1.46	Pass
Mean of Performance Group:			**1.67**				**3.37**	**1.96**	**Pass**
Performance Group No. PG-3SCB									
2SCBFDmin	2	D_{min}	1.38	1.73	5.8	1.12	1.94	1.56	Pass
3SCBFDmin	3	D_{min}	2.41	3.62	3.0	1.08	3.91	1.56	Pass
Mean of Performance Group:			**1.90**				**2.93**	**1.96**	**Pass**
Performance Group No. PG-4SCB									
6SCBFDmin	6	D_{min}	1.86	3.53	3.9	1.15	4.06	1.56	Pass
12SCBFDmin	12	D_{min}	2.18	5.00	1.4	1.10	5.50	1.56	Pass
16SCBFDmin	16	D_{min}	1.56	4.38	1.2	1.06	4.64	1.40	Pass
Mean of Performance Group:			**1.87**				**4.73**	**1.96**	**Pass**

In the case of BRBF archetypes, observed trends were less pronounced. Results showed more variation, but short-period BRBF archetypes generally had lower *ACMR* values, and the 2-story BRBF archetypes had especially low *ACMR* values in comparison with other BRBF archetypes. Results for 2-story and 6-story archetypes indicate that, for BRBF systems, archetypes designed for high seismic demands (SDC D_{max}) did not necessarily have lower *ACMR* values than archetypes designed for low seismic demands (SDC D_{min}).

The selection of analysis procedure used for design affected the performance evaluation. Taller archetypes designed using the RSA procedure had lower *ACMR* values than would have been expected given the apparent trend between short-period and long-period systems.

Table 5-10 Summary of Collapse Performance Evaluations of Buckling-Restrained Braced Frame Archetypes

Arch. Design ID No.	Design Configuration		Computed Overstrength and Collapse Margin Parameters					Acceptance Check	
	No. of Stories	SDC	Static Ω	*CMR*	μ_T	*SSF*	*ACMR*	Accept. *ACMR*	Pass/ Fail
Performance Group No. PG-1BRB									
2BRBFDmax	2	D_{max}	1.31	1.73	11.9	1.33	2.31	1.56	Pass
3BRBFDmax	3	D_{max}	1.48	2.85	22.7	1.39	3.96	1.56	Pass
Mean of Performance Group:			**1.40**				**3.13**	**1.96**	**Pass**
Performance Group No. PG-2BRB									
6BRBFDmax	6	D_{max}	1.47	3.29	15.5	1.53	5.03	1.56	Pass
12BRBFDmax	12	D_{max}	1.17	2.27	4.0	1.4	3.18	1.56	Pass
16BRBFDmax	16	D_{max}	1.00	3.14	3.1	1.32	4.15	1.56	Pass
Mean of Performance Group:			**1.21**				**4.12**	**1.96**	**Pass**
Performance Group No. PG-3BRB									
2BRBFDmin	2	D_{min}	1.44	1.71	6.6	1.13	1.94	1.56	Pass
3BRBFDmin	3	D_{min}	2.11	3.16	10.5	1.2	3.79	1.56	Pass
Mean of Performance Group:			**1.77**				**2.86**	**1.96**	**Pass**
Performance Group No. PG-4BRB									
6BRBFDmin	6	D_{min}	1.28	3.04	6.4	1.28	3.90	1.56	Pass
12BRBFDmin	12	D_{min}	1.44	2.86	3.1	1.21	3.46	1.56	Pass
16BRBFDmin	16	D_{min}	1.15	4.55	2.0	1.15	5.23	1.46	Pass
Mean of Performance Group:			**1.29**				**4.19**	**1.96**	**Pass**

Performance evaluation results by performance group are summarized in Table 5-11 for special SCBF archetypes and Table 5-12 for BRBF archetypes. To pass the performance evaluation criteria, the adjusted collapse margin ratio averaged across all archetypes in a performance group must exceed $ACMR_{10\%}$. For special SCBFs, the short-period SDC D_{min} performance group and all long-period performance groups passed this criterion. The short-period SDC D_{max} performance group did not. In the case of BRBFs, all performance groups passed this criterion.

Table 5-11 Summary of Results by Performance Group for Special Steel Concentrically Braced Frames

Performance Group Summary					
Group No.	Grouping Criteria				Performance Result
	Basic Config.	Design Load Level		Period Domain	
		Gravity	Seismic		
PG-1SCB	Double Story X-Braces	Typical	SDC D_{max}	Short	Fail
PG-2SCB				Long	Pass
PG-3SCB			SDC D_{min}	Short	Pass
PG-4SCB				Long	Pass

Table 5-12 Summary of Results by Performance Group for Buckling-Restrained Brace Frames

Performance Group Summary					
Group No.	Grouping Criteria				Performance Result
	Basic Config.	Design Load Level		Period Domain	
		Gravity	Seismic		
PG-1BRB	Double Story X-Braces	Typical	SDC D_{max}	Short	Pass
PG-2BRB				Long	Pass
PG-3BRB			SDC D_{min}	Short	Pass
PG-4BRB				Long	Pass

5.8 Evaluation of System Overstrength

In the Methodology, the system overstrength factor, Ω_0, is taken as the largest average value of the overstrength factor, Ω, computed for each performance group. Values of overstrength for individual archetypes and average values for each performance group are shown in Table 5-9 and Table 5-10. For special SCBFs, average values of overstrength varied between 1.3 and 2.4. Values did not show a specific trend among the performance groups and did not appear to be related to seismic design level. The resulting value of Ω_0 equal to 2.4 is larger but on the same order of magnitude as the value of 2.0 provided for special SCBF systems in ASCE/SEI 7-05.

For BRBFs, average values of overstrength varied between 1.0 and 2.1. The resulting value of Ω_0 equal to 2.1 is smaller but on the same order of magnitude as the value of 2.5 provided for BRBF systems in ASCE/SEI 7-05. Steel braced frame archetypes were deliberately configured to minimize the potential for overstrength. Close agreement between calculated and code-specified values of Ω_0 is likely to be related to this design objective.

5.9 Observations and Recommendations

5.9.1 Observations on System Performance

With the exception of the special SCBF, short-period, SDC D_{max} performance group, all special SCBF and BRBF archetypes met the acceptance criteria of the Methodology. System overstrength factors obtained in this study are comparable to values provided for both systems in ASCE/SEI 7-05.

In general, special SCBF archetypes had smaller values of *ACMR* than BRBF archetypes, and short-period archetypes had smaller values of *ACMR* than long-period archetypes. In some cases, archetypes designed for lower seismic demands had higher values of *ACMR* than archetypes designed for higher seismic demands. For the taller (i.e., long-period) archetypes, drift controlled the design in many cases, and member sizes were larger than would have otherwise been required considering the *R*-factor alone. This was likely a contributing factor in the observed trends in *ACMR* values between short-period and long-period archetypes. Observed trends were less pronounced in the case of BRBF archetypes.

Most of the special SCBF and BRBF archetypes passed the evaluation criteria, although some passed with greater margins than others. Archetypes that barely passed the criteria might possibly fail if the uncertainty were to increase, or if effects that were neglected (e.g., three-dimensional or torsional responses) were found to be significant.

The ELF and RSA procedures resulted in significantly different member sizes for tall and midrise braced frame archetypes. For the 16-story, special SCBF, SDC D_{max} archetype, member forces determined by ELF and RSA differed by as much as 50%. This difference was not as pronounced in low-rise archetypes. For the 6-story, special SCBF, SDC D_{max} archetype, member forces determined by both procedures were within 10%. When structures were controlled by drift, and member sizes became controlled by member stiffnesses needed to satisfy code drift requirements, the RSA procedure for computing drift resulted in much smaller member sizes.

Braced frame systems tend to concentrate damage at certain levels rather than distribute yielding over the height of a structure. Concentration of damage is related to the selection of member sizes. Because of limitations in the availability of member sizes, and the need to change member sizes to control drift and higher mode effects, the ratio of demand to capacity at each level is not uniform over height.

Figure 5-8 depicts demand and capacity profiles for the 16-story, BRBF, SDC D_{max} archetype. The demand profile is based on a pushover analysis, and the capacity is based on the strength of the braces at each level. As the lateral load increases, demand first meets the capacity at mid-height of the building, and the full capacity of the building at the base is never realized.

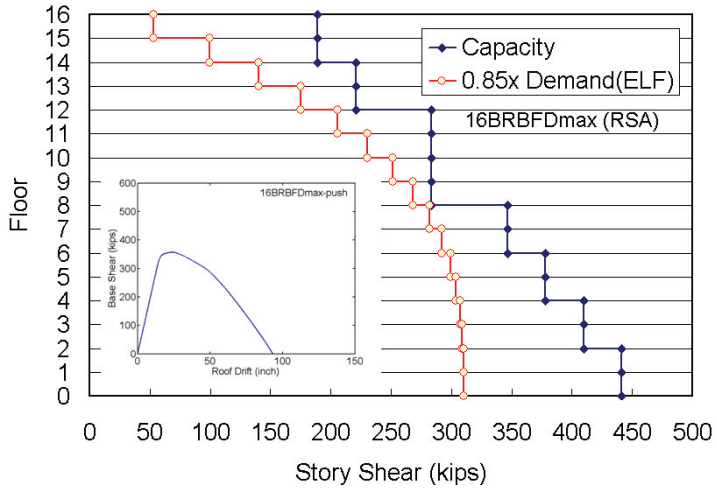

Figure 5-8 Demand profile of pushover analysis and approximate capacity of archetype 16BRBFD$_{max}$ (RSA).

When deformations are more uniformly distributed over the height of the building, overstrength is more likely to be large. When damage is concentrated in the lower levels, the impact on overstrength is relatively small because the capacity in the lower levels is more likely to be on the order of the design base shear. When damage is concentrated in the higher levels, however, the overall strength of the system is dominated by a level that is likely to be weaker, and overstrength could be 1.0 or less.

Pushover curves for SCBF archetypes showed a sudden drop in global strength upon brace buckling. This resulted in small estimated ductilities but could also result in an overestimation of system overstrength. In the numerical models, peak strength and drift at brace buckling are affected by the initial imperfection applied to the brace elements. A constant initial imperfection was assumed in the models, which implies that all of the braces were fabricated identically. In reality, the initial imperfection in each brace could vary, and the pushover responses may or may not be the same. Although overall collapse response of a frame with different initial imperfections would be expected to be similar under large deformations or after many cycles, values of peak strength and drift at brace buckling predicted by pushover analysis depend on the initial imperfection and should be used with caution.

In some analyses, archetypes did not collapse, even after all of the braces at a given level ruptured and lost all capacity in tension and compression. This was because the fully restrained beam-column connections in the model provided moment frame resistance to collapse. While the models included possible rupture due to low cycle fatigue, elements were not modeled to capture all of the substantial deterioration modes associated with beam plastic hinging.

Results suggest that *R* factors applied to short-period archetypes do not provide an acceptable margin against collapse. Structures with short fundamental periods are in

the energy-preserved region of the spectrum. Using a simple R-μ-T relation, the response modification factor, R, can be related to the ductility factor, μ:

$$R = \sqrt{2\mu - 1} \text{ or } \mu = \frac{R^2 + 1}{2} \quad (5\text{-}1)$$

For the short-period, 2-story, SCBF archetypes, an R factor of 6 would suggest a ductility factor of 18.5, which is much larger than a conventional buckling brace can develop. Smaller R factors for buildings with short periods might improve collapse resistance in the performance evaluation. For instance, if a target ductility of 6.0 is desired in this period range, the above equation would suggest that an R factor of 3.3 should be used. This effect might explain the failure of short-period archetypes in this and other trial applications.

5.9.2 Observations on the Methodology

The spectral shape factor (*SSF*) depends on the value of period-based ductility computed from a nonlinear static pushover analysis. In the case of special SCBF archetypes, pushover curves depended on assumptions of initial camber in the braces. Also, the negative post-yield tangent stiffness exhibited by special SCBF (and some BRBF) archetypes led to relatively small values of period-based ductility, resulting in possible underestimation of the *SSF*. As such, ductility estimates based on pushover analyses may be less accurate for determining values of *SSF* and *ACMR* for buckling braces than for other systems.

Quality ratings are determined on the basis of subjective judgment. These ratings should be reviewed across all systems on a consistent basis to have more confidence in the ratings. It is noted, however, that for most special SCBF and BRBF archetypes evaluated here, results were relatively insensitive to the quality ratings assumed.

Although all archetypes were designed to be in compliance with current code requirements, these same requirements could have been satisfied with different assumptions regarding structural layout, member size, proportions, and connection detailing. Variations in mechanical and dynamic properties would likely exist between the results obtained by different designers, or different sets of assumptions, and the potential for such differences should be considered in the performance evaluation of a proposed system.

5.9.3 Recommendations for Further Investigation

This study focused on a limited number of braced frame configurations, but steel braced frame buildings can have many different brace types and bracing configurations. In addition, code compliance can be achieved with many different sets of design assumptions. All these system variations would need to be studied in order to fully characterize the seismic performance of steel braced frame structures and identify appropriate seismic performance factors.

The SCBF archetypes designs utilized brace sizes that were larger than commonly considered in test programs. The local and global behavior of large braces is believed to be different from smaller braces, especially in the case of low-cycle fatigue. Ultimate behavior is also likely controlled by factors such as fracture of beams and columns near gusset plates and lateral torsional response of members. Additional testing is underway, but more data are needed to improve the ability of available analytical models to simulate all important deterioration behaviors for steel braced frame systems.

For practical reasons, analytical models were limited in their complexity. Additional studies with three-dimensional models are recommended to account for related failure modes at the local and global levels. Interaction of orthogonally oriented braced bays having shared columns should be addressed. The effect of in-plane torsional response due to brace buckling (or rupture) on one side of a building should be investigated considering two horizontal components of ground shaking. Use of finite element models, which can simulate yielding, local buckling, and low-cycle fatigue would also be desirable. Such models could account for the deterioration of beams and columns due to local buckling, and rupture of various members and connections not considered herein.

Chapter 6
Trial Application: Steel Moment Frame Structures

6.1 Introduction

This chapter presents a trial application of the FEMA P-695 Methodology on special steel moment frame (special SMF) structures. It summarizes design requirements and available test data for steel moment frames, explains the development of moment frame archetype configurations, documents the nonlinear modeling approach, presents the results of a performance evaluation, and summarizes observations on the Methodology specific to steel moment frame systems. Results are investigated for a range of building heights and design parameters.

6.2 Overview and Approach

In this trial application, the special steel moment frame system defined in AISC 341-05, *Seismic Provisions for Structural Steel Buildings* (AISC, 2005a), and AISC 358-05, *Prequalified Connections for Special and Intermediate Steel Moment Frames for Seismic Applications* (AISC, 2005b), was considered as if it was a new system proposed for inclusion in ASCE/SEI 7-05, *Minimum Design Loads for Buildings and Other Structures* (ASCE, 2006). Although the intent was to treat special steel moment frame systems as a new system, the purpose was not to re-derive or validate seismic performance factors (R, Ω_0, and C_d) for this system. Rather, it was to examine whether steel moment frame systems would satisfy the acceptance criteria of the FEMA P-695 Methodology, test the application of the Methodology with respect to these systems, and identify possible improvements to the Methodology or current steel moment frame design provisions.

The system design requirements of ASCE/SEI 7-05, including minimum base shear and story drift limits, were used as the basis for design, with the exception that C_d was taken equal to R, as specified in the FEMA P-695 Methodology. The value of R for special SMF systems is 8.

Steel moment frame systems can have many different configurations, and connection details can vary significantly. For practical reasons, the scope of the beta testing effort was necessarily limited, and only frames with reduced beam section (RBS) connections were investigated.

6.3 Structural System Information

6.3.1 Design Requirements

Special steel moment frame systems were designed and detailed in accordance with the strength design requirements in AISC 341-05 and the seismic design requirements in ASCE/SEI 7-05. The criteria given in AISC 358-05 were followed for the design of RBS connections.

6.3.2 Quality Rating of Design Requirements

Design requirements and connection design criteria for special SMF systems represent many years of development and include lessons learned from a number of major earthquakes. As a consequence, a quality rating of (A) Superior was assigned to the design requirements for special SMF systems.

6.3.3 Test Data

A large number of cyclic-load tests of beams and beam-to-column connections have been performed over the last 40 years. These tests form the basis of present code requirements for design and detailing of structural components and connections and for the component analytical model used for collapse prediction. The metadata and results of many of these tests are carefully documented in a database by Lignos and Krawinkler (2007).

Many tests have been performed in response to connection problems observed after the 1994 Northridge earthquake. These tests have been evaluated carefully and have resulted in detailed criteria for a set of pre-qualified connections published in AISC 358-05.

Considerable data are available, but a shortage of available test data is noted on the inelastic behavior of deep columns subjected to high axial forces and cyclic bending moments. More beam-to-column subassembly tests are needed to fully assess the effects of a composite slab on component strength and stiffness, and more substructure tests are needed to assess the restraining effects of the floor system on the deterioration characteristics of beams.

6.3.4 Quality Rating of Test Data

Although considerable test data are available, these data have limitations that reduce confidence in certain modeling parameters and failure criteria. As a consequence, a quality rating of (B) Good was assigned to the test data for special SMF systems.

6.4 Archetype Configurations

A rectangular plan configuration consisting of a three-bay perimeter frame on each side was selected for investigation of special SMF systems over a range of building heights and design parameters. The representative building plan, which was the same for all archetypes, is shown in Figure 6-1. In the design process it was assumed that

the moment frames resist all the seismic loading, but only receive tributary gravity loads as indicated in the shaded portion of figure. In addition to building height, the following additional design variables were also considered: period, level of seismic design loading (in terms of Seismic Design Category), and design basis (in terms of analysis procedure).

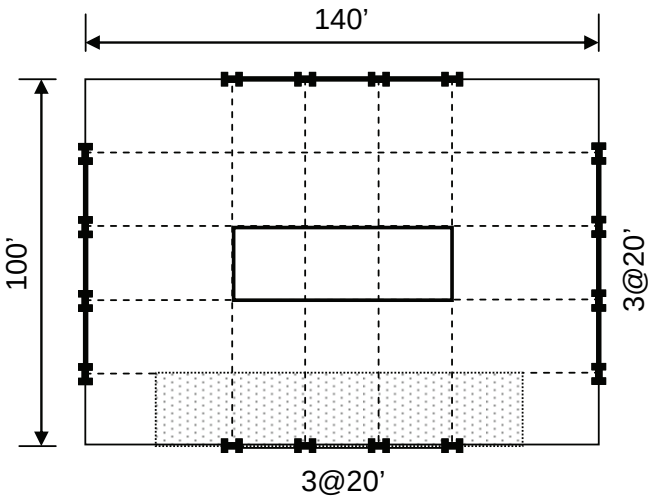

Figure 6-1 Typical plan configuration of special SMF archetypes.

Archetypes were grouped into performance groups containing a set of common features or behavioral characteristics, including Seismic Design Category (SDC), gravity load level, code-based period, and design basis. Considering the design variables listed above, a total of 20 archetypes were developed. These were divided into eight performance groups, four attributed to design using the Equivalent Lateral Force (ELF) procedure and four attributed to design using the Response Spectrum Analysis (RSA) procedure, as shown in Table 6-1 and Table 6-2. Performance groups with less than three archetypes did not meet the minimum number of archetypes per performance group required in a full application of the Methodology.

Building heights equal to 1, 2, 4, 8, 12, and 20 stories were considered. For the ELF design basis, it was decided to focus primarily on story heights for which the ELF procedure is widely used in practice (1-story to 4-story archetypes). An archetype of 20 stories was also investigated to push the envelope of ELF design procedures and potential system performance. This decision resulted in three ELF performance groups with less than three archetypes and one performance group with a significant variation in the number of stories (i.e., 2, 4, and 20 stories). In general, this is not an ideal distribution of archetype configurations within a performance group.

Table 6-1 Performance Groups for Evaluation of Special Steel Moment Frame Archetypes (ELF Design Basis)

Performance Group Summary					
Group No.	Grouping Criteria				Number of Archetypes
	Basic Config.	Design Load Level		Period Domain	
		Gravity	Seismic		
PG-1ELF	RBS Perimeter Frame 20-ft Bays	Typical	SDC D_{max}	Short	2[1]
PG-2ELF				Long	2[2]
PG-3ELF			SDC D_{min}	Short	1[3]
PG-4ELF				Long	3[4]

[1] Short-period, SDC D_{max}, PG-1, includes 1-story and 2-story archetypes.

[2] Long-period, SDC D_{max}, PG-2, includes 4-story and 20-story archetypes.

[3] Short-period, SDC D_{min}, PG-3, includes a single, 1-story archetype.

[4] Long-period, SDC D_{min}, PG-4, includes 2-story, 4-story, and 20-story archetypes.

Table 6-2 Performance Groups for Evaluation of Special Steel Moment Frame Archetypes (RSA Design Basis)

Performance Group Summary					
Group No.	Grouping Criteria				Number of Archetypes
	Basic Config.	Design Load Level		Period Domain	
		Gravity	Seismic		
PG-1RSA	RBS Perimeter Frame 20-ft Bays	Typical	SDC D_{max}	Short	2[1]
PG-2RSA				Long	4[2]
PG-3RSA			SDC D_{min}	Short	1[3]
PG-4RSA				Long	5[4]

[1] Short-period, SDC D_{max}, PG-1, includes 1-story and 2-story archetypes.

[2] Long-period, SDC D_{max}, PG-2, includes 4-story, 8-story, 12-story and 20-story archetypes.

[3] Short-period, SDC D_{min}, PG-3, includes a single, 1-story archetype.

[4] Long-period, SDC D_{min}, PG-4, includes 2-story, 4-story, 8-story, 12-story and 20-story archetypes.

Key seismic design parameters for the special SMF archetypes are summarized in Table 6-3 and Table 6-4. These include the code-based period, T (calculated using the equation, $T=C_u T_a$, provided in ASCE/SEI 7-05), fundamental period, T_1 (calculated from eigenvalue analysis), the seismic base shear coefficient, V/W, and the MCE-level spectral acceleration, S_{MT}. More detailed information on the design of all special SMF archetypes is provided in Appendix D.

Table 6-3 Special Steel Moment Frame Archetype Design Properties (ELF Design Basis)

Archetype Design ID Number	No. of Stories	Key Archetype Design Parameters						
		Gravity Loads	Seismic Design Criteria					$S_{MT}(T)$ (g)
			SDC	*R*	*T* (sec)	T_1 (sec)	*V*/*W* (g)	
Performance Group No. PG-1ELF								
1ELF	1	Typical	D_{max}	8	0.34	0.71	0.125	1.50
2ELF	2	Typical	D_{max}	8	0.56	0.87	0.125	1.50
Performance Group No. PG-2ELF								
3ELF	4	Typical	D_{max}	8	0.95	1.30	0.079	0.95
4ELF	20	Typical	D_{max}	8	3.37	2.48	0.044	0.32
Performance Group No. PG-3ELF								
5ELF	1	Typical	D_{min}	8	0.37	1.62	0.062	0.75
Performance Group No. PG-4ELF								
6ELF	2	Typical	D_{min}	8	0.60	1.74	0.042	0.50
7ELF	4	Typical	D_{min}	8	1.02	1.94	0.024	0.29
8ELF	20	Typical	D_{min}	8	3.61	3.44	0.022	0.08

Table 6-4 Special Steel Moment Frame Archetype Design Properties (RSA Design Basis)

Archetype Design ID Number	No. of Stories	Key Archetype Design Parameters						
		Gravity Loads	Seismic Design Criteria					$S_{MT}(T)$ (g)
			SDC	*R*	*T* (sec)	T_1 (sec)	*V*/*W* (g)	
Performance Group No. PG-1RSA								
1RSA	1	Typical	D_{max}	8	0.34	0.71	0.106	1.50
2RSA	2	Typical	D_{max}	8	0.56	0.91	0.106	1.50
Performance Group No. PG-2RSA								
3RSA	4	Typical	D_{max}	8	0.95	1.62	0.067	0.95
4RSA	8	Typical	D_{max}	8	1.64	2.29	0.039	0.55
5RSA	12	Typical	D_{max}	8	2.25	3.12	0.037	0.40
6RSA	20	Typical	D_{max}	8	3.37	4.47	0.037	0.27
Performance Group No. PG-3RSA								
7RSA	1	Typical	D_{min}	8	0.37	1.66	0.053	0.75
Performance Group No. PG-4RSA								
8RSA	2	Typical	D_{min}	8	0.60	1.83	0.035	0.50
9RSA	4	Typical	D_{min}	8	1.02	2.62	0.021	0.29
10RSA	8	Typical	D_{min}	8	1.75	3.55	0.019	0.17
11RSA	12	Typical	D_{min}	8	2.41	4.48	0.019	0.12
12RSA	20	Typical	D_{min}	8	3.61	5.74	0.019	0.08

6.4.1 Summary of Design Observations

Each archetype configuration was designed in accordance with requirements based on strength criteria, drift criteria, and P-Delta criteria. Member sizes were governed

by different phenomena, depending on the level of seismic design loading (SDC D_{max} versus SDC D_{min}) and on the number of stories. Key observations on the design of special SMF archetype are summarized below.

- Most beam sizes were controlled by stiffness considerations (either story drift limitation or P-Delta design requirements) rather than strength criteria. In the sections that follow, archetypes controlled by drift requirements are identified with a "D", and the archetypes controlled by P-Delta considerations are identified with a "P".
- Sizes of interior columns were usually controlled by beam sizes because of strong column-weak beam considerations. Sizes of end columns were often controlled by *P-M* interaction or by overstrength considerations. For taller SMF archetypes, the ASCE/SEI 7-05 P-Delta stability check often required an increase in the member sizes, particularly for the more flexible archetypes designed for SDC D_{min} seismic loading.
- Since archetype designs were based on $C_d = R$, a value of $C_d = 8.0$, rather than the code required 5.5, was used. Because drift considerations controlled many of the member sizes, the archetypes were often stiffer and stronger than required by ASCE/SEI 7-05 design requirements.
- For low-rise frames, story drift was governed by the shear mode of drift, caused by flexural and shear deformations in beams and columns and by shear deformations in the joint panel zone. For taller frames (above 4 stories), the flexural mode of drift, caused primarily by axial deformations in the end columns, became important. Control of the shear mode of drift (so that shear and flexural displacements were less than allowable values of drift) required larger beam sizes. In taller SMF archetypes, maximum beam sizes occurred several stories above the base. Control of the flexural mode of drift required larger end columns in the lower stories in some cases.
- Because of the inherent flexibility of special SMF systems, P-Delta considerations often controlled member sizes in the lower stories of tall archetypes. With the exception of the 1-story ELF archetype, member sizes in the lower stories of all SDC D_{min} archetypes, were controlled by P-Delta considerations. Explicit consideration of this is discussed in Appendix D.
- In low-rise archetypes, differences in member size between ELF and RSA designs were relatively small (with RSA member sizes being somewhat smaller). In high-rise 20-story SDC D_{max} and SDC D_{min} archetypes, differences became large. In the RSA procedure (per ASCE/SEI 7-05), minimum base shear requirements are explicitly excluded from consideration in the drift calculation, which is not the case when the ELF procedure is used. In long-period structures, differences in lateral loading under which story drifts were calculated became significant. In the case of 20-story SDC D_{max} archetypes, the ELF base shear for

drift calculation was about 3.0 times the RSA base shear for drift calculation. This resulted in a factor of three difference in the elastic stiffness between ELF and RSA archetypes, and was a significant contributor to observed differences in system performance based on design procedure.

- The large stiffness required for the 20-story, ELF, SDC D_{max} design could only be satisfied using very large beam and column sections. Heavy W36 sections were used for columns and heavy W30 and W40 sections were used for beams. AISC 358-05 specifies the use of beam sections weighing less than 300 lb/ft. Because this archetype was a special case intending to push the limits of the ELF design procedure to study broader system effects, this limitation was ignored and beam sections exceeding 300 lb/ft were used in this study.

6.5 Nonlinear Model Development

6.5.1 Modeling Approach

For nonlinear analysis, each archetype was idealized using two-dimensional models. Models were implemented in a modified version of the Drain-2DX analysis program (Prakash et al., 1993). P-Delta effects were modeled with a leaning column with zero flexural stiffness placed in parallel with the frame. This leaning column was loaded with a vertical load at each floor level representing half of the total system gravity load (taken as $1.05D + 0.25L$) that was not directly tributary to the column elements of the frame.

Components were modeled as elastic elements, with all inelastic behavior concentrated in plastic hinge regions at the member ends. A typical floor model is shown in Figure 6-2. Models consisted of three elastic beam elements spanning between points of RBS connections, six elastic beams between the RBS connections and the column faces, four rigid parallelogram models representing the joint panel zone, and elastic column elements framing into the parallelograms. The elements were connected with rotational springs representing inelastic behavior in a concentrated plasticity mode. Details of the spring models are presented below.

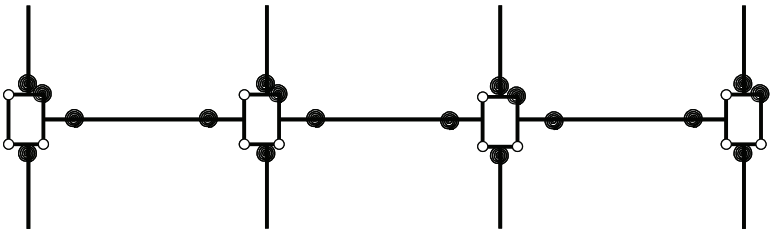

Figure 6-2 Typical floor model used for special SMF archetypes.

Nonlinear analysis models were based on concentrated plastic hinge concepts. The moment-rotation properties of plastic hinges were obtained from regression equations derived from experimental data of about 300 test specimens. All contributions to lateral strength and stiffness from the gravity system were neglected so that only the

SMFs were assumed to provide seismic resistance. The effects of the composite floor slab were not considered because of a lack of information available to model these effects with confidence. Fracture at beam-to-column connection welds was not considered. It was assumed that such fractures were adequately controlled by special SMF design requirements and the RBS connection configuration.

Collapse considered in the analyses was based on sidesway collapse modes. In sidesway collapse, structures lose lateral load-resisting capability in single-story or multistory mechanisms due to a combination of P-Delta effects and structural component deterioration. Vertical collapse, caused by effects such as column buckling or connection failure, was not considered. Although vertical collapse due to these effects can be represented using non-simulated collapse modes, connection fracture was considered an unlikely failure mode for RBS connections, and column buckling was spot-checked in the analytical results and found not to be critical.

Bases of 1-story and 2-story SMF columns were assumed to be pinned, and bases of taller SMF columns were assumed to be fixed. Analyses showed that plastic rotation demands at these locations were large. It was assumed that deterioration at column base hinge locations could be modeled similar to beam hinges. Actual plastic rotation capacity depends strongly on column base detailing. Although this detailing could have an effect on collapse capacity of special SMFs, potential differences in column base details were not considered in the collapse analyses.

6.5.2 Joint Panel Zone Model

Panel zones were modeled with eight rigid elements connected by hinges and bilinear rotational springs, as shown in Figure 6-3a. The rotational springs were used to represent the panel zone shear force-shear deformation behavior with a tri-linear model of the type shown in Figure 6-3b.

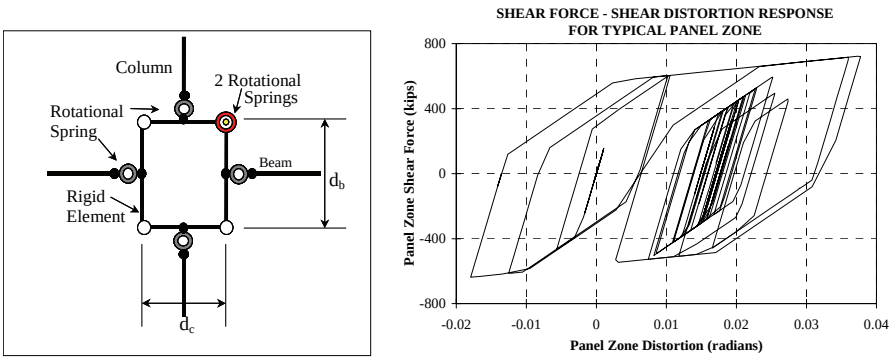

(a) Parallelogram model (b) Shear force–deformation behavior

Figure 6-3 Joint panel zone model (PEER/ATC, 2010).

Details of this model, along with recommended strength and stiffness properties, were taken from the PEER/ATC 72-1 report, *Modeling and Acceptance Criteria for*

Seismic Design and Analysis of Tall Buildings (PEER/ATC, 2010). Panel zone deterioration was not considered.

6.5.3 Beam Plastic Hinge Model

Inelastic behavior at beam plastic hinge locations was represented by rotational springs with appropriate strength, stiffness, and deterioration properties. These properties were determined in accordance with guidelines for steel beam deterioration modeling in PEER/ATC 72-1, based on the following:

- A monotonic backbone curve of the type shown in Figure 6-4, in which the force quantity is moment, M, and the deformation quantity is rotation, θ.

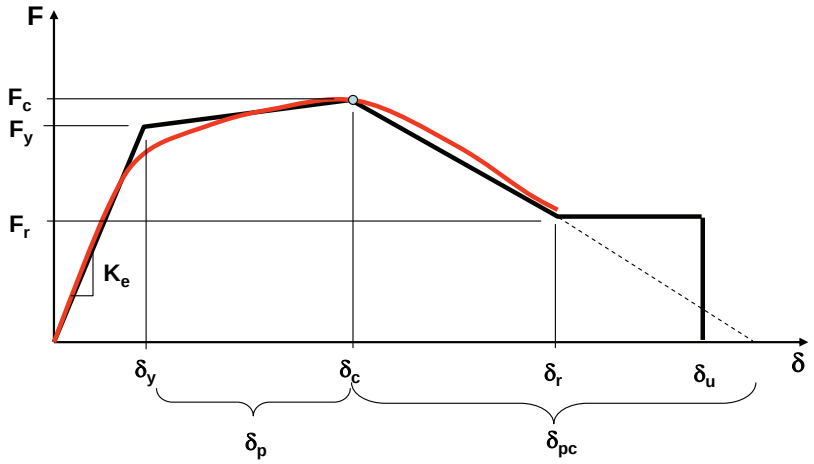

Effective yield strength and deformation (F_y and δ_y)
Effective elastic stiffness, $K_e = F_y/\delta_y$
Strength cap and associated deformation for monotonic loading (F_c and δ_c)
Pre-capping plastic deformation for monotonic loading, δ_p
Effective post-yield tangent stiffness, $K_p = (F_c\text{-}F_y)/\ \delta_p$
Post-capping deformation range, δ_{pc}
Effective post-capping tangent stiffness, $K_{pc} = F_c/\ \delta_{pc}$
Residual strength, $F_r = \kappa F_y$
Ultimate deformation, δ_u

Figure 6-4 Parameters of the initial (monotonic) backbone curve of the Ibarra-Krawinkler model (PEER/ATC, 2010).

- A simple bilinear hysteresis model used to simulate the basic cyclic characteristics of plastic hinges in steel beams.
- A set of cyclic deterioration rules developed by Ibarra et al. (2005) and modified by Lignos and Krawinkler (2009), as summarized in PEER/ATC 72-1. Use of these cyclic deterioration rules permitted modeling of basic and post-capping strength deterioration as illustrated in Figure 6-5, as well as unloading stiffness deterioration.

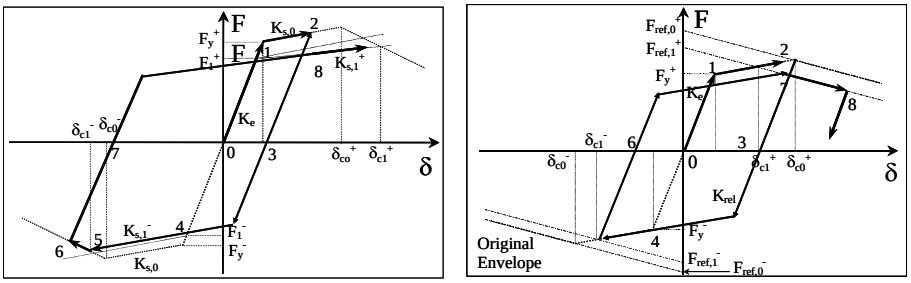

Figure 6-5 Basic and post-capping strength deterioration.

Parameters of this deterioration model have been calibrated against experimentally obtained moment rotation relationships assembled in a database of about 300 component or assembly tests (Lignos and Krawinkler, 2007 and 2009). A typical calibration result is shown in Figure 6-6. Examples of backbone curves (ignoring the elastic range) are shown in Figure 6-7.

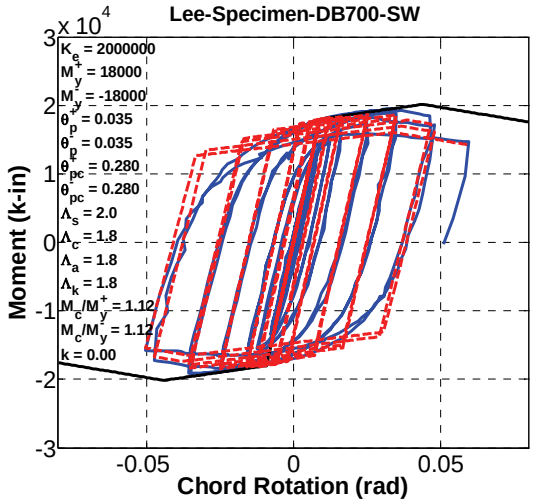

Figure 6-6 Calibration between deterioration model and experimental results (data from Lee et al., 2005).

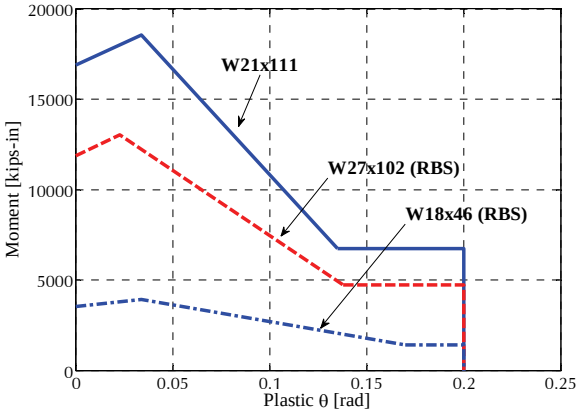

Figure 6-7 Example moment-rotation backbone curves.

6.5.4 Column Plastic Hinge Model

Experimental data on plastic hinging in columns with relatively high axial loads are rare. The study by Newell and Uang (2008) demonstrated that the plastic rotation capacity of heavy W14 sections is large, and that reduced bending strength in the presence of an axial load is well represented by the column *P-M* interaction equations given in AISC/ANSI 360-05, *Specification for Structural Steel Buildings*, (AISC, 2005c). The Newell and Uang tests, however, were concerned only with heavy W14 sections and do not permit extrapolation to deeper sections. For this reason, modeling parameters obtained from the Lignos and Krawinkler (2009) regression equations for "other than RBS" beams have also been used for columns. All other parameters are defined in the same manner as for the beam plastic hinge model.

To approximately account for the effect of axial force on column bending strength, a representative axial force was estimated from pushover analyses, taken as P_{grav} + $0.5P_{E,max}$, where $P_{E,max}$ is the maximum axial force due to lateral loading. A reduced bending strength was then determined using this axial force and the AISC *P-M* interaction equation and subsequently used in the response history analysis models. Although the column bending strength should change as a function of the variable axial force occurring in the analysis, such a compromise was necessary because presently employed deterioration models cannot account for the effect of constantly varying axial forces on bending strength.

6.5.5 Quality Rating of Analytical Models

Special SMF designs are controlled by many detailing and capacity design requirements that limit the extent of possible failure modes. Analytical models used in this study are able to simulate the primary expected failure mode reasonably well by capturing flexural hinging and post-peak degrading response under both monotonic and cyclic loading. They are also able to directly simulate structural response up to sidesway collapse and have been well calibrated to experimental data. There are, however, some limitations, specifically with regard to column axial load and plastic hinge modeling, as well as slab effects on beam properties. Recognizing that the modeling approach is able to directly simulate structural response up to collapse, but that some limitations exist, a quality rating of (B) Good was assigned to the analytical models for special SMF systems.

6.6 Nonlinear Analyses

For each archetype, a pushover analysis was conducted with a lateral load distribution corresponding to the fundamental mode shape and mass distribution of the structure. Nonlinear static pushover analyses were used to evaluate system overstrength and period-based ductility, as well as to help verify the structural model. Figure 6-8 shows an example pushover curve for the set of 4-story special SMF archetypes.

For the 4-story, ELF, SDC D_{max} archetype, global yielding occurred at a roof drift of about 0.85%. The overstrength factor for this archetype was computed as $\Omega = 2.88$, and the period-based ductility capacity was computed as $\mu_T = 5.3$.

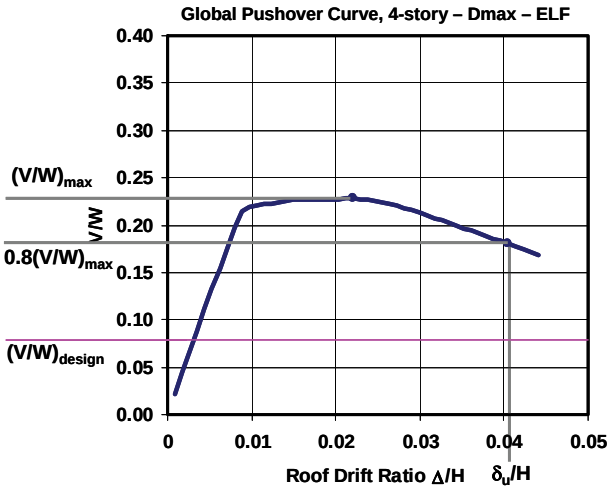

Figure 6-8 Example pushover curve and illustration of overstrength, Ω, and ultimate displacement, δ_u.

The archetype was analyzed using Rayleigh damping of 2.5% at the first mode period T_1 and at $T = 0.2T_1$. Complete incremental dynamic analyses (IDA) were not performed. Instead, target scale factors for the 44 ground motion records provided as part of the Methodology were selected and scaled until 22 collapses were obtained. The spectral acceleration at collapse, S_{CT}, was computed for each of the 44 ground motion records, and the median collapse level, $\hat{S}_{CT}$, was determined to be 1.72 g. The collapse margin ratio, calculated as the ratio of $\hat{S}_{CT}$ to the Maximum Considered Earthquake (MCE) ground motion spectral demand, S_{MT}, was equal to 1.81 for this archetype.

Values of overstrength, Ω, from pushover analysis, and the collapse margin ratio, *CMR*, from incremental dynamic analysis, are summarized in Table 6-5 for ELF designs, and Table 6-6 for RSA designs.

Table 6-5 Summary of Collapse Results for Special Steel Moment Frame Archetypes (ELF Design Basis)

Archetype Design ID Number	Design Configuration			Pushover and IDA Results			
	No. of Stories	Gravity Loads	SDC	Static Ω	S_{MT} [T] (g)	S_{CT} [T] (g)	*CMR*
Performance Group No. PG-1ELF							
1ELF	1	Typical	D_{max}	4.63	1.50	3.81	2.54
2ELF	2	Typical	D_{max}	3.69	1.50	3.42	2.28
Performance Group No. PG-2ELF							
3ELF	4	Typical	D_{max}	2.88	0.95	1.72	1.81
4ELF	20	Typical	D_{max}	4.45	0.27	0.35	1.33
Performance Group No. PG-3ELF							
5ELF	1	Typical	D_{min}	2.55	0.75	1.63	2.18
Performance Group No. PG-4ELF							
6ELF	2	Typical	D_{min}	3.44	0.50	1.15	2.31
7ELF	4	Typical	D_{min}	4.71	0.29	0.95	3.24
8ELF	20	Typical	D_{min}	4.67	0.08	0.18	2.14

Table 6-6 Summary of Collapse Results for Special Steel Moment Frame Archetypes (RSA Design Basis)

Archetype Design ID Number	Design Configuration			Pushover and IDA Results			
	No. of Stories	Gravity Loads	SDC	Static Ω	S_{MT} [T] (g)	S_{CT} [T] (g)	*CMR*
Performance Group No. PG-1RSA							
1RSA	1	Typical	D_{max}	5.46	1.50	3.81	2.54
2RSA	2	Typical	D_{max}	3.94	1.50	3.33	2.22
Performance Group No. PG-2RSA							
3RSA	4	Typical	D_{max}	2.21	0.95	1.38	1.46
4RSA	8	Typical	D_{max}	3.27	0.55	0.78	1.42
5RSA	12	Typical	D_{max}	2.68	0.40	0.55	1.38
6RSA	20	Typical	D_{max}	2.27	0.27	0.32	1.21
Performance Group No. PG-3RSA							
7RSA	1	Typical	D_{min}	2.84	0.75	1.77	2.36
Performance Group No. PG-4RSA							
8RSA	2	Typical	D_{min}	3.59	0.50	1.49	2.97
9RSA	4	Typical	D_{min}	3.27	0.29	0.62	2.10
10RSA	8	Typical	D_{min}	2.71	0.17	0.43	2.52
11RSA	12	Typical	D_{min}	2.48	0.12	0.37	2.99
12RSA	20	Typical	D_{min}	2.61	0.08	0.20	2.40

6.7 Performance Evaluation

In the Methodology, adjusted collapse margin ratios (*ACMR*s) are obtained by multiplying the *CMR*s, computed from nonlinear dynamic analysis results by the spectral shape factor (*SSF*). The acceptable average value of *ACMR* for each performance group is denoted by $ACMR_{10\%}$. The acceptable value of *ACMR* for individual archetypes within a performance group is denoted by $ACMR_{20\%}$.

Values of $ACMR_{10\%}$ and $ACMR_{20\%}$ are determined based on total system collapse uncertainty, β_{TOT}. Collapse uncertainty is a function of the quality ratings associated with the design requirements, test data, and nonlinear models, as well as record-to-record uncertainty. Quality ratings assigned to design requirements, test data, and nonlinear models for steel moment frame systems are summarized in Table 6-7.

Table 6-7 Summary of Quality Ratings for Special Steel Moment Frame Systems

System	Design Requirements	Test Data	Nonlinear Modeling
Special SMFs	A	B	B

6.7.1 Summary of Performance Evaluation Results

Performance evaluation results for individual special SMF archetypes are summarized in Table 6-8 for ELF designs and Table 6-9 for RSA designs.

Table 6-8 Summary of Collapse Performance Evaluations of Special Steel Moment Frame Archetypes (ELF Design Basis)

Arch. Design ID No.	Design Configuration			Computed Overstrength and Collapse Margin Parameters					Acceptance Check	
	No. of Stories	Gravity Loads	SDC	Static Ω	*CMR*	μ_T	*SSF*	*ACMR*	Accept. *ACMR*	Pass/ Fail
Performance Group No. PG-1ELF										
1ELF	1	Typ.	D_{max}	4.63	2.54	3.76	1.21	3.08	1.52	Pass
2ELF	2	Typ.	D_{max}	3.69	2.28	4.72	1.26	2.86	1.52	Pass
Mean of Performance Group:				**4.16**				**2.97**	**1.90**	**Pass**
Performance Group No. PG-2ELF										
3ELF	4	Typ.	D_{max}	2.88	1.81	5.3	1.35	2.45	1.52	Pass
4ELF	20	Typ.	D_{max}	4.45	1.33	1.09	1.08	1.43	1.36	Pass
Mean of Performance Group:				**3.67**				**1.94**	**1.75**	**Pass**
Performance Group No. PG-3ELF										
5ELF	1	Typ.	D_{min}	2.55	2.18	2.50	1.16	2.53	1.47	Pass
Mean of Performance Group:				**2.55**				**2.53**	**1.81**	**Pass**
Performance Group No. PG-4ELF										
6ELF	2	Typ.	D_{min}	3.44	2.31	2.17	1.15	2.66	1.44	Pass
7ELF	4	Typ.	D_{min}	4.71	3.24	3.98	1.31	4.23	1.52	Pass
8ELF	20	Typ.	D_{min}	4.67	2.14	1.50	1.17	2.51	1.39	Pass
Mean of Performance Group:				**4.27**				**3.13**	**1.77**	**Pass**

Table 6-9 Summary of Collapse Performance Evaluations of Special Steel Moment Frame Archetypes (RSA Design Basis)

Arch. Design ID No.	Design Configuration			Computed Overstrength and Collapse Margin Parameters					Acceptance Check	
	No. of Stories	Gravity Loads	SDC	Static Ω	*CMR*	μ_T	*SSF*	*ACMR*	Accept. *ACMR*	Pass/ Fail
Performance Group No. PG-1RSA										
1RSA	1	Typ.	D_{max}	5.46	2.54	3.76	1.21	3.08	1.52	Pass
2RSA	2	Typ.	D_{max}	3.94	2.22	4.02	1.23	2.73	1.52	Pass
Mean of Performance Group:				**4.70**				**2.91**	**1.90**	**Pass**
Performance Group No. PG-2RSA										
3RSA	4	Typ.	D_{max}	2.21	1.46	4.84	1.33	1.95	1.52	Pass
4RSA	8	Typ.	D_{max}	3.27	1.42	2.74	1.30	1.85	1.50	Pass
5RSA	12	Typ.	D_{max}	2.68	1.38	2.35	1.27	1.75	1.46	Pass
6RSA	20	Typ.	D_{max}	2.27	1.21	1.91	1.22	1.49	1.42	Pass
Mean of Performance Group:				**2.61**				**1.76**	**1.81**	**Fail**
Performance Group No. PG-3RSA										
7RSA	1	Typ.	D_{min}	2.84	2.36	2.34	1.15	2.72	1.46	Pass
Mean of Performance Group:				**2.84**				**2.72**	**1.78**	**Pass**
Performance Group No. PG-4RSA										
8RSA	2	Typ.	D_{min}	3.59	2.97	2.90	1.19	3.55	1.51	Pass
9RSA	4	Typ.	D_{min}	3.27	2.10	2.69	1.24	2.60	1.49	Pass
10RSA	8	Typ.	D_{min}	2.71	2.52	3.55	1.29	3.24	1.48	Pass
11RSA	12	Typ.	D_{min}	2.48	2.99	3.03	1.33	3.97	1.52	Pass
12RSA	20	Typ.	D_{min}	2.61	2.40	2.32	1.27	3.04	1.46	Pass
Mean of Performance Group:				**2.93**				**3.28**	**1.84**	**Pass**

Performance evaluation results by performance group are summarized in Table 6-10 for ELF designs and Table 6-11 for RSA designs. To pass the performance evaluation criteria, individual archetypes must have adjusted collapse margin ratios exceeding $ACMR_{20\%}$ and the adjusted collapse margin ratio averaged across all archetypes in a performance group must exceed $ACMR_{10\%}$.

All individual archetypes and almost all performance groups pass the acceptability criteria. The exception is the long-period, SDC D_{max}, RSA performance group (PH-2RSA), in which relatively poor performance is dominated by the low *ACMR*s of the 12- and 20-story archetypes.

For special SMFs designed using the ELF procedure, all performance groups passed the acceptance criteria. In the case of special SMFs designed using the RSA procedure, the long-period SDC D_{min} performance group and all short-period performance groups passed the criteria. The long-period SDC D_{max} performance group did not.

Table 6-10 Summary of Results by Performance Group for Special Steel Moment Frames (ELF Design Basis)

Performance Group Summary					
Group No.	Grouping Criteria				Performance Result
	Basic Config.	Design Load Level		Period Domain	
		Gravity	Seismic		
PG-1ELF	RBS Perimeter Frame 20-ft Bays	Typical	SDC D_{max}	Short	Pass
PG-2ELF				Long	Pass
PG-3ELF			SDC D_{min}	Short	Pass
PG-4ELF				Long	Pass

Table 6-11 Summary of Results by Performance Group for Special Steel Moment Frames (RSA Design Basis)

Performance Group Summary					
Group No.	Grouping Criteria				Performance Result
	Basic Config.	Design Load Level		Period Domain	
		Gravity	Seismic		
PG-1RSA	RBS Perimeter Frame 20-ft Bays	Typical	SDC D_{max}	Short	Pass
PG-2RSA				Long	Fail
PG-3RSA			SDC D_{min}	Short	Pass
PG-4RSA				Long	Pass

Computed *ACMRs* are presented graphically in Figure 6-9. For each archetype, the criterion that dominated member design is identified. The letter "D" implies that drift design controlled, and the letter "P" implies that P-Delta design controlled most of the beam sizes in the lower stories. It is seen that P-Delta considerations governed most of the SDC D_{min} archetypes. With the exception of some members near the top of some archetypes, almost none of the members were controlled by strength.

Calculated *ACMRs* did not follow predictable patterns. For SDC D_{max} archetypes, values of *ACMR* usually decreased with the number of stories, but for SDC D_{min} archetypes, values of *ACMR* often increased with the number of stories. Possible reasons are many, including the dominance of different design criteria for different structures. Member sizes of SDC D_{max} archetypes were usually drift controlled, whereas lower story member sizes of SDC D_{min} archetypes were mostly P-Delta controlled. Variations in controlling design criteria had a dominant effect on the collapse capacity of individual archetypes.

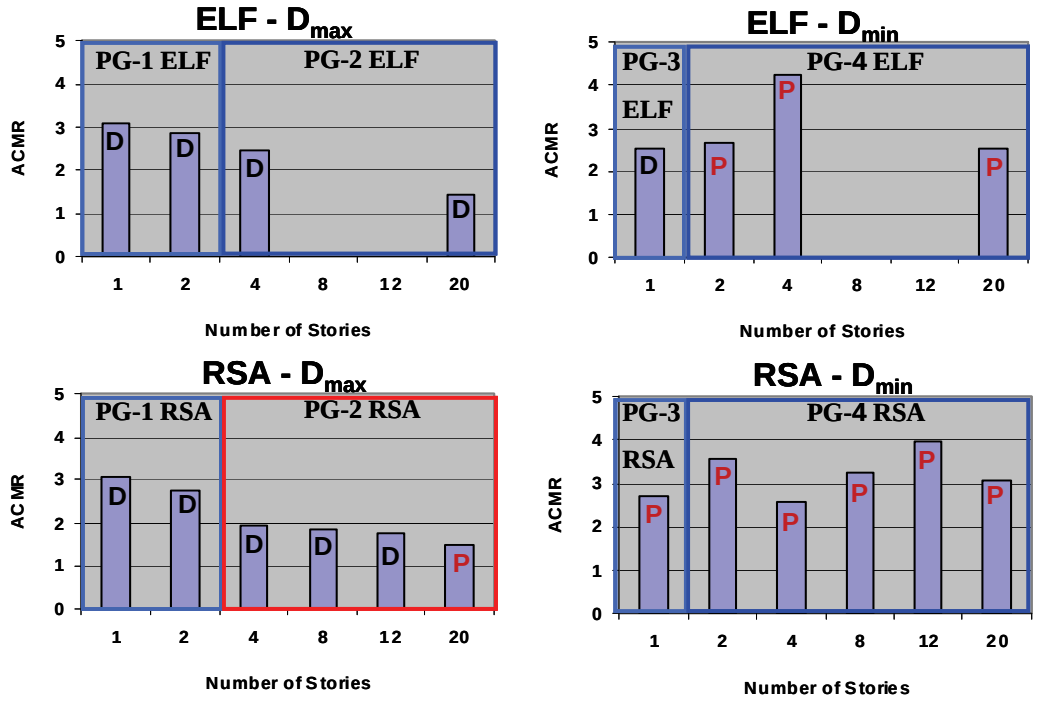

Figure 6-9 Graphical representation of ACMRs for all archetypes.

6.8 Evaluation of System Overstrength

In the Methodology, the system overstrength factor, Ω_0, is taken as the largest average value of the overstrength factor, Ω, computed for each performance group. Values of overstrength for individual archetypes and average values for each performance group are shown in Table 6-8 and Table 6-9 and presented graphically in Figure 6-10. For individual special SMF archetypes, overstrength factors varied between 2.2 and 5.5. Observed patterns for overstrength did not follow the trends observed for computed values of *ACMR*, demonstrating that strength alone is not necessarily a controlling consideration for collapse capacity. For most special SMF archetypes, strength design had little to do with the actual strength of each archetype because overstrength was usually controlled by allowable drift or P-Delta stiffness criteria.

Considering the dominance of drift and P-Delta crtieria in member sizes, it is noteworthy that in many cases the overstrength factor was relatively small (between 2 and 3). The implication is that overstrength could be very small if strength were indeed the controlling design condition. Gravity moments in typical perimeter frame structures were small, and rarely required an increase in beam size. This is an indication that the collapse margin ratio for most special SMF archetypes was not a test of the adequacy of the assigned *R* factor, rather, it was more a test of auxiliary design considerations, such as drift and P-Delta control, which depend on the *R* factor only indirectly.

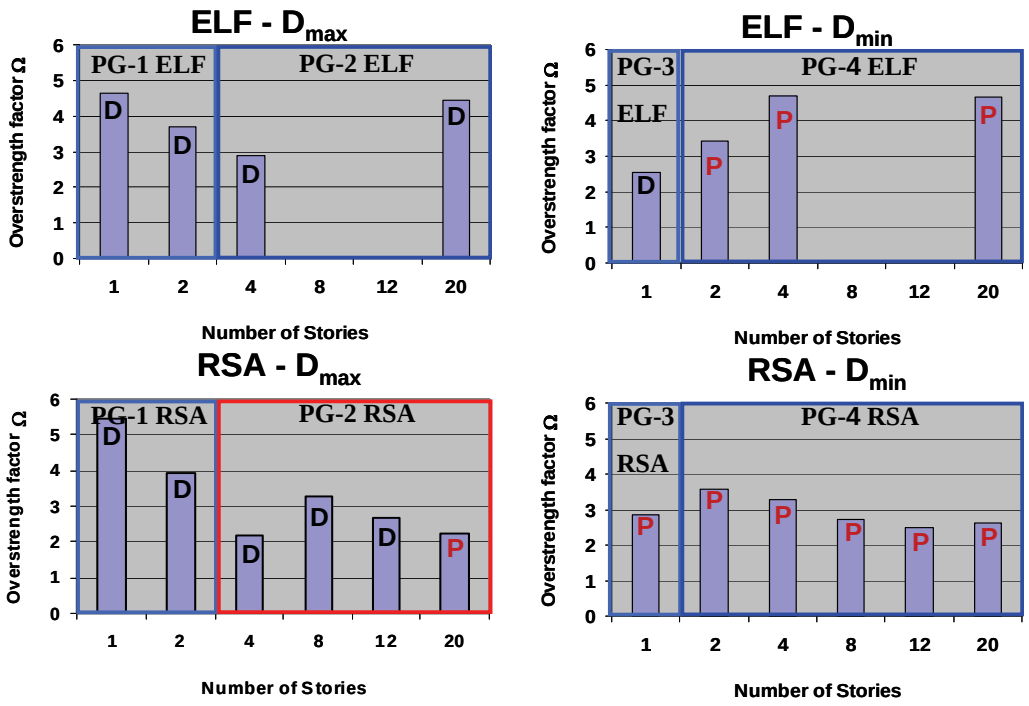

Figure 6-10 Graphical representation of overstrength factor for all archetypes.

6.9 Observations and Recommendations

6.9.1 Observations on System Performance

With the exception of the long-period, SDC D_{max} performance group designed using the RSA procedure, special SMF archetypes met the acceptance criteria of the Methodology. In general, special SMF archetypes had significant overstrength compared to designs based on strength requirements alone. This was attributed to drift criteria and P-Delta considerations.

Added lateral strength due to compliance with stiffness requirements varied with the number of stories, design procedure (ELF versus RSA), and Seismic Design Category. For taller SMF archetypes, the added strength was larger. Because of strong column-weak beam requirements, interior column sizes were controlled by beams that were oversized to control stiffness, so column overstrengths followed the same patterns observed in the beams.

In the tallest archetypes, the overstrength factor differed significantly, but the adjusted collapse margin ratio did not. A large increase in strength (which could also come from a decrease in the *R*-factor) did not guarantee a proportional increase in the collapse margin in special SMFs.

P-Delta effects controlled the nonlinear dynamic response of special SMFs. It led to amplification of story drifts in the lower stories, and in most cases triggered a partial (single-story or multistory) mechanism. Formation of this partial mechanism in addition to strength deterioration in beams (and columns if the latter are made of

slender deep sections) led to collapse. This phenomenon was observed in most archetypes, especially archetypes more than four stories tall.

This was evident in the global pushover curves for 1-, 2-, 4-, and 20-story archetypes presented in Figure 6-11. These curves show the effects of analysis procedure selection (ELF versus RSA), the anticipated behavior under nonlinear dynamic analysis, and the collapse potential of the archetypes. Differences between ELF and RSA designs can be evaluated from differences in strength and elastic stiffness. Differences were observed to increase rapidly with the number of stories, and became dominant in the 20-story archetypes.

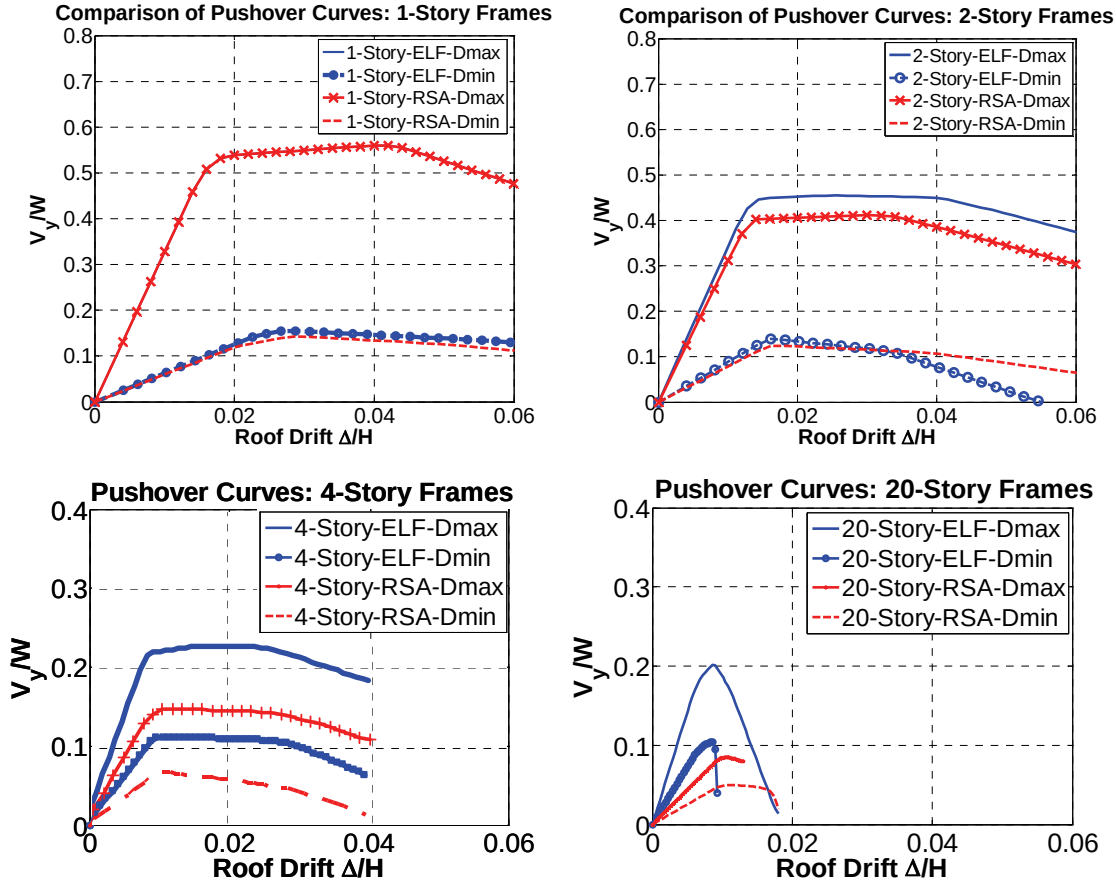

Figure 6-11 Global pushover curves for 1-, 2-, 4-, and 20-story special SMFs.

The global pushover curves in Figure 6-11 indicate that special SMF archetypes become less “ductile” as the number of stories increases. Possible explanations for this include more rapid strength deterioration in structural components of the ELF frame (particularly in the W36 columns) and differences in P-Delta dominated collapse mechanisms (which vary from ground motion to ground motion).

A word of caution is necessary regarding the potential misuse of pushover analysis results for quantification of demand parameters for tall SMF archetypes. The concept of applying an invariant load pattern is a reasonable approach for first mode

dominated structures but is not representative of the dynamic response of structures in which higher modes become important or inelastic redistribution takes place. For tall SMFs, pushover analyses serve to provide a qualitative representation of response but they should not be used to draw quantitative conclusions on seismic demands.

P-Delta effects often cause the formation of partial mechanisms, usually in the lower stories, leading to an amplification of story drifts where axial load, *P*, is large and elastic story drifts are comparable to drifts in the upper stories. In the inelastic range, drifts in the lower stories get amplified more than in the upper stories, which can result in changes in the deflected shape of the structure. This can be seen in the case of the 20-story, RSA, SDC D_{max} archetype results shown in Figure 6-12.

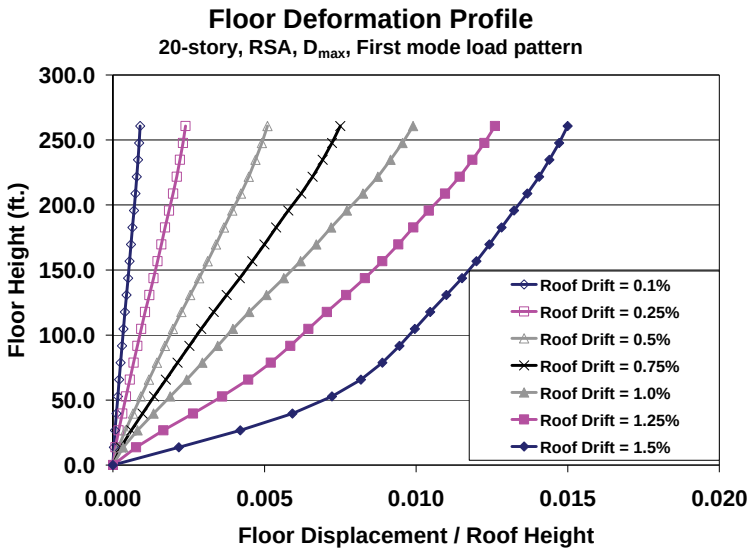

Figure 6-12 Deformation profile of the 20-story, RSA, SDC D_{max} archetype showing the change in deflected shape with increasing roof displacement.

Amplification of story drifts in the lower stories dominates response in the inelastic range, and leads to a mechanism that involves the bottom stories only. Typical plots of roof drift, first story drift, and moment-rotation responses in a bottom story beam and the base of an exterior column for the 20-story, RSA, SDC D_{max} archetype are shown in Figure 6-13 and Figure 6-14. The increase in ground motion intensity from Figure 6-13 to Figure 6-14 is small (7%), but the increase in deformation demand in the first story is sufficient to cause collapse.

Although increases in P-Delta effects were at least partially responsible for the relatively low collapse margin ratios observed in some of the taller archetypes, the pattern was not consistent. Collapse capacity was also affected by component deterioration properties, higher mode effects, and overstrength relative to ground motion intensity.

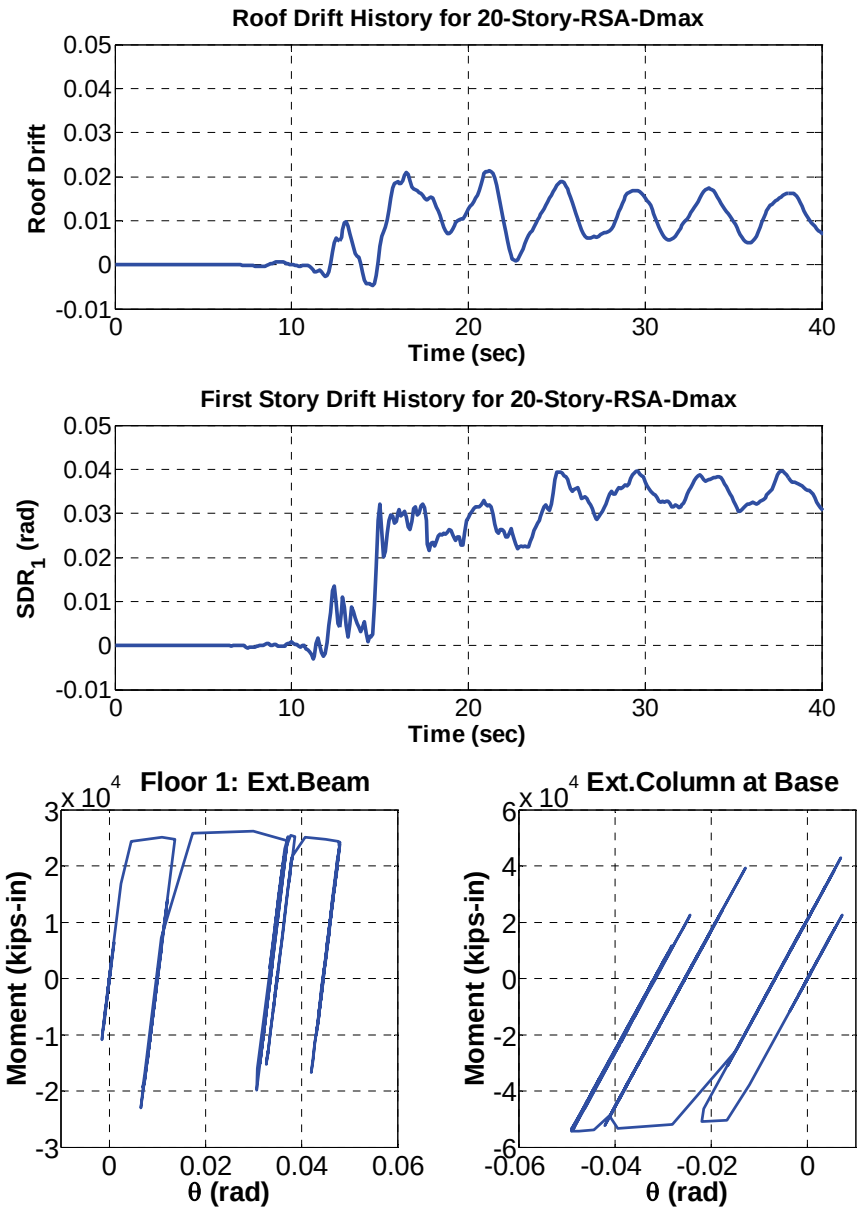

Figure 6-13 Response characteristics of the 20-story, RSA, SDC D_{max} archetype at a scale factor of 4.1.

It was also observed that increasing the pre-capping plastic rotation, θ_p, of all components by 50% increased the median collapse capacity by only 5%. It is believed that increasing the stiffness of the structure would be more effective, and that increasing the strength of the columns relative to the strength of the beams (in order to delay or prevent lower story collapse mechanisms) would be most effective at improving collapse capacity. These effects should be explored in more detail.

The FEMA P-695 requirement to ignore all contributions of the gravity system to lateral strength and stiffness penalizes special SMFs perhaps more than any other system. A large portion of the total system gravity load is supported by gravity framing consisting of beams and columns with so-called shear connections. Such

connections have some level of moment resistance, and the presence of gravity columns provides additional lateral resistance because these members must conform to the deflected shape of the structure under seismic loading. Considering the flexibility of the primary seismic force-resisting system, contributions from the gravity system to overall lateral strength and stiffness is likely to have a large effect on the collapse capacity of special SMF systems.

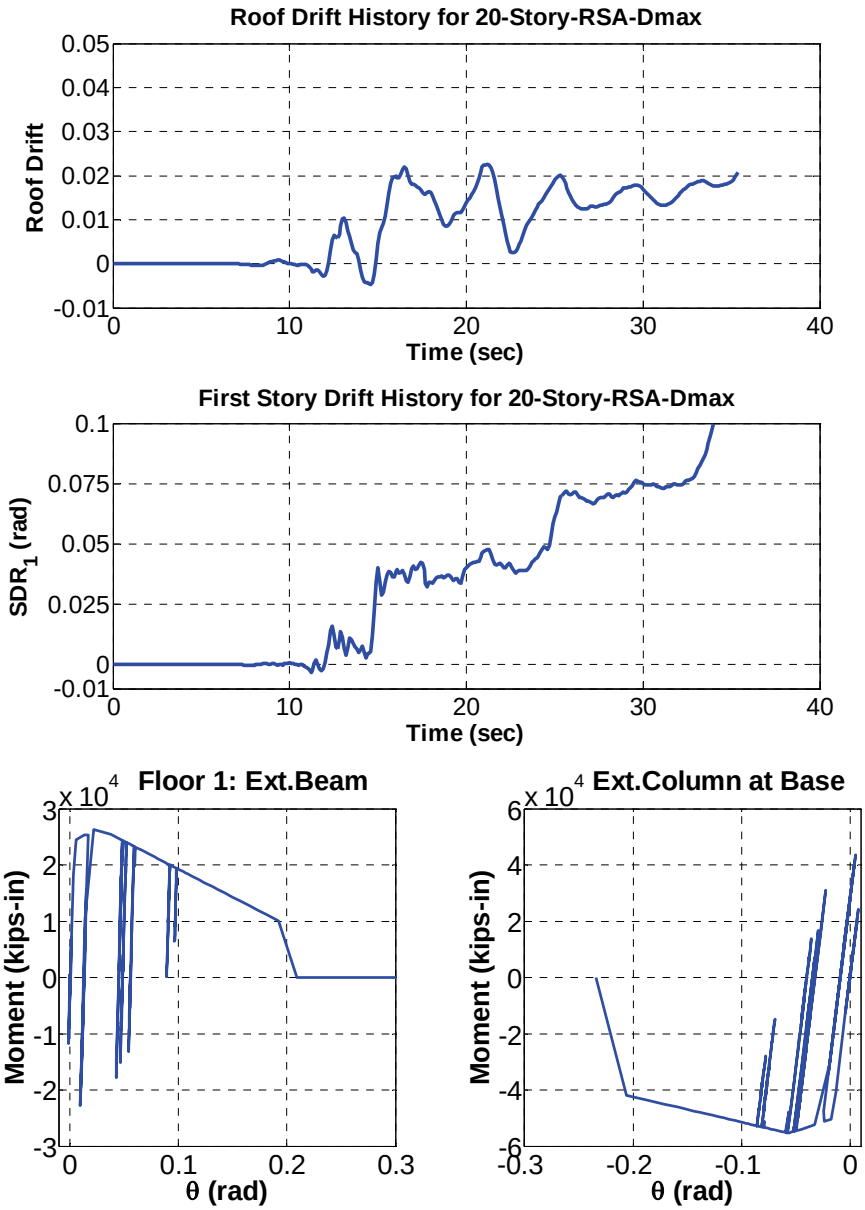

Figure 6-14 Response characteristics of the 20-story, RSA, SDC D_{max} archetype at a scale factor of 4.4 (structure collapses).

6.9.2 Observations on the Methodology

For special SMF systems, the response of the structure can be traced to collapse (total loss of lateral load resistance) using current analytical technologies. This study demonstrated that the Methodology can be implemented on special SMF systems,

provided that strength, stiffness, and deterioration properties of all important structural components are appropriately modeled.

Most member sizes in special SMF systems were controlled by stiffness requirements (drift limitations and P-Delta considerations) and not by strength requirements that are directly related to an *R* factor. As such, the collapse margin ratio for most special SMF archetypes was not a test of the adequacy of the assigned *R* factor, rather, it was more a test of auxiliary design considerations, such as drift and P-Delta control, which depend on the *R* factor only indirectly.

Because the Methodology specifies the use of $C_d = R$, archetypes that were drift controlled were stronger than would be required by present code design. This overstrength had an effect on the calculated collapse margin ratios and should impact judgment on acceptable levels of collapse safety and adequacy of current code-specified *R* factors for special SMF systems.

Additionally, specific guidance is needed on how to compute an acceptable value of *ACMR* for performance groups in which individual archetypes have different values of total collapse uncertainty (β_{TOT}).

6.9.3 Recommendations for Further Investigation

This study focused on a single frame configuration, but special SMF archetypes with different bay width, number of bays, story height, tributary floor area, types of beam-column connection, and site classes are possible. All such system variations would need to be studied in order to fully characterize the seismic performance of special SMF structures and identify appropriate seismic performance factors.

The required use of $C_d = R$ resulted in additional system overstrength in drift controlled systems that was observed to have an effect on the collapse margin ratio. The impact of this requirement should be evaluated through direct comparison with results for special SMF designs based on code-specified values of C_d.

More experimental and analytical work is needed to quantify, with confidence, steel column moment-rotation deterioration characteristics in the presence of varying axial loads, and to incorporate the effects of composite floor slabs on the moment-rotation characteristics of steel beams.

It was noted that the overstrength factor was much larger in long-period ELF designs than for long-period RSA designs. This was attributed to the required use of the ASCE/SEI 7-05 minimum base shear in ELF designs, which is not a requirement in RSA designs. Inequities such as this should be rectified by seismic code committees.

The observed collapse behavior of the 20-story, RSA, SDC D_{max} archetype design warrants further consideration. Models of 20-story SMF archetypes had first mode elastic periods as long as 5.74 seconds. Considering period elongation, effective first

mode periods may be even longer. Additional study is needed to investigate whether or not the ground motion record set has frequency domain characteristics that adequately represent seismic demands at very long periods (5 seconds and longer).

Considering that tall SMFs exhibit susceptibility to P-Delta effects that cause large amplifications of drifts in lower stories, there is a need to develop design concepts that prevent (or at least delay) the formation of partial mechanisms in lower stories of special SMF systems.

Chapter 7
Trial Application: Full Archetype Design Space

7.1 Introduction

This chapter illustrates an expanded application of the FEMA P-695 Methodology on steel braced frame structures utilizing the buckling-restrained braced frame (BRBF) system. In contrast to the limited number of BRBF configurations considered in Chapter 5, this application attempts to develop an archetype design space that would be consistent with a full application of the Methodology on a BRBF system. It then presents a systematic process for identifying and eliminating archetype configurations, and associated performance groups, that are not critical to the collapse performance evaluation of the system. Nonlinear models of archetypes were not developed or evaluated as part of this trial application, but the analytical work would be similar in nature and scope to that of the BRBF trial application presented in Chapter 5.

7.2 Overview and Approach

In this trial application, the buckling-restrained braced frame system with moment-resisting beam-column connections designated as Seismic Force-Resisting System No. 26 in ASCE/SEI 7-05, *Minimum Design Loads for Buildings and Other Structures* (ASCE, 2006), was studied. This is one of two BRBF systems permitted in ASCE/SEI 7-05, the second of which does not require moment-resisting beam-column connections. Although bracing configurations would likely be the same in both BRBF systems, the seismic performance factors and related seismic design criteria are not the same, so only system No. 26 is considered here.

The Methodology requires that a sufficient number of archetype configurations and performance groups be developed to adequately represent the archetype design space, which defines the overall range of permissible configurations, structural design parameters, and other properties that limit application of the seismic force-resisting system. The Methodology, however, permits elimination of configurations that do not control the collapse performance evaluation of the seismic force-resisting system of interest. A systematic process of identifying and eliminating non-controlling BRBF archetype configurations is illustrated and described below.

In an actual application, evaluation of archetype configurations and controlling performance groups would be determined based on nonlinear analysis results. This

trial application did not include development of analytical models, so engineering judgment (rather than analysis) was used to identify controlling features and characteristics of BRBF archetypes.

Peer review is a required element of the Methodology, and concurrence on the selected design space, archetype configurations, and associated performance groups is essential. This trial application is intended to represent the final product of a developmental team that engaged a peer review panel during the process. If nonlinear analyses were performed, it is possible that different archetype configurations and performance groups might be found to control performance of the system. It is also possible that another developmental team could select different archetypes, with somewhat different characteristics, that would equally bound the BRBF design space. The necessary design work and resulting number of archetype configurations and performance groups, however, are expected to be consistent with the order of magnitude minimum number of archetypes sufficient for collapse performance evaluation of the BRBF system under consideration.

7.3 Structural System Information

7.3.1 Design Requirements

Buckling-restrained brace frame systems were designed and detailed in accordance with the design requirements in ANSI/AISC 341-05, *Seismic Provisions for Structural Steel Buildings* (AISC, 2005a) and ASCE/SEI 7-05. Height limits were assumed to include the increase to 240 feet permitted by Section 12.2.5.4 of ASCE/SEI 7-05, and the Response Spectrum Analysis (RSA) procedure was used to design all archetypes.

A number of alternative beam-column-brace connection details are possible. ANSI/AISC 341-05 prescribes the required strength of connections, but permits latitude in determining the connection details. Also, buckling-restrained brace manufacturers specify their own proprietary methods for attachment of the brace elements to the connection plates. Under ANSI/AISC 341-05 requirements, these attachment details must be qualified by testing. In this study, beam-column connections and brace-to-framing connections were not designed in detail. It was assumed that these connections have adequate stiffness and strength, and are detailed such that they will not fail before the braces rupture. Considering the above noted uncertainties in connection detailing, along with requirements for qualification testing, BRBF design requirements were assigned a quality rating of (B) Good.

7.3.2 Test Data

There is a considerable amount of test data available from buckling-restrained brace manufacturers such as Nippon, Star Seismic, and CoreBrace. Test data are also available from limited research on BRBF assemblies and components (Merritt et al., 2003a, 2003b, 2003c; Fahnestock et al., 2006). Most testing, however, has not tested

buckling-restrained brace components to failure, so there is limited information on measured inelastic properties at or near failure displacements. As a consequence, BRBF test data were assigned a quality rating of (B) Good.

7.4 Archetype Configurations

The BRBF system is used primarily in larger, multistory structures and important government and institutional buildings, including university facilities and hospitals. There are, however, many examples of low-rise structures using BRBF systems, where it has proven to be more economical. Variations in building plan, elevation, size, and configuration were considered to cover the range of BRBF system occupancy and use.

A broad range of bracing configurations, design parameters, and related physical characteristics are possible in the full BRBF design space. Important parameters include brace type (in terms of brace configuration and end-connection), building height, bay size, brace size, building configuration (in plan and elevation), seismic design level (in terms of Seismic Design Category), and variation in gravity load levels. The following sections summarize behavior and performance-related issues for each BRBF system parameter and describe the specific selections made to represent the BRBF design space.

7.4.1 Brace Configuration

Buckling-restrained braces can be configured in a number different ways. The brace configuration that controls collapse performance was not known in advance, so different archetypes were developed to consider potential differences in performance. In this study, four brace configurations were selected to represent the range of possible BRBF system applications: (1) one diagonal per bay “zigzag” bracing (designated as ZZ-diagonal bracing); (2) one diagonal per bay “lightening bolt” bracing (designated as LB-diagonal bracing); (3) two diagonals per bay “chevron” bracing; and (4) two diagonals per bay, 2-story “X-bracing”. These brace configurations are shown in Figure 7-1 for 2-story, single-bay archetypes.

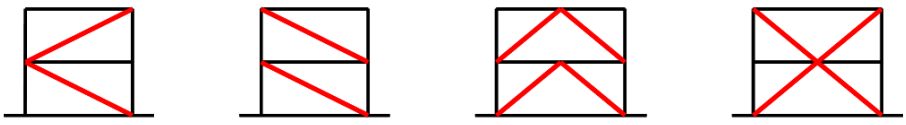

a. ZZ-diagonal b. LB-diagonal c. chevron d. X-brace

Figure 7-1 Brace configurations considered in the BRBF archetype design space.

Each brace configuration has a different impact on beam behavior. In the ZZ-diagonal and X-brace configurations, beams act as drag struts. In the LB-diagonal brace configuration, beams are heavily loaded in axial tension or compression. In the chevron configuration, beams are heavily loaded in flexure.

Another possible configuration is an X-brace configuration with a column in the middle (i.e., back-to-back, adjacent bays of ZZ-diagonal bracing). This type of bracing was judged to be less critical than the X-brace and ZZ-diagonal brace configurations described above, and was not investigated further.

7.4.2 Brace End Connections

The connection of a bucking-restrained brace to the gusset plate assembly can be fixed or pinned (free to rotate). The degree of rotational restraint at the end of a brace can affect performance, and ANSI/AISC 341-05 requires testing to verify that the connection does not adversely affect brace behavior at design load levels. Behavior at the point of failure is generally not known, and could possibly be different for different connection types.

Although brace end connections can affect brace behavior, it was assumed that pinned-end connections would be critical to overall system performance, and the same pinned-end modeling assumptions used in Chapter 5 were used to model the BRBFs in this study. This assumption should be verified through a comparison of the performance of pinned-end archetypes with the performance of fixed-end archetypes that have the same basic configuration and design loading, but are modeled with a different degree of rotational restraint at the brace end connections.

7.4.3 Plan and Elevation Configuration

Archetypes considered plan and elevation configurations representative of typical BRBF system applications. A symmetric (square) plan configuration with one bay of bracing per side was selected as the basis for archetype configurations. Floor plan dimensions were either 120 feet or 125 feet, as shown in Figure 7-2 and Figure 7-3.

In elevation, the same floor plan and brace layout were used at each floor to avoid vertical strength and stiffness irregularities. When practical limits on brace size required two bays of bracing per side (e.g., 18-story archetypes), then two bays of bracing were used at all floor levels.

Building size and plan configuration influence the magnitude of tributary seismic design forces. Building size also influences gravity loads on beam and column elements, although these effects were observed to be of secondary importance to BRBF system performance.

7.4.4 Bay Size

Bay size (along with story height) determines brace angle, which is important to BRBF system stiffness, the geometry of the end connection gusset plates and their effect on connection restraint, and ultimately, the propensity of a brace to buckle and fracture. In this trial application, bay sizes ranged from 15 feet to 25 feet for ZZ and LB brace configurations, and 20 feet to 30 feet for chevron and X-brace configurations, as shown in Figure 7-2 and Figure 7-3. These bay sizes were

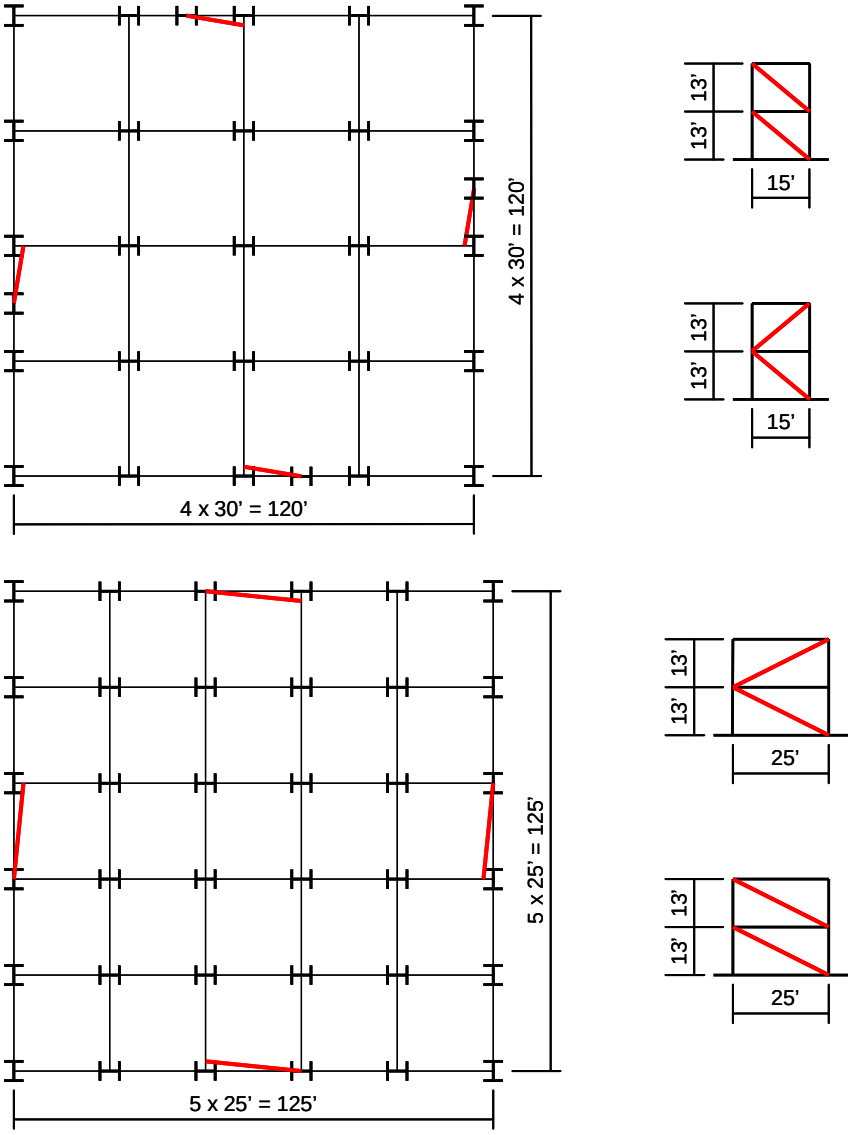

Figure 7-2 Plan configurations for ZZ- and LB-diagonal brace configurations illustrated for 2-story archetypes with bay widths of 15 feet and 25 feet.

considered representative of typical BRBF applications and sufficiently broad to bound anticipated performance issues related to bay size.

7.4.5 Brace Size

Brace sizes were designed considering a variety of load levels and building heights, typically using one bay of bracing per side. This design approach tended to challenge the practical limit on brace yield capacity, particularly in the taller archetype configurations. In some cases, design using one bay of bracing per side was not feasible, and an additional bay of bracing was provided. As designed, brace sizes reflected the range of sizes possible in BRBF component applications (about 100 kips to 1,500 kips).

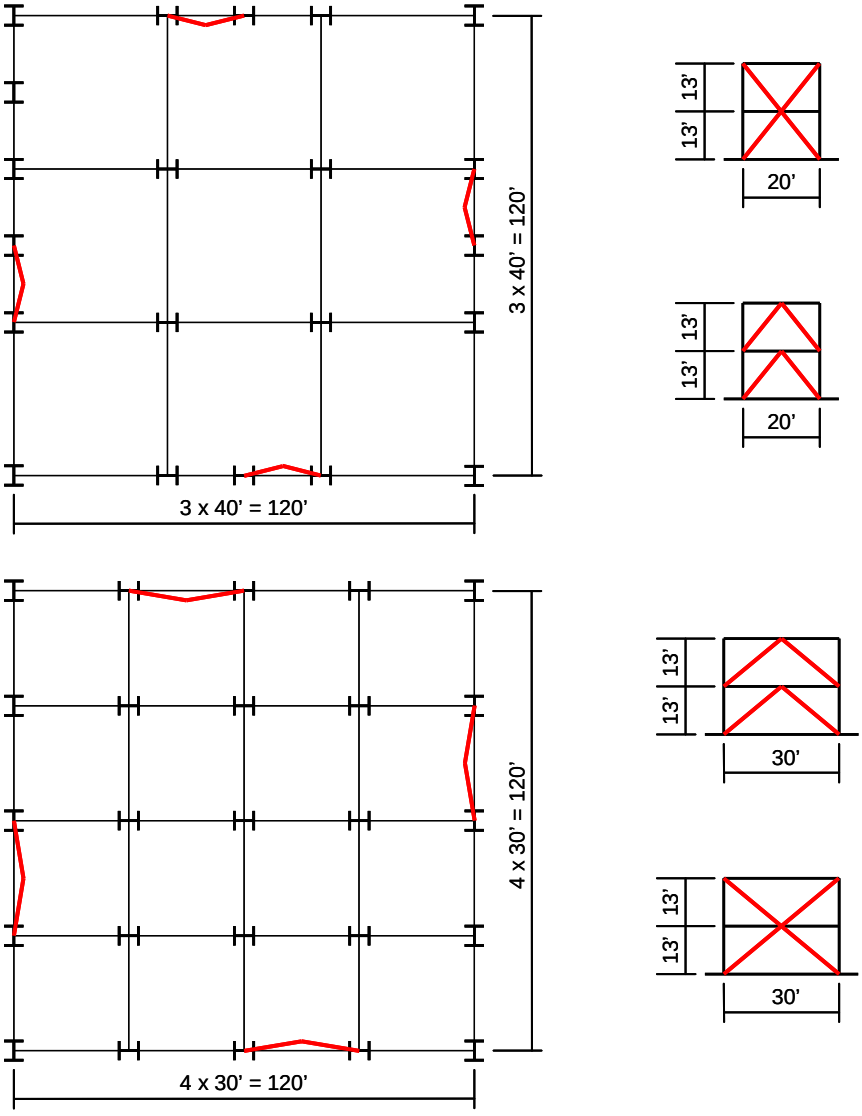

Figure 7-3 Plan configurations for chevron and X-brace configurations illustrated for 2-story archetypes with bay widths of 20 feet and 30 feet.

7.4.6 Building Height

Archetype configurations with 1, 2, 3, 4, 6, 9, 12, and 18 stories were selected to represent the range of building heights and building periods permitted in BRBF systems. For all archetype configurations, a story height of 13 feet was selected. Although a slightly taller height is not uncommon in the first story of multistory buildings, this potential variation was not judged critical to the overall behavior of the system. In addition, a uniform story height was selected to maintain consistency in the brace angle for each bay size.

The Methodology requires consideration of short-period performance groups and long-period performance groups, ideally with at least three different building heights in each group. Although only three archetypes are required in each performance group, additional archetypes (i.e., five to seven archetypes with different building

heights) were used to populate long-period performance groups for each Seismic Design Category. This period range is quite broad and is, by far, the most common period range for BRBF systems. The use of additional archetypes provided a better understanding of the trends in performance related to building height and period. Figure 7-4 shows the archetypes considered for the chevron brace configuration with SDC D_{max} seismic loading.

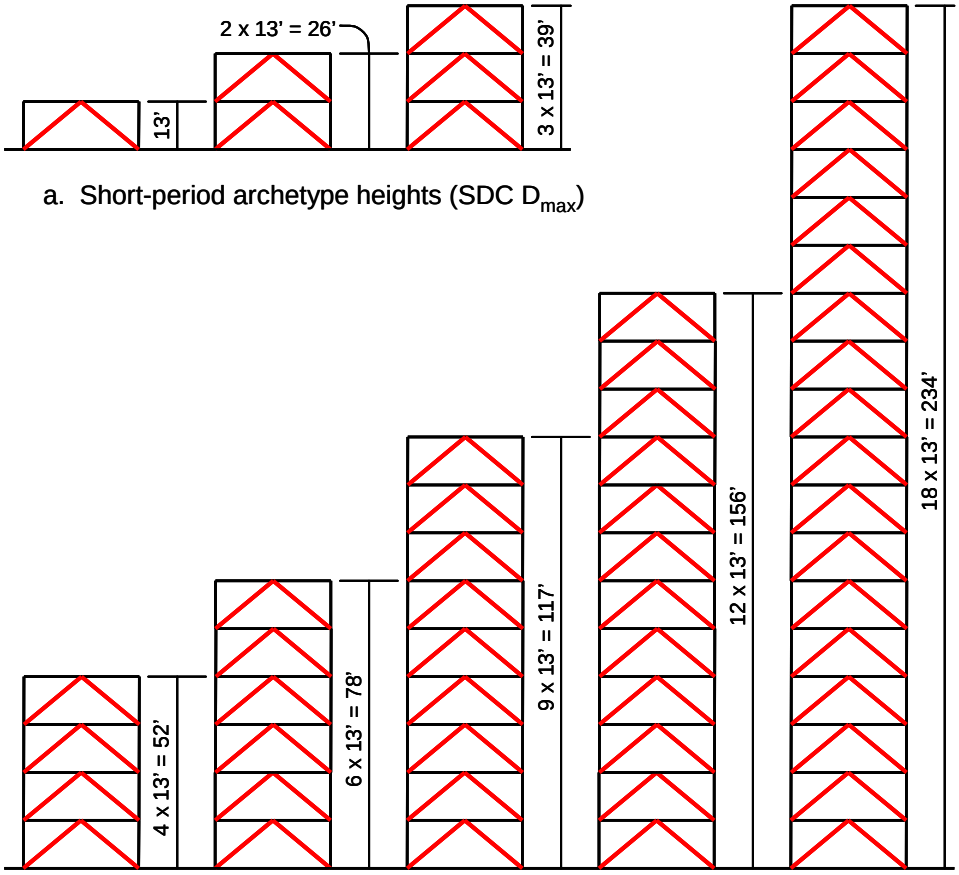

a. Short-period archetype heights (SDC D_{max})

b. Long-period archetype heights (SDC D_{max})

Figure 7-4 Building heights considered for single-bay, chevron archetype configurations designed for SDC D_{max} seismic loading.

Periods were calculated in accordance with the Methodology, and were determined for each of the four seismic design levels (SDC D_{max}, D_{min}/ C_{max}, C_{min}/B_{max}, and B_{min}). For SDC D_{max}, the transition period, T_s, is 0.6 seconds, and archetypes with 1-, 2-, and 3-story configurations were used in short-period performance groups.

For lower seismic design levels, the transition period, T_s, is 0.4 seconds, and only 1-story configurations had periods low enough to be considered for use in short-period performance groups. For SDC D_{min} and lower seismic design levels, the minimum requirement for 3 archetypes per performance group was met by varying brace type or bay spacing in 1-story archetypes. The number of stories, along with

corresponding building heights and building periods for BRBF archetypes, are summarized in Table 7-1.

Table 7-1 Building Height and Period for Buckling-Restrained Brace Frame Archetypes

Building Height		Building Period (sec.)			
Stories	h_n (ft.)	D_{max}	D_{min}/C_{max}	C_{min}/B_{max}	B_{min}
1	13	0.29	0.31	0.33	0.35
2	26	0.48	0.52	0.56	0.59
3	39	0.66	0.70	0.76	0.80
4	52	0.81	0.87	0.95	0.99
6	78	1.10	1.18	1.28	1.34
9	117	1.49	1.60	1.74	1.81
12	156	1.85	1.99	2.16	2.25
18	234	2.51	2.69	2.93	3.05

7.4.7 Seismic Design Category

The Methodology requires archetype configurations to be designed (and evaluated) for the range of seismic loading over which the system will be permitted for use. Although BRBF systems are permitted for use in all Seismic Design Categories, applications typically occur in regions of high or very high seismicity.

Previous studies have shown that archetypes designed for SDC D_{max} seismic loads likely control the value of the *R* factor, and that archetypes designed for SDC D_{min} seismic loads likely control the value of overstrength factor. In this application, SDC D_{max} and SDC D_{min} were selected for the design of most archetypes. SDC B_{max} was selected for design of a limited number of archetypes to verify that the higher seismic design levels governed system performance.

7.4.8 Gravity Design Load

The Methodology requires archetype configurations to be designed (and evaluated) for a range of gravity loads. In the braced frame trial applications in Chapter 5, the potential for variation in design gravity loads was considered irrelevant to the design of brace elements, and insignificant in comparison with column axial forces due to brace component forces and overturning effects. Based on these findings, a typical level of gravity load was assumed in the design of all BRBF archetypes.

7.5 Determination of Performance Groups

Archetypes were organized into performance groups with common features or behavioral characteristics, including brace configuration, gravity load level, Seismic Design Category, and period domain. A total of 128 different archetype

configurations across 32 performance groups were needed to represent the full design space of the BRBF system. These 32 performance groups are a product of four different brace configurations, two different bay sizes, one gravity load level, two seismic design levels (SDC D_{max} and SDC D_{min}), and two period ranges (short-period and long-period), as summarized in Table 7-2.

Table 7-2 Performance Groups for Evaluation of Buckling-Restrained Braced Frame Archetypes

Performance Group Summary					
Group No.	Grouping Criteria				Number of Archetypes[1]
	Basic Configuration	Design Load Level		Period Domain	
		Gravity	Seismic		
PG-1	ZZ-Diagonal Bracing 15-Foot Bays	Typical	SDC D_{max}	Short	3
PG-2				Long	5
PG-3			SDC D_{min}	Short	3[1]
PG-4				Long	7
PG-5	ZZ-Diagonal Bracing 25-Foot Bays	Typical	SDC D_{max}	Short	3
PG-6				Long	5
PG-7			SDC D_{min}	Short	3[1]
PG-8				Long	7
PG-9	LB-Diagonal Bracing 15-Foot Bays	Typical	SDC D_{max}	Short	3
PG-10				Long	5
PG-11			SDC D_{min}	Short	3[1]
PG-12				Long	7
PG-13	LB-Diagonal Bracing 25-Foot Bays	Typical	SDC D_{max}	Short	3
PG-14				Long	5
PG-15			SDC D_{min}	Short	3[1]
PG-16				Long	7
PG-17	Chevron Bracing 20-Foot Bays	Typical	SDC D_{max}	Short	3
PG-18				Long	5
PG-19			SDC D_{min}	Short	3[1]
PG-20				Long	7
PG-21	Chevron Bracing 30-Foot Bays	Typical	SDC D_{max}	Short	3
PG-22				Long	5
PG-23			SDC D_{min}	Short	3[1]
PG-24				Long	7
PG-25	2-Story X-Bracing 20-Foot Bays	Typical	SDC D_{max}	Short	3
PG-26				Long	5
PG-27			SDC D_{min}	Short	3[1]
PG-28				Long	7
PG-29	2-Story X-Bracing 20-Foot Bays	Typical	SDC D_{max}	Short	3
PG-30				Long	5
PG-31			SDC D_{min}	Short	3[1]
PG-32				Long	7

1. Additional archetypes for short period SDC D_{min} performance groups were developed by varying brace type or bay spacing in 1-story archetypes.

7.6 Identification of Controlling Performance Groups

While nothing precludes the evaluation of all archetypes in the full design space, the Methodology permits elimination of archetypes and associated performance groups that are not critical to the performance of the system. This section illustrates a systematic process for identifying performance groups that control the performance evaluation of the BRBF design space and eliminating performance groups that are determined to be non-controlling.

7.6.1 Phase I: Sensitivity Studies

Sensitivity studies can be used to determine the controlling features and characteristics of an archetype design space. In this trial application, sensitivity studies were used to determine the controlling values of seismic design level, bay size, and brace configuration.

Each parameter was investigated using both short-period and long-period configurations. Two-story archetypes were used to investigate short-period performance, and 12-story archetypes were used to investigate long-period performance. In each sensitivity study, a set of archetype configurations was established by varying the parameter of interest and holding all other parameters constant. A design was prepared for 14 unique archetype configurations, and the resulting features of each design were used to evaluate criticality based on judgment informed by results from prior analytical studies. Design properties for archetype configurations used in the sensitivity studies are summarized in Table 7-3. More detailed design information is provided in Appendix E.

Sensitivity Study 1 – Controlling Seismic Design Level. In this study, the collapse performance of one brace configuration designed for different levels of seismic design loading (e.g., SDC D_{max}, SDC D_{min} and SDC B_{max}) was investigated to confirm that SDC D_{max} controls the value of R and that SDC D_{min} (or the limit of 3.0) controls the value of Ω_0. The baseline seismic design level was assumed to be SDC D_{max}.

Sensitivity Study 2 – Controlling Bay Size. In this study, the collapse performance of archetypes that differ only in bay size was investigated to confirm that the 25-foot bay size controls short-period archetype performance and the 15-foot bay size controls long-period archetype performance. Baseline bay sizes were assumed to be 25-feet for short-period archetypes and 15-feet for long-period archetypes.

Sensitivity Study 3 – Controlling Brace Configuration. In this study, the collapse performance of archetypes with different brace configurations was investigated. The baseline brace configuration was assumed to be LB-diagonal bracing for both short-period and long-period archetype configurations.

Table 7-3 Buckling-Restrained Braced Frame Archetype Design Properties for Phase I Sensitivity Studies

Archetype ID Number	No. of Stories	Key Archetype Design Parameters						
		Analysis Procedure	Seismic Design Criteria					$S_{MT}(T)$ (g)
			SDC	*R*	*T* (sec)	T_1 (sec)	*VIW* (g)	
Sensitivity Study 1 – Controlling Seismic Design Level								
2S-LB-25B-Dmax	2	RSA	D_{max}	8	0.48	0.58	0.112	1.50
2S-LB-25B-Dmin	2	RSA	D_{min}	8	0.52	0.94	0.041	0.579
2S-LB-25B-Bmax	2	RSA	B_{max}	8	0.56	1.46	0.025	0.355
12S-LB-15B-Dmax	12	RSA	D_{max}	8	1.85	2.78	0.037	0.485
12S-LB-15B-Dmin	12	RSA	D_{min}	8	1.99	5.38	0.019	0.151
12S-LB-15B-Bmax	12	RSA	B_{max}	8	2.16	6.28	0.013	0.093
Sensitivity Study 2 – Controlling Bay Size								
2S-LB-25B-Dmax	2	RSA	D_{max}	8	0.48	0.58	0.112	1.50
2S-LB-15B-Dmax	2	RSA	D_{max}	8	0.48	0.67	0.106	1.50
12S-LB-25B-Dmax	12	RSA	D_{max}	8	1.85	3.19	0.038	0.485
12S-LB-15B-Dmax	12	RSA	D_{max}	8	1.85	2.78	0.037	0.485
Sensitivity Study 3 – Controlling Brace Configuration								
2S-LB-25B-Dmax	2	RSA	D_{max}	8	0.48	0.58	0.112	1.50
2S-ZZ-25B-Dmax	2	RSA	D_{max}	8	0.48	0.70	0.106	1.50
2S-CV-30B-Dmax	2	RSA	D_{max}	8	0.48	0.59	0.114	1.50
2S-2X-30B-Dmax	2	RSA	D_{max}	8	0.48	0.57	0.114	1.50
12S-LB-15B-Dmax	12	RSA	D_{max}	8	1.85	2.78	0.037	0.485
12S-ZZ-15B-Dmax	12	RSA	D_{max}	8	1.85	2.75	0.037	0.485
12S-CV-20B-Dmax	12	RSA	D_{max}	8	1.85	2.76	0.037	0.485
12S-2X-20B-Dmax	12	RSA	D_{max}	8	1.85	2.80	0.037	0.485

7.6.2 Phase I: Sensitivity Study Results

Since this trial application did not include the development of analytical models, engineering judgment, informed by results from prior analytical studies, was used to determine controlling features and characteristics. Results are summarized in Table 7-4 and described below. If actual nonlinear analyses were performed, it is possible that different configurations might be found to be critical, but the number of controlling archetype configurations and performance groups is expected to be consistent with the order of magnitude minimum number of archetypes sufficient for collapse performance evaluation of the selected BRBF system.

Table 7-4 Summary of Phase I Sensitivity Study Results

Archetype ID Number	No. of Stories	Bracing Type	Bay Size (feet)	Seismic Design Level	Controls?
Sensitivity Study 1 – Controlling Seismic Design Level					
2S-LB-25B-Dmax	2	LB-Diagonal	25	SDC Dmax	Yes (*R*)
2S-LB-25B-Dmin				SDC Dmin	Yes (Ω)
2S-LB-25B-Bmax				SDC Bmax	No
12S-LB-15B-Dmax	12	LB-Diagonal	15	SDC Dmax	Yes (*R*)
12S-LB-15B-Dmin				SDC Dmin	Yes (Ω)
12S-LB-15B-Bmax				SDC Bmax	No
Sensitivity Study 2 – Controlling Bay Size					
2S-LB-25B-Dmax	2	LB-Diagonal	25	SDC Dmax	Yes
2S-LB-15B-Dmax			15		No
12S-LB-25B-Dmax	12	LB-Diagonal	25	SDC Dmax	No
12S-LB-15B-Dmax			15		Yes
Sensitivity Study 3 – Controlling Brace Configuration					
2S-LB-25B-Dmax	2	LB-Diagonal	25	SDC Dmax	Yes
2S-ZZ-25B-Dmax		ZZ-Diagonal			No
2S-CV-30B-Dmax		Chevron	30		No
2S-2X-30B-Dmax		2X-Bracing			No
12S-LB-15B-Dmax	12	LB-Diagonal	15	SDC Dmax	Yes
12S-ZZ-15B-Dmax		ZZ-Diagonal			No
12S-CV-20B-Dmax		Chevron	20		No
12S-2X-20B-Dmax		2X-Bracing			No

Sensitivity Study 1 – Controlling Seismic Design Level. Previous analytical studies have consistently shown that SDC D_{max} controls value of the *R* factor and that lower levels of seismic design loading typically govern the overstrength factor, Ω_0. Similar results were assumed for this study, and SDC B_{max} archetypes were eliminated as non-controlling.

Sensitivity Study 2 – Controlling Bay Size. Previous studies have shown that collapse performance tends to worsen for archetypes with very short periods, all else being equal. A similar result was assumed for this study, and the larger bay size of 25 feet was selected as critical for short-period archetypes, since wider bays correspond to stiffer archetypes and relatively shorter periods.

Previous studies have also shown that collapse performance tends to worsen for archetypes with longer periods and larger lateral displacements, all else being equal. The smaller bay size of 15 feet was selected for long-period archetypes, since narrow bays correspond to more flexible systems and relatively longer periods.

Sensitivity Study 3 – Controlling Brace Configuration. While prior analytical studies provided information in support of the controlling parameters identified in other sensitivity studies, selection of the controlling brace configuration in this study is purely judgmental. LB-diagonal bracing was assumed to be critical for both short-period and long-period archetype configurations. This type of bracing was judged to be more vulnerable to collapse than chevron or X-brace configurations. Furthermore, multistory systems with the LB-diagonal brace configuration were considered to be more vulnerable to collapse than those with the ZZ-diagonal bracing configuration. It is possible that actual nonlinear analyses might determine that a different brace configuration is more critical in controlling BRBF system performance.

7.6.3 Identification of Controlling Performance Groups

Based on the results of Phase I sensitivity studies, the controlling performance groups summarized in Table 7-5 were identified.

Table 7-5 Summary of Controlling Performance Groups for the Buckling-Restrained Braced Frame System

Performance Group Summary					
Group No.	Grouping Criteria				Archetype ID Number
	Basic Configuration	Design Load Level		Period Domain	
		Gravity	Seismic		
PG-10	LB-Diagonal Bracing 15-Foot Bays	Typical	SDC D_{max}	Long	4S-LB-15B-Dmax
					6S-LB-15B-Dmax
					9S-LB-15B-Dmax
					12S-LB-15B-Dmax
					18S-LB-15B-Dmax
PG-12			SDC D_{min}	Long	2S-LB-15B-Dmin
					3S-LB-15B-Dmin
					4S-LB-15B-Dmin
					6S-LB-15B-Dmin
					9S-LB-15B-Dmin
					12S-LB-15B-Dmin
					18S-LB-15B-Dmin
PG-13	LB-Diagonal Bracing 25-Foot Bays	Typical	SDC D_{max}	Short	1S-LB-25B-Dmax
					2S-LB-25B-Dmax
					3S-LB-25B-Dmax
PG-15 PG-11 PG-23	Varies	Typical	SDC D_{min}	Short	1S-LB-25B-Dmin
					1S-LB-15B-Dmin
					1S-CV-30B-Dmin

After elimination of non-controlling archetype configurations, only six of the original 32 performance groups were found to be critical for performance evaluation of the selected BRBF system. It should be noted that three of the original performance groups (PG-15, PG-11 and PG-23), each with only one archetype, have been combined into a single new performance group meeting the minimum requirement of 3 archetypes per group.

7.6.4 Phase II: Performance Evaluation

Based on the controlling performance groups listed in Table 7-5, designs for an additional 15 unique archetype configurations were prepared for the Phase II performance evaluation of the BRBF system. Design properties are summarized in Table 7-6. More detailed design information is provided in Appendix E.

Table 7-6 Buckling-Restrained Braced Frame Archetype Design Properties for Phase II Performance Evaluation

Archetype ID Number	No. of Stories	Key Archetype Design Parameters						
		Analysis Procedure	Seismic Design Criteria					$S_{MT}(T)$ (g)
			SDC	*R*	*T* (sec)	T_1 (sec)	*V*/*W* (g)	
Performance Group PG-10, SDC D_{max}, Long-Period								
4S-LB-15BDmax	4	RSA	D_{max}	8	0.81	1.15	0.078	1.11
6S-LB-15B-Dmax	6	RSA	D_{max}	8	1.10	1.68	0.058	0.816
9S-LB-15B-Dmax	9	RSA	D_{max}	8	1.49	2.35	0.047	0.602
12S-LB-15B-Dmax	12	RSA	D_{max}	8	1.85	2.78	0.037	0.485
18S-LB-15B-Dmax	18	RSA	D_{max}	8	2.51	3.96	0.037	0.358
Performance Group PG-12, SDC D_{min}, Long-Period								
2S-LB-15B-Dmin	2	RSA	D_{min}	8	0.52	0.86	0.063	0.579
3S-LB-15B-Dmin	3	RSA	D_{min}	8	0.70	1.25	0.063	0.427
4S-LB-15B-Dmin	4	RSA	D_{min}	8	0.87	1.71	0.063	0.344
6S-LB-15B-Dmin	6	RSA	D_{min}	8	1.18	2.61	0.019	0.254
9S-LB-15B-Dmin	9	RSA	D_{min}	8	1.60	3.93	0.019	0.187
12S-LB-15B-Dmin	12	RSA	D_{min}	8	1.99	5.38	0.019	0.151
18S-LB-15B-Dmin	18	RSA	D_{min}	8	2.69	9.07	0.019	0.111
Performance Group PG-13, SDC D_{max}, Short-Period								
1S-LB-25B-Dmax	1	RSA	D_{max}	8	0.29	0.47	0.125	1.50
2S-LB-25B-Dmax	2	RSA	D_{max}	8	0.48	0.58	0.112	1.50
3S-LB-25B-Dmax	3	RSA	D_{max}	8	0.66	0.89	0.097	1.37
Performance Groups PG-15/PG-11/PG-20, SDC D_{min}, Short-Period								
1S-LB-25B-Dmin	1	RSA	D_{min}	8	0.31	0.53	0.053	1.50
1S-LB-15B-Dmin	2	RSA	D_{min}	8	0.31	0.49	0.053	1.50
1S-CV-30B-Dmin	3	RSA	D_{min}	8	0.31	0.39	0.062	1.50

This set of designs utilized the controlling values of seismic design level, bay size and brace configuration identified in the Phase I sensitivity studies. To complete the performance evaluation, they also considered variation in: (1) period range (short and long period); and (2) Seismic Design Category (SDC D_{max} and SDC D_{min}).

7.7 Observations

7.7.1 Observations on the Methodology

In this trial application, a total of 128 different archetype configurations across 32 performance groups were needed to represent the full design space of the BRBF system. In a series of Phase I sensitivity studies, 14 different archetypes were used to eliminate non-controlling conditions from consideration. Based on these studies, 15 unique archetype configurations across six controlling performance groups were needed for a Phase II performance evaluation of the BRBF system.

This trial application demonstrated how systematic identification of controlling characteristics can be used to reduce a full design space into a manageable number of archetype configurations and associated performance groups. In the case of BRBF systems, it was found that development of a full set of archetypes was reasonable and practical. Assumptions were made in selecting controlling features and characteristics in the Phase I sensitivity studies. Arguably, additional Phase I designs could be required if archetype configurations were not optimally selected for these studies. The important observation to note, however, is that the number of controlling performance groups would remain on the order of what has been shown here. While a different parameter might be found to control, only that parameter would need to be evaluated, and other parameters could be eliminated from consideration. In the end, a different controlling performance group would be substituted, but not added, into the mix for the final Phase II performance evaluation.

7.7.2 Estimated Level of Effort

The approximate level of effort associated with the work conducted on this trial application was on the order of 240 hours of engineering time. This included approximately 120 hours for design of archetype configurations, 40 hours of review associated with the selection of appropriate archetype configurations, and 80 hours for preparation of report and summary materials.

This information is provided as a data point based on actual work conducted, but it excludes some significant aspects of the overall process that should be considered in estimating the total level of effort involved in a full application of the Methodology. Because this trial application did not include nonlinear analyses, the reported level of effort does not include time to develop nonlinear models of archetype configurations, perform nonlinear static and dynamic analyses of the models, and evaluate system collapse performance using nonlinear analysis results. Similarly, it does not include additional time that might be required for working with the peer review panel and

responding to peer review comments on the analyses and performance evaluation results.

Completely outside consideration in this trial application is time for research, testing, development of design requirements, and other system developmental efforts that would be under the control of the system developer, and beyond what could be hypothetically considered in this example.

What has been demonstrated by this trial application, however, is that regardless of the specific parameters that are found to control system behavior, once the controlling parameters are identified, the level engineering effort needed to evaluate system performance in a full application of the Methodology can be reduced to a finite (and manageable) level.

Chapter 8

Summary, Conclusions, and Recommendations

This chapter summarizes the results of beta testing of the FEMA P-695 Methodology and provides recommendations for its possible improvement and future use. General findings and recommendations are based on the collective results for different seismic force-resisting systems. Additional, more in-depth findings specific to the systems of interest are contained in the relevant chapters for each system.

8.1 Summary of Beta Testing Work

A number of seismic force-resisting systems were investigated during development of the Methodology as part of example applications or supporting studies. Such investigations included special reinforced concrete moment frames, ordinary reinforced concrete moment frames, and light-framed walls with wood structural panel sheathing. Results from these investigations were used to test and refine the Methodology as it was being developed. While this effort was considerable, it covered only a small portion of the more than 75 individual systems contained in ASCE/SEI 7-05.

The trial applications documented in this report augment the original work by applying the Methodology to additional seismic force-resisting systems. The purpose of this work was to test the Methodology on additional seismic force-resisting systems, evaluate the results for the system of interest, develop recommendations for improving the Methodology (if needed), and to recommend areas for further study.

The scope of the beta testing effort was structured to cover a broad range of system types with different seismic response characteristics and detailing requirements. The following systems were investigated:

- Special reinforced masonry shear walls (special RMSW)
- Ordinary reinforced masonry shear walls (ordinary RMSW)
- Special reinforced concrete shear walls (special RCSW)
- Ordinary reinforced concrete shear walls (ordinary RCSW)
- Special steel concentrically braced frames (special SCBF)
- Buckling-restrained braced frames (BRBF)
- Special steel moment frame (special SMF)

In general, archetypes were designed using Equivalent Lateral Force (ELF) procedure. Certain archetypes were designed using the Response Spectrum Analysis (RSA) procedure when this procedure is more commonly used in practice. In the case of the special SMF system, both ELF and RSA procedures were used to explicitly investigate the significance of analysis procedure selection on system performance.

The Methodology defines seismic loads in terms of the Seismic Design Category (SDC). In general, the Methodology requires archetypes to be designed and evaluated for each SDC for which the system of interest will be used. In general, example applications that were part of the original Methodology development showed that archetypes designed for seismic loads associated with the highest SDC tended to govern collapse performance (and the resulting values of the *R*-factor). For systems with unrestricted use, the highest Seismic Design Category would be SDC D. The same studies showed that archetypes designed for lower Seismic Design Categories tended to govern the value of the overstrength factor.

To limit the number of archetypes investigated, each system was designed for seismic loads corresponding to the highest SDC for which the system is permitted. On this basis, systems with "special" seismic detailing were designed for SDC D seismic loads, and systems with "ordinary" seismic detailing were designed for SDC C seismic loads. The Methodology requires archetypes to be designed and evaluated for bounding values of the Seismic Design Category of interest (e.g., values of D_{max}/D_{min} for SDC D, and C_{max}/C_{min} for SDC C).

Similar to seismic loading, the Methodology requires the use of bounding values of gravity load for design of archetypes in which performance is influenced by gravity load. Accordingly, "high" and "low" levels of gravity load were used for design of reinforced masonry and reinforced concrete shear wall archetypes. A single "typical" value of gravity load was used for design of steel braced frame and steel moment frame archetypes in which performance was assumed to be essentially independent of gravity load.

Finally, archetypes were configured to have a number of different building heights, typically five for each seismic force-resisting system, to investigate the potential effect of period on performance. Because of necessary limitations in scope, the number of short- or long-period archetypes in some performance groups was less than the prescribed minimum of three per performance group. Also, the number of different system configurations (e.g., difference brace configurations for braced frame systems or different wall configurations for shear wall systems) was limited.

Although system performance was evaluated using a large number of archetypes (total of 120 archetypes for all seven systems), full implementation of the Methodology would require an even larger number of archetypes and performance groups. Additional archetypes would be needed to meet the minimum number of

three archetypes required per performance group, and additional performance groups would be required to evaluate system performance for other configurations and design variables that were not considered. For the purpose of beta testing the Methodology, it was considered more useful to evaluate a larger number of systems with a carefully selected, but limited, number of archetypes for each system, rather than to evaluate fewer systems using a larger number of archetypes for each system.

8.2 General Findings

Trial applications of the Methodology on reinforced masonry shear wall structures (Chapter 3), reinforced concrete shear wall structures (Chapter 4), steel braced frame structures (Chapter 5), and steel moment frame structures (Chapter 6) provided insight into the collapse performance of these systems, and a basis for judging the appropriateness and usefulness of the Methodology. Chapters outlining the results for each system conclude with observations on system performance, observations on the Methodology, and recommendations for further experimental or analytical investigation.

8.2.1 Does the Methodology Meet Its Intended Purpose?

The purpose of the Methodology, as stated in the FEMA P-695 report, is to provide a rational basis for determining building system performance and response parameters (i.e., R, C_d and Ω_O factors) that, when properly implemented in the seismic design process, will result in "equivalent safety against collapse in an earthquake, comparable to the inherent safety against collapse intended by current seismic codes, for buildings with different seismic force-resisting systems," (FEMA, 2009).

FEMA P-695 recommends the Methodology for use with model building codes and resource documents to set minimum acceptable design criteria for standard code-approved seismic force-resisting systems and to provide guidance in the selection of appropriate design criteria for other systems when linear design methods are applied. FEMA P-695 also notes that the Methodology provides a basis for evaluation of current code-approved systems for their ability to achieve intended seismic performance objectives.

In the trial applications, current code-approved systems were evaluated for their ability to achieve the intended collapse performance objectives inherent in the code. Seismic force-resisting systems were designed using "trial" values of the R factor based on values contained in Table 12.2-1 of ASCE/SEI 7-05. In a departure from current practice, the Methodology specifies the use of $C_d = R$, so values of C_d provided in Table 12.2-1 were not used in the preparation of trial designs. In the case of drift-controlled systems, this difference had an effect on the observed results.

For the purpose of evaluating the Methodology, the pass/fail rate across all tested systems was considered. It would be unrealistic to expect that the current set of code-approved systems, in which values of the R factor have been based primarily on

engineering judgment, would result in uniform collapse performance and equivalent safety against collapse over the entire code-permitted design space. Systems with documented acceptable performance in past earthquakes, however, would not be expected to fail the criteria miserably, and systems with less robust characteristics would not be expected to pass the criteria easily.

If most individual archetypes (or performance groups) were found to generally meet the acceptance criteria of the Methodology, then it could be concluded that the Methodology is appropriately "calibrated" in terms of evaluating collapse performance. Furthermore, if the few archetypes (or performance groups) not meeting the acceptance criteria could be associated with a design characteristic or configuration that has been shown to consistently affect collapse performance, then it could also be concluded that the Methodology is capable of identifying potential design or configuration shortcomings in a system of interest.

Table 8-1 is a summary of collapse performance evaluation results indicating the number of archetypes meeting the acceptance criterion for individual archetypes (adjusted collapse margin ratios exceeding $ACMR_{20\%}$). Table 8-2 is a summary indicating the number of performance groups meeting the acceptance criterion, on average, within a performance group (average adjusted collapse margin ratio exceeding $ACMR_{10\%}$). To meet the acceptance criteria of the Methodology, systems must meet both the individual criterion for each archetype, and the average criterion for each performance group.

Table 8-1 Number of Archetypes Passing the Acceptance Criterion for Evaluation of Individual Archetypes

Seismic Force-Resisting System			Primary Analysis Procedure	Short-Period Configurations		Long-Period Configurations	
No.	Type	Detailing		High Gravity	Low Gravity	High Gravity	Low Gravity
1	RMSW	Special	ELF	2 of 5 pass	3 of 5 pass	All pass	All pass
2	RMSW	Ordinary	ELF	1 of 4 pass	3 of 4 pass	3 of 6 pass	All pass
3	RCSW	Special	ELF	2 of 5 pass	2 of 5 pass	All pass	All pass
4	RCSW	Ordinary	ELF	All pass	All pass	All pass	All pass
5	SCBF	Special	ELF	3 of 4 pass		All pass	
6	BRBF	n/a	ELF	All pass		All pass	
7a	SMF	Special	ELF	All pass		All pass	
7b	SMF	Special	RSA	All pass		All pass	

Table 8-2 Number of Performance Groups Passing the Average Acceptance Criterion for Evaluation of Performance Groups

Seismic Force-Resisting System			Primary Analysis Procedure	Short-Period Configurations		Long-Period Configurations	
No.	Type	Detailing		High Gravity	Low Gravity	High Gravity	Low Gravity
1	RMSW	Special	ELF	0 of 2 pass	0 of 2 pass	All pass	All pass
2	RMSW	Ordinary	ELF	0 of 2 pass	0 of 2 pass	0 of 2 pass	All pass
3	RCSW	Special	ELF	0 of 2 pass	0 of 2 pass	All pass	All pass
4	RCSW	Ordinary	ELF	1 of 2 pass	1 of 2 pass	All pass	All pass
5	SCBF	Special	ELF	1 of 2 pass		All pass	
6	BRBF	n/a	ELF	All pass		All pass	
7a	SMF	Special	ELF	All pass		All pass	
7b	SMF	Special	RSA	All pass		1 of 2 pass	

In general, trial applications found that most individual archetypes and performance groups of the tested systems met the acceptance criteria of the Methodology, although for certain systems, some archetypes and performance groups did not fully comply with the criteria. Specific findings and the observed trends are summarized in the sections that follow.

Based on these results, it was concluded that the acceptance criteria of Methodology, and its underlying collapse objectives, are reasonably well calibrated with the inherent safety goals of ASCE/SEI 7-05 when design is primarily controlled by strength considerations (*R* factor). Also, it was concluded that most code-approved systems would generally meet the acceptance criteria of the Methodology. Systems not meeting the acceptance criteria would not be expected to fail by a large margin, although certain configurations or design characteristics of such systems might be expected to have significantly inferior performance. In addition, the Methodology was able to identify design and configuration shortcomings that were indicative of potentially inadequate collapse performance.

These conclusions are consistent with findings from previous example applications of the Methodology documented in the FEMA P-695 report. As a result, building codes and standards organizations can consider the use of the Methodology to provide calibrated seismic performance factors as long as the acceptance criteria used in the Methodology is equivalent to the expected (or intended) collapse risk.

8.2.2 Is the Methodology Practical to Implement?

In all cases, trial applications reported difficulty in capturing the full archetype design space for an existing code-approved system. The range of permissible configurations and possible variations in important design parameters led to more archetypes and performance groups than could be evaluated given the resources

available for the beta testing effort. In each case, the scope of the investigation was limited for practical reasons.

To investigate the feasibility of full implementation of the Methodology, the BRBF system was selected for further study, and the process for developing a full set of archetypes for evaluation of the complete design space was tested. The scope of this effort was again limited by available resources. Designs were prepared, but analyses were not performed and hypothetical decisions were made based on engineering judgment. Although nonlinear analyses and performance evaluations were not conducted, the study demonstrated how systematic identification of controlling characteristics can be used to limit the number of archetypes needed for full implementation of the Methodology. In the case of BRBF systems, the engineering effort needed to evaluate system performance was reduced to a finite level that was judged to be reasonable and practical.

In the case of new systems, the level of effort for full implementation of the Methodology is intended to be scalable, and is at the discretion of the system proponent. Archetype development and performance evaluation need only be performed on those configurations and seismic design levels for which the new system will be proposed for use. The design requirements and limits of application can then be adjusted accordingly.

8.3 Findings Related to System Performance

Trial applications of the Methodology revealed the following overarching findings related to the behavior of the systems that were evaluated. More detailed findings specific to individual systems of interest are contained in the relevant chapters.

8.3.1 Short-Period Systems

Reinforced masonry shear wall, reinforced concrete shear wall, and steel braced frame systems exhibited a similar trend in that short-period archetypes had smaller collapse margin ratios. This was observed in 1-, 2-, 3-story, and selected 4-story archetypes. In most cases, short-period performance groups failed the collapse performance evaluation criteria. In cases where short-period archetypes passed the criteria, they had smaller collapse margin ratios than corresponding long-period archetypes.

A significant exception to this trend existed in the special SMF system, in which lower collapse margin ratios were not observed in short-period archetypes. Due to the flexibility of steel moment frame systems, the calculated fundamental period of "short-period" archetypes was relatively long (greater than the transition period, T_s, which defines the boundary between the acceleration (short-period) and velocity (long-period) domains of the design spectrum). Thus, the analytical models of "short-period" special SMF archetypes that were used to evaluate collapse

performance did not respond dynamically as short-period systems, even though they were designed as such.

The trend observed in most short-period systems was not unexpected. It is consistent with previous findings during the development of the Methodology, and consistent with prior research studies demonstrating larger inelastic demands on short-period systems, regardless of the seismic force-resisting system. These findings suggest a possible need for period-dependent seismic performance factors. In such a formulation, the *R* factor could be reduced as a function of period, such that design strength increases as building period decreases and a uniform margin against collapse is maintained.

8.3.2 Partially Grouted Masonry Walls

Design of special RMSW archetypes assumed fully grouted construction, while design of ordinary RMSW archetypes assumed partially grouted construction. This is not a code requirement for design of masonry shear walls, but is generally consistent with engineering practice. The trial application on RMSW systems found the performance of ordinary RMSW archetypes to be inferior to special RMSW archetypes. This was largely attributed to the behavior of partially grouted walls. If special RMSW performance groups had also included partially grouted construction, then their collapse performance would have been adversely affected.

These results showed that the Methodology is capable of identifying design features that systematically affect seismic performance. These results also showed that, while not an *R* factor issue in itself, restricting the use of partially grouted walls in taller configurations of RMSW systems would seem to be an issue that should be considered by code committees. Such an adjustment in the design requirements would appear necessary for RMSW systems to comply with the collapse performance objectives of the Methodology and inherent in the code.

8.3.3 Drift and Stability Design Requirements

The design of special SMF system archetypes was governed by code drift limits and checks on stability rather than strength. This was attributed to the inherent flexibility of these systems, which necessitated adding stiffness to meet drift and stability criteria. Some of the taller archetypes in other systems were similarly affected. Because the addition of stiffness is often accompanied by a corresponding addition of strength, the value of the *R* factor is effectively reduced. Hence, drift and stability criteria can be as important as the *R* factor in the design and collapse performance of flexible systems.

For flexible systems, the Methodology effectively addresses drift and stability criteria through the deflection amplification factor, C_d, which is taken as equal to the *R* factor. There are many design requirements and other factors that influence system performance, which are defined in ASCE/SEI 7-05 (or the governing code or

standard). These are assumed to be in effect unless otherwise defined in the design requirements of a proposed system. The Methodology does not preclude use of different system-specific values of drift limits or stability criteria, which may be appropriate for flexible systems and taller configurations controlled by such criteria.

For evaluation of existing code-approved systems, results indicate that drift limits and stability criteria should be re-evaluated considering their effect on the collapse behavior of flexible, drift-controlled systems. Furthermore, any further investigation of the adequacy of the current *R* factor formulation should explicitly consider the interaction between strength, drift, and stability criteria, particularly in taller, more flexible systems and configurations.

8.3.4 Design Assumptions

In all cases, trial applications noted that performance evaluation results were affected by certain key assumptions made in the design process. Although the code specifies minimum strength and stiffness requirements, exactly how these requirements are met is left to the discretion of the designer. As a result, design solutions are not unique, and different design assumptions can affect system behavior.

In the trial applications, key design assumptions included: (1) the use of fully grouted or partially grouted masonry walls in RMSW archetypes; (2) the use of maximum shear stresses in RCSW archetypes; (3) the use of fully-restrained beam-column connection in SCBF archetypes; and (4) the choice of steel beam and column sections over the height of the building in SMF archetypes. Each of these assumptions was in compliance with the code, and a different set of assumptions could have been equally compliant. The resulting design choices, however, had a bearing on the collapse behavior of each system.

The Methodology recognizes the importance of design assumptions on archetype development and performance evaluation. Control occurs through extensive and detailed guidance regarding development of archetypes and review and concurrence through the peer review process. The Methodology does not (and cannot) define prototypical configurations for archetypes of new systems whose characteristics are not yet known. For evaluation of existing code-approved systems, however, it would seem possible, and appropriate, to develop prototypical archetype configurations and consensus design assumptions that reflect the collective wisdom of a broad range of stakeholders.

8.3.5 Nonlinear Modeling Assumptions

In all cases, trial applications noted that performance evaluation results were similarly affected by certain key assumptions made in nonlinear modeling. Nonlinear modeling is a challenging and evolving science that relies heavily on the expertise of the analyst and familiarity with current experimental data pertinent to the system of interest. In the trial applications, key modeling assumptions centered on

limitations in the ability to simulate certain behaviors and on decisions regarding criteria for non-simulated failure modes that were used to define collapse where limited or no data exist.

The Methodology recognizes the importance of modeling assumptions on performance evaluation. Control occurs through the use of non-simulated collapse modes, and review and concurrence through the peer review process.

8.4 Findings Related to the Methodology

Trial applications of the Methodology revealed the following findings related to specific aspects of the Methodology and its procedures.

8.4.1 Selection of Analysis Procedure

The Methodology states that the Equivalent Lateral Force (ELF) procedure of ASCE/SEI 7-05 should be used for design of archetypes, in general, but that the Response Spectrum Analysis (RSA) procedure should be used when the ELF procedure is not allowed. It further states that the RSA procedure is permitted for the design of archetypes where RSA methods of analysis are commonly used in practice. The underlying assumption is that either method would produce similar designs and similar collapse performance.

In general, trial applications found significant differences in the stiffness (period), strength, and collapse performance of archetypes designed using the RSA and ELF procedures. Performance of archetypes designed using the RSA procedure was typically inferior to that of archetypes designed using the ELF procedure, for the same configuration and level of seismic design loading.

The special SMF system was used to investigate the effect of analysis procedure selection on collapse performance. Large differences were reflected in the fundamental period (T_1) and strength (V_{max}) of special SMF archetypes designed using the RSA and ELF procedures. Table 8-3 compares the fundamental period of special SMF archetypes as a function of archetype height and level of seismic design loading. Similarly, Table 8-4 compares the normalized strength, V_{max}/W, of the same set of archetypes.

Values of the fundamental period and normalized strength were nearly identical for 1-story archetypes, but diverged significantly as height increased. For 20-story archetypes, normalized strength using an RSA design basis was about half the strength of corresponding archetypes using an ELF design basis. Collapse performance was found to be essentially the same for 1-story archetypes, but varied in the taller archetypes. Trends in collapse performance were not as well defined, and the differences were less pronounced.

Table 8-3 Comparison of Fundamental Period, T_1, of Special SMF Archetypes Designed Using ELF and RSA Procedures

Number of Stories	Fundamental Period, T_1 (seconds)			
	ELF		RSA	
	SDC D_{max}	SDC D_{min}	SDC D_{max}	SDC D_{min}
1	0.71	1.62	0.71	1.66
2	0.87	1.74	0.91	1.83
4	1.30	1.94	1.62	2.62
8	n/a	n/a	2.29	3.55
12	n/a	n/a	3.12	4.48
20	2.48	3.44	4.47	5.74

Table 8-4 Comparison of Normalized Strength, V_{max}/W, of Special SMF Archetypes Designed Using ELF and RSA Procedures

Number of Stories	Fundamental Period, T_1 (seconds)			
	ELF		RSA	
	SDC D_{max}	SDC D_{min}	SDC D_{max}	SDC D_{min}
1	0.58	0.16	0.58	0.15
2	0.46	0.14	0.42	0.13
4	0.23	0.11	0.15	0.07
8	n/a	n/a	0.13	0.05
12	n/a	n/a	0.10	0.05
20	0.20	0.10	0.08	0.05

Results suggest that archetypes should be designed using the more critical of the ELF or RSA procedures (if both are permitted). Differences in stiffness, strength, and performance suggest a need to revise seismic design requirements to achieve better collapse parity between the ELF and RSA design procedures.

8.4.2 Quality Ratings

Many trial applications noted the subjective nature of the quality ratings used to define uncertainty associated with design requirements, test data, and nonlinear modeling. Table 8-5 summarizes the quality ratings for all systems evaluated as part of the beta testing effort or the original development of the Methodology.

Some trial applications found that collapse performance was somewhat insensitive to changes in quality ratings. Nonetheless, there is a need for a consistent and reliable method for selection of quality ratings, and a fair assessment of the quality of design requirements, test data, and nonlinear modeling capabilities across all systems. The Methodology recognizes this need, and control occurs through review and concurrence in the peer review process. For evaluation of existing code-approved

systems, it would seem possible and appropriate to develop a consensus set of quality ratings that reflect the collective opinion of a broad range of stakeholders.

Table 8-5 Summary of Quality Ratings for All Systems Evaluated

Seismic Force-Resisting System			Quality Rating		
No.	Type	Detailing	Design Requirements	Test Data	Nonlinear Modeling
1	RMSW	Special	B	B	B
2	RMSW	Ordinary	C	C	B
3	RCSW	Special	B	B	B
4	RCSW	Ordinary	B	B	B
5	SCBF	Special	B	B	B
6	BRBF	n/a	B	B	B
7a	SMF	Special	A	B	B
7b	SMF	Special	A	B	B
	RCMF[1]	Special	A	B	B
	RCMF[1]	Ordinary	A	B	C
	SMF[1]	Special	A	B	B
	WLFSW[1,2]	n/a	A	B	B[3]/D[4]

[1] System evaluated as part of original Methodology development.

[2] WLFSW = Wood Light-Frame Shear Wall system with wood structural panel sheathing.

[3] Quality rating associated with low-aspect ratio archetypes.

[4] Quality rating associated with high-aspect ratio archetypes.

8.4.3 Period-Based Ductility

Trial applications showed a wide range in the calculated period-based ductility factor, μ_T. Values ranged from 1.1 for a 20-story special SMF archetype (a tall, flexible system) to about 50 for a 4-story special RCSW archetype (a relatively short, stiff system).

The period-based ductility factor is used for determining the value of the Spectral Shape Factor (*SSF*). It is intended to be a measure of the elongation of the elastic period of the building as a result of yielding in the structural system. The effect of the *SSF* saturates at a period-based ductility factor of $\mu_T = 8$, so larger values are of no consequence to the collapse performance evaluation. Nonetheless, variations in the calculated values of this parameter appear counterintuitive, and large values appear unreasonable in systems that are not normally considered to be "ductile."

Problems were attributed to the effective yield displacement of an archetype, which is based on the fundamental-mode period, T_1, unless the code-based period, T, is larger. It was suggested that changes in the estimation of the initial stiffness, effective yield displacement, and effective ductility could be warranted.

Another problem was identified with the measurement of period-based ductility for elements with extremely limited ductility. Evaluation of special SCBF archetypes showed a potential problem with the calculation of period-based ductility when there was a rapid loss of strength due to buckling of braces in compression. When buckling occurred, strength dropped rapidly (below 80 percent of the maximum strength used to define the ultimate displacement of the archetype) and the value of the period-based ductility factor was very low. In addition, estimation of peak buckling strength was quite sensitive to modeling assumptions and was extremely variable.

Because the Methodology caps the effect of period-based ductility, there is no real problem with the factor when it is used solely to determine the value of the *SSF*. It is recognized, however, that there are other methods of defining effective yield strength and ductility, which would result in different values of predicted ductility. Regardless of the measure, the resulting effects would need to be calibrated for use in defining the *SSF*, and the net result would be expected to be the same. There is a need to better define maximum strength for elements like braces, which experience a rapid loss in strength due to buckling behavior, for the purpose of calculating values of ultimate displacement and period-based ductility.

8.4.4 Acceptance Criteria for Archetypes with Low Ductility

Trial applications on special SMF archetypes revealed a small, but important, shortcoming for systems with very limited period-based ductility. The Methodology is ambiguous with respect to acceptable values of adjusted collapse margin ratio (*ACMR*) when archetypes have very small values of period-based ductility and should be clarified for use with such systems.

8.5 Recommendations for Improving the Methodology

Recommendations are divided into two groups: (1) recommendations directly affecting the Methodology and its procedures, as applied to new systems; and (2) recommendations for implementation of the Methodology in the evaluation of existing code-approved systems.

8.5.1 Methodology Improvements

Based on the results of trial applications studied herein, recommendations for improving the Methodology as it is applied to new systems include the following:

- Additional guidance on the appropriate use of the ELF or RSA procedures in the design of archetypes.
- Improved consistency and reliability in the selection and determination of quality ratings.

- Additional guidance on determining acceptable values of adjusted collapse margin ratio, *ACMR*, for systems with extremely low period-based ductility or systems with archetypes that have different values of β_{TOT}.
- Verification of the applicability of the Far-Field ground motion set to long-period systems with $T > 4$ seconds.

8.5.2 Methodology Implementation

Based on the results of trial applications studied herein, recommendations for implementing the Methodology in the evaluation of existing code-approved systems include the following:

- Investigation of an improved framework for seismic performance factors, in terms of possible adjustments to the *R* factor formulation, considering observations made in the trial applications and lessons learned regarding system performance.
- Investigation and quantification of the effects of the requirement for $C_d = R$ on drift controlled systems through direct comparison with results for designs based on code-specified values of C_d.
- Investigation of modified material-specific design requirements to improve collapse behavior of selected systems, considering observations made in the trial applications and lessons learned regarding individual system performance documented in the relevant chapters.
- Standardization of design configurations for each system in terms of representative index archetype configurations and necessary variations in design parameters (e.g., design assumptions, span lengths, story heights, member sizes, and member shapes).
- Standardization of nonlinear modeling in terms of guidelines on nonlinear analysis techniques, and selection of non-simulated collapse criteria.
- Standardization of quality ratings in terms of consensus opinions from a large group of stakeholders on quality of design requirement and test data across all systems.
- Augmentation of existing experimental data with new testing to better quantify nonlinear deteriorating behavior of primary seismic force-resisting components considering: (1) shear failure and loss of vertical load-carrying ability in reinforced masonry and reinforced concrete shear walls; (2) behavior of large brace sections and fracture near steel gusset plate connections in steel braced frames; and (3) moment-rotation deterioration for deep slender steel column sections under varying axial loads.

Appendix A
Design Details of Reinforced Masonry Shear Wall Archetypes

This appendix presents detailed design information for reinforced masonry shear wall (RMSW) archetypes considered in Chapter 3. Seismic criteria, design loads, and other related requirements that were used as a basis for design of special RMSW and ordinary RMSW archetypes are described, and the resulting plan configurations, wall sections, and reinforcing patterns at each floor level for each archetype are summarized. Calibration of reinforced masonry shear wall models is explained, and results from supplemental model validation studies are presented.

A.1 Introduction

Index archetypes for special RMSW and ordinary RMSW systems were designed in accordance with design requirements contained within ACI 530-08/ASCE 5-08/TMS 402-08, Masonry Standards Joint Committee (MSJC), *Building Code Requirements for Masonry Structures* (ACI, 2008b), and ASCE/SEI 7-05, *Minimum Design Loads for Buildings and Other Structures* (ASCE, 2006). Test data were used to support the designs, as necessary.

A.2 Material Properties and Gravity Loads

Material properties for masonry and reinforcing steel are summarized in Table A-1. Masonry walls are constructed of hollow concrete masonry blocks with nominal thicknesses varying from 8 inches to 16 inches. The unit weight of masonry was taken as 120 pcf, and the weight of partially grouted walls was determined considering the volumetric void ratio. Floor and roof systems were assumed to consist of cast-in-place concrete slabs in the corridors and precast hollow core planks with a cast-in-place concrete topping slab elsewhere. Gravity load assumptions for floor and roof dead load and live load are summarized in Table A-2.

Table A-1 Material Properties for Special RMSW and Ordinary RMSW Archetypes

Material	Properties
Concrete Masonry Units	f'_m=1.5 ksi (minimum); 3.0 ksi (maximum)
Steel Reinforcing	ASTM A615 Grade 60 ksi

Table A-2 Gravity Load Assumptions for Special RMSW and Ordinary RMSW Archetypes

Load	Value
Roof Loading	
Typical Dead Load (single-story)	30 psf
Typical Dead Load (multistory)	85 psf
Typical Live Load	20 psf
Floor Loading	
Typical Dead Load	100 psf
Typical Live Load	28 psf
Corridor Dead Load	73 psf
Corridor Live Load	60 psf
Masonry Walls	
Fully grouted	120 pcf
Partially grouted	Determined by volumetric void ratio

A.3 Structural Configurations

Plan configurations for special RMSW and ordinary RMSW archetypes are shown in Figure A-1 and Figure A-2. Two plan configurations were selected as representative of realistic reinforced masonry shear wall arrangements in single-story and multistory buildings. Story heights were 12 feet for the single-story archetypes and 10 feet for the multistory archetypes.

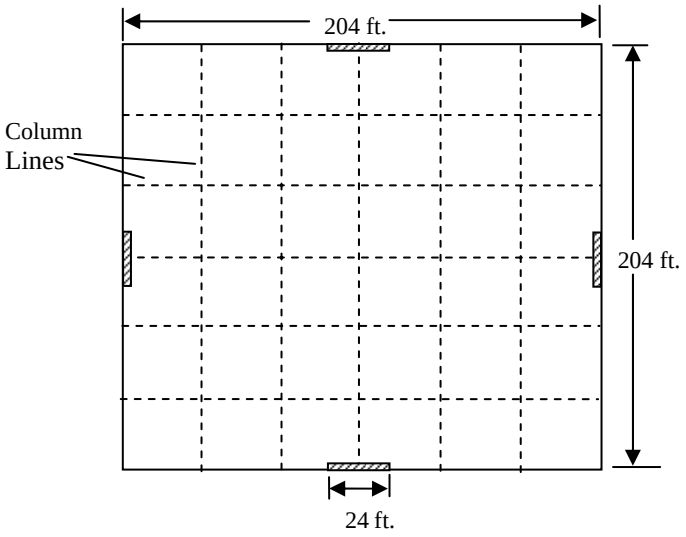

Figure A-1 Single-story reinforced masonry shear wall building configuration (design for SDC D_{max} shown).

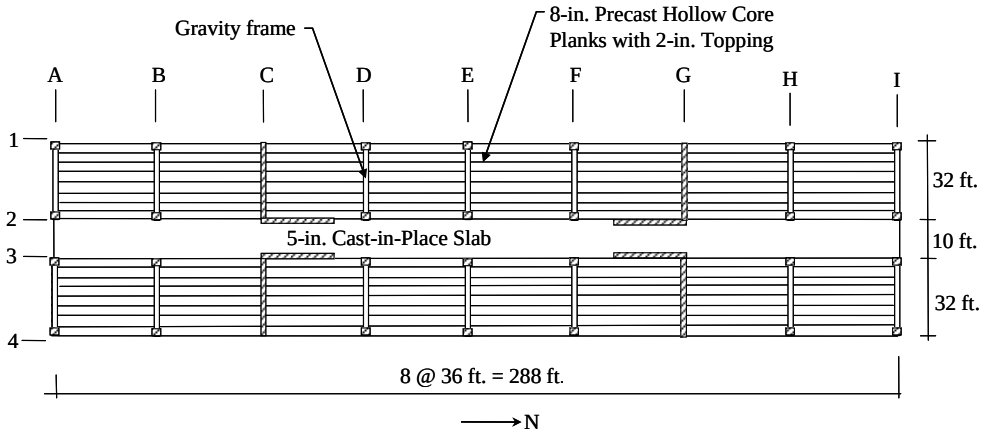

(a) 2-story building (4 walls per direction, 8 bays)

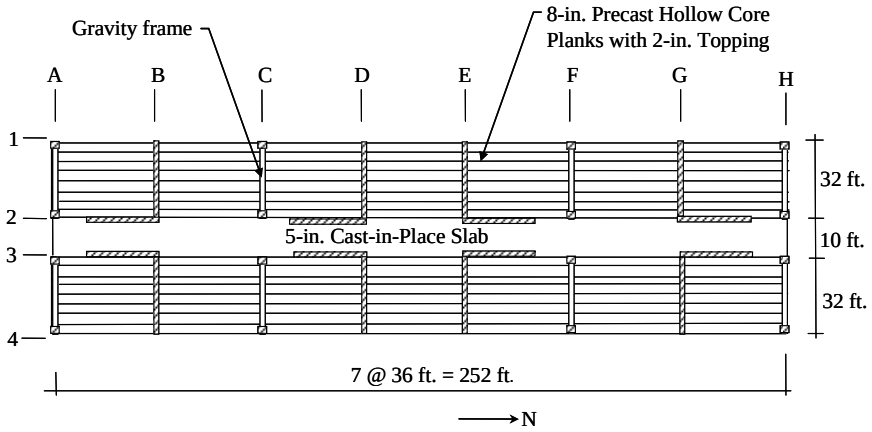

(b) 4-story building (8 walls per direction, 7 bays)

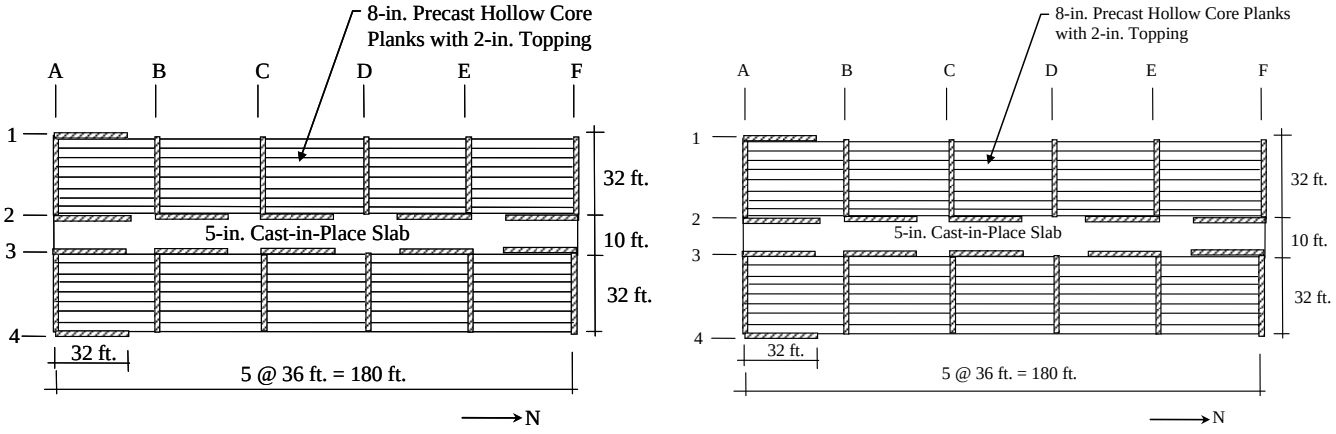

(c) 8-story and 12-story buildings (12 walls per direction, 5 bays)

Figure A-2 Multistory reinforced masonry shear wall building configurations (designs for SDC D_{max} shown).

To avoid biasing of performance evaluation results with excessive overstrength, building size and number of shear walls in each direction were adjusted in each archetype to suit the level of seismic design loading. Table A-3 summarizes the number of stories, number of bays, number of walls in each direction, and wall aspect ratio (height/length) for each archetype and seismic design category.

Table A-3 Reinforced Masonry Shear Wall Building Archetype Configurations

No. of Stories	Story Height (ft.)	SDC	Length (bays)	Width (bays)	No. of Walls (each direct.)	Wall Aspect Ratio Height/Length (ft.)
1	12	D_{max}	6	6	2	12/24
		D_{min}	10	10	2	
		C_{max}	6	6	4	
		C_{min}	10	10	4	
2	10	D_{max}	8	3	4	20/32
		D_{min}	14	3	4	
		C_{max}	6	3	4	
		C_{min}	10	3	4	
4	10	D_{max}	7	3	8	40/32
		D_{min}	10	3	4	
		C_{max}	5	3	8	
		C_{min}	5	3	4	
8	10	D_{max}	5	3	12	80/32
		D_{min}	6	3	4	
		C_{max}	5	3	12	
		C_{min}	6	3	8	
12	10	D_{max}	5	3	12	120/32
		D_{min}	6	3	4	
		C_{max}	5	3	12	
		C_{min}	5	3	8	

A.4 Shear Wall Designs

Shear wall design parameters are summarized in Table A-4 through Table A-23 by ductility classification (special versus ordinary) and Seismic Design Category (D_{max}, D_{min}, C_{max}, and C_{min}). In the tables, the design story shear, V_u, is the larger of the shear demand and the shear force corresponding to 1.25 times the nominal moment capacity of the wall. In most cases the shear corresponding to the flexural strength governed. Tables include minimum and maximum design axial load ratios determined for each wall (based on the net cross-sectional area), nominal wall thickness, nominal specified masonry compressive strength, shear and flexural

demands, nominal shear and flexural capacities, and horizontal and vertical reinforcing steel quantities.

Plan sections showing wall reinforcing patterns at the base of each wall are provided in Figures A-3 through A-6. When different bars sizes were necessary, larger bars were placed closer to the ends of the wall. When the number of bars is reduced in the upper stories, bars were placed to keep the bar spacing as uniform as possible.

Table A-4 1-Story Special Reinforced Masonry Shear Wall Designs, SDC D_{max}

Story	t (in.)	f'_m (ksi)	M_u (kip-ft)	ρ_v	Vert. Reinf.	ϕM_n (kip-ft)	V_u (kips)	ρ_h	Horiz. Reinf.	ϕV_n (kips)
High/Low Axial Load, $P_u / A_n f'_m$ = 0.008 - 0.022										
1	8	1.5	1,551	0.00113	8#5	1,837	254	0.00085	#5@48"	272

Table A-5 2-Story Special Reinforced Masonry Shear Wall Designs, SDC D_{max}

Story	t (in.)	f'_m (ksi)	M_u (kip-ft)	ρ_v	Vert. Reinf.	ϕM_n (kip-ft)	V_u (kips)	ρ_h	Horiz. Reinf.	ϕV_n (kips)
High Axial Load, $P_u / A_n f'_m$ = 0.025 - 0.053										
1, 2	8	2.5	3,685	0.00082	12#4	4,416	567	0.00180	#6@32"	569
Low Axial Load, $P_u / A_n f'_m$= 0.007 - 0.014										
1, 2	8	2.5	3,685	0.00127	12#5	3,755	382	0.00082	#4@32"	443

Table A-6 4-Story Special Reinforced Masonry Shear Wall Designs, SDC D_{max}

Story	t (in.)	f'_m (ksi)	M_u (kip-ft)	ρ_v	Vert. Reinf.	ϕM_n (kip-ft)	V_u (kips)	ρ_h	Horiz. Reinf.	ϕV_n (kips)
High Axial Load, $P_u / A_n f'_m$ = 0.042 - 0.092										
1, 2	8	3.0	6,342	0.00082	12#4	6,899	544	0.00127	#5@32"	543
3, 4	8	3.0	2,229	0.00082	12#4	4,460	367	0.00127	#5@32"	573
Low Axial Load, $P_u / A_n f'_m$= 0.007 - 0.014										
1, 2	8	2.0	6,342	0.00246	12#7	6,849	387	0.00180	#6@32"	421
3, 4	8	2.0	2,229	0.00127	12#5	3,708	261	0.00082	#4@32"	411

Table A-7 8-Story Special Reinforced Masonry Shear Wall Designs, SDC D_{max}

Story	t (in.)	f'_m (ksi)	M_u (kip-ft)	ρ_v	Vert. Reinf.	ϕM_n (kip-ft)	V_u (kips)	ρ_h	Horiz. Reinf.	ϕV_n (kips)
High Axial Load, $P_u/A_n f'_m$ = 0.103 - 0.224										
1, 2	8	2.5	10,579	0.00127	12#5	11,813	455	0.00082	#4@32"	468
3, 4	8	2.5	6,873	0.00127	12#5	9,860	421	0.00082	#4@32"	468
5, 6	8	1.5	3,562	0.00127	12#5	7,159	295	0.00082	#4@32"	407
7, 8	8	1.5	1,107	0.00127	12#5	5,180	163	0.00082	#4@32"	425
Low Axial Load, $P_u/A_n f'_m$ = 0.034 - 0.072										
1, 2	8	2.0	10,579	0.00410	12#9	10,948	318	0.00082	#4@32"	378
3, 4	8	2.0	6,873	0.00246	12#7	7,405	294	0.00082	#4@32"	356
5, 6	8	1.5	3,562	0.00127	12#5	4,238	231	0.00082	#4@32"	333
7, 8	8	1.5	1,107	0.00127	12#5	3,641	128	0.00082	#4@32"	369

Table A-8 12-Story Special Reinforced Masonry Shear Wall Designs, SDC D_{max}

Story	t (in.)	f'_m (ksi)	M_u (kip-ft)	ρ_v	Vert. Reinf.	ϕM_n (kip-ft)	V_u (kips)	ρ_h	Horiz. Reinf.	ϕV_n (kips)
High Axial Load, $P_u/A_n f'_m$ = 0.092 - 0.199										
1, 2	12	3.0	20,462	0.00167	12x2#5	20,560	526	0.00107	2x#4@32"	782
3, 4	12	3.0	15,661	0.00108	12x2#4	16,691	512	0.00107	2x#4@32"	782
5, 6	12	2.0	11,046	0.00108	12x2#4	13,568	472	0.00107	2x#4@32"	639
7, 8	12	2.0	6,869	0.00108	12x2#4	11,395	400	0.00107	2x#4@32"	639
9, 10	12	2.0	3,422	0.00108	12x2#4	9,044	295	0.00107	2x#4@32"	707
11, 12	12	2.0	1,019	0.00108	12x2#4	6,523	154	0.00107	2x#4@32"	712
Low Axial Load, $P_u/A_n f'_m$ = 0.029 - 0.064										
1, 2	12	3.0	20,462	0.00481	6x2#8 10x2#7	20,831	415	0.00072	2x#4@48"	688
3, 4	12	3.0	15,661	0.00344	4x2#7 12x2#6	16,076	404	0.00072	2x#4@48"	659
5, 6	12	2.0	11,046	0.00234	2x2#6 14x2#5	11,339	372	0.00072	2x#4@48"	549
7, 8	12	2.0	6,869	0.00143	16x2#4	7,704	316	0.00072	2x#4@48"	518
9, 10	12	2.0	3,422	0.00143	16x2#4	6,904	233	0.00072	2x#4@48"	550
11, 12	12	2.0	1,019	0.00143	16x2#4	6,088	121	0.00072	2x#4@48"	617

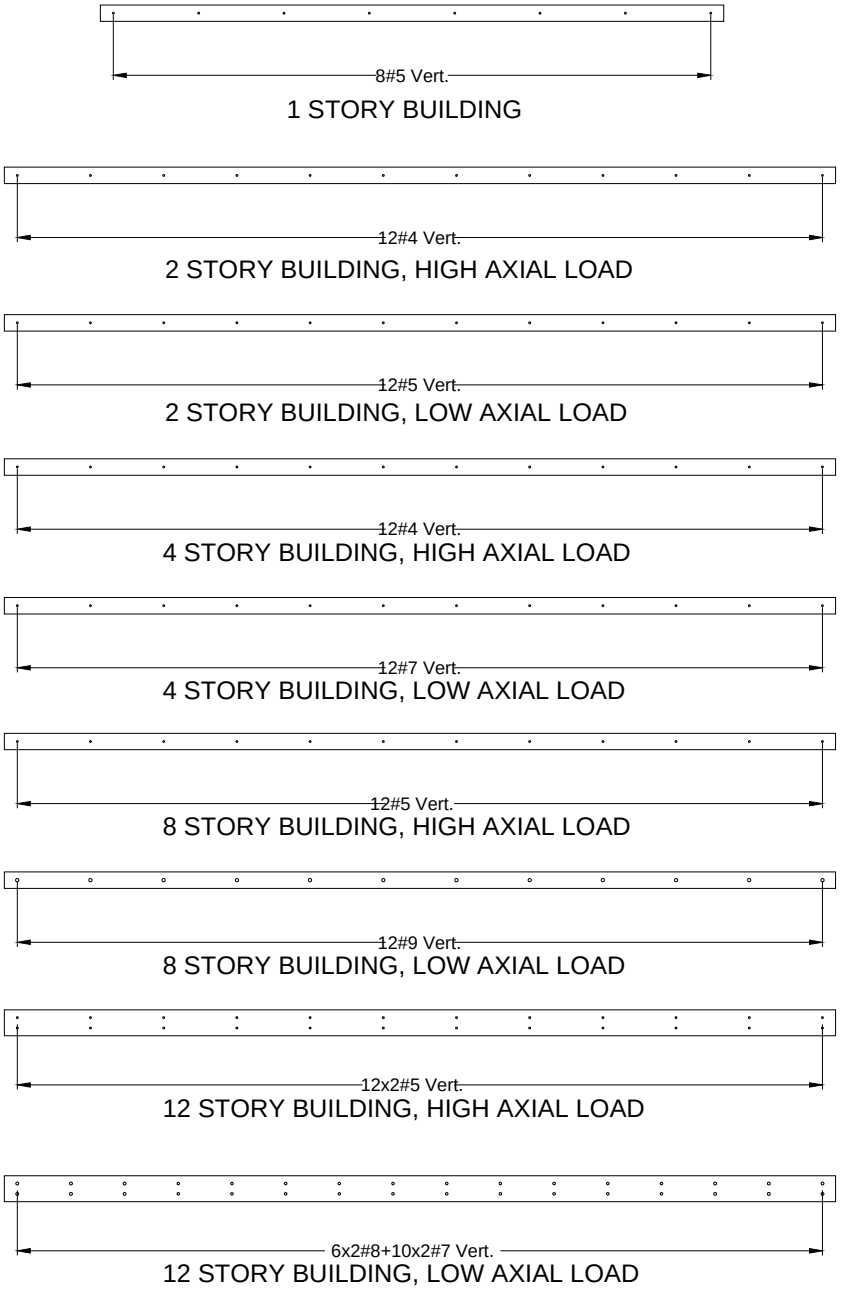

Figure A-3 Plan sections of fully grouted special reinforced masonry shear walls, SDC D_{max}.

Table A-9 1-Story Special Reinforced Masonry Shear Wall Designs, SDC D_{min}

Story	t (in.)	f'_m (ksi)	M_u (kip-ft)	ρ_v	Vert. Reinf.	ϕM_n (kip-ft)	V_u (kips)	ρ_h	Horiz. Reinf.	ϕV_n (kips)
High/Low Axial Load, $P_u / A_n f'_m$ = 0.008 - 0.015										
1	8	2.0	2,107	0.00137	4#6,4#5	2,214	290	0.00085	#5@48”	304

Table A-10 2-Story Special Reinforced Masonry Shear Wall Designs, SDC D_{min}

Story	t (in.)	f'_m (ksi)	M_u (kip-ft)	ρ_v	Vert. Reinf.	ϕM_n (kip-ft)	V_u (kips)	ρ_h	Horiz. Reinf.	ϕV_n (kips)
High Axial Load, $P_u / A_n f'_m$ = 0.035 - 0.062										
1,2	8	2.0	3,169	0.00082	12#4	4,674	486	0.00127	#5@32"	487
Low Axial Load, $P_u / A_n f'_m$= 0.013 - 0.022										
1,2	8	2.0	3,169	0.00105	6#5,6#4	3,235	320	0.00127	#5@32"	391

Table A-11 4-Story Special Reinforced Masonry Shear Wall Designs, SDC D_{min}

Story	t (in.)	f'_m (ksi)	M_u (kip-ft)	ρ_v	Vert. Reinf.	ϕM_n (kip-ft)	V_u (kips)	ρ_h	Horiz. Reinf.	ϕV_n (kips)
High Axial Load, $P_u/A_n f'_m$ = 0.048 - 0.085										
1, 2	8	3.0	7,198	0.00082	12#4	7,550	534	0.00127	#5@32"	542
3, 4	8	3.0	2,551	0.00082	12#4	4,793	363	0.00127	#5@32"	568
Low Axial Load, $P_u / A_n f'_m$= 0.019 - 0.034										
1, 2	8	2.0	7,198	0.00259	2#8 10#7	7,298	389	0.00180	#6@32"	418
3, 4	8	2.0	2,551	0.00106	12#5	3,797	265	0.00109	#4@24"	428

Table A-12 8-Story Special Reinforced Masonry Shear Wall Designs, SDC D_{min}

Story	t (in.)	f'_m (ksi)	M_u (kip-ft)	ρ_v	Vert. Reinf.	ϕM_n (kip-ft)	V_u (kips)	ρ_h	Horiz. Reinf.	ϕV_n (kips)
High Axial Load, $P_u/A_n f'_m$ = 0.098 - 0.174										
1, 2	8	3	10,357	0.00082	12#4	12,466	381	0.00127	#5@32"	513
3, 4	8	2	6,770	0.00082	12#4	9,488	353	0.00127	#5@32"	419
5, 6	8	1.5	3,549	0.00082	12#4	6,913	281	0.00127	#5@32"	471
7, 8	8	1.5	1,133	0.00082	12#4	4,554	159	0.00127	#5@32"	450
Low Axial Load, $P_u/A_n f'_m$ = 0.038 - 0.067										
1, 2	8	2.0	10,357	0.00410	12#9	11,128	307	0.00082	#4@32"	372
3, 4	8	1.5	6,770	0.00246	12#7	7,316	284	0.00082	#4@32"	320
5, 6	8	1.5	3,549	0.00127	12#5	4,402	226	0.00082	#4@32"	328
7, 8	8	1.5	1,133	0.00127	12#5	3,728	128	0.00082	#4@32"	363

Table A-13 12-Story Special Reinforced Masonry Shear Wall Designs, SDC D_{min}

Story	t (in.)	f'_m (ksi)	M_u (kip-ft)	ρ_v	Vert. Reinf.	ϕM_n (kip-ft)	V_u (kips)	ρ_h	Horiz. Reinf.	ϕV_n (kips)
High Axial Load, $P_u/A_n f'_m$ = 0.106 - 0.186										
1, 2	12	3.0	18,399	0.00108	12x2#4	20,697	482	0.00108	2#4@32"	782
3, 4	12	2.0	14,129	0.00108	12x2#4	16,887	439	0.00108	2#4@32"	639
5, 6	12	2.0	10,015	0.00108	12x2#4	14,714	406	0.00108	2#4@32"	639
7, 8	12	2.0	6,276	0.00108	12x2#4	12,322	346	0.00108	2#4@32"	639
9, 10	12	2.0	3,167	0.00108	12x2#4	9,710	258	0.00108	2#4@32"	691
11, 12	12	2.0	974	0.00108	12x2#4	6,871	138	0.00108	2#4@32"	703
Low Axial Load, $P_u/A_n f'_m$ = 0.050 - 0.090										
1, 2	12	2.0	18,399	0.00430	16x2#7	18,439	343	0.00072	2#4@48"	596
3, 4	12	2.0	14,129	0.00315	16x2#6	14,801	335	0.00072	2#4@48"	569
5, 6	12	2.0	10,015	0.00222	16x2#5	11,360	309	0.00072	2#4@48"	542
7, 8	12	2.0	6,276	0.00143	16x2#4	8,043	264	0.00072	2#4@48"	513
9, 10	12	2.0	3,167	0.00143	16x2#4	7,134	197	0.00072	2#4@48"	542
11, 12	12	2.0	974	0.00143	16x2#4	6,206	106	0.00072	2#4@48"	612

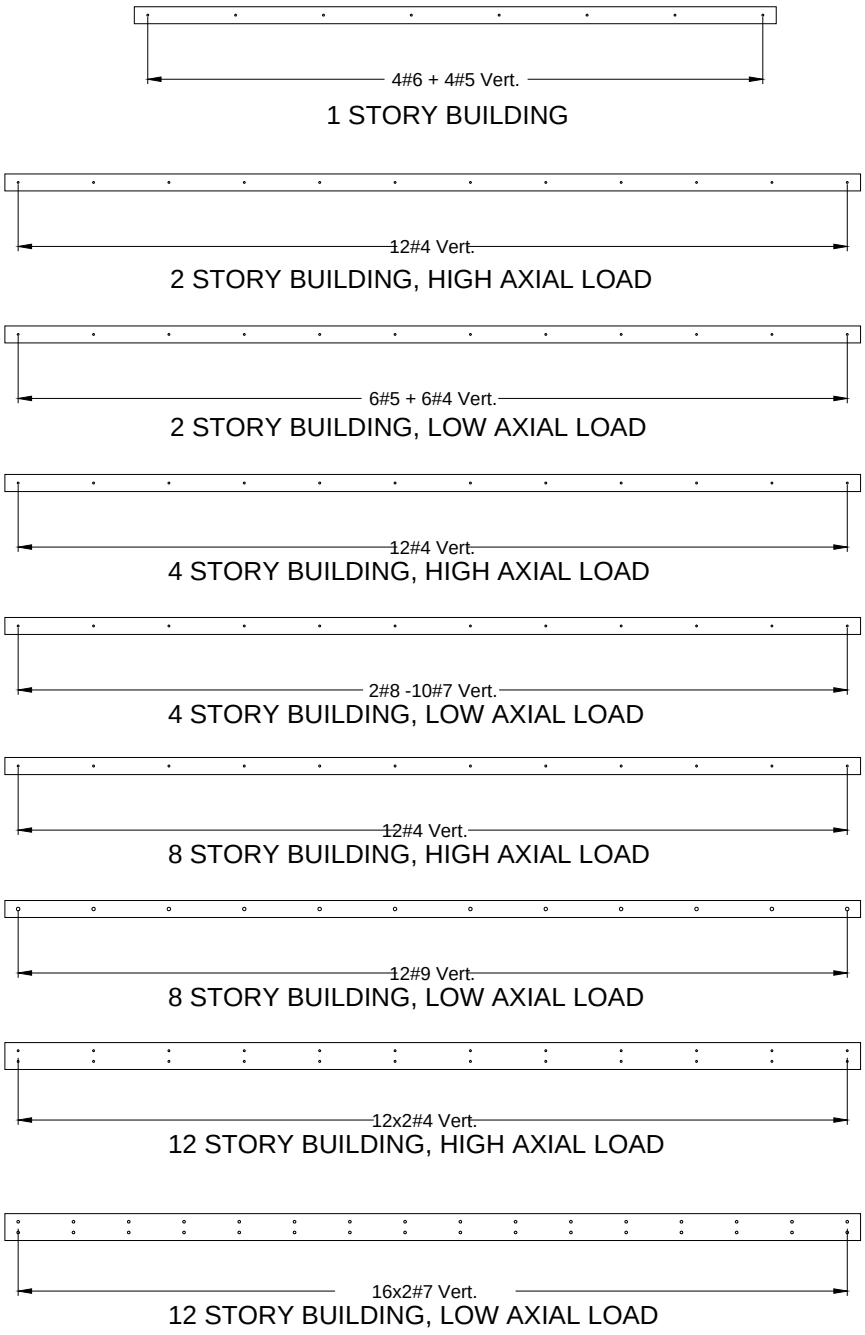

Figure A-4 Plan sections of fully grouted special reinforced masonry shear walls, SDC D_{min}.

Table A-14 1-Story Ordinary Reinforced-Masonry Shear Wall Designs, SDC C_{max}

Story	t (in.)	f'_m (ksi)	M_u (kip-ft)	ρ_v	Vert. Reinf.	ϕM_n (kip-ft)	V_u (kips)	ρ_h	Horiz. Reinf.	ϕV_n (kips)
High/Low Axial Load, $P_u / A_n f'_m$ = 0.016 - 0.029										
1	8	1.5	954	0.00057	4#5	1,064	80	0.000219	#4@120"	133

Table A-15 2-Story Ordinary Reinforced Masonry Shear Wall Designs, SDC C_{max}

Story	t (in.)	f'_m (ksi)	M_u (kip-ft)	ρ_v	Vert. Reinf.	ϕM_n (kip-ft)	V_u (kips)	ρ_h	Horiz. Reinf.	ϕV_n (kips)
High Axial Load, $P_u / A_n f'_m$ = 0.079 – 0.139										
1, 2	8	1.5	3,382	0.00056	4#5,2#4	3,445	208	0.00021	#4@120"	208
Low Axial Load, $P_u / A_n f'_m$= 0.012 - 0.023										
1, 2	8	2.0	3,382	0.00136	2#8,4#7	3,642	208	0.00052	#4@48"	226

Table A-16 4-Story Ordinary Reinforced Masonry Shear Wall Designs, SDC C_{max}

Story	t (in.)	f'_m (ksi)	M_u (kip-ft)	ρ_v	Vert. Reinf.	ϕM_n (kip-ft)	V_u (kips)	ρ_h	Horiz. Reinf.	ϕV_n (kips)
High Axial Load, $P_u/A_n f'_m$ = 0.107 - 0.190										
1, 2	10	2.0	4,592	0.00033	6#4	5,315	157	0.00017	#4@120"	255
3, 4	10	1.5	1,616	0.00033	6#4	3,281	106	0.00017	#4@120"	237
Low Axial Load, $P_u / A_n f'_m$= 0.025 - 0.040										
1, 2	8	2.0	4,515	0.00176	2#9,4#8	4,811	155	0.00021	#4@120"	170
3, 4	8	2.0	1,591	0.00049	2#5,4#4	1,756	105	0.00021	#4@120"	206

Table A-17 8-Story Ordinary Reinforced Masonry Shear Wall Designs, SDC C_{max}

Story	t (in.)	f'_m (ksi)	M_u (kip-ft)	ρ_v	Vert. Reinf.	ϕM_n (kip-ft)	V_u (kips)	ρ_h	Horiz. Reinf.	ϕV_n (kips)
High Axial Load, $P_u/A_n f'_m$ = 0.130 - 0.231										
1, 2	12	3	7,633	0.00027	6#4	9,722	134	0.00014	#4@120"	371
3, 4	12	2.5	4,975	0.00027	6#4	7,674	125	0.00014	#4@120"	329
5, 6	12	2.0	2,590	0.00027	6#4	5,552	99	0.00014	#4@120"	291
7, 8	12	2.0	813	0.00027	6#4	3,553	55	0.00014	#4@120"	296
Low Axial Load, $P_u/A_n f'_m$ = 0.037 - 0.068										
1, 2	10	2.5	7,506	0.00217	8#9	7,760	132	0.00017	#4@120"	226
3, 4	10	2.0	4,892	0.00130	8#7	5157	122	0.00017	#4@120"	199
5, 6	10	2.0	2,549	0.00067	8#5	3,169	97	0.00017	#4@120"	212
7, 8	10	2.0	801	0.00043	8#4	1,964	54	0.00017	#4@120"	247

Table A-18 12-Story Ordinary Reinforced Masonry Shear Wall Designs, SDC C_{max}

Story	t (in.)	f'_m (ksi)	M_u (kip-ft)	ρ_v	Vert. Reinf.	ϕM_n (kip-ft)	V_u (kips)	ρ_h	Horiz. Reinf.	ϕV_n (kips)
High Axial Load, $P_u/A_n f'_m$ = 0.124 – 0.219										
1, 2	16	3.0	14,878	0.00053	16#4	16,700	174	0.00011	2#3@120"	636
3, 4	16	3.0	11,407	0.00053	16#4	15,011	170	0.00011	2#3@120"	600
5, 6	16	2.0	7,643	0.00027	8#4	9,745	148	0.00011	2#3@120"	434
7, 8	16	2.0	4,772	0.00027	8#4	8,310	126	0.00011	2#3@120"	391
9, 10	16	2.0	2,391	0.00027	8#4	6,432	94	0.00011	2#3@120"	385
11, 12	16	2.0	722	0.00027	8#4	4,078	49	0.00011	2#3@120"	406
Low Axial Load, $P_u/A_n f'_m$ = 0.036 - 0.065										
1, 2	16	3.0	14,878	0.00320	16x2#7	17,286	174	0.00011	2#3@120"	452
3, 4	16	3.0	11,407	0.00235	16x2#6	14,047	170	0.00011	2#3@120"	439
5, 6	16	2.0	7,643	0.00117	8x2#6	7,835	146	0.00011	2#3@120"	307
7, 8	16	2.0	4,772	0.00083	8x2#5	5,945	126	0.00011	2#3@120"	296
9, 10	16	2.0	2,391	0.00053	8x2#4	4,143	94	0.00011	2#3@120"	323
11, 12	16	2.0	722	0.00053	8x2#4	3,458	49	0.00011	2#3@120"	376

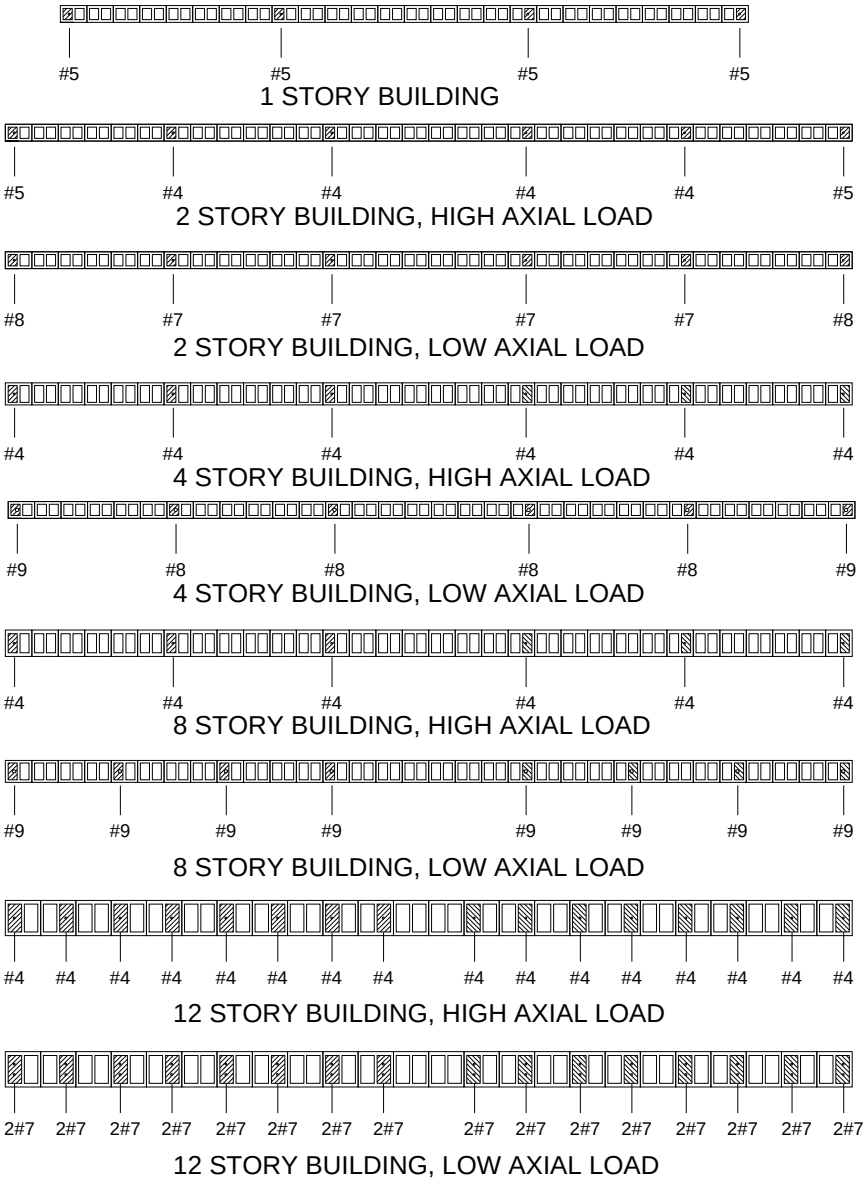

Figure A-5 Plan sections of partially grouted ordinary reinforced masonry shear walls, SDC C_{max}.

Table A-19 1-Story Ordinary Reinforced Masonry Shear Wall Designs, SDC C_{min}

Story	t (in.)	f'_m (ksi)	M_u (kip-ft)	ρ_v	Vert. Reinf.	ϕM_n (kip-ft)	V_u (kips)	ρ_h	Horiz. Reinf.	ϕV_n (kips)
High/Low Axial Load, $P_u / A_n f'_m$ = 0.017 - 0.029										
1	8	1.5	1,571	0.00109	4#7	1,728	131	0.00021	#4@120"	133

Table A-20 2-Story Ordinary Reinforced Masonry Shear Wall Designs, SDC C_{min}

Story	t (in.)	f'_m (ksi)	M_u (kip-ft)	ρ_v	Vert. Reinf.	ϕM_n (kip-ft)	V_u (kips)	ρ_h	Horiz. Reinf.	ϕV_n (kips)
High Axial Load, $P_u / A_n f'_m$ = 0.082 - 0.135										
1, 2	8	1.5	3,352	0.00048	2#5,4#4	3,412	206	0.00021	#4@120"	210
Low Axial Load, $P_u / A_n f'_m$= 0.013 - 0.022										
1, 2	8	2.0	3,352	0.00123	6#7	3,382	206	0.00021	#4@120"	226

Table A-21 4-Story Ordinary Reinforced Masonry Shear Wall Designs, SDC C_{min}

Story	t (in.)	f'_m (ksi)	M_u (kip-ft)	ρ_v	Vert. Reinf.	ϕM_n (kip-ft)	V_u (kips)	ρ_h	Horiz. Reinf.	ϕV_n (kips)
High Axial Load, $P_u/A_n f'_m$ = 0.103 – 0.169										
1, 2	8	2.5	5,416	0.00041	6#4	5,690	184	0.00021	#4@120"	252
3, 4	8	1.5	1,927	0.00041	6#4	3,263	126	0.00021	#4@120"	213
Low Axial Load, $P_u / A_n f'_m$= 0.021 - 0.035										
1, 2	8	2.5	5,416	0.00205	6#9	5,524	184	0.00021	#4@120"	186
3, 4	8	1.5	1,927	0.00064	6#5	2,080	126	0.00021	#4@120"	182

Table A-22 8-Story Ordinary Reinforced Masonry Shear Wall Designs, SDC C_{min}

Story	t (in.)	f'_m (ksi)	M_u (kip-ft)	ρ_v	Vert. Reinf.	ϕM_n (kip-ft)	V_u (kips)	ρ_h	Horiz. Reinf.	ϕV_n (kips)
High Axial Load, $P_u/A_n f'_m$ = 0.135 - 0.225										
1, 2	12	3.0	8,042	0.00027	6#4	9,951	140	0.00014	#4@120"	371
3, 4	12	2.0	5,264	0.00027	6#4	7,165	131	0.00014	#4@120"	303
5, 6	12	1.5	2,762	0.00027	6#4	5,193	104	0.00014	#4@120"	267
7, 8	12	1.5	880	0.00027	6#4	3,455	59	0.00014	#4@120"	265
Low Axial Load, $P_u/A_n f'_m$ = 0.032 - 0.055										
1, 2	10	3.0	7,963	0.00216	8#9	8,091	139	0.00017	#4@120"	245
3, 4	10	2.0	5,213	0.00130	8#7	5,215	129	0.00017	#4@120"	200
5, 6	10	2.0	2,731	0.00067	8#5	3,213	103	0.00017	#4@120"	212
7, 8	10	2.0	872	0.00043	8#4	1,989	58	0.00017	#4@120"	247

Table A-23 12-Story Ordinary Reinforced Masonry Shear Wall Designs, SDC C_{min}

Story	t (in.)	f'_m (ksi)	M_u (kip-ft)	ρ_v	Vert. Reinf.	ϕM_n (kip-ft)	V_u (kips)	ρ_h	Horiz. Reinf.	ϕV_n (kips)
High Axial Load, $P_u/A_n f'_m$ = 0.139 - 0.230										
1, 2	16	3.0	12,444	0.00040	12#4	1,5909	144	0.00010	#4@120"	584
3, 4	16	3.0	9,567	0.00040	12#4	14,326	141	0.00010	#4@120"	575
5, 6	16	2.0	6,594	0.00020	6#4	9,195	127	0.00010	#4@120"	413
7, 8	16	2.0	4,138	0.00020	6#4	8,069	109	0.00010	#4@120"	382
9, 10	16	2.0	2,089	0.00020	6#4	6,205	81	0.00010	#4@120"	371
11, 12	16	2.0	640	0.00020	6#4	3,887	43	0.00010	#4@120"	388
Low Axial Load, $P_u/A_n f'_m$ = 0.038 - 0.065										
1, 2	16	3.0	12,444	0.00240	12x2#7	14,377	144	0.00011	2#3@120"	421
3, 4	16	3.0	9,567	0.00176	12x2#6	11,656	141	0.00011	2#3@120"	409
5, 6	16	2.0	6,594	0.00088	6x2#6	6,704	127	0.00011	2#3@120"	296
7, 8	16	2.0	4,138	0.00040	6x2#4	4,284	109	0.00011	2#3@120"	284
9, 10	16	2.0	2,089	0.00040	6x2#4	3,592	81	0.00011	2#3@120"	308
11, 12	16	2.0	640	0.00040	6x2#4	2,837	43	0.00011	2#3@120"	358

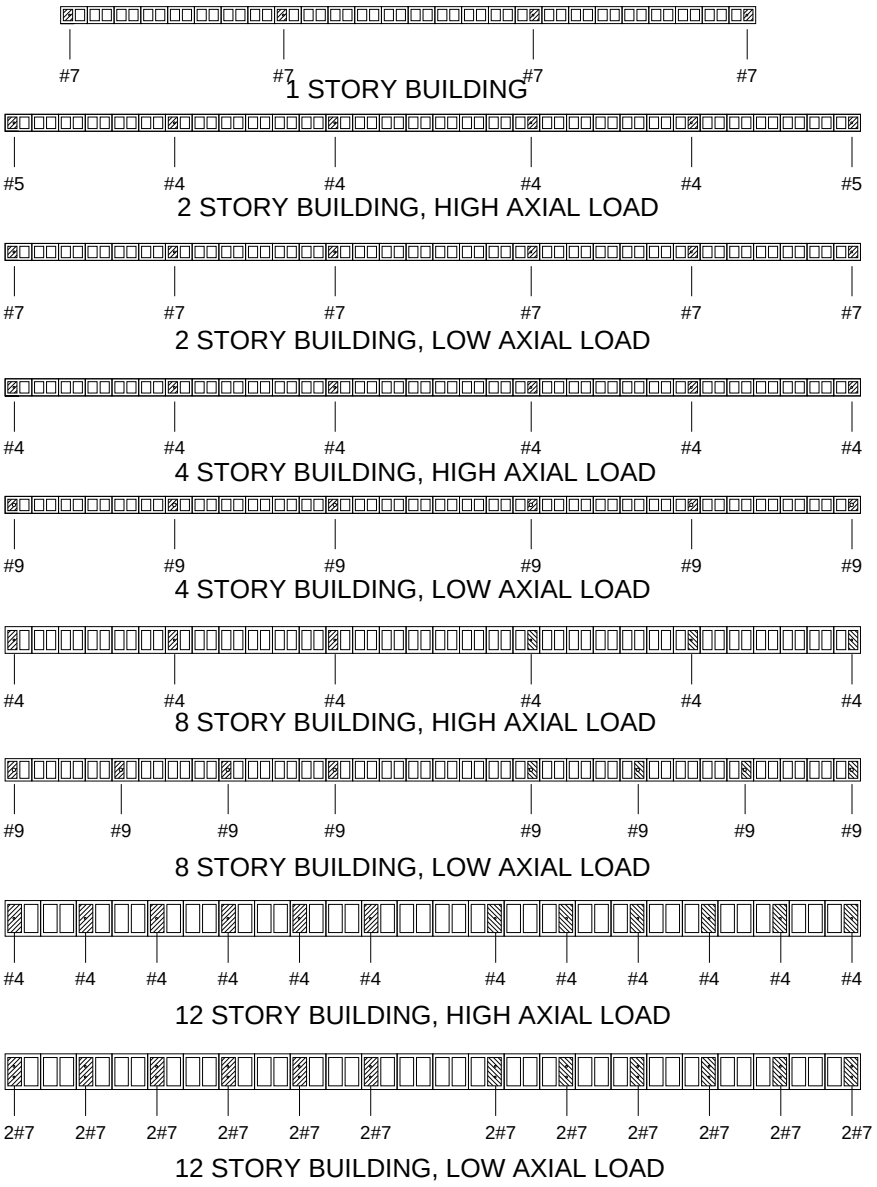

Figure A-6 Plan sections of partially grouted ordinary reinforced masonry shear walls, SDC C_{min}.

A.5 Calibration of Reinforced Masonry Shear Wall Models

In displacement-based beam-column elements with distributed plasticity and strain-softening material laws, there is a potential for strain localization to occur. This phenomenon can lead to numerical results that are sensitive to the length of the element in which the plastic strain is localized. To circumvent this problem, the reference material stress-strain relations should be modified according to the element size to obtain realistic total fracture-energy dissipation. This modification is called regularization, which ensures that the numerical solution will be objective and not sensitive to element size.

Regularization can be achieved by determining ε_r according to the following formula (Coleman and Spacone, 2001):

$$\varepsilon_r = \frac{G_m^f}{0.6 f_m' L_e} - \frac{0.8 f_m'}{E_m} + \varepsilon_p \tag{A-1}$$

In this formula f_m' is the compressive strength of masonry, ε_p is the strain at the peak stress, and E_m is the modulus of elasticity, which is assumed to remain the same during loading and unloading even though it is not exactly the case for the material model used here. With the Kent-Park model, $E_m = 667\ f_m'$.

The fracture energy G_m^f is to be determined from the effective plastic-hinge length L_p of the wall and the reference material model shown in Figure 3-5 by means of the following equation:

$$G_m^f = 0.6(0.01 - \varepsilon_p) f_m' L_p + \frac{0.48 f_m'^2 L_p}{E_m} \tag{A-2}$$

As to the steel stress-strain law, it is important to maintain the objectivity of the bar fracture and buckling as a function of the total wall rotation in a plastic-hinge region. To this end, the fracture strain, ε_u, and the strain, ε_o, at which the tensile strength reaches zero, as shown in Figure 3-6a, are to be determined according to the ratio of the element length to the effective plastic-hinge length as follows:

$$\varepsilon_u = \varepsilon_y + \left(0.05 - \varepsilon_y\right)\frac{L_p}{L_e} \tag{A-3}$$

$$\varepsilon_o = \varepsilon_u + \frac{0.05 L_p}{L_e} \tag{A-4}$$

The above equations retain the objectivity of the rate of tensile stress gain in the strain hardening regime and the bar rupture point as the element size changes. When the length ratio is one, the values shown in Figure 3-6a are recovered. Because the compressive strain signifying the onset of bar buckling is set equal to the strain at which the masonry compressive strength drops to 40% of the peak value, it will change with the ε_r value for masonry as L_e changes to maintain the objectivity of the bar buckling point.

A.6 Supplemental Model Validation Studies

This section presents results from additional validation studies on reinforced masonry shear wall models. Figure A-7 compares the experimental and numerical results for a two-story coupled wall system (Specimen 2a) tested by Merryman et al. (1990). The specimen consisted of two walls coupled by a reinforced concrete slab at each level. The coupling slabs were modeled with beam-column elements with concentrated plastic hinges at the two ends. The effective bending width of the slabs was based on

the value suggested in the report by Merryman et al. It can be seen from the figure that the numerical results matched the test results well.

Another analysis was conducted on a cantilever wall with a height/length ratio equal to 2 and an axial load ratio of 0.10 (Specimen 6) tested by Shedid et al. (2008). Figure A-8 shows that both the strength and hysteretic behavior are well captured by the model.

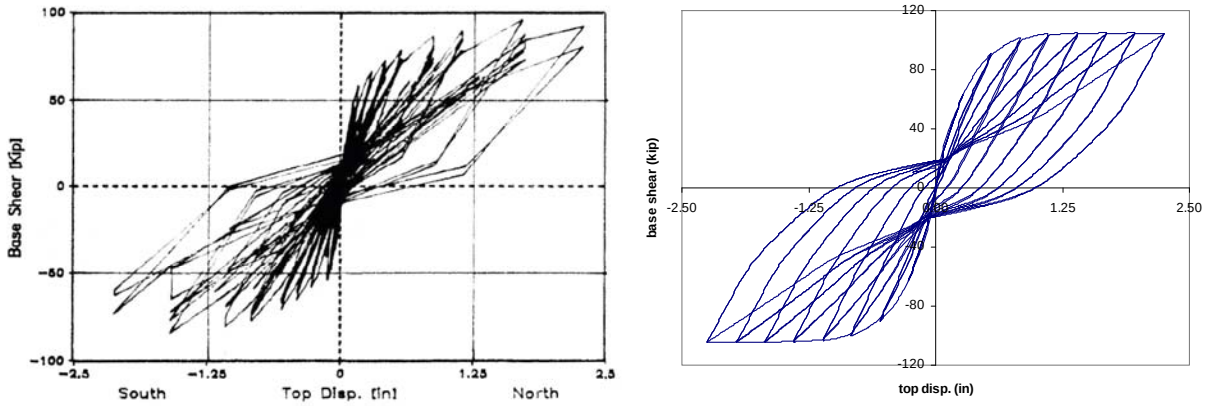

(a) (b)

Figure A-7 Lateral load versus displacement curves for Specimen 2a tested by Merryman et al. (1990): (a) experimental results; (b) analytical model.

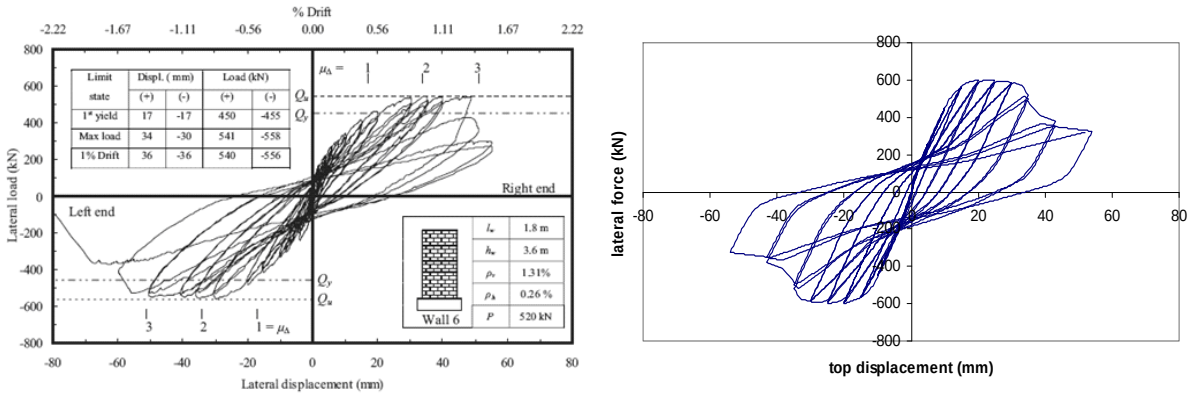

(a) (b)

Figure A-8 Lateral load versus displacement curves for Specimen 6 tested by Shedid et al. (2008): (a) experimental results; (b) analytical model.

Figure A-9 shows experimental and numerical results for a single-story, one-third scale, partially grouted, wall tested by Ghanem et al. (1992). The specimen was subjected to a monotonically increasing lateral displacement and exhibited a flexure-dominated behavior. The analysis agreed with the test results reasonably well, especially in terms of the initial stiffness and softening behavior.

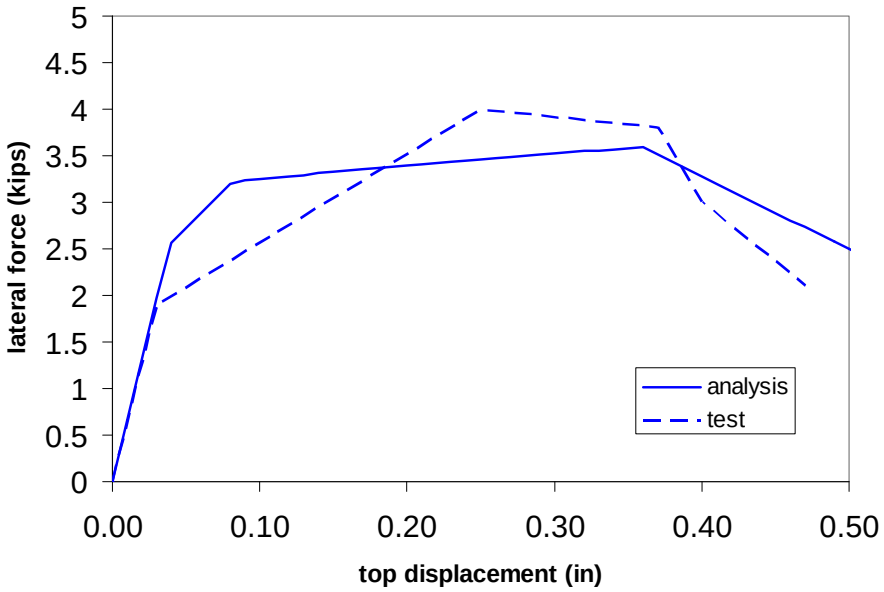

Figure A-9 Lateral load versus lateral displacement for a wall tested by Ghanem et al. (1992).

Appendix B

Design Details of Reinforced Concrete Shear Wall Archetypes

This appendix presents detailed design information for reinforced concrete shear wall (RCSW) archetypes considered in Chapter 4. Design loads and other requirements that were used as a basis for design of special RCSW and ordinary RCSW archetypes are described, and the resulting plan configurations, wall sections, and reinforcing patterns at each floor level for each archetype are summarized. Results of modeling sensitivity studies and an investigation of axial failure criteria are presented.

B.1 Introduction

Index archetypes for special RCSW and ordinary RCSW systems were designed in accordance with design requirements contained within ACI 318-08, *Building Code Requirements for Structural Concrete* (ACI, 2008a), and ASCE/SEI 7-05, *Minimum Design Loads for Buildings and Other Structures* (ASCE, 2006). Test data were used to support the designs, as necessary.

B.2 Material Properties and Gravity Loads

Material properties for concrete and reinforcing steel are summarized in Table B-1. Concrete was assumed to be normal weight concrete (150 pcf), and wall thicknesses varied between 10 inches and 16 inches. Floor and roof systems were assumed to consist of cast-in-place concrete slabs on a building frame system. Gravity load assumptions are summarized in Table B-2.

Table B-1 Material Properties for Special RCSW and Ordinary RCSW Archetypes

Material	Properties
Concrete	f'_c=5000 psi
Steel Reinforcing	f_y=60,000 psi

Table B-2 Gravity Load Assumptions for Special RCSW and Ordinary RCSW Archetypes

Load	Value
Typical Dead Load	150 psf
Typical Live Load	50 psf

B.3 Structural Configurations

A rectangular configuration with two walls resisting lateral forces in each direction was selected as representative of non-load-bearing shear walls in a building frame system. Story heights were taken as 13 feet in the first story and 12 feet in other stories. To avoid biasing of performance evaluation results with excessive overstrength, the size of the floor plan and length of shear walls in each direction were adjusted in each archetype to suit the level of seismic design loading and to achieve certain design objectives. Archetypes were configured to maximize the shear stress in the wall sections and to investigate both shear-controlled and flexural-controlled behavior.

Configurations are summarized in Table B-3 for special RCSW archetypes and Table B-4 for ordinary RCSW archetypes. For each archetype, the resulting design axial load ratio, shear stress, and shear capacity to demand ratio are reported.

Table B-3 Special Reinforced Concrete Shear Wall Archetype Configurations

Archetype ID	No. of Stories	SDC	Plan Dimensions (ft x ft)	L_w (ft)	t_w (in)	Axial Load ($A_g f'_c$)	Shear Stress ($\sqrt{f'_c}$)	$\phi V_n/V_u$
1	1	D_{max}	400 x 350	26	10	0.075	7.9	1.2
2	2	D_{max}	280 x 240	25	10	0.075	7.9	1.2
3	4	D_{max}	150 x 140	24	12	0.2	4.3	1.1
4	8	D_{max}	110 x 100	32	14	0.2	2.0	1.65
5	12	D_{max}	105 x 100	41	16	0.2	1.5	2.1
6	1	D_{min}	400 x 350	26	10	0.075	4.0	1.03
7	2	D_{min}	280 x 240	25	10	0.075	3.9	1.03
8	4	D_{min}	150 x 140	24	12	0.2	1.7	2.0
9	8	D_{min}	110 x 100	32	14	0.2	0.7	4.95
10	12	D_{min}	105 x 100	41	16	0.2	0.5	6.4
11	1	D_{max}	400 x 350	26	10	0.075	7.9	1.17
12	2	D_{max}	280 x 240	25	10	0.075	7.9	1.17
13	4	D_{max}	150 x 140	24	12	0.075	4.3	1.1
14	8	D_{max}	110 x100	32	14	0.075	2.0	1.65
15	12	D_{max}	105 x 100	41	16	0.075	1.5	2.13
16	1	D_{min}	400 x 350	26	10	0.075	4.0	1.03
17	2	D_{min}	280 x 240	25	10	0.075	3.9	1.03
18	4	D_{min}	150 x 140	24	12	0.075	1.7	2.0
19	8	D_{min}	110 x 100	32	14	0.075	0.7	4.95
20	12	D_{min}	105 x 100	41	16	0.075	0.5	6.37

Table B-4 Ordinary Reinforced Concrete Shear Wall Archetype Configurations

Archetype ID	No. of Stories	SDC	Plan Dimensions (ft x ft)	L_w (ft)	t_w (in)	Axial Load ($A_g f'_c$)	Shear Stress ($\sqrt{f'_c}$)	$\phi V_n/V_u$
21	1	C_{max}	400 x 350	26	10	0.075	4.7	1.15
22	2	C_{max}	280 x 240	25	10	0.075	4.7	1.15
23	4	C_{max}	150 x 140	41	16	0.2	2.0	1.05
24	8	C_{max}	110 x 100	32	14	0.2	0.8	3.3
25	12	C_{max}	105 x 100	32	14	0.2	0.6	4.25
26	1	C_{min}	400 x 350	26	10	0.075	3.2	1.1
27	2	C_{min}	280 x 240	25	10	0.075	3.2	1.0
28	4	C_{min}	150 x 140	24	12	0.2	1.3	2.0
29	8	C_{min}	110 x 100	32	14	0.2	0.8	3.3
30	12	C_{min}	105 x 100	41	16	0.2	0.6	4.25
31	1	C_{max}	400 x 350	26	10	0.075	4.7	1.15
32	2	C_{max}	280 x 240	25	10	0.075	4.7	1.15
33	4	C_{max}	150 x 140	24	12	0.075	2.0	1.3
34	8	C_{max}	110 x 100	32	14	0.075	0.8	3.3
35	12	C_{max}	105 x 100	41	16	0.075	0.6	4.25
36	1	C_{min}	400 x 350	26	10	0.075	3.2	1.1
37	2	C_{min}	280 x 240	25	10	0.075	3.2	1.0
38	4	C_{min}	150 x 140	24	12	0.075	1.3	2.0
39	8	C_{min}	110 x 100	32	14	0.075	0.5	5.0
40	12	C_{min}	105 x 100	41	16	0.075	0.4	6.4

B.4 Reinforced Concrete Shear Wall Designs

Shear wall design base shear and moment demands were calculated based on the Equivalent Lateral Force (ELF) procedure. Axial loads were assumed to be the result of the axial load combination that created the highest demand. Wall reinforcement was determined through axial load-moment interaction, using the BIAX software program (Wallace, 1989). An example *P-M* interaction diagram for Archetype 12 is shown in Figure B-1.

A displacement-based approach was used to determine the need for special boundary elements. The approach was based on the procedure in ACI 318-08, which requires compression zones to be reinforced with special boundary elements when:

$$c \geq \frac{l_w}{600(\delta_u / h_w)} \qquad \text{(B-1)}$$

where c is the largest neutral axis depth calculated for the factored axial force and nominal moment strength consistent with the design displacement δ_u, calculated by summing the roof deflections caused by lateral forces acting at each level.

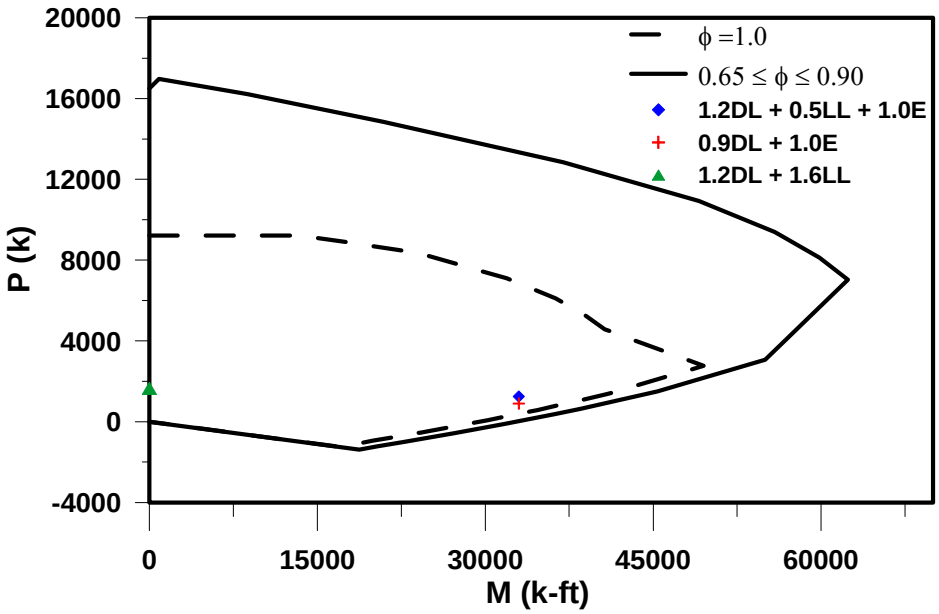

Figure B-1 Axial load-moment (*P-M*) interaction diagram for Archetype 12.

An example shear wall section with boundary element reinforcing is shown in Figure B-2. The figure shows the dimensions and resulting reinforcing for Archetype 12. Shear wall design parameters for all archetypes are summarized in Table B-5 through Table B-14 by Archetype ID, ductility classification (special versus ordinary), and Seismic Design Category (D_{max}, D_{min}, C_{max}, and C_{min}). In the tables, typical web reinforcing size and spacing are shown. Number and size of longitudinal boundary element reinforcing are shown when boundary elements are required.

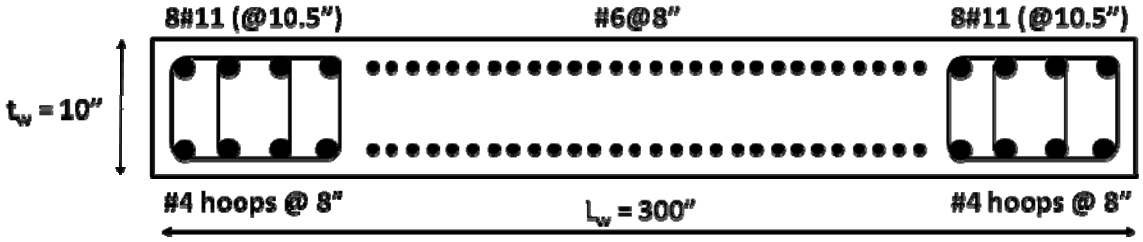

Figure B-2 Example shear wall section with boundary element reinforcing.

Table B-5 1-Story Special Reinforced Concrete Shear Wall Designs

Archetype ID	SDC	Story	Web Reinforcement	Boundary Reinforcement
1	D_{max}	1	#6 @ 8”	-
6	D_{min}	1	#5 @ 14”	-
11	D_{max}	1	#6 @ 8”	-
16	D_{min}	1	#5 @ 14”	-

Table B-6 2-Story Special Reinforced Concrete Shear Wall Designs

Archetype ID	SDC	Story	Web Reinforcement	Boundary Reinforcement
2	D_{max}	1, 2	#6 @ 8”	-
7	D_{min}	1, 2	#4 @ 14”	10#6
12	D_{max}	1, 2	#4 @ 10”	14#11
17	D_{min}	1, 2	#4 @ 14”	-

Table B-7 4-Story Special Reinforced Concrete Shear Wall Designs

Archetype ID	SDC	Story	Web Reinforcement	Boundary Reinforcement
3	D_{max}	1, 2	#5 @ 10”	12#9
		3, 4	#5 @ 18”	-
8	D_{min}	1, 2	#5 @ 18”	8#5
		3, 4	#5 @ 18”	-
13	D_{max}	1, 2	#5 @ 10”	14#11
		3, 4	#5 @ 18”	-
18	D_{min}	1, 2	#5 @ 18”	-
		3, 4	#5 @ 18”	-

Table B-8 8-Story Special Reinforced Concrete Shear Wall Designs

Archetype ID	SDC	Story	Web Reinforcement	Boundary Reinforcement
4	D_{max}	1, 2	#4 @ 10"	16#4
		3, 4	#4 @ 10"	16#4
		5, 6	#4 @ 10"	-
		7, 8	#4 @ 10"	-
9	D_{min}	1, 2	#4 @ 10"	-
		3, 4	#4 @ 10"	-
		5, 6	#4 @ 10"	-
		7, 8	#4 @ 10"	-
14	D_{max}	1, 2	#4 @ 10"	14#11
		3, 4	#4 @ 10"	8#11
		5, 6	#4 @ 10"	-
		7, 8	#4 @ 10"	-
19	D_{min}	1, 2	#4 @ 10"	-
		3, 4	#4 @ 10"	-
		5, 6	#4 @ 10"	-
		7, 8	#4 @ 10"	-

Table B-9 12-Story Special Reinforced Concrete Shear Wall Designs

Archetype ID	SDC	Story	Web Reinforcement	Boundary Reinforcement
5	D_{max}	1, 2	#4 @ 10"	20#4
		3, 4	#4 @ 10"	16#4
		5, 6	#4 @ 10"	-
		7, 8	#4 @ 10"	-
		9, 10	#4 @ 10"	-
		11, 12	#4 @ 10"	-
10	D_{min}	1, 2	#4 @ 10"	-
		3, 4	#4 @ 10"	-
		5, 6	#4 @ 10"	-
		7, 8	#4 @ 10"	-
		9, 10	#4 @ 10"	-
		11, 12	#4 @ 10"	-
15	D_{max}	1, 2	#4 @ 10"	12#11
		3, 4	#4 @ 10"	8#11
		5, 6	#4 @ 10"	-
		7, 8	#4 @ 10"	-
		9, 10	#4 @ 10"	-
		11, 12	#4 @ 10"	-
20	D_{min}	1, 2	#4 @ 10"	-
		3, 4	#4 @ 10"	-
		5, 6	#4 @ 10"	-
		7, 8	#4 @ 10"	-
		9, 10	#4 @ 10"	-
		11, 12	#4 @ 10"	-

Table B-10 1-Story Ordinary Reinforced Concrete Shear Wall Designs

Archetype ID	SDC	Story	Web Reinforcement	Boundary Reinforcement
21	D_{max}	1	#6 @ 8"	-
26	D_{min}	1	#6 @ 14"	-
31	D_{max}	1	#6 @ 8"	-
36	D_{min}	1	#6 @ 14"	-

Table B-11 2-Story Ordinary Reinforced Concrete Shear Wall Designs

Archetype ID	SDC	Story	Web Reinforcement	Boundary Reinforcement
22	D_{max}	1, 2	#6 @ 8"	-
27	D_{min}	1, 2	#6 @ 16"	-
32	D_{max}	1, 2	#6 @ 8"	-
37	D_{min}	1, 2	#6 @ 16"	-

Table B-12 4-Story Ordinary Reinforced Concrete Shear Wall Designs

Archetype ID	SDC	Story	Web Reinforcement	Boundary Reinforcement
23	D_{max}	1, 2	#4 @ 12"	-
		3, 4	#4 @ 12"	-
28	D_{min}	1, 2	#4 @ 12"	-
		3, 4	#4 @ 12"	-
33	D_{max}	1, 2	#4 @ 12"	-
		3, 4	#4 @ 12"	-
38	D_{min}	1, 2	#4 @ 12"	-
		3, 4	#4 @ 12"	-

Table B-13 8-Story Ordinary Reinforced Concrete Shear Wall Designs

Archetype ID	SDC	Story	Web Reinforcement	Boundary Reinforcement
24	D_{max}	1, 2	#4 @ 10"	-
		3, 4	#4 @ 10"	-
		5, 6	#4 @ 10"	-
		7, 8	#4 @ 10"	-
29	D_{min}	1, 2	#4 @ 10"	-
		3, 4	#4 @ 10"	-
		5, 6	#4 @ 10"	-
		7, 8	#4 @ 10"	-
34	D_{max}	1, 2	#4 @ 10"	-
		3, 4	#4 @ 10"	-
		5, 6	#4 @ 10"	-
		7, 8	#4 @ 10"	-
39	D_{min}	1, 2	#4 @ 10"	-
		3, 4	#4 @ 10"	-
		5, 6	#4 @ 10"	-
		7, 8	#4 @ 10"	-

Table B-14 12-Story Ordinary Reinforced Concrete Shear Wall Designs

Archetype ID	SDC	Story	Web Reinforcement	Boundary Reinforcement
25	D_{max}	1, 2	#4 @ 10"	-
		3, 4	#4 @ 10"	-
		5, 6	#4 @ 10"	-
		7, 8	#4 @ 10"	-
		9, 10	#4 @ 10"	-
		11o 12	#4 @ 10"	-
30	D_{min}	1, 2	#4 @ 10"	-
		3,4	#4 @ 10"	-
		5, 6	#4 @ 10"	-
		7, 8	#4 @ 10"	-
		9, 10	#4 @ 10"	-
		11, 12	#4 @ 10"	-
35	D_{max}	1, 2	#4 @ 10"	-
		3, 4	#4 @ 10"	-
		5, 6	#4 @ 10"	-
		7, 8	#4 @ 10"	-
		9, 10	#4 @ 10"	-
		11, 12	#4 @ 10"	-
40	D_{min}	1, 2	#4 @ 10"	-
		3, 4	#4 @ 10"	-
		5, 6	#4 @ 10"	-
		7, 8	#4 @ 10"	-
		9, 10	#4 @ 10"	-
		11, 12	#4 @ 10"	-

B.5 Model Sensitivity Studies

Model sensitivity studies were conducted on each archetype to determine the most reliable model configurations (i.e., the number of elements and integration points) to minimize the impact of modeling parameters on the results. Pushover analyses using different element configurations and number of integration points were conducted, and the resulting curvatures and roof displacements were compared with estimates obtained using commonly employed "rules" to ensure that predicted results did not substantially deviate from expected results (within 15%) unless the variation could be justified. Using one such rule, the displacement at the top of a wall can be written as:

$$\delta_u = \frac{11}{40}\varphi_y h_w^{\,2} + (\varphi_u - \varphi_y) l_p (h_w - \frac{l_p}{2}) \qquad \text{(B-2)}$$

where δ_u is the ultimate displacement, ϕ_y and ϕ_u are the yield and ultimate curvatures, h_w is the wall height, and l_p is the plastic hinge length. Estimated plastic hinge lengths and number of elements per story are summarized in Table B-15.

Table B-15 Estimated Plastic Hinge Lengths and Number of Elements Per Story

Number of stories	Plastic hinge length (inches)	Number of Elements per Story	Element length (inches)
1	$L_w/6 = 52$	2	78
2	$L_w/4 = 75$	2	78[1] and 72[2]
4	$L_w/2 = 144$	1	156[1] and 144[2]
8	$L_w/2 = 192$	1	156[1] and 144[2]
12	$L_w/2 = 246$	1	156[1] and 144[2]

[1] Element length in the first story

[2] Element length in other stories

The most reliable results are obtained when element lengths (heights) are close to the expected length of the plastic hinge. Based on this approach, two elements per story were investigated for the 1- and 2-story walls, and one element per story was investigated for the 4-, 8-, and 12-story walls. Curvature values obtained from the analyses were compared with estimates based on an assumed plastic hinge length and Equation B-2. Results for the one-story archetypes are provided in Table B-16.

Results show that increasing the number of integration points from 3 to 5 leads to an increase in curvature at high drift ratios. Although the use of more elements led to better curvature approximations at lower drift values, deviations from estimated curvature values were observed at higher drift ratios, where failures occur, which was considered more important for this study. Based on these results, two elements and three integration points were used for the one-story archetypes.

Table B-16 Results of Sensitivity Studies for 1-story Archetype

Drift (%)	Estimated Curvature	Analysis (3 points)	Analysis (5 points)	Element Assembly
2 equal-length elements per story				
0.32	7.41E-05	2.91E-05	2.91E-05	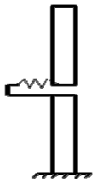
0.64	1.48E-04	8.48E-05	8.44E-05	
0.80	1.85E-04	1.17E-04	1.17E-04	
0.96	2.22E-04	1.52E-04	1.56E-04	
1.28	2.96E-04	2.49E-04	2.82E-04	
3 equal-length elements per story				
0.32	7.41E-05	3.80E-05	3.78E-05	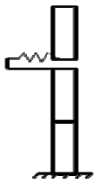
0.64	1.48E-04	1.11E-04	1.11E-04	
0.80	1.85E-04	1.57E-04	1.59E-04	
0.96	2.22E-04	2.26E-04	2.46E-04	
1.28	2.96E-04	3.83E-04	4.40E-04	
4 equal-length elements per story				
0.32	7.41E-05	4.36E-05	4.36E-05	
0.64	1.48E-04	1.37E-04	1.38E-04	
0.80	1.85E-04	2.10E-04	2.28E-04	
0.96	2.22E-04	3.26E-04	3.72E-04	
1.28	2.96E-04	5.25E-04	6.21E-04	

Similar results were observed for the 2-story archetypes, where the use of two elements per story was necessary for capturing nonlinear behavior. One element per story was used for the 4-, 8-, and 12-story archetypes, because estimated plastic hinge lengths were large enough to justify this modeling assumption. Use of a Multiple-Vertical-Line-Element (MVLE) model, which averages strain values over a specified element length, would have been a preferred modeling approach; however, the MVLE model implemented in OpenSees does not work for dynamic loading.

B.6 Axial Failure Model

An axial failure model was applied to all archetypes to estimate the drift ratio at axial failure. According to the model, axial load capacity of a shear critical column can be investigated using a shear friction model, where the axial load supported by a column must be transferred across the diagonal crack plane through shear friction (Figure B-3).

Axial load failure is assumed to result from sliding along the critical crack plane when the shear friction demand exceeds the shear friction capacity. Equilibrium of forces in horizontal and vertical directions in leads to the following equations:

$$P = N\cos\theta + V_{sf}\sin\theta + \frac{d_c}{s_h}P_{s,web} \qquad \text{(B-3)}$$

$$N \sin\theta = V_{sf} \cos\theta + A_{st} f_{st} \frac{h}{s_v} - V_r \qquad \text{(B-4)}$$

where, θ is the critical crack angle relative to the horizontal, s_h is the horizontal spacing of the vertical web bars, s_v is the vertical spacing of the horizontal web bars, d_c is the depth of the core measured center line to center line of the ties, $P_{s,web}$ is the axial load supported by a single vertical web bar, h is the height of the wall, and V_r is the residual shear force.

The shear friction force transferred across the crack, V_{sf}, is dependent upon the normal force, N, and an effective coefficient of friction, μ as:

$$V_{sf} = \mu N \qquad \text{(B-5)}$$

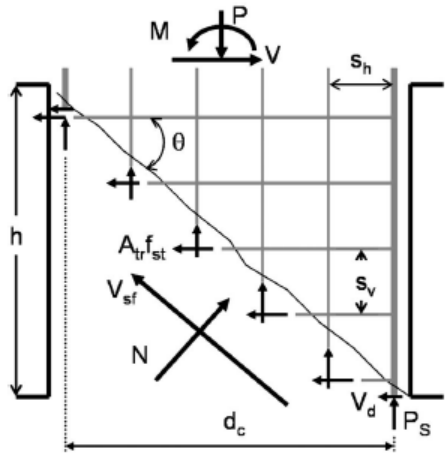

Figure B-3 Cracked pier free-body diagram (Wallace et al., 2008)

The critical crack angle, θ, is defined relative to the horizontal, based on the wall geometry as indicated in Figure B-4.

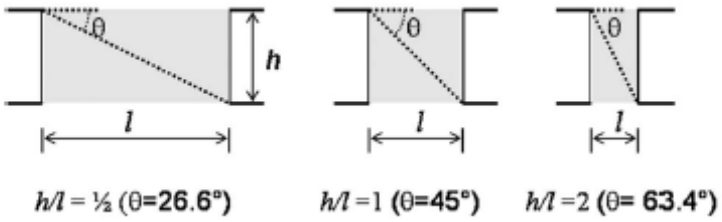

Figure B-4 Wall pier geometry and critical crack angles (Wallace et al., 2008).

Substitution of Equation B-5 into Equations B-3 and B-4 yields Equation B-6, which states that the total axial load, P_t, is the summation of the axial load carried by shear friction and the axial load carried by the web reinforcement.

$$P_t = \left(\frac{A_s f_{yt} h}{s_v} - V_r\right)\left(\frac{1+\mu\tan\theta}{\tan\theta-\mu}\right) + n_{bars,web} P_{s,web} \quad \text{(B-6)}$$

It is likely that when the axial capacity due to shear friction is reached, the axial load is transferred to the longitudinal reinforcement as sliding begins to occur on the shear failure plane. Elwood and Moehle (2005) referred to this as the maximum capacity model as in Equation B-7, which was used to produce a lower estimate of the axial load capacity.

$$P_m = \max\left[\left(\frac{A_s f_{yt} h}{s_v} - V_r\right)\left(\frac{1+\mu\tan\theta}{\tan\theta-\mu}\right), n_{bars,web} P_{s,web}\right] \quad \text{(B-7)}$$

Elwood and Moehle (2005) developed the following relationship between the coefficient of friction and drift at axial failure based on column tests:

$$\mu = C_1 - C_2\left(\frac{\Delta}{h}\right)_{axial} \geq 0 \quad \text{(B-8)}$$

where shear friction at zero drift, C_1, was taken as 2.14, and C_2 was taken as 25 to achieve a close approximation to the data. Because of a lack of available test data, values of $C_1 = 2.14$ and $C_2 = 25$ were used for the walls in this study. Substitution of Equation B-8 into Equation B-7 results in the following general expression:

$$\frac{\Delta}{L} = \frac{(1+C_1\tan\theta) + (P/C_3)(C_1 - \tan\theta)}{C_2(P/C_3 + \tan\theta)} \quad \text{(B-9)}$$

where,

$$C_3 = (A_{st} f_{yt} h / s_v - V_r) \quad \text{(B-10)}$$

A graph of pier lateral drift ratio (Δ/L) versus pier properties, $(A_{st}f_{yt}h/s_v)/P_0$, was plotted for different critical crack angle values and axial load levels (Figure B-5), and the corresponding drift ratios for each archetype were obtained. Because drift values obtained from the plot were higher than deemed reasonable, lower drift values at axial failure were selected based on judgment for each archetype. Drift ratios obtained from the axial failure model and those selected by judgment are summarized in Table B-17 and Table B-18. Axial failure was assumed to occur if the lateral drift ratio reached 3% in the 1- and 2-story archetypes and 5% in the 4-, 8-, and 12-story archetypes.

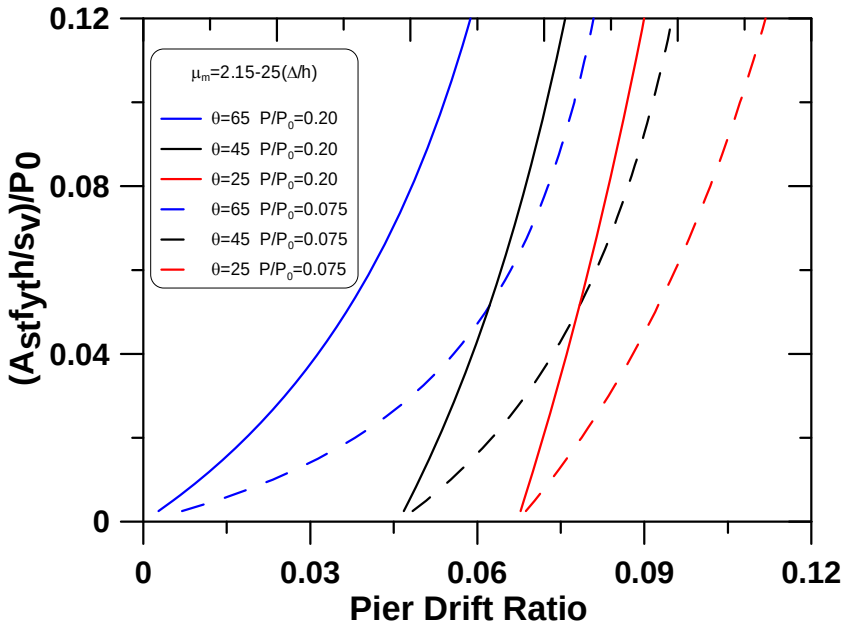

Figure B-5 Drift ratio at axial failure for different critical crack angles and axial load levels.

Table B-17 Modeled and Assumed Drift at Axial Failure for Special Reinforced Concrete Shear Wall Archetypes

Archetype ID	No. of Stories	SDC	Axial Load ($A_g f'_c$)	Drift at Axial Failure – Model (%)	Drift at Axial Failure – Judgment (%)
1	1	D_{max}	0.075	9.6	3
2	2	D_{max}	0.075	9.5	3
3	4	D_{max}	0.2	5.9	5
4	8	D_{max}	0.2	5.4	5
5	12	D_{max}	0.2	5.4	5
6	1	D_{min}	0.075	7.9	3
7	2	D_{min}	0.075	6.9	3
8	4	D_{min}	0.2	4.5	5
9	8	D_{min}	0.2	5.4	5
10	12	D_{min}	0.2	5.4	5
11	1	D_{max}	0.075	9.6	3
12	2	D_{max}	0.075	9.5	3
13	4	D_{max}	0.075	8.1	5
14	8	D_{max}	0.075	7.7	5
15	12	D_{max}	0.075	7.7	5
16	1	D_{min}	0.075	7.9	3
17	2	D_{min}	0.075	6.9	3
18	4	D_{min}	0.075	7	5
19	8	D_{min}	0.075	7.7	5
20	12	D_{min}	0.075	7.7	5

Table B-18 Modeled and Assumed Drift at Axial Failure for Ordinary Reinforced Concrete Shear Wall Archetypes

Archetype ID	No. of Stories	SDC	Axial Load ($A_g f'_c$)	Drift at Axial Failure – Model (%)	Drift at Axial Failure – Judgment (%)
21	1	C_{max}	0.075	9.6	3
22	2	C_{max}	0.075	9.5	3
23	4	C_{max}	0.2	4.1	5
24	8	C_{max}	0.2	5.4	5
25	12	C_{max}	0.2	5.4	5
26	1	C_{min}	0.075	8.8	3
27	2	C_{min}	0.075	8.1	3
28	4	C_{min}	0.2	4.1	5
29	8	C_{min}	0.2	5.4	5
30	12	C_{min}	0.2	5.4	5
31	1	C_{max}	0.075	9.6	3
32	2	C_{max}	0.075	9.5	3
33	4	C_{max}	0.075	6.6	5
34	8	C_{max}	0.075	7.7	5
35	12	C_{max}	0.075	7.7	5
36	1	C_{min}	0.075	8.8	3
37	2	C_{min}	0.075	8.1	3
38	4	C_{min}	0.075	6.6	5
39	8	C_{min}	0.075	7.7	5
40	12	C_{min}	0.075	7.7	5

Given the uncertainty associated with axial failure, two sets of analyses were conducted on selected archetypes, and two separate adjusted collapse margin ratio (*ACMR*) values were obtained. One set of results was generated including all failure modes (e.g., steel fracture, concrete crushing, shear failure) along with axial failure, and the other set was generated excluding axial failure.

Adjusted collapse margin ratio values obtained based on the axial failure criteria are compared to the *ACMR* values obtained considering other failure modes in Table B-19. The axial failure criteria generally yielded higher *ACMR* values for the 1- and 2-story archetypes, because the drift at axial failure (3%) is higher than the drift at shear failure (1.5%), which was the governing failure mode for low-rise archetypes. The axial failure criteria resulted in lower *ACMR* values for the 4- and 12-story archetypes studied.

Table B-19 Comparison of ACMR Values Considering All Failure Modes and Axial Failure Modes

Archetype ID	SDC	Axial load level	*ACMR* – all modes	*ACMR* - axial failure
1-story Archetypes				
1, 11	D_{max}	low/high	1.05	1.28
6, 16	D_{min}	low/high	1.60	1.03
21, 31	C_{max}	low/high	1.90	2.19
26, 36	C_{min}	low/high	2.51	3.03
2-story Archetypes				
2, 12	D_{max}	low/high	1.50	2.03
7, 17	D_{min}	low/high	1.40	1.84
22, 32	C_{max}	low/high	1.63	1.88
27, 37	C_{min}	low/high	2.05	2.55
4- story Archetypes				
13	D_{max}	low	2.7	2.35
12-story Archetypes				
15	D_{max}	low		2.92

B.7 Shear Model Sensitivity Studies

Tests on lightly reinforced wall piers by Massone (2006) indicate that diagonal cracking occurs at roughly $2.5\sqrt{f_c'}$ to $3.0\sqrt{f_c'}$ and that the uncracked shear modulus is reasonably approximated by $G_c = E_c/2(1+\nu) = 0.4E_c$. Tests on cantilever walls with rectangular cross sections by Thomsen and Wallace (1995, 2004), however, indicate that the peak shear stress is limited by flexural yielding to $2.3\sqrt{f_c'}$, which is well below the pure shear diagonal cracking shear stress value observed by Massone (2006). Results indicate that nonlinear shear deformations occur due to coupling between axial-bending and shear behavior, and available cyclic material models in OpenSees do not include this coupled behavior.

A sensitivity study using tests on cantilever walls with rectangular cross sections performed by Thomsen and Wallace (1995, 2004), was conducted to determine the most appropriate shear backbone behavior. In this study, the cracking force (stress) level was varied between 8 and 20 kips, and the post-crack slope was set at $0.1E_c$, $0.05E_c$, and $0.01E_c$. Results obtained from this study are shown in Figures B-6 to B-8 for a cracking load of 12 kips. Results for post-crack stiffness of $0.1E_c$ and $0.05E_c$ were too stiff, whereas the results for a post-crack slope $0.01E_c$ closely matched the test results. These results indicate that reducing the shear modulus as shown in Figure B-9 is necessary to account for nonlinear shear deformations.

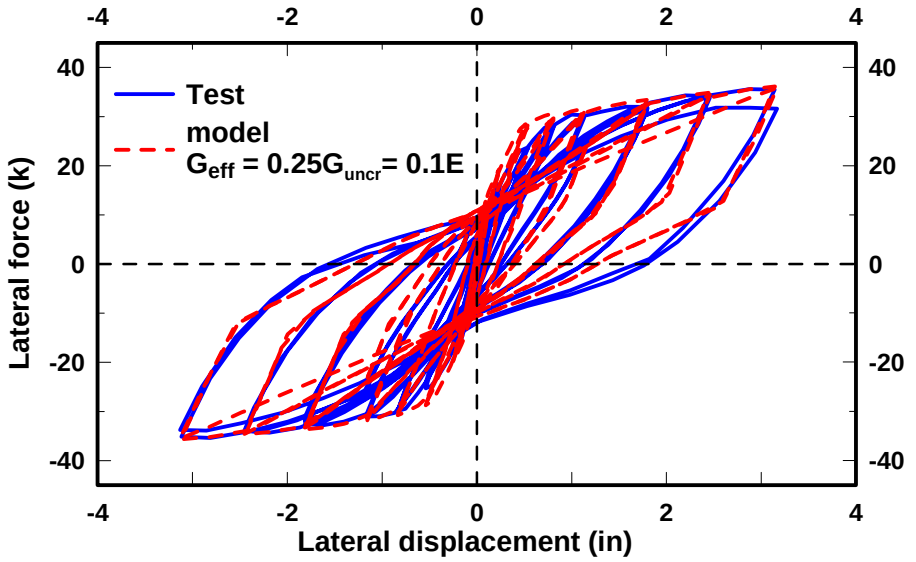

Figure B-6 Model results with an effective shear modulus of 0.1E.

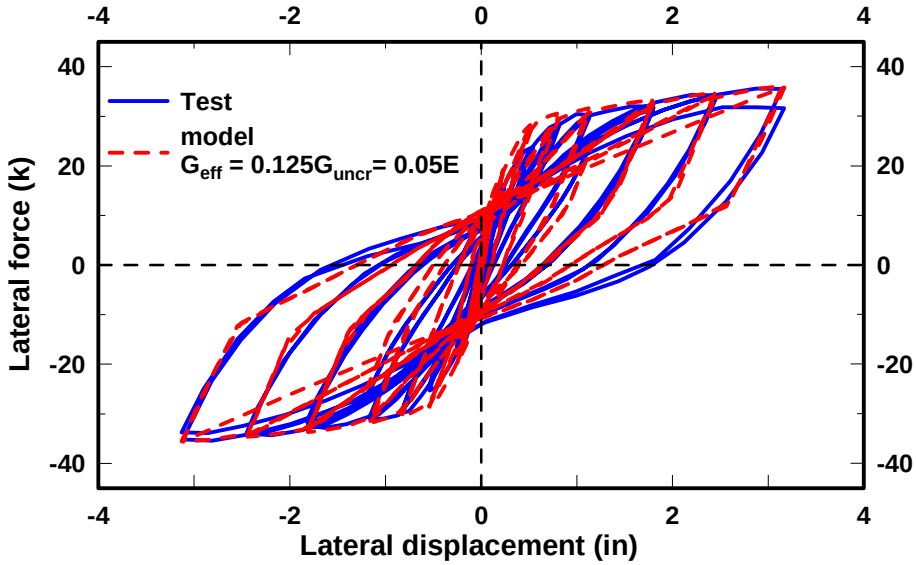

Figure B-7 Model results with an effective shear modulus of 0.05E.

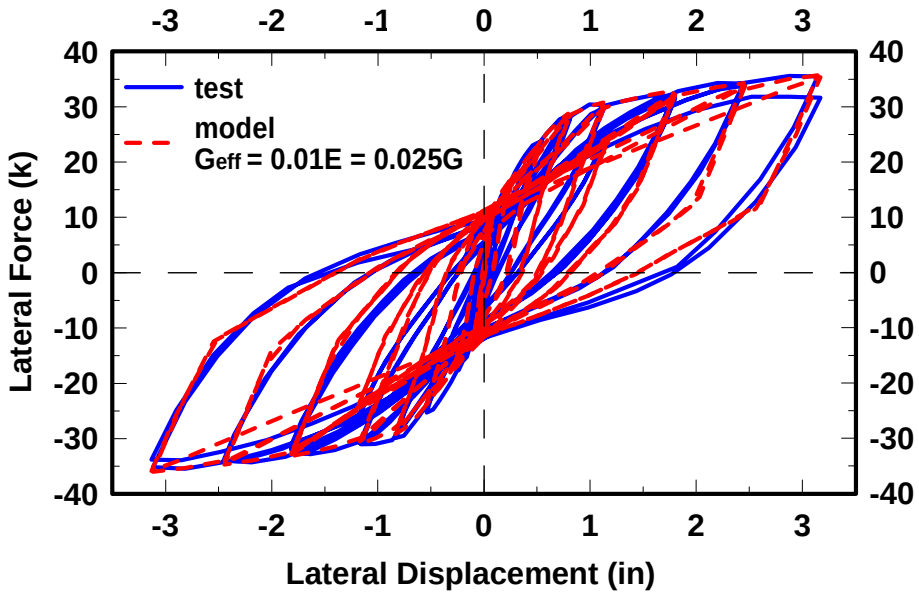

Figure B-8 Model results with an effective shear modulus of 0.01E.

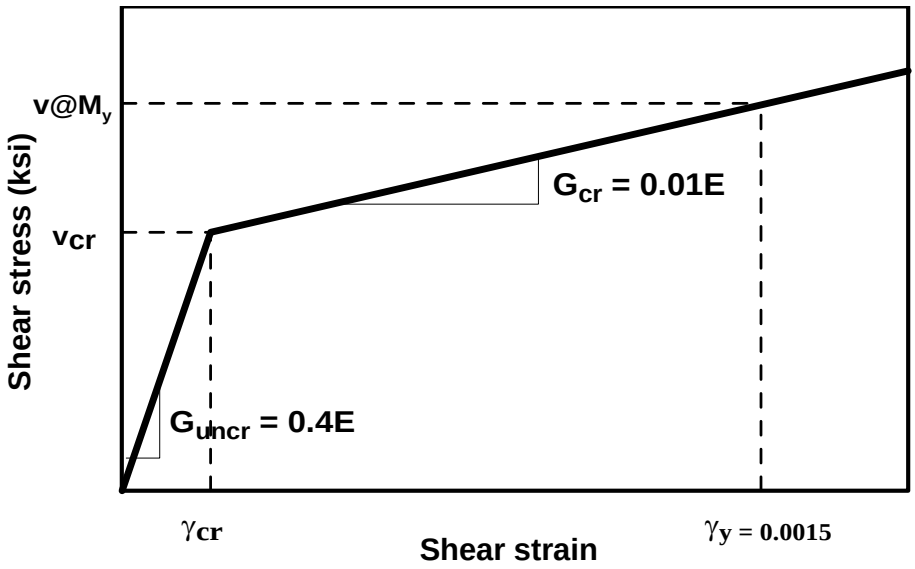

Figure B-9 Shear model with reduced shear modulus for calibration with specimen RW2.

Appendix C

Design Details of Steel Braced Frame Archetypes

This appendix presents detailed design information for steel braced frame archetypes considered in Chapter 5. Seismic criteria, design loads, load combinations, and related requirements that were used as a basis for design of special steel concentrically braced frame (SCBF) and buckling-restrained braced frame (BRBF) archetypes are described, and the resulting beam, column, and brace member sizes in each story for each archetype are summarized.

C.1 Introduction

Index archetypes for special SCBF and BRBF systems were designed in accordance with design requirements contained within AISC 341-05, *Seismic Provisions for Structural Steel Buildings* (AISC, 2005a), and ASCE/SEI 7-05 *Minimum Design Loads for Buildings and Other Structures* (ASCE, 2006). Test data were used to support the designs, as necessary. Beams, columns, and brace components were designed in strict compliance with code requirements to avoid undue overstrength in the system.

C.2 Material Properties and Gravity Loads

Material properties and gravity loads were based on modified values taken from Steel TIPS reports, *Design of Special Concentric Braced Frames* (Cochran and Honeck, 2004) and *Seismic Design of Buckling-Restrained Braced Frames* (López and Sabelli, 2004) as well as building designs prepared for the SAC Project (Gupta and Krawinkler, 1999).

Material properties for structural steel sections are summarized in Table C-1. Gravity load assumptions for floor and roof dead load and live load are summarized in Table C-2. In addition, gravity loads were determined including an average exterior curtain wall weight of 15 psf, which includes an allowance for column and spandrel cladding.

C.3 Seismic Design Loading

Seismic Design Category (SDC) is a combination of ground motion intensity and Occupancy Category. Occupancy Category II, with a corresponding importance factor equal to unity was selected for the design of special SCBF and BRBF archetypes in this study. Key seismic design parameters are summarized in Table C-3.

Table C-1 Structural Materials for Special SCBF and BRBF Archetypes

Steel Section	Material Properties
W sections	ASTM A992 F_y=50 ksi; F_u=65 ksi
HSS sections	ASTM A500 Grade B F_y=42 ksi; F_u=58 ksi for square tube sections F_y=46 ksi; F_u=58 ksi for circular pipe sections
BRB Steel Core	ASTM A36 or JIS G3136 SN 400B with supplemental yield requirements: F_{ysc}=42 ksi
Gusset plates	ASTM A572, Grade 50 F_y=50 ksi; F_u=65 ksi
Weld electrodes	E70XX notch toughness: 20 ft-lb at –20 degrees Fahrenheit

Table C-2 Gravity Loads for Special SCBF and BRBF Archetypes

Component	Gravity Load (psf)
Roof Loading	
Roofing and insulation	7
Metal deck and concrete fill	47
Steel framing and fireproofing	8
Ceiling	3
Mechanical/Electrical	2
Total Roof Loading:	67
Floor Loading	
Metal deck and concrete fill	47
Steel framing and fireproofing	13
Partition walls	20
Ceiling	3
Mechanical/Electrical	2
Total Floor Loading:	85
Live Loads	
Roof	20
Floor	50

Table C-3 Seismic Design Parameters for Special SCBF and BRBF Archetypes

Parameter	Value
Occupancy Category	II (office)
Importance Factor	1.0
Design Spectral Acceleration at short periods, S_{DS}	D_{max} 1.0g D_{min} 0.5g
Design Spectral Acceleration at 1-second period, S_{D1}	D_{max} 0.6g D_{min} 0.2g
F_a	1.0
F_v	1.5
R	SCBF 6 BRBF 8
C_d	SCBF 6 BRBF 8
$_0$	SCBF 2.0 BRBF 2.5

Seismic design forces and displacements were calculated using Equivalent Lateral Force (ELF) or the Response Spectrum Analysis (RSA) procedures. The analysis procedure was determined for each archetype per Section 12.6 in ASCE/SEI 7-05. The ELF procedure was used in most cases, except for the 12- and 16-story archetypes, in which the RSA procedure was used.

In ASCE/SEI 7-05 (as amended), calculation of the seismic response coefficient in the ELF procedure is constrained by a lower bound equal to $0.044S_{DS}$, which controlled in many of the long-period archetypes, especially the taller BRBFs.

C.4 Story Drift and P-Delta Effects

The value for displacement and drift quantities were multiplied by C_d, which was equal to R for the SCBF and BRBF archetype designs. In the RSA procedure, the modal responses are combined using SRSS method. In accordance with ASCE/SEI 7-05, drift calculations are based on the modal base shear, V_t, for each archetype, which can be less than 85 percent of the base shear, V, calculated using the ELF procedure. For archetype designs that were controlled by drift, the demand was dramatically reduced when the RSA procedure was used in lieu of the ELF procedure.

The design story drift calculated by the ELF or RSA procedure is limited by the maximum allowable story drift in ASCE/SEI 7-05. The story drift was limited to 2.5% for 2- and 3-story archetypes and to 2.0% for 6-, 12-, and 16-story archetypes.

P-Delta effects, as evaluated per ASCE/SEI 7-05, were not expected to control the design of braced frame archetypes for high seismic demands. In the case of special SCBF and BRBF archetypes designed for SDC D_{max} and SDC D_{min}, low-rise archetypes were controlled by strength, high-rise archetypes were controlled by drift, and no archetypes were controlled by P-delta effects.

C.5 Load Combinations

Archetypes were designed in accordance with the load combinations of Section 12.4 of ASCE/SEI 7-05 and guidance provided in FEMA P-695. Archetype designs ignored snow load, *S*, foundation loads, *H*, and wind loads, *W*. Where consideration of overstrength is required to determine the seismic load effect for the design of some structural components (e.g., columns) the overstrength factor Ω_0 specified in ASCE/SEI 7-05 was considered.

C.6 Structural Configurations

Plan configurations for special SCBF and BRBF archetypes are shown in Figures C-1 through C-3. A rectangular configuration with braced bays located around the perimeter was chosen to minimize the potential for torsional effects. Structural layouts of 3- and 6-story archetypes are similar to braced frames designed by others (DASSE, 2009).

The typical floor plan is 180 feet by 120 feet. To avoid biasing of performance evaluation results with excessive overstrength, the size and number of braced bays were adjusted in each archetype to suit the level of seismic design loading. For 2-, 3- and 6-story archetypes, one braced bay was used on each side of the building. For 12- and 16-story archetypes, two braced bays were used on each side of the building. Column bay spacing was 30 feet in the typical case and 20 feet for the 2-story archetypes.

Story heights were 15 feet in the typical case and 10 feet for the 2-story archetypes. Bracing was arranged in a two-story X-configuration.

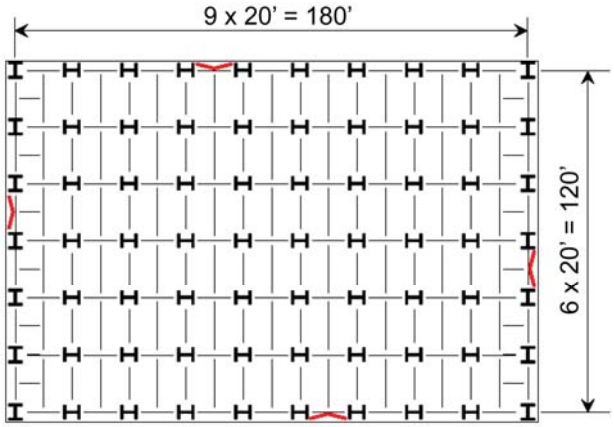

Figure C-1 Plan configuration of 2-story braced frame archetypes.

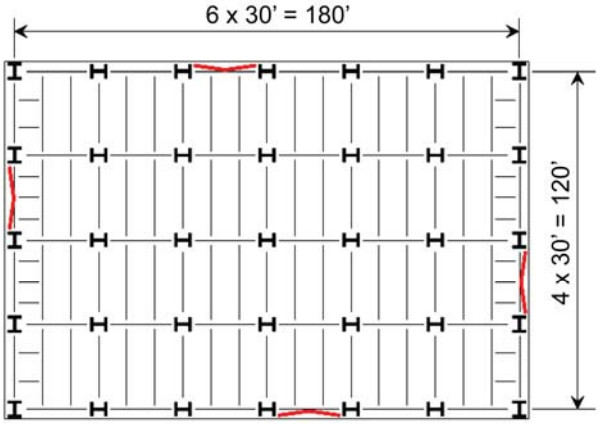

Figure C-2 Plan configuration of 3-story and 6-story braced frame archetypes.

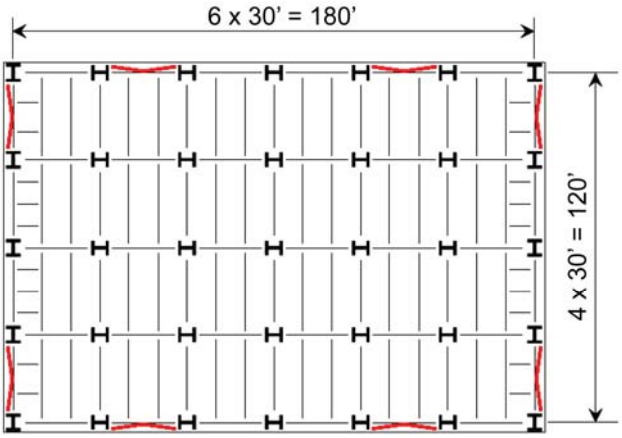

Figure C-3 Plan configuration of 12-story and 16-story braced frame archetypes.

C.7 Member Sizes

Braces were assumed to have pinned end connections, and fully restrained connections were assumed for the beam-column connection. The braces were designed to resist more than 70% of the lateral forces. Round hollow structural sections (HSS) were used in most cases for special SCBF archetypes, except at locations where wide-flange sections were needed because the demand was too large. Buckling-restrained braces were sized based on the area of the steel core.

Beams were assumed to be laterally supported at quarter points along the span and were designed to carry the axial force from braces. For beams where the braces intersected at midspan, unbalanced forces due to differences in capacity of braces above and below the beams were considered. The beams were also designed to carry tributary gravity loads distributed along the span.

Columns were assumed to be fixed at the base and orientated to resist lateral forces in strong-axis bending. Wide-flange (W14 and W12) sections were designed using appropriate load combinations, including the overstrength factor, Ω_o. Column sizes

were changed a maximum of every two stories, and the splices were assumed to be above the floor level and outside any potential plastic hinge regions.

Column, brace, and beam member sizes for special SCBF and BRBF archetypes are summarized in Tables C-4 through C-9.

Table C-4 Member Sizes for 2-Story Braced Frame Archetypes

Story	Columns		Braces		Beams	
	SDC D_{max}	SDC D_{min}	SDC D_{max}	SDC D_{min}	SDC D_{max}	SDC D_{min}
Special SCBF Archetypes						
2	W10x45	W10x30	HSS6x6x3/8	HSS6x0.25	W24x117	W18x35
1	W10x45	W10x30	HSS6x6x3/8	HSS6x0.25	W24x117	w18x50
BRBF Archetypes						
2	W10x39	W10x26	5 in^2	2.5 in^2	W18x35	W18x35
1	W10x39	W10x26	5 in^2	2.5 in^2	w18x50	W18x35

Table C-5 Member Sizes for 3-Story Braced Frame Archetypes

Story	Columns		Braces		Beams	
	SDC D_{max}	SDC D_{min}	SDC D_{max}	SDC D_{min}	SDC D_{max}	SDC D_{min}
Special SCBF Archetypes						
3	W12x120	W12x72	HSS8-3/4x0.312	HSS6-1/8x0.25	W30x173	W21x132
2	W12x120	W12x72	HSS8-3/4x0.5	HSS6-7/8x0.312	W21x111	W18x76
1	W12x120	W12x72	HSS9-5/8x0.5	HSS7-1/2x0.312	W18x65	W18x46
BRBF Archetypes						
3	W12x120	W14x82	3 in^2	1 in^2	W21x62	W21x62
2	W12x120	W14x82	5.5 in^2	2 in^2	W18x76	W21x55
1	W12x120	W14x82	6 in^2	2 in^2	W21x62	W21x62

Table C-6 Member Sizes for 6-Story Braced Frame Archetypes

Story	Columns		Braces		Beams	
	SDC D_{max}	SDC D_{min}	SDC D_{max}	SDC D_{min}	SDC D_{max}	SDC D_{min}
Special SCBF Archetypes						
6	W14x68	W12x53	HSS7-1/2x0.312	HSS6x0.25	W18x97	W18x76
5	W14x68	W12x53	HSS9x5/8x0.375	HSS6-5/8x0.25	W24x104	W18x76
4	W14x176	W12x106	HSS9x5/8x0.5	HSS7x0.312	W24x131	W18x76
3	W14x176	W12x106	HSS11-1/4x0.5	HSS7x0.375	W18x76	W21x68
2	W14x342	W14x159	HSS12-1/2x0.5	HSS8-3/4x0.312	W24x146	W18x86
1	W14x342	W14x159	HSS12-1/2x0.5	HSS8-3/4x0.312	W21x62	W21x62
BRBF Archetypes						
6	W14x90	W14x53	2.5 in^2	1 in^2	W18x76	W21x55
5	W14x90	W14x53	5 in^2	1.5 in^2	W21x62	W21x62
4	W14x193	W14x90	5.5 in^2	1.5 in^2	W18x76	W21x55
3	W14x193	W14x90	7 in^2	2 in^2	W21x62	W21x62
2	W14x342	W14x176	8 in^2	2 in^2	W18x76	W21x55
1	W14x342	W14x176	8 in^2	2 in^2	W21x62	W21x62

Table C-7 Member Sizes for 12-Story Braced Frame Archetypes

Story	Columns		Braces		Beams	
	SDC D_{max}	SDC D_{min}	SDC D_{max}	SDC D_{min}	SDC D_{max}	SDC D_{min}
Special SCBF Archetypes						
12	W12x45	W12x40	HSS6-5/8x0.312	HSS5x0.25	W18x55	W18x40
11	W12x45	W12x40	HSS6-5/8x0.312	HSS5x0.25	W18x35	W18x35
10	W14x99	W14x53	HSS8-3/4x0.312	HSS6-5/8x0.25	W18x60	W18x46
9	W14x99	W14x53	HSS8-3/4x0.312	HSS6-5/8x0.25	W18x35	W18x35
8	W14x193	W14x74	HSS10x0.375	HSS6-7/8x0.312	W18x65	W18x46
7	W14x193	W14x74	HSS10x0.375	HSS6-7/8x0.312	W18x35	W18x35
6	W14x283	W14x99	HSS10x0.375	HSS7x0.312	W18x65	W18x46
5	W14x283	W14x99	HSS10x0.375	HSS7x0.312	W18x35	W18x35
4	W14x398	W14x132	HSS9-5/8x0.5	HSS7x0.312	W18x71	W18x46
3	W14x398	W14x132	HSS9-5/8x0.5	HSS7x0.312	W18x35	W18x35
2	W14x550	W14x176	HSS9-5/8x0.5	HSS7x0.312	W18x71	W18x46
1	W14x550	W14x176	HSS9-5/8x0.5	HSS7x0.312	W18x35	W18x35
BRBF Archetypes						
12	W12x40	W12x40	3 in^2	1.5 in^2	W18x46	W18x35
11	W12x40	W12x40	3 in^2	1.5 in^2	W18x35	W18x35
10	W14x74	W14x61	3.5 in^2	2 in^2	W18x46	W18x35
9	W14x74	W14x61	3.5 in^2	2 in^2	W18x35	W18x35
8	W14x99	W14x74	4 in^2	2.5 in^2	W18x46	W18x35
7	W14x99	W14x74	4 in^2	2.5 in^2	W18x35	W18x35
6	W14x145	W14x90	4.5 in^2	3 in^2	W18x46	W18x35
5	W14x145	W14x90	4.5 in^2	3 in^2	W18x35	W18x35
4	W14x176	W14x120	5.5 in^2	3.5 in^2	W18x50	W18x35
3	W14x176	W14x120	5.5 in^2	3.5 in^2	W18x35	W18x35
2	W14x257	W14x176	6 in^2	3.5 in^2	W18x50	W18x35
1	W14x257	W14x176	6 in^2	3.5 in^2	W18x35	W18x35

Table C-8 Member Sizes for 16-Story Braced Frame Archetypes

Story	Columns		Braces		Beams	
	SDC D_{max}	SDC D_{min}	SDC D_{max}	SDC D_{min}	SDC D_{max}	SDC D_{min}
Special SCBF Archetypes						
16	W12x45	W12x40	HSS9-5/8x0.375	HSS5x0.312	W18x65	W18x50
15	W12x45	W12x40	HSS9-5/8x0.375	HSS5x0.312	W18x35	W18x35
14	W14x82	W14x53	HSS8-5/8x0.5	HSS6x0.312	W18x71	W18x50
13	W14x82	W14x53	HSS8-5/8x0.5	HSS6x0.312	W18x35	W18x35
12	W14x120	W14x68	HSS11-1/4x0.5	HSS6x0.312	W18x86	W18x50
11	W14x120	W14x68	HSS11-1/4x0.5	HSS6x0.312	W18x35	W18x35
10	W14x176	W14x90	HSS10x0.625	HSS6x0.312	W18x86	W18x50
9	W14x176	W14x90	HSS10x0.625	HSS6x0.312	W18x35	W18x35
8	W14x233	W14x109	HSS11-1/4x0.625	HSS6-5/8x0.312	W18x97	W18x50
7	W14x233	W14x109	HSS11-1/4x0.625	HSS6-5/8x0.312	W18x35	W18x35
6	W14x283	W14x132	HSS11-1/4x0.625	HSS6-5/8x0.312	W18x97	W18x50
5	W14x283	W14x132	HSS11-1/4x0.625	HSS6-5/8x0.312	W18x35	W18x35
4	W14x342	W14x159	HSS11-1/4x0.625	HSS6-5/8x0.5	W21x93	W18x60
3	W14x342	W14x159	HSS11-1/4x0.625	HSS6-5/8x0.5	W18x35	W18x35
2	W14x370	W14x193	W12x96	HSS6-5/8x0.5	W24x146	W18x60
1	W14x370	W14x193	W12x96	HSS6-5/8x0.5	W18x35	W18x35
BRBF Archetypes						
16	W12x40	W12x40	3 in^2	1.5v	W18x46	W18x35
15	W12x40	W12x40	3 in^2	1.5 in^2	W18x35	W18x35
14	W14x82	W14x61	3.5 in^2	2.5 in^2	W18x46	W18x35
13	W14x82	W14x61	3.5 in^2	2.5 in^2	W18x35	W18x35
12	W14x109	W14x82	4.5 in^2	3 in^2	W18x46	W18x35
11	W14x109	W14x82	4.5 in^2	3 in^2	W18x35	W18x35
10	W14x159	W14x99	4.5 in^2	3 in^2	W18x46	W18x35
9	W14x159	W14x99	4.5 in^2	3 in^2	W18x35	W18x35
8	W14x193	W14x120	5.5 in^2	3.5 in^2	W18x50	W18x40
7	W14x193	W14x120	5.5 in^2	3.5 in^2	W18x35	W18x35
6	W14x233	W14x145	6 in^2	3.5 in^2	W18x50	W18x40
5	W14x233	W14x145	6 in^2	3.5 in^2	W18x35	W18x35
4	W14x342	W14x176	6.5 in^2	4 in^2	W18x50	W18x40
3	W14x342	W14x176	6.5 in^2	4 in^2	W18x35	W18x35
2	W14x426	W14x233	7 in^2	4.5 in^2	W18x55	W18x40
1	W14x426	W14x233	7 in^2	4.5 in^2	W18x35	W18x35

Appendix D

Design Details of Special Steel Moment Frame Archetypes

This appendix presents detailed design information for special steel moment frame (SMF) archetypes considered in Chapter 6. Seismic criteria, design loads, and other related requirements that were used as a basis for design of special SMF archetypes are described, and the member sizes for each archetype are summarized. In addition, discussions regarding on P-Delta considerations and the relationship between design and analytical models are presented.

D.1 Introduction

Index archetypes for special SMF systems were designed in accordance with design requirements contained within AISC 341-05, *Seismic Provisions for Structural Steel Buildings* (AISC, 2005a), AISC 358-05, *Prequalified Connections for Special and Intermediate Steel Moment Frames for Seismic Applications* (AISC, 2005b) and ASCE/SEI 7-05, *Minimum Design Loads for Buildings and Other Structures* (ASCE, 2006). Test data were used to support the designs, as necessary.

D.2 Structural Configuration

The plan configuration for special SMF archetypes is shown in Figure D-1. This configuration was selected as representative of single-story and multistory SMF buildings. The height of the first story was assumed to be 15 feet, and height for all other stories was 13 feet. The bay width (centerline dimension between columns) was taken as 20 feet.

D.3 Special Steel Moment Frame Designs

Member sizes were based on the following specific design decisions:

- Members were designed using ASTM A992 steel, and f_y = 50 ksi.
- The dead load was 90 psf uniformly distributed over each floor. A cladding load was applied as a perimeter load of 25 psf. Unreduced life load was 50 psf on all floors and 20 psf on the roof. Wind loads were not considered.
- Whenever applicable, the minimum base shear was determined in accordance with Supplement 2 of ASCE/SEI 7-05.
- Column splices were provided every two stories.
- Column sizes in the lower stories were never smaller than in the upper stories.

- End columns could be different sizes than interior columns.
- All beams at a floor level were the same size.

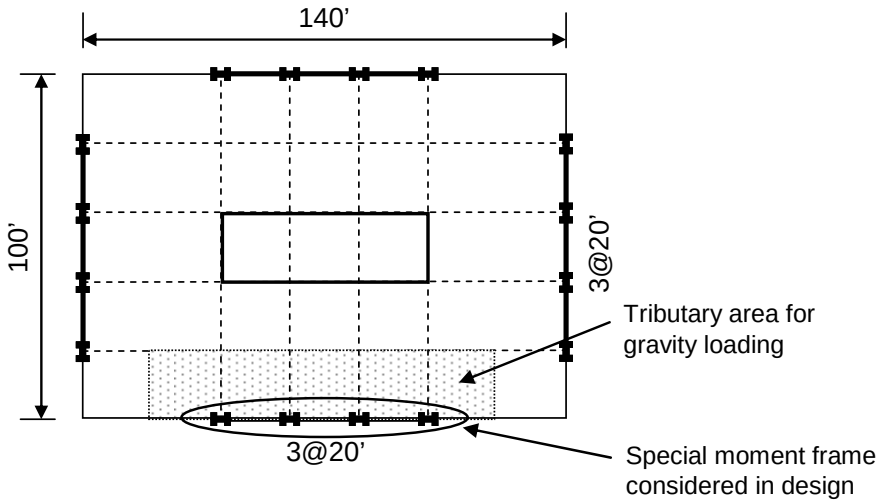

Figure D-1 Typical plan view of buildings used for archetype selection.

- Unbraced column length was taken as the clear story height.
- Preference was given to W24 column sections unless economic or constructability constraints demanded a different nominal depth.
- The seismic non-compactness of several light W14 and W24 sections sometimes resulted in considerable changes in section size.
- The shear design of joint panel zones was based on AISC-360 Equations J10-11 and J10-12. When doubler plates were required, the thickness was rounded up to the nearest 1/16 of an inch.
- All connections were reduced beam section (RBS) connections, as shown in Figure D-2, designed in accordance with AISC 358-05, using $a = 0.625b_f$, $b = 0.75d_b$, and $c = 0.250b_f$.

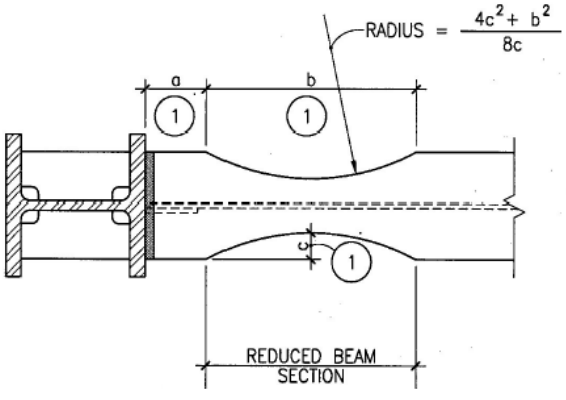

Figure D-2 Definition of terms for reduced beam section design.

Beam and column member sizes for special SMF designs are summarized by performance group in Tables D-1 through D-8.

Table D-1 Member Sizes for Special SMF Performance Group PG-1ELF, SDC D_{max}

Story	Elevation (in.)	Beam Size	Exterior Column Size	Interior Column Size	Doubler Plate Size	
					Exterior Col.	Interior Col.
1-story						
1	170.95	W27X102	W21X111	W21X111	1/4	1-1/8
2-story						
1	164.65	W30X148	W24X131	W24X176	7/16	1-5/16
2	320.65	W16X31	W24X131	W24X176	0	0

Table D-2 Member Sizes for Special SMF Performance Group PG-2ELF, SDC D_{max}

Story	Elevation (in.)	Beam Size	Exterior Column Size	Interior Column Size	Doubler Plate Size	
					Exterior Col.	Interior Col.
4-story						
1	166.55	W24X103	W24X103	W24X131	1/16	5/8
2	322.55	W24X103	W24X103	W24X131	1/16	7/16
3	478.55	W24X76	W24X76	W24X84	1/16	1/2
4	634.55	W24X76	W24X76	W24X84	1/16	1/2
20-story						
1	165.00	W40X183	W36X487	W36X652	0	0
2	321.00	W40X183	W36X487	W36X652	0	0
3	477.00	W40X362	W36X441	W36X652	0	7/16
4	633.00	W40X362	W36X441	W36X652	0	7/16
5	789.00	W40X397	W36X441	W36X652	1/16	11/16
6	945.00	W40X397	W36X441	W36X652	1/16	11/16
7	1101.00	W40X503	W36X441	W36X652	1/2	1-1/2
8	1257.00	W40X503	W36X441	W36X652	1/2	1-1/2
9	1413.00	W40X503	W36X441	W36X652	1/2	1-1/2
10	1569.00	W40X503	W36X441	W36X652	1/2	1-1/2
11	1725.00	W40X593	W36X441	W36X652	7/8	2-3/16
12	1881.00	W40X593	W36X441	W36X652	7/8	2-3/16
13	2037.00	W40X593	W36X441	W36X652	7/8	2-3/16
14	2193.00	W40X593	W36X441	W36X652	7/8	2-3/16
15	2349.00	W40X503	W36X441	W36X529	1/2	2-1/8
16	2505.00	W40X503	W36X441	W36X529	1/2	2-1/8
17	2661.00	W40X397	W36X441	W36X441	1/16	1-11/16
18	2817.00	W40X397	W36X441	W36X441	1/16	1-11/16
19	2973.00	W40X167	W36X330	W36X395	0	0
20	3129.00	W40X167	W36X330	W36X395	0	0

Table D-3 Member Sizes for Special SMF Performance Group PG-3ELF, SDC D_{min}

Story	Elevation (in.)	Beam Size	Exterior Column Size	Interior Column Size	Doubler Plate Size	
					Exterior Col.	Interior Col.
1-story						
1	170.95	W18X46	W14X68	W14X68	1/4	11/16

Table D-4 Member Sizes for Special SMF Performance Group PG-4ELF, SDC D_{min}

Story	Elevation (in.)	Beam Size	Exterior Column Size	Interior Column Size	Doubler Plate Size	
					Exterior Col.	Interior Col.
2-story						
1	168.05	W24X76	W18X55	W18X97	3/8	7/8
2	324.05	W12X19	W18X55	W18X97	0	0
4-story						
1	166.55	W18X71	W18X86	W18X97	1/16	9/16
2	322.55	W18X86	W18X86	W18X97	3/16	1/2
3	478.55	W18X71	W18X65	W18X86	1/16	11/16
4	634.55	W18X71	W18X65	W18X86	1/16	11/16
20-story						
1	165.00	W30X108	W36X302	W36X361	0	0
2	321.00	W40X183	W36X302	W36X361	0	1/4
3	477.00	W40X215	W36X247	W36X361	1/16	9/16
4	633.00	W40X215	W36X247	W36X361	1/16	9/16
5	789.00	W40X215	W36X231	W36X361	1/8	9/16
6	945.00	W40X215	W36X231	W36X361	1/8	9/16
7	1101.00	W40X277	W36X231	W36X361	3/8	1-1/16
8	1257.00	W40X277	W36X231	W36X361	3/8	1-1/16
9	1413.00	W40X277	W36X231	W36X361	3/8	1-1/16
10	1569.00	W40X277	W36X231	W36X361	3/8	1-1/16
11	1725.00	W40X297	W36X231	W36X361	1/2	1-1/4
12	1881.00	W40X297	W36X231	W36X361	1/2	1-1/4
13	2037.00	W40X297	W36X231	W36X361	1/2	1-1/4
14	2193.00	W40X297	W36X231	W36X361	1/2	1-1/4
15	2349.00	W40X264	W36X182	W36X302	1/2	1-1/8
16	2505.00	W40X264	W36X182	W36X302	1/2	1-1/8
17	2661.00	W40X211	W36X160	W36X231	1/4	1
18	2817.00	W40X211	W36X160	W36X231	1/4	1
19	2973.00	W30X108	W36X160	W36X182	0	3/16
20	3129.00	W30X108	W36X160	W36X182	0	3/16

Table D-5 Member Sizes for Special SMF Performance Group PG-1RSA, SDC D_{max}

Story	Elevation (in.)	Beam Size	Exterior Column Size	Interior Column Size	Doubler Plate Size	
					Exterior Col.	Interior Col.
1-story						
1	170.95	W27X102	W21X111	W21X111	1/4	1-1/8
2-story						
1	164.65	W30X132	W24X131	W24X162	3/8	1-3/16
2	320.65	W16X31	W24X131	W24X162	0	0

Table D-6 Member Sizes for Special SMF Performance Group PG-2RSA, SDC D_{max}

Story	Elevation (in.)	Beam Size	Exterior Column Size	Interior Column Size	Doubler Plate Size	
					Exterior Col.	Interior Col.
4-story						
1	166.55	W21X73	W24X103	W24X103	0	5/16
2	322.55	W21X73	W24X103	W24X103	0	5/16
3	478.55	W21X57	W24X62	W24X62	0	5/16
4	634.55	W21X57	W24X62	W24X62	0	5/16
8-story						
1	166.55	W30X108	W24X131	W24X162	1/16	9/16
2	322.55	W30X116	W24X131	W24X162	1/16	3/8
3	478.55	W30X116	W24X131	W24X162	1/16	11/16
4	634.55	W27X94	W24X131	W24X162	0	3/8
5	790.55	W27X94	W24X131	W24X131	0	9/16
6	946.55	W24X84	W24X131	W24X131	0	7/16
7	1102.55	W24X84	W24X94	W24X94	0	9/16
8	1258.55	W21X68	W24X94	W24X94	0	5/16
12-story						
1	166.55	W30X124	W24X207	W24X207	0	1/2
2	322.55	W30X132	W24X207	W24X207	0	7/16
3	478.55	W30X132	W24X162	W24X207	1/16	5/8
4	634.55	W30X132	W24X162	W24X207	1/16	5/8
5	790.55	W30X116	W24X146	W24X176	0	5/8
6	946.55	W30X116	W24X146	W24X176	0	5/8
7	1102.55	W30X116	W24X131	W24X162	1/16	11/16
8	1258.55	W30X116	W24X131	W24X162	1/16	11/16
9	1414.55	W27X94	W24X131	W24X131	0	9/16
10	1570.55	W27X94	W24X131	W24X131	0	9/16
11	1726.55	W24X84	W24X84	W24X94	1/16	9/16
12	1882.55	W24X84	W24X84	W24X94	1/16	9/16

Table D-6 Member Sizes for Special SMF Performance Group PG-2RSA, SDC D_{max} (continued)

Story	Elevation (in.)	Beam Size	Exterior Column Size	Interior Column Size	Doubler Plate Size	
					Exterior Col.	Interior Col.
20-story						
1	165.00	W33X169	W14X426	W24X335	0	1/4
2	321.00	W33X169	W14X426	W24X335	0	1/4
3	477.00	W33X169	W14X426	W24X335	0	1/4
4	633.00	W33X169	W14X426	W24X335	0	1/4
5	789.00	W33X169	W14X398	W24X335	0	1/4
6	945.00	W33X169	W14X398	W24X335	0	1/4
7	1101.00	W33X169	W14X370	W24X335	0	1/4
8	1257.00	W33X169	W14X370	W24X335	0	1/4
9	1413.00	W33X141	W14X311	W24X279	0	5/16
10	1569.00	W33X141	W14X311	W24X279	0	5/16
11	1725.00	W33X141	W14X283	W24X250	0	1/2
12	1881.00	W33X141	W14X283	W24X250	0	1/2
13	2037.00	W33X141	W14X233	W24X250	1/16	1/2
14	2193.00	W33X141	W14X233	W24X250	1/16	1/2
15	2349.00	W30X108	W14X159	W24X162	1/4	9/16
16	2505.00	W30X108	W14X159	W24X162	1/4	9/16
17	2661.00	W30X108	W14X132	W24X162	3/8	9/16
18	2817.00	W30X108	W14X132	W24X162	3/8	9/16
19	2973.00	W24X62	W14X132	W24X103	0	3/16
20	3129.00	W24X62	W14X132	W24X103	0	3/16

Table D-7 Member Sizes for Special SMF Performance Group PG-3RSA, SDC D_{min}

Story	Elevation (in.)	Beam Size	Exterior Column Size	Interior Column Size	Doubler Plate Size	
					Exterior Col.	Interior Col.
1-story						
1	170.95	W18X40	W14X68	W14X68	0	1/2

Table D-8 Member Sizes for Special SMF Performance Group PG-4RSA, SDC D_{min}

Story	Elevation (in.)	Beam Size	Exterior Column Size	Interior Column Size	Doubler Plate Size	
					Exterior Col.	Interior Col.
2-story						
1	168.05	W24X62	W18X86	W18X86	1/16	11/16
2	324.05	W12X19	W18X86	W18X86	0	0
4-story						
1	166.55	W16X57	W14X74	W14X82	1/8	11/16
2	322.55	W18X60	W14X74	W14X82	1/8	3/8
3	478.55	W18X60	W14X48	W14X74	5/16	13/16
4	634.55	W16X57	W14X48	W14X74	1/4	3/4
8-story						
1	166.55	W24X55	W24X131	W24X94	0	3/16
2	322.55	W24X55	W24X131	W24X94	0	3/16
3	478.55	W24X62	W24X84	W24X94	0	1/4
4	634.55	W24X62	W24X84	W24X94	0	1/4
5	790.55	W21X50	W24X76	W24X76	0	1/8
6	946.55	W21X50	W24X76	W24X76	0	1/8
7	1102.55	W21X50	W24X62	W24X76	0	1/8
8	1258.55	W21X50	W24X62	W24X76	0	1/8
12-story						
1	166.55	W24X94	W24X162	W24X162	0	3/8
2	322.55	W24X94	W24X162	W24X162	0	3/8
3	478.55	W24X94	W24X131	W24X146	0	7/16
4	634.55	W24X94	W24X131	W24X146	0	7/16
5	790.55	W24X76	W24X103	W24X131	0	5/16
6	946.55	W24X76	W24X103	W24X131	0	5/16
7	1102.55	W24X62	W24X84	W24X94	0	1/4
8	1258.55	W24X62	W24X84	W24X94	0	1/4
9	1414.55	W24X62	W24X76	W24X84	0	5/16
10	1570.55	W24X62	W24X76	W24X84	0	5/16
11	1726.55	W21X62	W24X76	W24X76	0	3/8
12	1882.55	W21X62	W24X76	W24X76	0	3/8

Table D-8 Member Sizes for Special SMF Performance Group PG-4RSA, SDC D_{min} (continued)

Story	Elevation (in.)	Beam Size	Exterior Column Size	Interior Column Size	Doubler Plate Size	
					Exterior Col.	Interior Col.
20-story						
1	166.55	W27X129	W24X335	W24X250	0	5/16
2	322.55	W27X129	W24X335	W24X250	0	5/16
3	478.55	W30X132	W24X229	W24X250	0	3/8
4	634.55	W30X132	W24X229	W24X250	0	3/8
5	790.55	W30X132	W24X207	W24X229	0	1/2
6	946.55	W30X132	W24X207	W24X229	0	1/2
7	1102.55	W27X129	W24X192	W24X207	0	9/16
8	1258.55	W27X129	W24X192	W24X207	0	9/16
9	1414.55	W27X129	W24X162	W24X207	0	9/16
10	1570.55	W27X102	W24X162	W24X207	0	1/4
11	1726.55	W27X102	W24X146	W24X192	0	5/16
12	1882.55	W27X102	W24X146	W24X192	0	5/16
13	2038.55	W27X102	W24X131	W24X176	0	7/16
14	2194.55	W27X94	W24X131	W24X176	0	5/16
15	2350.55	W27X94	W24X131	W24X131	0	9/16
16	2506.55	W24X94	W24X131	W24X131	0	9/16
17	2662.55	W24X94	W24X94	W24X131	1/16	9/16
18	2818.55	W24X94	W24X94	W24X131	1/16	9/16
19	2974.55	W21X44	W24X94	W24X62	0	1/8
20	3130.55	W21X44	W24X94	W24X62	0	1/8

D.4 Additional Modeling Considerations

For the special SMF archetypes, modeling parameters were based on the following assumptions:

- Effective yield strength $M_y = 1.1M_p$, with M_p based on expected yield strength of 55 ksi.
- $M_c/M_y = 1.10$
- $M_r/M_y = 0.4$
- $\theta_u = 0.2$
- θ_p, θ_{pc}, and Λ for RBS connections obtained from the regression equation derived by Lignos and Krawinkler (2009) and presented in PEER/ATC 72-1 report (PEER/ATC, 2010).
- The effects of a composite floor slab on modeling parameters were not considered.

D.5 P-Delta Considerations

Because of the flexibility of special SMFs, P-Delta considerations often controlled member sizes in the lower stories of tall frames. ASCE/SEI 7-05 requires explicit consideration of P-Delta effects for each story in which the elastic stability coefficient $\theta = (P\Delta)/(V_h C_d)$ exceeds 0.1 (Equation 12.8.7). In this equation, Δ is the "design story drift," which means it contains the deflection amplification factor C_d, i.e., $\Delta = \Delta_e C_d$. This implies that the elastic stability coefficient can be computed under any level of lateral load, provided that the structure remains elastic and that Δ_e and V come from the same lateral load condition. The load, P, is the total vertical design load, including the load tributary to gravity framing.

Equation 12.8-17 in ASCE/SEI 7-05 places an upper limit of $\theta_{max} = 0.5 / (\beta \times C_d) \leq 0.25$ on the permissible stability coefficient, where β is the ratio of shear demand to shear capacity for the story under consideration. When computer analyses are used to predict elastic design forces and drifts, P-Delta effects are usually accounted for automatically. The ASCE/SEI 7-05 upper limit on θ, however, is not automatically considered in such analyses and was found to control member sizes in the lower stories of several tall SMF archetypes.

Shear demand is the story design shear force for strength design, and shear capacity is the maximum shear force that can be resisted by the story. This shear capacity cannot be uniquely defined because the capacity in one story depends on the load pattern applied to the full structure. An estimate of the story shear capacity can be obtained by dividing the average of the "floor moment" capacities of the two floors by the story height. The "floor moment" capacity is the sum of the maximum beam or column moments that can be developed at the intersection of all beam-to-column centerlines at the floor level. For connections at which the strong column–weak beam concept is followed, this amounts to the quantity ΣM_{pb}^* employed in AISC 341-05 Equation 9-3, divided by 1.1 to eliminate the strain hardening effect. For connections with weak columns the quantity ΣM_{pc}^* from Equation 9-3 should be used. Results obtained from such estimates are illustrated in Figure D-3(a) for the 4-story, SDC D_{max} RSA archetype. The pushover curve shown in Figure D-3(b) indicates that these estimates are reasonable.

In most cases estimated demand/capacity ratios (β values) led to θ_{max} values clearly smaller than 0.25, and in many cases the requirement $\theta \leq \theta_{max}$ necessitated an increase in story stiffness. Member sizes in the lower stories of all SDC D_{min} archetypes, except for the 1-story, SDC D_{min} ELF archetype, were controlled by P-Delta considerations.

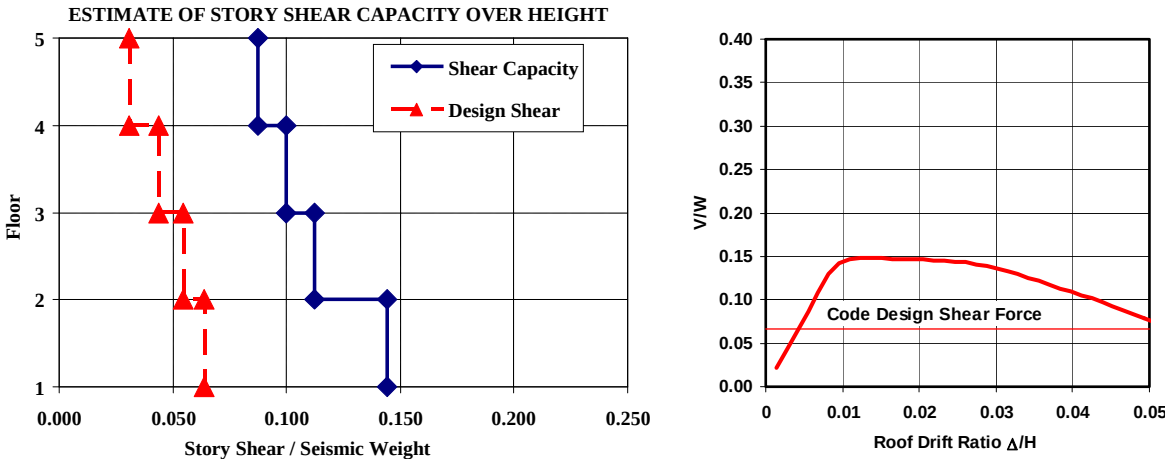

(a) Estimated story shear capacity (b) Pushover overstrength

Figure D-3 Estimated story shear capacity, 4-story, SDC D_{max} RSA archetype.

D.6 Assessment of Relationship between Design and Analytical Models for Special SMFs

In this example, a 1-story SMF archetype for SDC D_{min} seismic design loading was considered. For a building height of 15 feet, the code design period $T = C_u T_a$ is equal to 1.5*0.244 = 0.37 seconds, which is on the plateau (in the constant acceleration region) of the design spectrum, i.e., the base shear design value is $(0.5/8)W = 0.0625W$. Strength design considerations resulted in small member sizes, and drift requirements governed. The drift limitation under design forces is $0.025h/C_d = 0.025$ x 180/8 = 0.56" (for $C_d = R = 8$).

Equivalent Lateral Force (ELF) design based on this drift limit resulted in a structure with a calculated period of $T_1 = 1.62$ seconds and a base shear strength of $0.16W$ ($\Omega = 2.55$). For ELF designs, the minimum base shear of 0.022 must be considered.

A disconnect in the relationship between design and analytical models occurs in that a designer might have a stiff structure in mind ($T = 0.37$ seconds) with a base shear strength equal to 100(0.16/0.50) = 32% of the design spectrum value at a period of 0.37 seconds, but what is actually being modeled in the collapse analysis is a structure that is $(1.62/0.37)^2 = 19$ times as flexible, and whose base shear strength is 100(0.16/(0.2/1.62)) = 130% of the design spectrum value at $T = 1.62$ seconds. The analytical model, when subjected to seismic loading, experiences ground motion effects at a period of 1.62 seconds (and longer because of period elongation). In this period range, the structure has a strength that is almost as large as the elastic MCE demand.

The question that must be addressed is how the collapse capacity of this analytical model relates to the collapse safety of the actual 1-story archetype. At this time the transition back to the design archetype was made by computing the collapse margin ratio (*CMR* = median collapse capacity over MCE demand) using the spectral

acceleration demand and capacity at the code-specified period of 0.37 seconds and not the analytical period of 1.62 seconds. Whether or not this provides a realistic collapse assessment of a structure with an actual period that is somewhere between 0.37 and 1.62 seconds, and response that could be affected by the stiffness and strength of non-simulated structural and nonstructural components, needs further investigation.

Appendix E
Design Details of Buckling-Restrained Braced Frame Archetypes

This appendix presents detailed design information for buckling-restrained braced frame (BRBF) archetypes considered in the full archetype design space described in Chapter 7. Seismic criteria, design loads, load combinations, and related requirements that were used as a basis for design of BRBF archetypes are described, and the resulting beam, column, and brace member sizes in each story for each archetype are summarized.

E.1 Introduction

Index archetypes for special SCBF and BRBF systems were designed in accordance with design requirements contained within ANSI/AISC 341-05, *Seismic Provisions for Structural Steel Buildings* (AISC, 2005a), and ASCE/SEI 7-05 *Minimum Design Loads for Buildings and Other Structures* (ASCE, 2006). Test data were used to support the designs, as necessary.

All archetypes were designed using a response modification coefficient, $R = 8$, a deflection amplification factor, $C_d = R$, and redundancy factor, $\rho = 1$. Values of C_t and x used to determine the fundamental period were based on Appendix R of ANSI/AISC 341-05. The height limit for archetypes was taken as 240 feet, which is extended from the basic limit of 160 feet prescribed in ASCE/SEI 7-05.

The Response Spectrum Analysis (RSA) procedure was used for the design of all archetypes. Because of base shear scaling, the RSA procedure typically results in designs that are 15% weaker than the Equivalent Lateral Force (ELF) procedure in the case of strength-controlled designs, and somewhat lighter for drift-controlled designs.

A number of alternative beam-column-brace connection details are possible. ANSI/AISC 341-05 prescribes the required strength of connections, but permits a designer latitude in determining the connection details. In this study, beam-column connections and brace-to-framing connections were not designed in detail. It has been assumed that these connections have adequate stiffness and strength, and are detailed such that they will not fail before the braces rupture, which is the basic requirement in ANSI/AISC 341-05.

E.2 Material Properties and Design Loading

Material properties for structural steel sections are summarized in Table E-1.

Table E-1 Structural Materials for BRBF Archetypes

Steel Section	Material Properties
W sections	ASTM A992 F_y=50 ksi; F_u=65 ksi
BRB Steel Core	ASTM A36 or JIS G3136 SN 400B with supplemental yield requirements: F_{ysc}=42 ksi

All designs were checked for strength and checked for a drift limit of 0.02%. ASCE/SEI 7-05 limits on second-order effects were also observed. ASCE/SEI 7-05 load combinations were used for the design of the frame, with the following exceptions:

- Braces were designed for seismic forces only. The effects of gravity load were ignored, as is typical practice.
- Seismic forces in columns and beams were computed based on the maximum forces that can be developed in the braces, considering strain hardening effects. All braces were considered to yield simultaneously in tension or compression in a first-mode displacement, as required in ANSI/AISC 341-05.
- Flexural forces in columns were not considered in combination with maximum forces imposed by the braces, as permitted in ANSI/AISC 341-05.

E.3 Buckling-Restrained Braced Frame Designs

Buckling-restrained braced frame designs were prepared for 14 unique archetype configurations in the Phase I sensitivity studies. Designs for an additional 15 archetype configurations were prepared for the Phase II collapse performance evaluation. Brace, column, and beam member sizes for each archetype configuration at each story are summarized in the sections that follow.

E.3.1 Buckling-Restrained Frame Designs for Phase I Sensitivity Studies

Brace, column, and beam member sizes for BRBF archetypes used in the Phase I sensitivity studies are summarized in Tables E-2 through E-4.

Table E-2 Member Sizes for Buckling-Restrained Braced Frame Archetypes for Sensitivity Study 1

Story	Brace Area (in^2)	Column Size	Beam Size
Archetype ID No. 2S-LB-25B-Dmax			
2	6.0	W14x82	W21x50
1	9.0	W14x82	W21x73
Archetype ID No. 2S-LB-25B-Dmin			
2	2.0	W14x38	W21x44
1	3.0	W14x38	W21x62
Archetype ID No. 2S-LB-25B-Bmax			
2	1.0	W14x38	W18x35
1	1.0	W14x38	W18x35
Archetype ID No. 12S-LB-15B-Dmax (2 bays of bracing per side)			
12	3.0	W14x145	W21x50
11	4.0	W14x145	W21x50
10	5.0	W14x145	W21x62
9	6.0	W14x145	W21x62
8	6.0	W14x211	W21x62
7	6.0	W14x211	W21x62
6	7.0	W14x211	W21x62
5	7.0	W14x211	W21x62
4	8.0	W14x257	W21x62
3	8.0	W14x257	W21x73
2	9.0	W14x283	W21x73
1	9.0	W14x283	W21x73

Table E-2 Member Sizes for Buckling-Restrained Braced Frame Archetypes for Sensitivity Study 1 (continued)

Story	Brace Area (in^2)	Column Size	Beam Size
Archetype ID No. 12S-LB-15B-Dmin			
12	3.0	W14x82	W18x35
11	3.0	W14x82	W21x50
10	3.0	W14x132	W21x50
9	4.0	W14x132	W21x62
8	4.0	W14x132	W21x62
7	5.0	W14x132	W21x62
6	5.0	W14x159	W21x62
5	5.0	W14x159	W21x62
4	6.0	W14x193	W21x62
3	7.0	W14x193	W21x62
2	7.0	W14x257	W21x62
1	7.0	W14x257	W21x62
Archetype ID No. 12S-LB-15B-Bmax			
12	3.0	W14x74	W18x35
11	3.0	W14x74	W21x50
10	3.0	W14x132	W21x50
9	3.0	W14x132	W21x50
8	3.0	W14x132	W21x50
7	3.0	W14x132	W21x50
6	3.0	W14x132	W21x50
5	3.0	W14x132	W21x50
4	3.0	W14x145	W21x50
3	4.0	W14x145	W21x62
2	4.0	W14x176	W21x62
1	4.0	W14x176	W21x62

Table E-3 Member Sizes for Buckling-Restrained Braced Frame Archetypes for Sensitivity Study 2

Story	Brace Area (in^2)	Column Size	Beam Size
Archetype ID No. 2S-LB-25B-Dmax			
2	6.0	W14x82	W21x50
1	9.0	W14x82	W21x73
Archetype ID No. 2S-LB-15B-Dmax			
2	5.0	W14x74	W21x44
1	6.0	W14x74	W21x62
Archetype ID No. 12S-LB-25B-Dmax			
12	4.0	W14x211	W21x50
11	5.0	W14x211	W21x62
10	7.0	W14x257	W21x73
9	7.0	W14x257	W24x76
8	9.0	W14x311	W24x76
7	9.0	W14x311	W24x94
6	10.0	W14x370	W24x94
5	11.0	W14x370	W24x94
4	12.0	W14x455	W24x103
3	12.0	W14x455	W24x103
2	12.0	W14x500	W24x103
1	12.0	W14x500	W24x103
Archetype ID No. 12S-LB-15B-Dmax (2 bays of bracing per side)			
12	3.0	W14x145	W21x50
11	4.0	W14x145	W21x50
10	5.0	W14x145	W21x62
9	6.0	W14x145	W21x62
8	6.0	W14x211	W21x62
7	6.0	W14x211	W21x62
6	7.0	W14x211	W21x62
5	7.0	W14x211	W21x62
4	8.0	W14x257	W21x62
3	8.0	W14x257	W21x73
2	9.0	W14x283	W21x73
1	9.0	W14x283	W21x73

Table E-4 Member Sizes for Buckling-Restrained Braced Frame Archetypes for Sensitivity Study 3

Story	Brace Area (in^2)	Column Size	Beam Size
Archetype ID No. 2S-LB-25B-Dmax			
2	6.0	W14x82	W21x50
1	9.0	W14x82	W21x73
Archetype ID No. 2S-ZZ-25B-Dmax			
2	4.0	W14x53	W21x50
1	6.0	W14x53	W21x44
Archetype ID No. 2S-CV-30B-Dmax			
2	3.0	W14x53	W24x55
1	4.0	W14x53	W24x55
Archetype ID No. 2S-2X-30B-Dmax			
2	3.0	W14x53	W24x62
1	4.0	W14x53	W21x44
Archetype ID No. 12S-LB-15B-Dmax (2 Bays of Bracing per Side)			
12	3.0	W14x145	W21x50
11	4.0	W14x145	W21x50
10	5.0	W14x145	W21x62
9	6.0	W14x145	W21x62
8	6.0	W14x211	W21x62
7	6.0	W14x211	W21x62
6	7.0	W14x211	W21x62
5	7.0	W14x211	W21x62
4	8.0	W14x257	W21x62
3	8.0	W14x257	W21x73
2	9.0	W14x283	W21x73
1	9.0	W14x283	W21x73

Table E-4 Member Sizes for Buckling-Restrained Braced Frame Archetypes for Sensitivity Study 3 (continued)

Story	Brace Area (in^2)	Column Size	Beam Size
Archetype ID No. 12S-ZZ-15B-Dmax (2 Bays of Bracing per Side)			
12	3.0	W14x159	W18x40
11	5.0	W14x159	W18x40
10	6.0	W14x159	W18x40
9	6.0	W14x159	W18x40
8	6.0	W14x176	W18x40
7	6.0	W14x176	W18x40
6	7.0	W14x211	W18x40
5	7.0	W14x211	W18x40
4	8.0	W14x257	W18x40
3	8.0	W14x257	W18x40
2	9.0	W14x311	W18x40
1	9.0	W14x311	W18x40
Archetype ID No. 12S-CV-20B-Dmax			
12	5.0	W14x132	W24x62
11	8.0	W14x132	W24x76
10	8.0	W14x257	W24x76
9	9.0	W14x257	W24x76
8	9.0	W14x311	W24x76
7	10.0	W14x311	W24x76
6	10.0	W14x398	W24x76
5	10.0	W14x398	W24x76
4	11.0	W14x455	W24x76
3	11.0	W14x455	W24x76
2	12.0	W14x605	W24x76
1	12.0	W14x605	W24x76

Table E-4 Member Sizes for Buckling-Restrained Braced Frame Archetypes for Sensitivity Study 3 (continued)

Story	Brace Area (in^2)	Column Size	Beam Size
Archetype ID No. 12S-2X-20B-Dmax			
12	6.0	W14x132	W24x62
11	7.0	W14x132	W24x62
10	8.0	W14x257	W21x50
9	9.0	W14x257	W24x62
8	9.0	W14x311	W21x50
7	10.0	W14x311	W24x62
6	10.0	W14x398	W21x50
5	10.0	W14x398	W24x62
4	11.0	W14x455	W21x50
3	11.0	W14x455	W24x62
2	12.0	W14x605	W21x50
1	12.0	W14x605	W24x62

E.3.2 Buckling-Restrained Braced Frame Designs for Phase II Performance Evaluation

Brace, column, and beam member sizes for BRBF archetypes used in the Phase II designs are summarized in Tables E-5 through E-8.

Table E-5 Member Sizes for Buckling-Restrained Braced Frame Performance Group PG-10

Story	Brace Area (in^2)	Column Size	Beam Size
Archetype ID No. 4S-LB-15B-Dmax			
4	5.0	W14x74	W21x50
3	7.0	W14x82	W21x62
2	9.0	W14x132	W21x73
1	10.0	W14x145	W21x73
Archetype ID No. 6S-LB-15B-Dmax			
6	8.0	W14x132	W21x73
5	9.0	W14x159	W21x73
4	10.0	W14x159	W24x76
3	10.0	W14x193	W24x76
2	11.0	W14x211	W27x94
1	11.0	W14x233	W27x94

Table E-5 Member Sizes for Buckling-Restrained Braced Frame Performance Group PG-10 (continued)

Story	Brace Area (in^2)	Column Size	Beam Size
Archetype ID No. 9S-LB-15B-Dmax			
9	9.0	W14x370	W21x62
8	9.0	W14x370	W24x76
7	10.0	W14x370	W24x76
6	10.0	W14x398	W24x76
5	11.0	W14x398	W27x94
4	11.0	W14x455	W27x94
3	11.0	W14x455	W27x94
2	12.0	W14x500	W27x94
1	12.0	W14x500	W27x94
Archetype ID No. 12S-LB-15B-Dmax (2 Bays of Bracing per Side)			
12	3.0	W14x145	W21x50
11	4.0	W14x145	W21x50
10	5.0	W14x145	W21x62
9	6.0	W14x145	W21x62
8	6.0	W14x211	W21x62
7	6.0	W14x211	W21x62
6	7.0	W14x211	W21x62
5	7.0	W14x211	W21x62
4	8.0	W14x257	W21x62
3	8.0	W14x257	W21x73
2	9.0	W14x283	W21x73
1	9.0	W14x283	W21x73

Table E-5 Member Sizes for Buckling-Restrained Braced Frame Performance Group PG-10 (continued)

Story	Brace Area (in^2)	Column Size	Beam Size
Archetype ID No. 18S-LB-15B-Dmax (2 Bays of Bracing per Side)			
18	4.0	W14x176	W21x50
17	5.0	W14x176	W21x62
16	5.0	W14x342	W21x62
15	5.0	W14x342	W21x62
14	6.0	W14x342	W21x62
13	6.0	W14x342	W21x62
12	8.0	W14x426	W21x62
11	8.0	W14x426	W24x76
10	8.0	W14x426	W24x76
9	8.0	W14x426	W24x76
8	8.0	W14x500	W24x76
7	10.0	W14x500	W24x76
6	10.0	W14x500	W24x76
5	10.0	W14x500	W24x76
4	10.0	W14x605	W24x76
3	12.0	W14x605	W24x94
2	12.0	W14x605	W24x94
1	12.0	W14x605	W24x94

Table E-6 Member Sizes for Buckling-Restrained Braced Frame Performance Group PG-12

Story	Brace Area (in^2)	Column Size	Beam Size
Archetype ID No. 2S-LB-15B-Dmin			
2	3.0	W14x38	W18x35
1	3.0	W14x53	W21x50
Archetype ID No. 3S-LB-15B-Dmin			
3	3.0	W14x38	W18x35
2	3.0	W14x53	W21x50
1	3.0	W14x74	W21x50
Archetype ID No. 4S-LB-15B-Dmin			
4	3.0	W14x74	W18x35
3	3.0	W14x74	W21x50
2	3.0	W14x74	W21x50
1	3.0	W14x82	W21x50
Archetype ID No. 6S-LB-15B-Dmin			
6	3.0	W14x74	W18x35
5	3.0	W14x74	W21x50
4	3.0	W14x74	W21x50
3	3.0	W14x82	W21x50
2	3.0	W14x132	W21x50
1	3.0	W14x132	W21x50
Archetype ID No. 9S-LB-15B-Dmin			
9	3.0	W14x74	W18x35
8	3.0	W14x74	W21x50
7	3.0	W14x74	W21x50
6	3.0	W14x132	W21x50
5	4.0	W14x132	W21x50
4	4.0	W14x132	W21x62
3	6.0	W14x159	W21x62
2	6.0	W14x159	W21x62
1	6.0	W14x176	W21x62

Table E-6 Member Sizes for Buckling-Restrained Braced Frame Performance Group PG-12 (continued)

Story	Brace Area (in^2)	Column Size	Beam Size
Archetype ID No. 12S-LB-15B-Dmin			
12	3.0	W14x82	W18x35
11	3.0	W14x82	W21x50
10	3.0	W14x132	W21x50
9	4.0	W14x132	W21x62
8	4.0	W14x132	W21x62
7	5.0	W14x132	W21x62
6	5.0	W14x159	W21x62
5	5.0	W14x159	W21x62
4	6.0	W14x193	W21x62
3	7.0	W14x193	W21x62
2	7.0	W14x257	W21x62
1	7.0	W14x257	W21x62
Archetype ID No. 18S-LB-15B-Dmin			
18	3.0	W14x132	W18x35
17	4.0	W14x132	W21x62
16	4.0	W14x132	W21x62
15	5.0	W14x132	W21x62
14	5.0	W14x132	W21x62
13	5.0	W14x132	W21x62
12	5.0	W14x211	W21x62
11	6.0	W14x211	W21x62
10	6.0	W14x211	W21x62
9	6.0	W14x211	W21x62
8	6.0	W14x257	W21x62
7	7.0	W14x257	W21x62
6	8.0	W14x283	W21x73
5	8.0	W14x283	W21x73
4	9.0	W14x342	W21x73
3	10.0	W14x342	W24x76
2	11.0	W14x398	W24x94
1	11.0	W14x398	W24x94

Table E-7 Member Sizes for Buckling-Restrained Braced Frame Performance Group PG-13

Story	Brace Area (in^2)	Column Size	Beam Size
Archetype ID No. 1S-LB-25B-Dmax			
1	4.0	W14x38	W21x62
Archetype ID No. 2S-LB-25B-Dmax			
2	6.0	W14x82	W21x50
1	9.0	W14x82	W21x73
Archetype ID No. 3S-LB-25B-Dmax			
3	5.0	W14x38	W21x62
2	7.0	W14x74	W21x73
1	8.0	W14x82	W24x76

Table E-8 Member Sizes for Buckling-Restrained Braced Frame Performance Groups PG-15, PG-11, and PG-20

Story	Brace Area (in^2)	Column Size	Beam Size
Archetype ID No. 1S-LB-25B-Dmin			
1	3.0	W14x38	W21x50
Archetype ID No. 1S-LB-15B-Dmin			
1	3.0	W14x38	W18x35
Archetype ID No. 1S-CV-30B-Dmin			
1	3.0	W14x38	W21x50

References

ACI, 2008a, *Building Code Requirements for Structural Concrete*, ACI 318-08, American Concrete Institute, Farmington Hills, Michigan.

ACI, 2008b, *Building Code Requirements for Masonry Structures*, ACI 530-08/ASCE 5-08/TMS 402-08, Masonry Standards Joint Committee of the American Concrete Institute, Farmington Hills, Michigan; Structural Engineering Institute of the American Society of Civil Engineers, Reston, Virginia; and The Masonry Society, Boulder, Colorado.

AISC, 2005a, *Seismic Provisions for Structural Steel Buildings*, ANSI/AISC 341-05, American Institute for Steel Construction, Chicago, Illinois.

AISC, 2005b, *Prequalified Connections for Special and Intermediate Steel Moment Frames for Seismic Applications*, ANSI/AISC 358-05, American Institute for Steel Construction, Chicago, Illinois.

AISC, 2005c, *Specification for Structural Steel Buildings*, AISC/ANSI 360-05, American Institute of Steel Construction, Chicago, Illinois.

Aktan A. E., Bertero V., and Sakino K., 1985, "Lateral stiffness characteristics of reinforced concrete frame-wall structures," *Structural Journal*, ACI, Vol. 86, No. 10, pp. 231-262.

ANSI/AF&PA, 2005, *National Design Specification for Wood Construction*, ANSI/AF&PA NDS-2005, American National Standards Institute and American Forest and Paper Association, Washington, D.C.

ASCE, 2006, *Minimum Design Loads for Buildings and Other Structures*, ASCE/SEI 7-05, American Society of Civil Engineers, Reston, Virginia.

ASCE, 2007, *Seismic Rehabilitation of Existing Buildings*, ASCE Standard ASCE/SEI 41-06, American Society of Civil Engineers, Reston, Virginia.

ATC, 1978, *Tentative Provisions for the Development of Seismic Regulations for Buildings*, Report No. ATC-3-06, Applied Technology Council, Redwood City, California.

Atkinson, R.H. and Kingsley, G.R., 1985, *A Comparison of the Behavior of Clay and Concrete Masonry in Compression*, Report No. 1.1-1, US-Japan Coordinated Program for Masonry Building Research, Atkinson-Noland & Associates, Boulder, Colorado.

Black, R.G., Wenger, W.A., and Popov, E.P., 1980, *Inelastic Buckling of Steel Struts Under Cyclic Load Reversals*, UCB/EERC-80/40, Earthquake Engineering Research Center, University of California, Berkeley, California.

Black, C., Makris, N., and Aiken, I.D., 2004, "Component testing, seismic evaluation and characterization of buckling-restrained braces," *Journal of Structural Engineering*, ASCE, Vol. 130, No. 6, pp. 880-894.

Bournonville, M., Dahnke, J., and Darwin, D., 2004, *Statistical Analysis of the Mechanical Properties and Weight of Reinforcing Bars*, SL Report 04-1, University of Kansas Structural Engineering and Engineering Materials, 198 pp.

Chang, G.A. and Mander, J.B., 1994, *Seismic Energy Based Fatigue Damage Analysis of Bridge Columns: Part I – Evaluation of Seismic Capacity*, NCEER Technical Report No. NCEER-94-0006; State University of New York, Buffalo, New York.

Cochran, M. and Honeck, W., 2004, *Design of Special Concentric Braced Frames*, Steel TIPS Report, Structural Steel Educational Council, Moraga, California.

Coleman, J. and Spacone, E., 2001, "Localization issues in forced-based frame elements," *Journal of Structural Engineering*, ASCE, Vol. 127, No. 11, pp. 1257-1265.

Corley, W.G., Fiorato, A.E., and Oesterle, R.G., 1981,"Structural walls," *Structural Journal*, ACI, Vol. 72, No. 4, pp. 77-131.

DASSE, 2009, *Cost Advantages of Buckling Restrained Braced Frame Buildings*, prepared by DASSE Design Inc for Star Seismic, Park City, Utah. Available at http://www.starseismic.net/pdf/Dasse_Cost_Study.pdf.

Elwood, K.J., and Moehle, J.P., 2005, "Axial Capacity Model for Shear-Damaged Columns," *Structural Journal*, ACI, Vol. 102, No. 4, pp. 578-587.

Fahnestock, L.A., Ricles, J.M., and Sause, R., 2006, "Experimental study of a large-scale buckling-restrained braced frame using the pseudo-dynamic testing method," *Proceedings of the 8th National Conference on Earthquake Engineering*, San Francisco, California.

FEMA, 2004a, *NEHRP Recommended Provisions for Seismic Regulations for New Buildings and Other Structures, Part 1: Provisions*, FEMA 450-1, 2003 Edition, Federal Emergency Management Agency, Washington, D.C.

FEMA, 2004b, *NEHRP Recommended Provisions for Seismic Regulations for New Buildings and Other Structures, Part 2: Commentary*, FEMA 450-2, 2003 Edition, Federal Emergency Management Agency, Washington, D.C.

FEMA, 2009, *Quantification of Building Seismic Performance Factors*, FEMA P-695, prepared by Applied Technology Council for the Federal Emergency Management Agency, Washington, D.C.

Ghanem, G.M., Essawy, A.S., and Hamid, A.A., 1992, "Effect of steel distribution on the behavior of partially-grouted reinforced masonry shear walls," *Proceedings of the 6th Canadian Masonry Symposium*, University of Saskatchewan, Saskatoon, Canada.

Goodsir, W.J., 1985, *The Design of Coupled Frame-Wall Structures for Seismic Actions*, Research Report 85-8, Department of Civil Engineering, University of Canterbury, Christchurch, New Zealand.

Gupta, A. and Krawinkler, H., 1999, *Seismic Demands for Performance Evaluation of Steel Moment-Resisting Frame Structures*. Rep. No. 132, John A. Blume Earthquake Engineering Center, Dept. of Civil and Environmental Engineering, Stanford Univ., Stanford, California.

Hidalgo, P.A., Ledezma, C.A., and Jordan, R.M., 2002, "Seismic behavior of squat reinforced concrete shear walls," *Earthquake Spectra*, Vol. 18, No. 2, pp. 287-308.

Ibarra L.F., Medina R.A., and Krawinkler, H., 2005, "Hysteretic models that incorporate strength and stiffness deterioration," *Earthquake Engineering and Structural Dynamics*, Vol. 34, No. 12, pp. 1489-1511.

Ingham, J.M., Davidson, B.J., Brammer, D.R., and Voon, K.C., 2001, "Testing and codification of partially grout-filled nominally-reinforced concrete masonry subjected to in-plane cyclic loads," *The Masonry Society Journal*, Vol. 19, No. 1, pp. 83-94.

Kent, D.C. and Park, R., 1971, "Flexural members with confined concrete," *Journal of the Structural Division*, ASCE, Vol. 97, No. 7, pp. 1969-1990.

Khatib, I.F., Mahin, S.A., and Pister, K.S., 1988, *Seismic Behavior of Concentrically Braced Steel Frames*, UCB/EERC-88/01, Earthquake Engineering Research Center, University of California, Berkeley, California.

Kingsley, G.R., Seible, F., Priestley, M.J.N., and Hegemier, G.A., 1994, *The U.S.-TCCMAR Full-Scale Five-Story Reinforced Masonry Research Building Test: Part II, Design, Construction, and Testing*, Report No. 9.4-2, US-Japan Coordinated Program for Masonry Building Research, University of California at San Diego, La Jolla, California.

Lignos, D.G. and Krawinkler, H., 2007, "A database in support of modeling of component deterioration for collapse prediction of steel frame structures," *ASCE Structures Congress*, Long Beach, California.

Lignos, D.G. and Krawinkler, H., 2009, *Sidesway Collapse of Deteriorating Structural Systems under Seismic Excitations*, Report No. TR-172, John A. Blume Earthquake Engineering Center, Department of Civil Engineering, Stanford University, California.

López, W. and Sabelli, R., 2004, *Seismic Design of Buckling-Restrained Braced Frames*, Steel TIPS Report, Structural Steel Educational Council, Moraga, California.

Massone, L.M., 2006, *RC Wall Shear – Flexure Interaction: Analytical and Experimental Responses*, PhD Dissertation, University of California, Department of Civil & Environmental Engineering, Los Angeles, California.

Massone, L.M. and Wallace, J.W., 2004, "Load – deformation responses of slender reinforced concrete walls," *Structural Journal*, ACI, Vol. 101, No. 1, pp. 103-113.

Massone, L.M., Orakcal, K., and Wallace, J.W., 2006, "Modeling flexural/shear interaction in RC walls," *Special Publication 236*, ACI, Paper 7, pp. 127-150.

Massone, L.M., Orakcal, K., and Wallace, J.W., 2009, "Modeling of squat structural walls controlled by shear," *Structural Journal*, ACI, Vol. 106, No 5, pp. 646-655.

Merritt, S., Uang, C.M., and Benzoni, G., 2003a, *Subassemblage Testing of CoreBrace Buckling Restrained Braces*, in Report No. TR-2003/01, University of California, San Diego, La Jolla, California.

Merritt, S., Uang, C.M., and Benzoni, G., 2003b, *Subassemblage Testing of Star Seismic Buckling Restrained Braces*, in Report No. TR-2003/04, University of California, San Diego, La Jolla, California.

Merritt, S., Uang, C.M., and Benzoni, G., 2003c, *Uniaxial Testing of Associated Bracing Buckling Restrained Braces*, in Report No. TR-2003/05, University of California, San Diego, La Jolla, California.

Merryman, K.M., Leiva, G., Antrobus, N., and Klingner, R.E., 1990, *In-plane Seismic Resistance of Two-Story Concrete Masonry Coupled Shear Walls*, Report No. 3.1(c)-1, US-Japan Coordinated Program for Masonry Building Research, University of Texas at Austin, Texas.

Mirza, S.A. and MacGregor, J.G., 1979, "Variability of mechanical properties of reinforcing bars," *Journal of the Structural Division*, ASCE, Vol. 105, No. 5, pp. 921-937.

Newell, J. and Uang, C.M., 2006, *Cyclic Behavior of Steel Columns with Combined High Axial Load and Drift Demand*, Report No. SSRP-06/22, Structural

Systems Research Project, Department of Structural Engineering, University of California, San Diego, California.

Newell, J., and Uang, C.M., 2008, "Cyclic Behavior of Steel Wide-Flange Columns Subjected to Large Drift," *Journal of Structural Engineering*, Vol. 134, No. 8, pp. 1334-1342.

Nowak, A.S., Szerszen, M.M., Szeliga, E.K., Szwed, A., and Podhorecki, P.J., 2008, *Reliability-Based Calibration for Structural Concrete, Phase 3*, Serial No. 2849, Portland Cement Association, Skokie, Illinois.

Oesterle, R.G., Fiorato, A.E., Johal, L.S., Carpenter, J.E., Russle, H.E., and Corley, W.G., 1976, *Earthquake Resistant Structural Walls – Tests of Isolated Walls*, Report to the National Science Foundation, Construction Technology Laboratories, Portland Cement Association, Skokie, Illinois, 315 pp.

Oesterle, R.G., Aristizabal-Ochoa, J.D., Fiorato, A.E., Russel, H.E., and Corley, W.G., 1979, *Earthquake Resistant Structural Walls – Tests of Isolated Walls – Phase II*, Report to the National Science Foundation, Construction Technology Laboratories, Portland Cement Association, Skokie, Illinois, 325 pp.

OpenSees, 2007, *Open System for Earthquake Engineering Simulation*, Pacific Earthquake Engineering Research Center, University of California, Berkeley, California, available at http://opensees.berkeley.edu/.

Orakcal, K. and Wallace, J.W., 2006, "Flexural modeling of reinforced concrete walls-Experimental verification," *Structural Journal*, ACI, Vol. 103, No. 2, pp. 196-206.

Orakcal, K., Conte, J.P., and Wallace, J.W., 2004, "Flexural modeling of reinforced concrete walls – Model attributes," *Structural Journal*, ACI, Vol. 101, No. 5, pp. 688-698.

Orakcal, K., Massone, L.M., and Wallace, J.W., 2006, *Analytical Modeling of Reinforced Concrete Walls for Predicting Flexural and Coupled– Shear-Flexural Responses*, Report No. 2006/07, Pacific Earthquake Engineering Research Center, University of California, Berkeley, California, 228 pp.

Orakcal, K., Massone, L.M., and Wallace, J.W., 2009, "Shear strength of lightly reinforced wall piers and spandrels," *Structural Journal*, ACI, Vol. 106, No. 4, pp. 455-465.

Pantazopoulou S.J., 1998, "Detailing for reinforcement stability in RC members," *Journal of Structural Engineering*, ASCE, Vol. 124, No. 6, pp. 623-632.

Paulay, T., 1986, "The design of ductile reinforced concrete structural walls for earthquake resistance," *Earthquake Spectra*, Vol. 2, No. 4, pp. 783-823.

Paulay, T. and Priestley, M.J.N., 1993, "Stability of ductile structural walls," *Structural Journal*, ACI, Vol. 90, No. 4, pp. 385-392.

PEER, 2006, *PEER Next-Generation Attenuation (NGA) Database*, Pacific Earthquake Engineering Research Center, University of California, Berkeley, California. Available at http://peer.berkeley.edu/nga/.

PEER/ATC, 2010, *Modeling and Acceptance Criteria for Seismic Design and Analysis of Tall Buildings*, PEER/ATC 72-1 report, prepared by the Applied Technology Council for the Pacific Earthquake Engineering Research Center, Redwood City, California.

Powell, J., Clark, K., Tsai, K.C., Roeder, C., and Lehman, D., 2008, "Test of a full scale concentrically braced frame with multi-story X-bracing," *ASCE 2008 Structures Congress*, Vancouver, BC, Canada.

Prakash, V., Powell, G.H., and Campbell, S., 1993, "DRAIN-2DX: Basic program description and user guide," *Report No. UCB/SEMM-1993/17*, University of California, Berkeley, California.

Razvi, S. and Saatcioglu, M., 1999, "Confinement model for high-strength concrete," *Journal of Structural Engineering*, ASCE, Vol. 125, No.3, pp. 281-289.

Rodriguez, M.E., Botero, J.C., and Villa, J., 1999, "Cyclic stress-strain behavior of reinforcing steel including effect of buckling," *Journal of Structural Engineering*, ASCE, Vol. 125, No. 6, pp 605-612.

Salonikios, T.N., 2002, "Shear strength and deformation patterns of R/C walls with aspect ratio 1.0 and 1.5 designed to Eurocode 8 (EC8)," *Engineering Structures*, Vol. 24, No. 1, pp. 39-49.

Salonikios, T.N., Kappos, A.J., Tegos, I.A., and Penelis, G.G., 1999, "Cyclic load behavior of low-slenderness RC walls: design basis and test results," *Structural Journal*, ACI, Vol. 96, No. 4, pp. 649–660.

Scott, B.D., Park, R., and Priestley, M.J.N., 1982, "Stress-strain behavior of concrete confined by overlapping hoops at high and low strain rates," ACI Journal Proceedings, Vol. 79, No. 1, pp.13–27.

Shedid, M.T., Drysdale, R.G., and El-Dakhakhni, W.W., 2008, "Behavior of fully-grouted reinforced concrete masonry shear walls failing in flexure: Experimental results," *Journal of Structural Engineering*, ASCE, Vol. 134, No, 11, pp. 1754-1767.

Shing, P.B., Noland, J.L., Spaeh, H.P., Klamerus, E.W., and Schuller, M.P., 1991, *Response of Single-Story Reinforced Masonry Shear Walls to In-Plane Lateral Loads*, Report No. 3.1(a)-2, US-Japan Coordinated Program for Masonry Building Research, University of Colorado at Boulder.

Shiu, K.N., Daniel, J.I., Aristizabal-Ochoa, J.D., Fiorato, A.W., and Corley, W.G., 1981, *Earthquake Resistant Structural Walls – Tests of Walls with and without Openings*, Report to the National Science Foundation, Construction Technology Laboratories, Portland Cement Association, Skokie, Illinois.

Thomsen, J.H. and Wallace J.W., 1995, *Displacement-Based Design of RC Structural Walls: An Experimental Investigation of Walls with Rectangular and T-Shaped Cross-Sections*, Report No. CU/CEE-95/06, Department of Civil Engineering, Clarkson University, Potsdam, New York, 353 pp.

Thomsen IV, J.H. and Wallace, J.W, 2004, "Displacement-based design of slender reinforced concrete structural walls – Experimental verification," *Journal of Structural Engineering*, ASCE, Vol. 130, No. 4, pp. 618-630.

Tremblay, R., 2002, "Inelastic seismic response of bracing members," *J. of Const. Steel Research*, Vol. 58, pp. 665-701.

Tremblay, R., 2008, "Influence of brace slenderness on the fracture life of rectangular tubular steel bracing members subjected to seismic inelastic loading," *Proceedings*, ASCE 2008 Structures Congress, Vancouver, BC, Canada.

Uriz, P, 2005, *Towards Earthquake Resistant Design of Concentrically Braced Steel Structures*, Ph.D. Dissertation, University of California, Berkeley, California.

Voon, K.C. and Ingham, J.M., 2006, "Experimental in-plane shear strength investigation of reinforced concrete masonry walls," *Journal of Structural Engineering*, ASCE, Vol. 132, No. 3, pp. 400-408.

Wallace, J.W., 1989, *BIAX: Revision 1, A Computer Program for the Analysis of Reinforced Concrete Sections*, Clarkson University, Department of Civil Engineering, Potsdam, New York.

Wallace, J.W., 1996, "Evaluation of UBC-94 provisions for seismic design of RC structural walls," *Earthquake Spectra*, Vol. 12, No. 2, pp. 327-348.

Wallace, J.W., 2007, "Modeling issues for tall reinforced concrete core wall buildings," *The Structural Design of Tall and Special Buildings*, Vol. 16, No. 5, pp. 615-632.

Wallace, J.W., Elwood, K.J., and Massone L.M., 2008, "An axial load capacity model for shear critical RC wall piers," *Journal of Structural Engineering*, ASCE, Vol. 134, No. 9, pp. 1548-1557.

Waugh, J., Aaleti, S., Sritharan, S., and Zhao, J., 2008, *Nonlinear Analysis of Rectangular and T-Shaped Concrete Walls*, ISU-ERI-Ames Report ERI-09327, Department of Civil, Construction, and Environmental Engineering, Iowa State University, 351 pp.

Wood, S.L., 1990, "Shear strength of low-rise reinforced concrete walls," *Structural Journal*, ACI, Vol. 87, No. 1, pp. 99-107.

Wood, S.L., 1991,"Observed behavior of slender RC walls subjected to cyclic loadings," *Inelastic Response and Design of Earthquake-Resistant Concrete Structures, SP-127*, S. K. Ghosh, ed., American Concrete Institute, Farmington Hills, Mich., pp. 334-344.

Yang, F. and Mahin, S.A., 2005, *Limiting Net Section Fracture in Slotted Tube Braces*, Steel Tips Report, Structural Steel Education Council, Moraga, California.

Yassin, M.H.M., 1994, *Nonlinear Analysis of Prestressed Concrete Structures under Monotonic and Cyclic Loads*, PhD Dissertation, University of California, Berkeley, California.

Yoo, J.H., Roeder, C.W., and Lehman, D.E., 2008, "Analytical performance simulation of special concentrically braced frames," *Journal of Structural Engineering*, ASCE, Vol. 134, No. 6, pp. 881-889.

Zayas, V.A., Popov, E.P., and Mahin, S.A., 1980, *Cyclic Inelastic Buckling of Tubular Steel Braces*, UCB/EERC-80/16, University of California, Berkeley, California.

Project Participants

National Institute of Standards and Technology

John (Jack) R. Hayes
Engineering Laboratory (MS8604)
National Institute of Standards and Technology
100 Bureau Drive
Gaithersburg, Maryland 20899

John (Jay) L. Harris III
Engineering Laboratory (MS8603)
National Institute of Standards and Technology
100 Bureau Drive
Gaithersburg, Maryland 20899

NEHRP Consultants Joint Venture

APPLIED TECHNOLOGY COUNCIL
201 Redwood Shores Parkway, Suite 240
Redwood City, California 94065
www.ATCouncil.org

CONSORTIUM OF UNIVERSITIES FOR
RESEARCH IN EARTHQUAKE ENGINEERING
1301 S. 46th Street, Building 420
Richmond, California 94804
www.CUREE.org

Joint Venture Management Committee

James R. Harris
J.R. Harris & Company
1775 Sherman Street, Suite 1525
Denver, Colorado 80203

Christopher Rojahn
Applied Technology Council
201 Redwood Shores Parkway, Suite 240
Redwood City, California 94065

Robert Reitherman
Consortium of Universities for Research in
Earthquake Engineering
1301 S. 46th Street, Building 420
Richmond, California 94804

Andrew Whittaker
Dept. of Civil, Structural, and Environ. Engin.
230 Ketter Hall
University at Buffalo
Buffalo, New York 14260

Joint Venture Program Committee

Jon A. Heintz (Program Manager)
Applied Technology Council
201 Redwood Shores Parkway, Suite 240
Redwood City, California 94065

William T. Holmes
Rutherford and Chekene
55 Second Street, Suite 600
San Francisco, California 94105

Michael Constantinou
Dept. of Civil, Structural, and Environ. Engin.
University at Buffalo
132 Ketter Hall
Buffalo, New York 14260

Jack Moehle
University of California Berkeley
325 Davis Hall – MC 1792
Berkeley, California 94720

James R. Harris (ex-officio)
Andrew Whittaker (ex-officio)

C.B. Crouse
URS Corporation
1501 4th Avenue, Suite 1400
Seattle, Washington 98101

Project Technical Committee

Charles Kircher (Project Director)
Kircher & Associates, Consulting Engineers
1121 San Antonio Road, Suite D-202
Palo Alto, California 94303

Gregory Deierlein
Stanford University
Dept. of Civil and Environmental Engineering
Blume Earthquake Engineering Center
Stanford, California 94305

John Hooper
Magnusson Klemencic Associates
1301 Fifth Avenue, Suite 3200
Seattle, Washington 98101

Helmut Krawinkler
Stanford University
Dept. of Civil and Environmental Engineering
473 Via Ortega
Stanford, California 94305

Steve Mahin
University of California, Berkeley
Department of Civil Engineering
777 Davis Hall, MC 1710
Berkeley, California 94720

Benson Shing
University of California, San Diego
Dept of Structural Engineering
409 University Center
9500 Gilman Drive, MC 0085
La Jolla, California 92093

John Wallace
University of California, Los Angeles
Dept. of Civil Engineering
5731 Boelter Hall,
Los Angeles, California 90095

Working Group Members

Chui-Hsin Chen
University of California, Berkeley
1301 South 46th Street
Richmond, California 94804

Brian Dean
Walter P. Moore
595 Market Street, Suite 950
San Francisco, California 94105

Aysegul Gogus
University of California, Los Angeles
5730 Boelter Hall
Los Angeles, California 90095

Ioannis Koutromanos
University of California, San Diego
409 University Center, Room 145
9500 Gilman Drive, MC 0085
La Jolla, California 92093

Dimitrios Lignos
Dept. of Civil Engineering and Applied Mechanics
McGill University
Macdonald Engineering Building
817 Sherbrooke West, Room 488
Montreal, Quebec, H3A 2K6

Farzin Zareian
University of California, Irvine
The Henry Samueli School of Engineering
Dept. of Civil and Environmental Engineering
Irvine, California 92697

Project Review Panel

Ronald O. Hamburger
Simpson Gumpertz & Heger
The Landmark @ One Market, Suite 600
San Francisco, California 94105

James R. Harris
J.R. Harris & Company
1775 Sherman Street, Suite 1525
Denver, Colorado 80203

William T. Holmes
Rutherford and Chekene
55 Second Street, Suite 600
San Francisco, California 94105

Richard E. Klingner
University of Texas at Austin
10100 Burnet Road
Austin, Texas 78758

Philip Line
(American Forest and Paper Association representative)
URS Corporation
200 Orchard Ridge Drive, Suite 101
Gaithersburg, Maryland 20878

Nicolas Luco
US Geological Survey
Box 25046 – DFC – MS 966
Denver, Colorado 80225

Bonnie E. Manley
AISI Regional Director
41 Tucker Road
Norfolk, Massachusetts 02056

Laurence Novak
Portland Cement Association
5420 Old Orchard Road
Skokie, Illinois 60077

Rafael Sabelli
Walter P. Moore
595 Market Street, Suite 950
San Francisco, California 94105

Kurt Stochlia
International Code Council
5360 Workman Mill Road
Whittier, California 90601

FEMA Representatives

Michael Mahoney
Federal Emergency Management Agency
500 C Street, SW
Washington, D.C. 20472

Robert D. Hanson
Federal Emergency Management Agency
2926 Saklan Drive
Walnut Creek, California 94595